UNIVERSITY OF ZULULAND

Development of a Point-of-Care Biomedical Imaging Diagnostics for Cancer Screening

By

Edwina Olohirere UZUNUIGBE

Student number: 201546690

Thesis submitted in fulfilment of the requirements for the award of

Doctor of Philosophy (PhD) in the field of Biochemistry

Department of Biochemistry and Microbiology, Faculty of Science and Agriculture,

University of Zululand, KwaDlangezwa, South Africa

Supervisor: Prof. Abidemi Paul Kappo

Co-Supervisor: Prof. Mervin Meyer and Prof Martin Onani

DECLARATION

I, Edwina Olohirere UZUNUIGBE (Student No: 201546690), declare that the experimental work described in this thesis was carried out in the Department of Biochemistry and Microbiology, Faculty of Science and Agriculture, University of Zululand. Also in the Department of Biotechnology, University of the Western Cape (UWC), from April 2015 to October 2017, under the supervision of Prof. Abidemi Paul Kappo and co-supervision of Prof. Mervin Meyer and Prof. Martin Onani. Hence this "Development of a Point-of-Care Biomedical Imaging Diagnostics for Cancer Screening" is my original work, therefore has never been submitted in any form to another University. Every work of others used has been correctly cited and acknowledged in the text and references. Hence, I UZUNUIGBE Olohirere Edwina firmly declared the above statement to be true.

Candidate:

Signature: .....

Date: .....

Supervisor:

Signature: .....

Date: .....

Co-supervisors:

Signature: ..... Date: .....

Signature: ..... Date: .....

DEDICATION

This thesis is dedicated to the Almighty God, the giver of life, who is the source of wisdom, knowledge, inspiration, and understanding in life.

AND

To my husband, Engr Eghosa Osagie Uzunuigbe and Children.

ACKNOWLEDGEMENTS

My deepest gratitude goes to the Almighty God, the Author and Finisher of our faith who keeps Life and provided all that was needed to complete this program. Thanks, dear Lord, Jesus Christ for mercy and great grace. He took care of everything that would have stopped the work and strengthened me throughout the most challenging times.

An earnest and most sincere gratitude go to my supervisor Prof Abidemi Paul Kappo, for his guidance, cooperation, patience, and support during this program and without him this work would not have been possible. Also, appreciation goes to my co-supervisors; Prof Mervin Meyer for his soft-spoken advice that was inspiring, accurate guidance and support, which made this work a great success and Prof Onani Martins for his technical humour, guidance, and support, l appreciate greatly, Sirs. Especially, for giving the platform to develop new skills and techniques in this scientific pursuit.

To my lovely husband; Engr. Eghosa Osagie Uzunuigbe, for his love, patience, friendship, humour and unconditional support and to my children: The three Ns; Noyorion, Nirhoite and Nomweosa and niece in a daughter – Mary. Lots of love that can never be quantified.

To my parents and siblings: Special thanks to Daddy - Chief Gabriel.O. Iruolaje, (A man who loves education) for your encouragement and financial support; Mrs Winifred Irabor, my delightful sister, there can never be a sister like you and my other siblings, God bless you all. Mama, thanks for all your prayers, Loads of Love. God bless Mama, in Jesus name. All the in-laws; Mrs B.A Ogunmwonyi, Dr Etinosa and Dr. (Mrs) lsoken Igbinosa, Nosa and Pat Ogunmwonyi, Dr Uyi Idemudia and Osaze Inneh family, I appreciate you all.

Moreover, also wish to express warm thanks to the HOD - Prof A.K. Basson, and other members of staff in the Department of Biochemistry and Microbiology, University of Zululand for their support. Am grateful to the National Research Foundation (NRF) South

Africa and to the Research Office of the University of Zululand for funding this research work. Prof. Andrew Opoku, for his kind encouragement, warmest gratitude.

I wish to appreciate and acknowledge all the colleagues in the Biochemistry and Structural Biology (BSB) group who assisted, advised, and supported my research; Firstly, Dr Babatunji Oyinloye (MOG) l say a big thank you. Adenowo Fatima, Funmi Akapo, Priscilla Masamba Ntombikhona Koza, Makhosazana Mathenjwa, Ntando Buthelezi, Sbonelo Khanyile, Philisiwe Molefe, Noxolo Khuboni and the entire BSB Group. I especially want to appreciate these young colleagues in BSB group; Tayo Alex Adekiya, Taiwo Aruleba, and Paul Ikwegbue, I appreciate all your support at the last stage of this thesis write up. God bless them richly.

To the entire UWC crew, Dr Nicole, Dr Janet Okafor, Taahirah Boltman, Dr Marius, Riziki, and all the entire NIC and Biotechnology group, I cherish the time we spent together in the lab, thank you all. To the entire inorganic research group in chemistry, Dr Kiplagat Ayabei and others l extend sincere gratitude. I especially want to thank, Dr. (Mrs) Dorcas Wusu, whom l met in UWC, my meeting you was a divine arrangement, you have touched my life in such an excellent way, for all statistical analysis you taught me, just to mention but a few and also Dr Theresa and Dr (Mrs) Janet, I say thank you.

To Pastor Henock and his lovely wife, Renate and the entire Christ Assembly Parish RCCG, Esikhawini; Pastor and Mrs Fatoba and the entire RCCG Household of God family, Belhar, Cape Town, South Africa. God bless. Warm appreciation to the colleagues in Unizulu; Mr Kayode Oki, Bro. Kenny, Bro. Tosin, Bro. Joshua, Bro. Segun, Bro. Chinaza and Sister Toyin they are all blessed. A special appreciation goes to the Executive Director of Rubber Research Institute of Nigeria, Iyanomo, Benin City. Edo State; Dr A.I. Aigbodion. Dr O. Aghughu, (Head of Department; Crop Improvement and Management Department), Dr K.O. Omokhafe and the entire Physiology and Biochemistry division Staff; Especially

Franklin Ohikhena, Stanley Omorogbe, Joy Omorogbe, Doyin Chukwuka, Desmond, Uhimwen, and the Akpaka's. Special thanks go to an adorable and unassuming couple, Big Mama and the husband, Dr and Dr (Mrs). Emeudo, words cannot say it all, she has touched my life in unusual ways. To a fantastic friend in a sister, and her husband; Dr Ehi and Barr. (Mrs) Isoken Ogbeide, thanks for being there. To dear friends; Gloria Orih, Dr Anulika Okongwu, Ese Emebuome and others too numerous to mention, Lots of appreciation to you all.

TABLES OF CONTENTS

DECLARATION ..... **ii**

DEDICATION ..... **iii**

ACKNOWLEDGEMENTS ..... **iv**

TABLES OF CONTENTS ..... **vii**

LIST OF TABLES ..... **xv**

LIST OF ABBREVIATIONS ..... **xvi**

ABSTRACT ..... **xviii**

CHAPTER ONE **1**

1.1 General Introduction **1**

1.2 Extracellular Matrix (ECM) **3**

1.2.1 ECM remodelling and cancer 7

1.2.2 Extracellular Matrix Proteases 8

1.3 Matrix metalloproteinase (MMPS) **8**

1.3.1 Matrix metalloproteinase 2 (MMP-2) 10

1.3.2. Regulation of MMP-2 13

1.3.3 Role of MMP-2 in cancer 14

1.4 Cancer: an overview of distribution, occurrences and causes **15**

1.4.1 Some typical features of cancer cells 18

1.4.1.1 Sustenance of proliferative signalling 19

1.4.1.2 Insensitivity to antigrowth signals 19

1.4.1.3 Evading apoptosis 20

1.4.1.4 Limitless replicative potential 20

1.4.1.5 Sustained angiogenesis 21

1.4.1.6 Genome instability 21

1.4.1.7 Tissue invasion and metastasis 21

1.4.2 Cancer diagnosis and therapy 22

1.5 Chlorotoxin (CTX): origin and biochemical components **23**

1.5.1 Mode of action of CTX in tumour cells 24

1.5.2 MMP-2 and chlorotoxin interaction as a diagnostic tool 25

1.6 Gum Arabic **26**

1.6.1 Chemical Composition of GA 28

1.6.2 Uses of Gum Arabic 28
1.6.3 Gum Arabic as a Nanovector 30
1.7 Nanotechnology 33
1.7.1 Application of Nanotechnology 33
1.7.2 Types of Nanoparticles 34
1.8 Quantum Dots (QDs) 34
1.8.1 Characteristics of Quantum Dots 35
1.8.2 Uses of Quantum Dots 36
1.8.3 Cadmium Telluride (CdTe) QDs 37
1.9 Cancer-specific peptide a promising agent for cancer diagnosis and therapeutics. 38
1.9.1 Peptide for Cancer diagnosis and Therapeutic 39
1.9 Cytotoxicity of QDs 40
1.10 Flow Cytometry 41
1.11 Problem Statement 41
1.12 Aim and Objective of the Study 42
1.13 References 43
CHAPTER TWO 72
2.1 Introduction 73
2.2 Experiment 74
2.3 Synthesis and Characterization of CdTe-QDs 75
2.4 Preparation of QDs-GA Using Gum Arabic Polymer 76
2.5 Investigation of the effect of CdTe QDs in cancer cells 76
2.6 Results and discussion 78
2.6.1 Optical characterisation 78
2.6.2 X-Ray Diffraction (XRD) Powder Analysis 79
2.6.3 High-Resolution Transmission Electron Microscope 81
2.6.4 Fourier Transform Infrared Spectroscopy (FT-IR) 85
2.6.5 Zeta Potential, Hyrodynaymic Sizes and Polydispersity Index 87
2.7 Cytotoxicity Studies of the Bare and GA capped Quantum Dots 90
2.8 Conclusion 92
2.9 References 93
CHAPTER THREE 96

3.1 Introduction **96**
3.2 Experimental design **97**
3.2.1 Materials used 97
3.2.2 Method 97
3.3 Results and Discussion **97**
3.4 Stability of QDs-MPA and QDs-GA in 0.5% BSA **98**
3.5 Stability of QDs-MPA and QDs-GA in DMEM **102**
3.6 Stability of QDs-MPA and GA-QDs in 10% FBS **104**
3.7 Stability of QDs-MPA and QDs-GA in PBS **106**
3.8 Stability of QDs-MPA and QDs-GA in RPMI **108**
3.9 Conclusion **110**
3.10 References **111**
CHAPTER FOUR **114**
4.1 Introduction **114**
4.2 Types of cancer cell lines **115**
4.3 Immunocytochemistry **115**
4.4 Materials and Method **116**
4.4.1 Materials 116
4.4.2 Cell Culture 116
4.5 Cell binding study of FITC labelled Chlorotoxin peptide 1 and 2 ..... **117**
4.6 Seeding of cells in culture plate cells **118**
4.7 Fixing and permeabilisation of cells on slides **118**
4.8 Staining of fixed cells **119**
4.9 Immunocytochemistry Assay **119**
4.10 Results and Discussion **120**
4.10.1 WST-1 viability assay images of cells treated with different QDs concentrations 120
4.10.2 WST-1 cell viability of HeLa cells treated with different QDs concentrations 120
4.10.3 WST-1 cell viability of PC-3 cells treated with different QDs concentrations 121
4.10.4 WST-1 cell viability of MCF-7 cells treated with different QDs concentrations 121
4.10.5 WST-1 cell viability of U87 cells treated with different QDs concentrations 122
4.11 Cell binding studies using CTX-FITC (Peptide-1) and CTX-FITC (Peptide-2) **123**
4.11.1 Binding studies for HeLa cells using CTX-FITC (Peptide-1) and CTX-FITC (Peptide-2). 124

4.11.2 Binding studies for PC-3 cells using CTX-FITC (Peptide-1) and CTX-FITC (Peptide-2). 125
4.11.3 Binding studies for MCF-7 cells using CTX-FITC (Peptide-1) and CTX-FITC (Peptide-2). 126
4.11.4 Binding studies for U87 cells using CTX-FITC (Peptide-1) and CTX-FITC (Peptide-2)... 127
4.11.5 Binding studies for CHO cells using CTX-FITC (Peptide-1) and CTX-FITC (Peptide-2). 128
4.12 Percentage of cells binding of CTX-FITC Peptide 1 for all cell line 129
4.12.1 Percentage of cells binding of CTX-FITC Peptide 2 for all cell line 130
4.13 Cell Microscopy Studies 132
4.14 Immunocytochemistry Assay 137
4.15 References 142
CHAPTER FIVE 148
5.1 Introduction 148
5.2 Materials and Method 149
5.2.1 Materials 149
5.2.3 Transformation and Expression screening of Chlorotoxin (CTX) 149
5.2.4 Large Scale Expression of Chlorotoxin 150
5.3 Purification of Recombinant HIS-CTX-GST Protein 151
5.3.1 Preparation of Column 151
5.3.2 Purification of HIS-CTX-GST Protein 152
5.3.3 Analysis of Extracted HIS-CTX-GST Protein 152
5.3.4 The Cleavage of HIS-GST-CTX with 3C Protease. 153
5.3.5 Quantification of Chlorotoxin Protein 153
5.4 Analysis of Sequences 154
5.5 Results 155
5.5.1 SDS GEL of CTX Expression Screening 155
5.5.2 SDS GEL of CTX Purification 156
5.5.3 SDS Gel is showing the CTX Digestion. 156
5.6 Sequence of Chlorotoxin 157
5.7 Discussion on the purification and recombinant expression of chlorotoxin 158
5.8 Blocking Studies 159
5.8.1 Material and Method 159
5.8.2 Method 159
5.9 Results 160

5.9.1 Histogram of cell blocking studies using labelled chlorotoxin and purified chlorotoxin 160
5.9.2 HeLa Cells Block Study Analysis using CTX Peptides 1 161
5.9.3 PC-3 Cells Block Study Analysis using CTX Peptides 1 161
5.9.4 U87 Cells Block Study Analysis using CTX Peptides 1 162
5.9.5 MCF - 7 Cells Block Study Analysis using CTX Peptides 1 162
5.9.6 HeLa, PC-3, U87 and MCF-7 Blocked Cells Percentages 163
5.10 Discussion on Blocking Studies 163
5.11 Scratch Migration Assay 165
5.11.1 Experimental 165
5.11.2 Result and discussion of Scratch Migration Assay 166
5.11.2.1 HeLa cells percentage gap closure of scratch migration assay 166
5.11.2.2 U87 Cells Percentage Gap Closure of Scratch Migration Assay 166
5.11.2.3 MCF-7 Cells Percentage Gap Closure of Scratch Migration Assay 167
5.11.2.4 PC-3 Cells Percentage Gap Closure of Scratch Migration Assay 167
5.12 Discussion 168
5.13 References 170
CHAPTER SIX 173
6.1 Introduction 173
6.2 Materials and Method 173
6.2.1 Materials 173
6.2.2 Synthesis and characterisation of QDs-MPA and QDs-GA CdTe quantum dots 174
6.2.3 Bio-conjugation of quantum dots to Biotinylated Chlorotoxin Peptide 174
6.2.4 Cell culture and WST-1 cell viability 175
6.3 Results and Discussion 175
6.5 References 183
CHAPTER SEVEN 185
7.1 General Discussion 185
7.2 Conclusion 188
7.3 Recommendation for Further Work 189
7.4 References 190
APPENDIX 193

LIST OF FIGURES

Figure 1.1: Structure of the extracellular matrix. 5
Figure 1.2: The Structure showing the two primary classifications of the ECM. 6
Figure 1.5: The basic structure of MMP-2 (Gelatinases-2) showing it various domains. 13
Figure 1.6 Biochemical role of MMP-2 in cancer. 15
Figure 1.7: Stages of tumour cell development from a single mutated cell. 18
Figure 1.9: (A) Purified powder of Gum Arabic (B) Raw Gum Arabic freshly harvested from the tree. 27
Figure 1.10: Map of Africa showing the significant Gum Arabic producing countries. 27
Figure 1.11: Structure of Gum Arabic. 33
Figure 1.12: Structure of Quantum dots. 35
Figure 1.13: Diagram showing the different uses of quantum dots. 37
Figure2.1: UV–vis spectra of the QDs-MPA, QDs-GA2 and QDs-GA12 78
Figure 2.2: The photoluminescence spectrum of the QDs-MPA, QDs-GA2 and QDs-GA12 79
Figure2.3: XRD pattern of the QDs-MPA, QDs-GA2 and QDs-GA12 80
Figure2.4a: Particle size distribution of QDs-MPA 82
Figure2.4b: EDX Spectra of QDs-MPA 82
Figure2.4c: HRTEM and SAED images of QDs-MPA 82
Figure2.5a: Particle size distribution of QDs-GA2 83
Figure 2.5b: EDS spectra of QDs-GA2 83
Figure 2.5c: HRTEM and SAED images of QDs-GA2 83
Figure 2.6a: Particle size distribution of QDs-GA12 84
Figure2.6b: EDS spectra QDs-GA12 84
Figure 2.6c: HRTEM and SAED images of QDs-GA12 84
Figure2.7: The FT-IR plot of all three; QDs-MPA, QDs-GA2 and QDs-GA12 86
Figure 2.8: Histogram showing the Zeta potential, Polydispersity index (PDI) and hydrodynamic distribution of the different quantum dots. 88
Figure 2.9: Bar chart showing U87 Cytotoxicity assay using QDs-MPA and QDs-GA 90
Figure 2.10: Bar chart showing MCF-7 cytotoxicity assay using QDs-MPA and QDs-GA ... 90
Figure 2.11: Bar chart showing HeLa cytotoxicity assay using QDs-MPA and QDs-GA 91
Figure 2.12: Bar chart showing PC-3 cytotoxicity assay using QDs-MPA and QDs-GA 91
Figure 3.1: Stability of QDs-MPA in 0.5% BSA 99
Figure 3.2: Stability of QDs-GA2 in 0.5% BSA: 100
Figure 3.3: Stability of QDs-GA12 in 0.5% BSA: 101
Figure 3.4: Stability of QDs-MPA in DMEM: 102
Figure 3.5: Stability of QDs-GA2 in DMEM: 103
Figure 3.6: Stability of QDs-GA12 in DMEM: 103
Figure 3.7: Stability of QDs-MPA in 10% FBS: 104
Figure 3.8: Stability of QDs-GA2 in 10% FBS: 105
Figure 3.9: Stability of QDs-GA12 in 10% FBS: 105
Figure 3.10: Stability of QDs-MPA in PBS: 106
Figure 3.11: Stability of QDs-GA2 in PBS: 107
Figure 3.12: Stability of QDs-GA12 in PBS: 107
Figure 3.13: Stability of QDs-MPA in RPMI: 108
Figure 3.14: Stability of QDs-GA2 in RPMI: 109

Figure 3.15: Stability of QDs-GA12 in RPMI:.....109
Figure 4.1: Images of HeLa cells treated with different concentration of QDs-MPA, QDs-GA2, and QDs-GA12 respectively, in 96 well plates.....120
Figure 4.2: Images of PC-3 cells treated with different concentration of QDs-MPA, QDs-GA2 and QDs-GA12 respectively. 121
Figure 4.3: Images of MCF-7 cells treated at a different concentration of QDs-MPA, QDs-GA2, and QDs-GA12 respectively. 122
Figure 4.4: Images of U-87 cells treated at a different concentration of QDs-GA, QDs-GA2, and QDs-GA12 respectively. 122
Figure 4.5a: Histogram of HeLa cells treated with FITC peptide1 at various concentrations. 124
Figure 4.5b: Histogram of HeLa cells treated with various concentrations of FITC peptide-2. 124
Figure 4.6a: Histogram of PC-3 cells treated with FITC peptide1 at different concentrations. 125
Figure 4.6b: Histogram of PC-3 cells treated with FITC peptide-2 at varying concentrations. 125
Figure 4.7a: Histogram of MCF-7 cells treated with FITC peptide-1 at various concentrations. 126
Figure 4.7b: Histogram of MCF-7 cells treated with FITC peptide-2 at varying concentrations. 126
Figure 4.8a: Histogram of U87 cells treated with FITC peptide-1 at various concentrations. 127
Figure 4.8b: Histogram of U87 cells treated with FITC peptide-2 at varying concentrations. 127
Figure 4.9a: Histogram of CHO cells treated with FITC Peptide-1 at various concentrations. 128
Figure 4.9b: Histogram of cells treated with FITC peptide-2 at varying concentrations. 128
Figure 4.10: Plot of percentage binding of peptide 1 to cell lines (HeLa, PC-3, MCF-7, U87 and CHO cells).....129
Figure 4.11: Plot of percentage binding of peptide 2 to cell line (HeLa, PC-3, MCF-7, U87 and CHO cells). (HeLa, PC-3, MCF-7, U87 and CHO cells).....130
Figure 4.12: Microscopy study of the binding of the QDs to HeLa cells.....133
Figure 4.13: Microscopy study of the binding of the QDs to PC-3 cells.....134
Figure 4.14: Microscopy study of the binding of the QDs to MCF-7 cells.....135
Figure 4.15: Microscopy study of the binding of the QDs to U8-7 cells.....136
Figure 4.16: Immunocytochemistry images of HeLa Cells.....139
Figure 4.17: Immunocytochemistry images of PC-3 Cells.....139
Figure 4.18: Immunocytochemistry images of MCF-7 Cells.....140
Figure 4.19: Immunocytochemistry images of U87 Cell.....140
Figure 5.1a: Expression screening results of Chlorotoxin (CTX). 155
Figure 5.1b: SDS-PAGE analysis of Purification of Chlorotoxin protein.....156
Figure 5.1c: SDS Gel showing the Digestion of CTX.....157
Figure 5.2a: Amino acid sequence of Chlorotoxin 157
Figure 5.2b: Nucleotide sequence of CTX protein retrieved from ExPASy translate tool....158
Figure 5.3: Histogram of cell blocking studies.....160

Figure 5.4: Histogram showing is blocking experiment of HeLa cells using Chlorotoxin peptide. 161
Figure 5.5: Histogram showing is blocking experiment of PC-3 cells using chlorotoxin peptide. 161
Figure 5.6: Histogram showing is blocking experiment of U87 cells using chlorotoxin peptide. 162
Figure 5.7: Histogram showing is blocking experiment of MCF-7 cells using chlorotoxin peptide. 162
Figure 5.8: Chart showing percentage blocked cells of HeLa, PC-3, U87 and MCF-7. 163
Figure 5.9: Chart showing percentage gap closure of HeLa cells 166
Figure 5.10: Chart showing percentage gap closure of U87 cells 166
Figure 5.11: Chart showing percentage gap closure of MCF-7 cells 167
Figure 5.12: Chart showing percentage gap closure of PC-7 cells 167
Figure 6.1: Diagram showing the mechanism of conjugation of biotinylated chlorotoxin to Quantum dots. 174
Figure 6.2: UV absorbance of QDs-MPA, QDs-Streptavidin and QDs-MPA-CTX. 177
Figure 6.3 UVis absorbance of QDs-GA, QDs-GA-Strep and QDs-GA-CTX. 178
Figure 6.4: The cytotoxicity studies of QDs-GA chlorotoxin conjugate (QDs-GA-CTX) using HeLa, MCF-7, PC-3 and U87 cell line. 179
Figure 6.5: The cytotoxicity studies of QDs-MPA chlorotoxin conjugate. 179
Figure 6.6: Percentage QDs-MPA uptake at 25µg/mL (blue bar) and 50µg/mL (orange bar). 180
Figure 6.7: Percentage QDs-GA uptake at 25µg/mL (blue bar) and 50µg/mL (orange bar). 180
MCF-7 and U87 Cell lines (QDs -MPA-CTX) at 25 µg/mL and 50 µg/mL concentration. . 181
Figure 6.9: Percentage uptake of the QDs-GA chlorotoxin conjugate in HeLa, PC-3, MCF-7 and U87 Cell lines (QDs-GA-CTX) at 25 µg/mL and 50 µg/mL concentration. 181

LIST OF TABLES

Table1.1: Peptide applied in cancer diagnosis.....40

Table 4.1: The preparation of 12 % SDS-PAGE. 153

LIST OF ABBREVIATIONS

Amp	Ampicillin
APS	Ammonium per sulphate
C-terminal	Carboxyl terminus
CTX	Chlorotoxin
DNA	Deoxyribonucleic acid
DMEM	Dulbecco's Modified Eagle's Medium
DMSO	Dimethyl sulfoxide
DNA	Deoxyribonucleic Acid
dH_2O	Deionized Water
DTT	Dithiothreitol
ECM	Extracellular matrix
EDTA	Ethylene diamine tetraacetic acid
EDC	1-Ethyl-3-(3-dimethylaminopropyl) Carbodiimide
EDX/EDS	Energy-dispersive X-ray spectroscopy
FBS	Foetal Bovine Serum
FTIR	Fourier Transform Infrared Spectroscopy
FDA	Food and Drug Administration
FITC	Fluorescein isothiocyanite
GLOBOCAN	Global cancer statistics
GA	Gum Arabic
HRTEM	High-Resolution Transmission Electron Microscopy
IPTG	Isopropyl-β-D-thiogalactoside
KDa	Kilo Dalton
LB	Luria Brentani
mL	Millilitre
mm	Mille molar

mAb	monoclonal antibody
MMP-2	Matrix metalloproteinase-2
MEROPS	Database for peptidases
N	amino terminus
NCR	National Cancer Research
Nm	nanometre
OD	Optical density
PAGE	Polyacrylamide gel electrophoresis
PCR	Polymerase chain reaction
PBS	Phosphate buffered saline
PL	Photoluminescence
QDs	Quantum dot
QD-MPA	Quantum dots capped with Mecarptopionic acids
QDs-GA	Quantum Dots capped with gum Arabic.
SAED	Selected area (electron) diffraction
SD	Standard deviation
SDS	Sodium dodecyl sulphate
SEM	Scanning electron microscopy
TBS	Tris buffered saline
TEM	Transmission electron microscopy
UV-Vis	Ultraviolet-visible
μL	microlitre
μM	micro molar
WST-1	(2-[4-iodophenyl]-3-[4-nitrophenyl]-5-[2, 4-disulfophenyl]-2H-tetrazolium
WHO	World Health Organization
XRD	X-ray powder diffraction

ABSTRACT

Despite our improved understanding of cancer biology, this disease remains a global health phenomenon, affecting the populations in developed and developing countries, of every socioeconomic strata. It is the second leading cause of death worldwide with over 10 million new cases and over 5 million deaths annually. The point-of-care diagnostic approach holds important promise for the early detection of cancer since most cases are treatable at an early stage of the disease. Research has shown that over 90 per cent of cancer cells express some forms of proteins, which can serve as biomarkers for early detection, thereby increasing survival rate in cancer patients. Recently, nanotechnology has been used to develop nanoparticles like a quantum dot, known for their unique optical properties and sizes and applicable for diagnosis in cancer cells research. In this study, colloidal cadmium telluride quantum dots were synthesised, capped and stabilised with Gum Arabic polymer. These particles were characterised using UV absorption, Photoluminescence (PL), X-Ray diffraction (XRD), High-Resolution Transmission Electron Microscopy (HRTEM), Fourier transform infrared (FTIR) analysis and zeta potential to determine their stability in different media. These quantum dots were then used for *in-vitro* cytotoxicity studies on 4 different cancer cell lines (HeLa, MCF-7, PC-3 and U87) in a dose-dependent manner. Results: cells were found to have over 50% viability for almost all cell line. Binding studies were evaluated in-*vitro.* Chlorotoxin peptide labelled with FITC at the C and N-terminals respectively were used for this study while fluorescence intensity was used to determine the binding of the cell to the peptides and expressed in percentage. Results show that cells bind more to chlorotoxin peptide with FITC attached to the N-terminal of the CTX than CTX peptide with FITC at the C- terminal and this binding was dose-dependent. Chlorotoxin (HIS-CTX-GST tagged) was genetically recombined and expressed in *Escherichia coli* (*E. coli*) BL21 cells, purified using nickel beads. Sodium dodecyl sulphate polyacrylamide gel electrophoresis (SDS-PAGE) was

used to analyse the protein and results show noticeable bands at 30 kDa which corresponding to the HIS-GST-CTX protein. Block studies experiment was carried out using CTX-FITC labelled peptide and recombinantly expressed CTX to determine the binding effect of both peptides to the cells that is if they are specific or receptor-dependent. The results revealed that the binding of the CTX-FITC was receptor dependent. Biotinylated chlorotoxin was conjugated to quantum dots using streptavidin-biotin chemistry and cytotoxicity of this conjugates was carried out using WST-1 cell viability assay. Cell binding and uptake were also analysed. These studies will serve as a point-of-care diagnosis for cancer treatment as early diagnosis a key to surviving the disease. Also the *in vivo* studies cell uptake can be used to improve surgical procedure by ensuring total tumour removal, and this can prevent tumour reoccurrence.

Keywords: Chlorotoxin Peptide (CTX), MMP-2, WST-1 cell viability Assay, Nanoparticles, Quantum Dots, UV-Vis, HRTEM, XRD, Fluorescence, Cancer cells.

CHAPTER ONE

Introduction and Literature Review

1.1 General Introduction

The knowledge of cancer biology has increased appreciably in the last two decades. However, cancer remains a significant health challenge and one of the leading causes of death worldwide (Ma and Yu, 2006). Cancer has been classified as one of the non-communicable diseases (NCDs) with increasing prevalence globally (Bhandari *et al.*, 2014; Heneghan *et al*., 2013). Cancer is characterised by the uncontrolled growth of abnormal cells anywhere in the body, infiltrating normal body tissues in the process (NCI, 2014; WHO, 2014). This abnormal cell proliferation can be due to mutations, genetics and chronic inflammation as well as exposure to unhealthy lifestyles such as smoking, inadequate exercise, excessive alcohol intake, unhealthy diet, overweight and obesity (Cancer Research UK, 2014).

Cancer burden has been on the increase due to an ageing and growing world population. The recent upsurge in lifestyle-associated habits and behaviours such as smoking and unhealthy diets, especially in developed countries has contributed to the upsurge of cancers (Jemal *et al*., 2011). In 2008, an estimated 169.3 million people died of cancer globally (Torre *et al.*, 2015). In 2012, about 8.2 million people were estimated to have died of cancer from the 14.1 million new cases of cancers that were diagnosed (Global Cancer Statistics, 2012). Research has shown that 50% of global cancer death occurred in countries with low income or medium level human development index (HDI). Lungs, breast, prostate and colon cancers are the most commonly occurring cancers accounting for about 4 in 10 of all cancers diagnosed (Siegel *et al*., 2013; Cancer Research UK, 2014) with breast cancer having the highest mortality rate (Siegel *et al.,* 2014) while lung cancer is the most frequently diagnosed (Ferlay *et al.,* 2015).

The challenge at the moment is that most cancer drugs have no specificity. Early detection and removal of a tumour are one of the ways to prevent cancer cells from metastasising. This has prompted scientists to develop the strategy of targeted therapies, which entails tumour-specific targeting and bio-imaging for early detection of disease. Targeted imaging is a strategy that identify an appropriate molecule that is highly expressed at the cell surface and to develop this into an appropriate marker: antibodies, antibody-like ligands, proteins or peptides. These biomarkers can serve for detection or treatment of the disease by delivering the appropriate drug using a vector (Dardevet *et al*., 2015). It can also be used as a diagnostic tool to facilitate detection of the disease at an initial stage, thereby increasing the chances of survival. These vectors can be produced by bio-conjugating the molecules with a protein that is explicit in the disease site of interest, with an imaging agent for diagnostic purpose considering the fact most existing diagnostic tools detect disease at an advanced stage, there is the need to develop a more accessible, faster and affordable tool to replace existing ones and make tumours more visible during targeted surgery (Wang *et al.,* 2006).

The use of nanoparticles especially those synthesised from plants as biomedical molecules or anticancer agents has been termed safe, non-toxic, biodegradable, environmentally-friendly and of significant advantage in combating cancer challenges (Dubey *et al*., 2009; Oluwafemi *et al*., 2013; Raveendran *et al*., 2003). This technology can be used for the development of diagnostic tools to greatly enhance the chances of survival in cancer patients as well as ease the removal of tumours during surgery (Gaddala and Nataru, 2015).

The identification of an appropriate specific molecule that can bind cancer cells has been a problem in medicine until the discovery of Chlorotoxin (CTX); a 4kD protein made up of 36 amino acids from the venom of scorpion, *Leiurus quinquestriatus* (El-Ghlban *et al.,* 2014; Fu *et al.*, 2012; Wu *et al*., 2010). CTX has been shown to bind the family of proteases; the matrix metalloproteinase (MMPs), that are over-expressed in stroma cells found around

cancerous cells. A member of these proteinases, MMP-2, has been chosen as a promising target for cancer therapy because CTX has been shown to bind and inhibit MMP-2 activities (Hua *et al.,* 2011).

Quantum dots are semiconductor colloidal nanoparticles of sizes less than 10 nm that have found full usage in biological applications (Chan *et al*., 2002; Tang *et al*., 2002) They have distinctive optical and electronic properties, which can be manipulated and capped with different compounds using polymers such as Gum Arabic (Smith and Nie, 2008; Sun *et al*., 2006). This makes QDs good choice for cellular bio-imaging and tumour targeted therapy compared to other conventional dyes. Among the different types of QDs, Cadmium Telluride (CdTe) QDs is a unique probe in bio-imaging of living cells because of their distinctive photoluminescence characteristics when excited (Erogbogbo *et al*., 2010; Rizvet *et al.,* 2010; Zhang *et al.*, 2015), its photo-stability, well-regulated and narrow emission of light and high quantum yield (Bao *et al*. 2010; Zhang *et al.,* 2015). The method of synthesis and capping agent used in CdTe is very significant because it determines the solubility and application in biological processes. Therefore, this study is targeted at using conjugated chlorotoxin to Gum Arabic capped and CdTe-stabilized quantum dots for bio-imaging to serving as a point-of care-diagnostics for cancer.

1.2 Extracellular Matrix (ECM)

ECM contains a diversity of large matrix molecules whose exact arrangement structure vary from tissue to tissue. (Theocharis *et al.,* 2016). The extracellular matrix (ECM) can be defined as a three-dimensional, non-cellular structure found in all tissues and organs, which is essential for life (Bonnans *et al.,* 2014; Theocharis *et al.,* 2016)**.** It is the principal controller of cellular and tissue functions in the body (Cox and Erler, 2011). The ECM is a structural and functional part of the stromal microenvironment (Marastoni *et al.*, 2008), which at the molecular level alters cellular activities such as proliferation, structural organisation, cellular

differentiation and receptor signalling (Kass *et al*., 2007; Paszek and Weaver, 2004). It also controls activities such as apoptosis, angiogenesis (Noguera *et al.,* 2012) as well as cell functions that are fundamental for wound healing, vascular matrix remodelling, synthesis of connective tissues associated with diseases such as atherosclerosis (Heeneman *et al*., 2003), cancer and hypertension (Ingber, 2007; Mosher and Adams, 2012). The ECM is also concerned with transmitting extracellular signals to cells, thus regulating cell differentiation (Werb, 1997). The ECM is composed of numerous macromolecules such as proteins mixed with fibrous glycoproteins; like structural glycoproteins (collagen and elastin), specialised glycol proteins (fibrillin, fibronectin and laminin) and proteoglycans (Rauch, 1997). These macromolecules are made up of a protein core with long chains of repeating disaccharide units, glycosaminoglycan. However, most ECM components are a physical obstruction to cell movement; hence, an understanding of the different changes in processes involving ECM production, modification and remodelling, and linking these changes to the biochemical and structural properties of the ECM are vital to determining how the microenvironment affects cellular responses, especially in disease conditions. Currently, the disease microenvironment is assumed to be correspondingly vital as cell populations involved in the development of pathologic conditions. For instance, healthy microenvironment inhibits the cancerous outgrowth of epithelial cells, while perturbation of homeostasis aids the initiation and progression of malignancy that brings about resistance (Theocharis *et al.,* 2016). ECMs are classified into two main types; pericellular and interstitial matrices (Theocharis *et al*., 2016). These findings would be very significant in the development of anti-cancer therapies targeting different aspects of the disease (Cox and Erler, 2011).

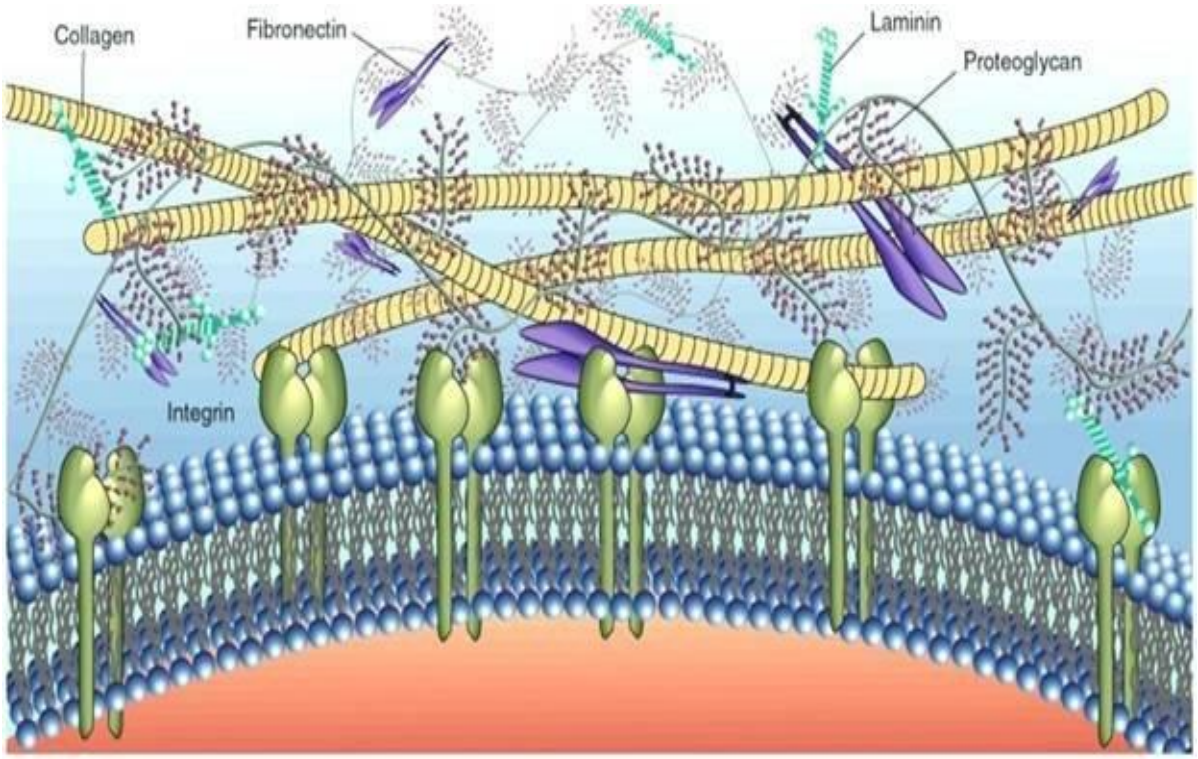

Figure 1.1: Structure of the extracellular matrix.
(Adopted from Meguid *et al.,* 2007)

The structure of the ECM showing its structural composition; Proteoglycan complex, collagen fibres, cytoskeleton and plasma membrane. These help to maintain the integrity of the ECM.)

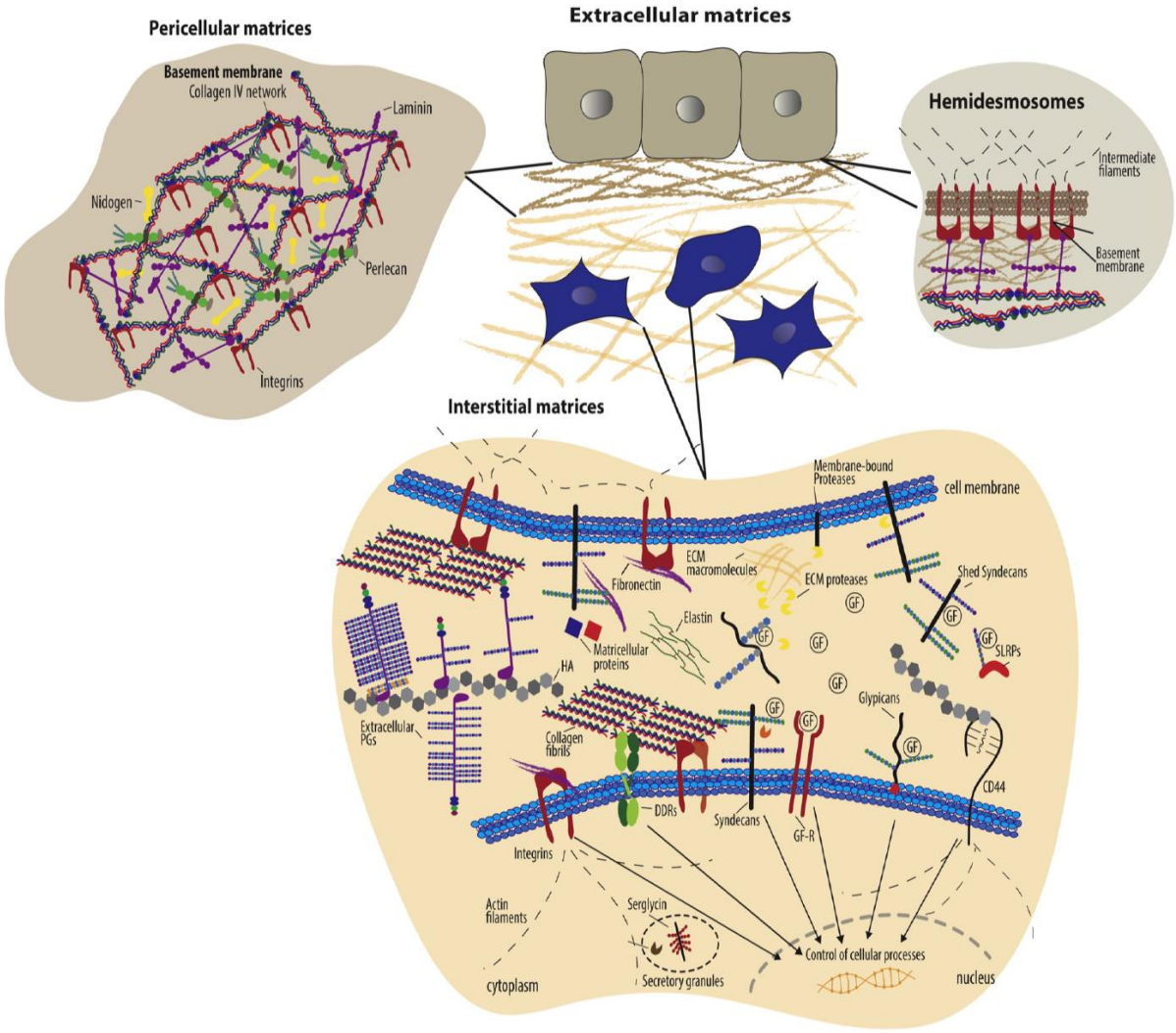

Figure 1.2: The Structure showing the two primary classifications of the ECM.
The Pericellular and interstitial matrices and their components. A type of the pericellular cells is the basement membrane found between the epithelial cells and connective tissues made up of collagens. Hemidesmosomes anchor the epithelial cells to the basement membranes in the ECM through the connections of integrins. Interstitial matrices comprise of, secreted PGs and HA, collagen fibrils, elastin, and matricellular proteins. Cells bind to ECM components by specific cell surface receptors, such as integrins; cell surface PGs; syndecans and glypicans. Some proteolytic enzymes, such as MMPs, ADAMs, ADAMTs, cathepsins, and plasminogen activators degrade the ECM. ECM degrading enzymes play critical roles in normal tissue remodelling and disease progression. (Figure adopted from Theocharis *et al.*, 2016).

1.2.1 ECM remodelling and cancer

The extracellular matrix is a dynamic structure that undergoes controlled changes known as remodelling. This remodelling occurs during disease and some physiological conditions, involving quantitative and qualitative changes in which both the proteinaceous and non-proteinaceous components of the ECM are deposited, degraded and modified (Bonnans *et al.,* 2014; Lu *et al.,* 2011; Schaefer and Dieter, 2016; Theocharis *et al.,* 2016). This process is facilitated by metalloproteinase and is connected with diseases progression (Bonnans *et al.,* 2014). ECM remodelling plays a crucial role in structural integrity and regulating cellular processes such as cell shape, cell movement and growth. In humans, these processes affect cell behaviour leading to diseases such as cancer and fibrosis (Frantz *et al.,* 2010). Severe injuries to tissues lead to excess ECM production resulting in an imbalance in the ECM, but without a corresponding balance in degradation it can lead to fibrosis, which in turn increases the risk of cancer development by 20–30%. The primary process that occurs in ECM remodelling is the cleavage of the component of the ECM by proteases such as MMPs. Hence, studies targeted at ECM remodelling enzymes and their receptors may thus have potential therapeutic properties. For instance, MMP inhibitors such as marimastat and prinomastat were potential anticancer agents who failed clinical trials due to non-specificity and poor tolerability (Coussens *et al.,* 2002). Therefore, MMPs alteration using monoclonal antibodies may be a more promising approach (Devy and Dransfield, 2011).

Cancer formation is a complex but gradual process that involves cellular and environmental factors as a result of alteration between cells and its microenvironment (Cox and Erler, 2011). These changes occur when the ECM is remodelled by increased ECM synthesis, assembly and alteration in matrix properties, totally disrupting normal tissue functions and encouraging disease progression (Cattell *et al.,* 1996). This disruption of the ECM microenvironment leads typically to an imbalance between ECM synthesis and secretion, mainly due to

alteration caused by matrix remodelling enzymes such as MMPs (Jodele *et al.*, 2006; Kessenbrock *et al.*, 2010; Strongin, 2006). Hence, the disruption in ECM homeostasis leads to pathological diseases which include cancer. For instance, ECM remodelling is one of the first steps in metastasis as it leads to tumour colonisation and circulation. For a tumour cell to metastasise from a primary tumour to other organs, it has to degrade constituents of the ECM. More so, the ECM also alters angiogenesis to promote tumour growth (Cheresh and Stupack, 2008) hence, targeting ECM enzymes involved in remodelling the receptors which transduce their signals offer promising therapeutic opportunities for many diseases.

1.2.2 Extracellular Matrix Proteases

They are also known as proteinases and were first presented as generic damaging enzymes linked to protein catabolism and generation of peptides and amino acids. Proteases make up more than 2% of the total genes in the human genome. This makes them a significant contributor in physiological cellular functions by regulating the fate, localisation and activity of a variety of proteins, modulating protein-protein interactions and generating new bioactive molecules (Theocharis *et al.*, 2016). The human degradome contains about 569 proteinases which are found distributed intracellularly and extracellularly according to the MEROPS database, and this is made up of five protease families (Theocharis *et al.*, 2016); Metalloproteases, Serine proteases, Cysteine proteases, Aspartic acid proteases and Threonine proteases. This classification is based on the chemical moiety that participates in the hydrolysis families (Theocharis *et al.*, 2016).

1.3 Matrix metalloproteinase (MMPS)

Matrix metalloproteinase (MMPs) belong to a family of protease or zinc-containing hydrolytic enzymes which specifically cleave components of the extracellular matrix and surface receptors such as collagen and proteoglycans (Brinckerhoff and Matrisian, 2002;

Gialeli *et al.,* 2011; Tentes *et al*., 2007; Theocharis *et al*., 2016). These enzymes are also involved in the cleavage of cell surface receptors, the release of apoptotic ligands and inactivation of chemokines/cytokines. MMPs are known to play a significant role in normal biological processes such as embryogenesis, tissue remodelling, wound healing, angiogenesis and in diseases such as tissue ulceration, atheroma, arthritis and cancer (Gialeli *et al.,* 2011; Raffetto and Khalil, 2008; Visse and Nagase, 2003). They were first discovered i n vertebrates including humans but have since been found in invertebrates and plants (Jackso n *et al*., 2010; Visse and Nagase, 2003). The MMPs family shares some essential secondary structural elements consisting of three common domains: the pro-peptide or N-terminal auto-inhibitory pro-domain, the catalytic domain and the hemopexin-like C-terminal domain (Amălinei *et al*., 2007; Visse and Nagase, 2003). They are classified into six groups based on their sequence similarity, domain organisation and substrate specificity as follows: collagenases, gelatinases, stromelysin, matrilysins, membrane-types MMPS (Mt-MMPs) and other M MPs (Amălinei *et al.,* 2007; Marchenko *et al*., 2003).

For this study, the focus was on a member of the gelatinase group known as MMP-2. Gelatinases are enzymes which are distinguished by the presence of a three repeat type-2 fibronectin domain inserted into their catalytic domain to form a compact collagen binding domain (Folgueras *et al*., 2004). The gelatin-binding area is located immediately before the zinc-binding motif and forms a separate folding unit which does not disrupt the structure of the catalytic domain. Members of this family of enzymes include MMP-2 and MMP-9. These enzymes are vital in ECM remodelling and degradation, especially in physiological states such as implantation, wound healing and in the disease state (Hashizume, 2007).

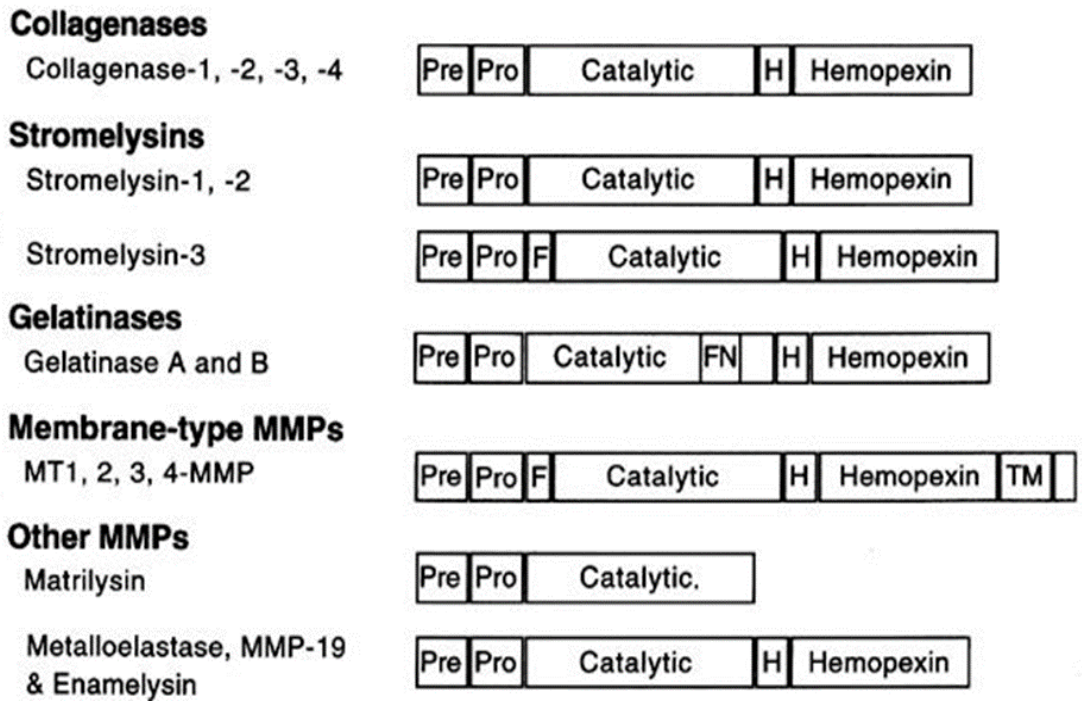

Figure 1.3: The MMPs individual family domain structures.
(Source: Uria and Werb, 1998)

Pre, signal peptide signal region; Pro, propeptide; Catalytic, domain comprising of the active and metal binding sites; F, furin recognition domain; FN domain with homology to the collagen-binding region of fibronectin; H is 'hinge' connecting region; the C-terminal with homology to hemopexin domain

1.3.1 Matrix metalloproteinase 2 (MMP-2)

Matrix metalloproteinase 2 (MMP-2) belongs to the family of gelatinases: gelatinase A and B. MMP-2 is classified as a gelatinase A (Murphy and Nagase, 2008; Visse and Nagase, 2003). It is a 72 kDa, type IV collagenase (Amăline *et al.*, 2007); a multi-domain protein found to be up-regulated in the stromal cells surrounding metastasising tumours as shown in figure 1.4 and 1.5 below (Cox and Erler, 2011). The enzyme is secreted in the inactive form and when cleaved, becomes a 64 kDa soluble protein (Arzamasov *et al.*, 2014). MMP-2 functions to degrade native and denatured collagens, elastin, aggrecan and fibronectin, cleave growth factors and cytokines by proteolysis (Murphy and Nagase, 2008; Xue and Jackson,

2008). It is highly expressed by various cell types including fibroblasts, keratinocytes. Comprise of four main domains viz signal, pro-peptide, a catalytic and the hemopexin domains (Amalinei *et al.*, 2007; Strongin, 2006; Vandooren *et al.*, 2013). The main thrust of this study will focus on the catalytic domain of the MMP-2 proteins.

The catalytic domain of the protein is a highly active, conserved, zinc ion (Zn^{2+}) binding site within the protein (Amălinei *et al.*, 2007; Vandooren *et al.,* 2013), made up of a 19 kDa amino acid sequence (Dhanaraj *et al*., 1999), with three repeating identical fibronectin (Fn) sequence, and two intramolecular disulphide bonds each, unique to the gelatinases. The fibronectin functions to enable smooth degradation of the sizeable gelatinous substrate and provide collagen with a site for binding. It is made up of two antiparallel β-strand sheets linked to a short α-helix and stabilised by two disulphide bonds (Amălinei *et al.*, 2007; Vandooren *et al.*, 2013). This domain is linked to the hemopexin region by a proline-rich hinge linker. This catalytically vital Zn^{2+} ion bound three histidine residues which are in the conserved sequence HExxHxxGxxH (zinc-binding motif). This domain is connected to the hemopexin-like C-terminal domain by a linker of 75 amino acids long, with no distinct structure. Gelatinases such as MMP-2, incorporate fibronectin type II modules which are inserted immediately before the zinc-binding motif in the catalytic domain (Trexler *et al*., 2003).

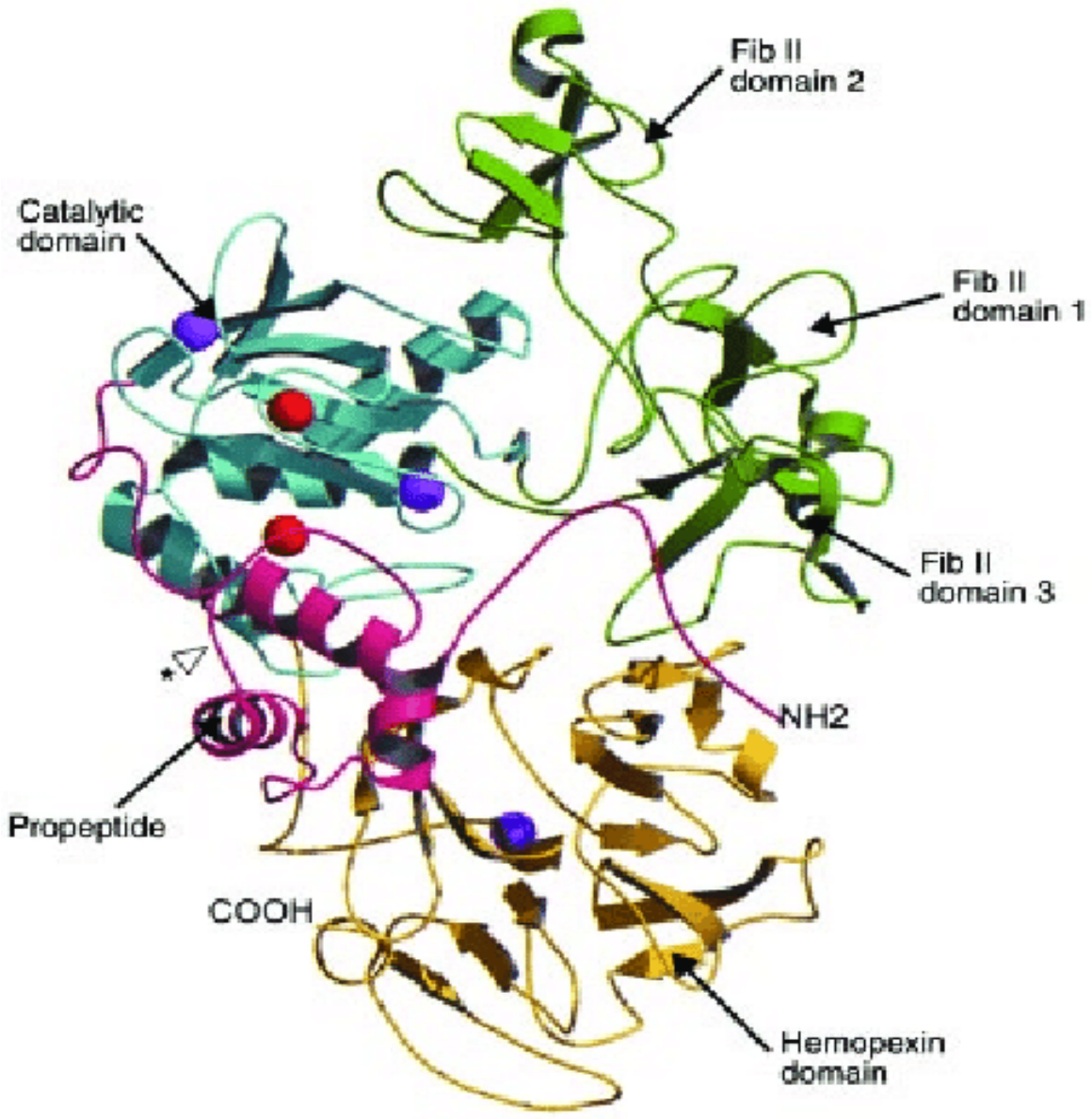

Figure 1.4: Pro-MMP2 Structure is showing the different domains.
(Figure adopted from Morgunova *et al.*, 1999).

The catalytic domain has two zinc cations (red) and two calcium cations (purple) indicated with bounds. The hemopexin domain (yellow) has one calcium cation (purple) bound is also known as the C-terminal.

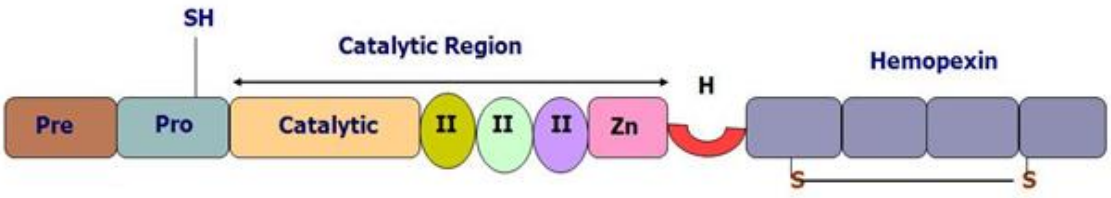

Figure 1.5: The basic structure of MMP-2 (Gelatinases-2) showing it various domains. (Figure taken from Chaudhary *et al.*, 2010; Visse and Nagase, 2003).

Pre domain is the signal sequence responsible for activation. Pro-peptide domain has zinc-ligating thiol group; fibronectin type II also known as the collagen binding site readily digest and binds to gelatin/collagen. The catalytic domain is the active site of the protein and contain Zn-binding site, H is a linker that connects the catalytic domain helps to link catalytic domain to hemopexin domain, and hemopexin made up of four repeat blade and a disulphide bond which is essential for collagenolytic activities of MMP-2.

1.3.2. Regulation of MMP-2

Regulation of MMP-2 helps in understanding the exact mechanisms that control the activity of enzymes in physiological and pathological conditions because it helps to prevent unwanted activities of other proteinases. These regulating mechanisms help to localise MMP degradative activities to the specific site, but tumour cells have acquired multiple ways to avoid these controls by up-regulating MMP proteolytic activity, a feature that leads to tumour growth and invasion (Folgueras *et al.*, 2004). All secreted proteinases have catalytic activities that are regulated at four points: gene expression, compartmentalization (that is, pericellular accumulation of enzymes), pro-enzymes activation (Folgueras *et al.*, 2004; Ra and Parks,

2007) and inhibition of enzyme activities by tissue inhibitors of metalloproteinase (Sariahmetoglu *et al.*, 2007).

MMP-2 is the most largely expressed MMP and found in several tissues and cells. It is widely known as an ECM degrading enzyme that can also act on some non-matrix substrates like interleukin 1, endothelin-1, monocyte chemoattractant protein-3- and stromal cell-derived factor 1 (Sariahmetoglu *et al.*, 2007). The enzymes can also be expressed in normal tissues, suggesting an involvement in regulating ECM homeostasis. However, like most MMPs, the enzymes are not expressed in a resting tissue but is generated during tissue repair or remodelling in a diseased state (Ra and Parks, 2007). This manner of regulating the functions of the proteinase have broadened its biological function (Sariahmetoglu *et al.*, 2007).

1.3.3 Role of MMP-2 in cancer

MMP-2 plays a very vital but complex role in cancer progression, but the mechanism is not well established. The major role of MMP-2 in cancer is in ECM degradation, which permits cancer cells to migrate and metastasize (Gialeli *et al*., 2011; Mook *et al.*, 2004), with its activities associated with breast, colorectal, lung and prostate cancers (Björklund and Koivunen, 2005; Said *et al.;* 2014). The enzymes have been found to play a crucial role in angiogenesis during cancer progression with the process vital for tumour cell survival.

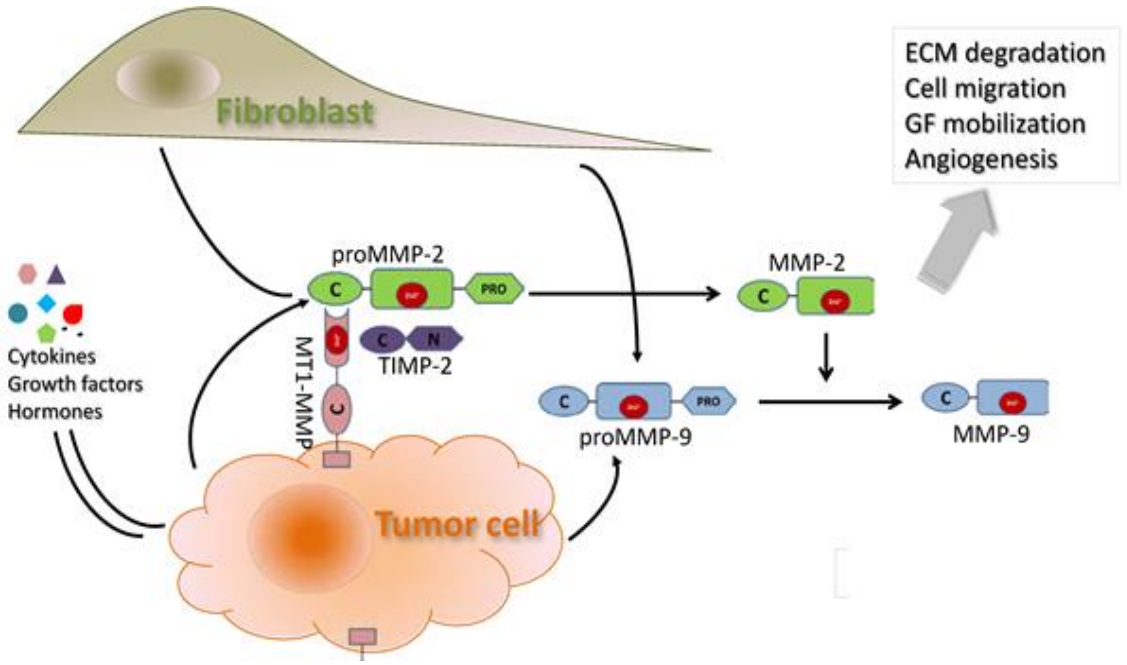

Figure 1.6 Biochemical role of MMP-2 in cancer.

Gelatinases (MMP-2 and MMP-9) are secreted as a pro-enzymes form by a tumour and fibroblast cells in the tumour microenvironment. The proMMP-2 is then activated by MT1-MMP thus leading to ECM degradation cell migration. Activated MMP-2 also activates other MMP-9 and other MMPs (Modified from Gong *et al.*, 2014)

1.4 Cancer: an overview of distribution, occurrences and causes

Cancer is classified as a non-communicable disease (NCD) (Bhandari *et al*., 2014; Heneghan *et al*., 2013); it is a disease condition that affects individuals over a period defined as idiopathic (Bhandari *et al.,* 2014). The biggest problem in cancer progression is that the immune system more often than not cannot tell the difference between a tumour and normal cells hence, this remains one of the most significant challenges in the fight against disease (Hahn *et al.,* 2009). During cancer cell formation, the typical regulator system that checks cell overgrowth and invasion of other tissues are deactivated. This abnormal behaviour can be said to be due to mutation, genetic and chronic inflammation factors (Colotta *et al.,* 2009).

Statistics have shown that cancer prevalence is increasing yearly and is expected to rise in the next two decades by 70 % (WHO, 2015) making the disease one of the main global public

health challenges (Arvizo *et al.*, 2010; Ferlay *et al.,* 2010; Siegel *et al* , 2017; Yu Gao *et al.,* 2013). The World Health Organization reports that one in six deaths is due to cancer hence, making this the second leading cause of death. A near 8.8 million deaths occurred from cancer in 2015 (WHO, 2015). About 100 different kinds of cancers are known (Cooper, 2000). Globally, the cancer burden is increasing due to ageing and an increase in cancer-causing behaviours such as smoking and unhealthy diet, especially in developed countries (Jemal *et al*., 2011). In the United States of America, and other low income or medium income countries, cancers remains the 2nd leading cause of death (DeVita and Chu, 2008; WHO, 2015 and Yu Gao *et al.,* 2014). Lungs, breast colon or bowel and prostate cancers are the most commonly occurring cancers; accounting for about 4 in 10 of all cancers diagnosed globally. Lung cancer is the most frequently diagnosed and the second leading cause of death. While prostate cancer remains the most common form of cancer in men and has the highest mortality rate of all cases of cancer deaths (Siegel *et al.,* 2014), it is most common in Europe and North America, probably due to exposure to environmental and occupational carcinogens like asbestos and polycyclic aromatic hydrocarbons (Spitz and Spitz, 2006). Breast cancer is the most common cancer diagnosed in females globally and the cause about 14 % of total cancer deaths in females (Siegel *et al.,* 2014), with the very high incidence in developed countries of Northern and Western Europe, North America. Although the incidence of breast cancer in sub-Saharan Africa and Asia is low, the mortality rate is high unexpectedly high in these low income and developing countries mainly due to inaccessibility to proper medical care, quality screening and early diagnosis (Ghafoor *et al., 2*003). In South Africa, one in every four South Africans has cancer, and the rate of survival is six in every ten patient. (Cancer Association of South Africa and NCR Report, 2011 (CANSA). A recent study by the South African Medical Research Council (SAMRC, 2014), listed four common cancers with a high mortality rate as follows; lung cancer (17%), oesophagus cancer (13%), cervical

cancer (8%) and breast cancer (8%). It has been projected that the rate of cancer in South Africa may increase by 78% in the year 2030 (Cancer Association of South Africa and the NCR report, 2011, CANSA). Studies have shown that ~ 90% of cancers are caused by environmental and lifestyle factors, behavioural and pollution factors (Forouzanfar, 2016; Manton *et al.,* 2008) with the remainder 10% driven by genetic factors and chronic inflammations (Anand *et al.,* 2008). However, genetic factors are known to play major roles in breast cancer with 70% of cases said to be hereditary and resulting from gene mutation of the BRCA 1 and BRCA 2 genes. In the normal physiological state, these genes produce proteins that help to check abnormal cell growth (Tutt and Ashworth, 2002 and Venkitaraman, 2002).

Cancer development (carcinogenesis) or tumorigenesis is a multi-step process in humans (Hanahan and Weinberg, 2000). At the cellular level, it involves mutation and epimutation of genetic materials of normal cells thereby increasing the ability of cells to proliferate and an unusual ability to survive, cause invasion and metastasise. The first step in carcinogenesis involves tumour initiation; this is the genetic mutation leading to an unprecedented

proliferation of a single cell giving rise to an outgrowth of a population of clone tumour cells. Tumour progression continues as the cells undergo different forms of mutations within the cells of the tumour population with the mutation leading to more rapid growth (figure 1.7). The progenies within the cell with such mutation then become dominant within the tumour population (Cooper and Hausman, 2000). This abnormality confers new competencies like the ability to release growth factors and digestive enzymes which invade nearby normal cells and often decreases the functions of the affected organ(s) or tissue(s). Another critical step in the growth of a tumour is the development of blood vessels for blood supply (angiogenesis). Angiogenesis supplies nutrients and transport waste material for the

tumour cells. During the abnormal cell division and proliferation, some genes are involved in their activities. These genes are mostly normal genes that became either ineffective (loss of their function) or over-expressed (gain of function).

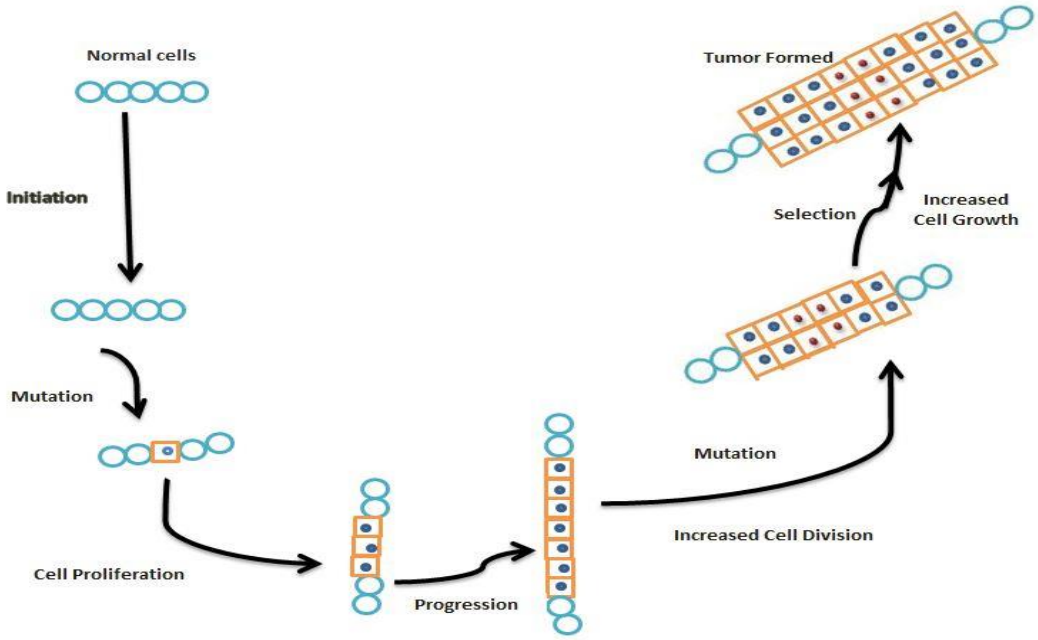

Figure 1.7: Stages of tumour cell development from a single mutated cell.

1.4.1 Some typical features of cancer cells

The framework of the human body is made up of billions of different kinds of cells. These cells can grow, divide normally and eventually form various tissues and organs in the body. The body system has its peculiar mechanism of removing worn out and dead cells through apoptosis (cell suicide or programmed cell death): a sensitive and well-controlled process that leads to the production of new cell components (Alberts *et al*., 2002; Elmore, 2007). To understand the biochemical processes involved in the development of a normal body cell into cancerous cells, some biochemical features of the cells which regulate their growth have to be

considered (DeVita and Chu, 2008). Tumours have multifaceted nature; these explain their ability to transform normal cells into tumour cells and give cancer cells some new abilities (Hanahan and Weinberg, 2000; 2011). These processes are commonly referred to as the hallmark of cancer and include sustenance of proliferative signalling, insensitivity to antigrowth signals, evading apoptosis, limitless replicative potential, sustained angiogenesis, genome instability, tissue invasion and metastasis.

1.4.1.1 Sustenance of proliferative signalling

Cancer cells can promote their growth continuously; they do not require signals from growth factors in the body before they grow and divide to sustain their continued proliferation. In the case of normal cells, growth factor signal like hormones is needed for cell division and in maintaining homeostasis in the number and function of these cells in their microenvironment. This process is closely controlled and well regulated. Most times in cancer cells, this process is disrupted and deregulated due to altered hormones controlling the process leading to disruption of homeostasis in the cell, resulting in an abnormal increase in cell division (Hanahan and Weinberg, 2000).

1.4.1.2 Insensitivity to antigrowth signals

Generally, in normal tissue, several anti-proliferative indicators function to keep cellular serenity and tissue homeostasis. These processes are controlled by tumour suppressor genes also known as anti-growth signals. These anti-growth signals prevent cell proliferation in two ways: firstly; by compulsorily stopping the active cell cycle division stage by taking it into an inactive state (G_0) to permit cell division when the cells are ready to divide. Secondly, the cells are caused to give up their ability to proliferate permanently by entering into the post-mitotic state (Hanahan and Weinberg, 2011). Tumour suppressor proteins in cancer cells are altered and damaged making them unable to control cell division when cells are deformed.

Contact inhibition is another way normal cells control cell growth. This is a kind of regulatory system which allows the cell to grow into a single layer thereby occupying its surrounding areas and eventually stops dividing when cells fill up the surrounding areas (Nelson and Chen, 2002). Cancerous cells lack these features of contact inhibition. Hence, they divide in a wild, unrestrained manner and continue to grow on each other, eventually causing invasion of the nearby surrounding, forming tumours in the process (McClatchey and Yap, 2012).

1.4.1.3 Evading apoptosis

Apoptosis is a type of cell death that plays a significant role in the removal of dead cells that are damaged and dysfunctional in the body (Vo and Leta, 2010). It is a well-organised process whereby the genome of these dysfunctional cells are broken down to smaller pieces and then cleaned up by phagocytes. This process helps organisms to grow well and accurately maintain body tissues (Elmore, 2007). Cancer cells can avoid this process and evade this complex mechanism by increasing the rate of cell proliferation by slowing down the cell death process, thereby changing the mechanism which detects these anomalies and cause mutation in the proteins involved in apoptotic pathways (Elmore, 2007; Hanahan and Weinberg, 2000).

1.4.1.4 Limitless replicative potential

Cancer cells can undergo an uncontrolled multiplication in a limitless manner, unlike a typical cell with regulated cell division (Blagosklonny, 2003). This uncontrolled multiplicatio n-n of cells is due to the shortening of the telomeres in the DNA chromosomes with each cell division occurring until it becomes too short and then triggers the death of the cell. Cancer cells, on the other hand, skip this step in cell division by manipulating the telomerase

enzymes involved in cell division: thereby making the cells to divide and grow in an unrestrained manner (Greenberg, 2005; Hanahan and Weinberg, 2011).

1.4.1.5 Sustained angiogenesis

Angiogenesis is an essential process in development and growth. It is a process that involves the production of new blood vessels in the body. In normal body tissues, blood supply for cell functions are highly coordinated, but in cancer cells, this is not. Cancers can start the angiogenesis process, thereby making sure that the tumour cell repeatedly gets blood supply by interrupting the normal process (Cavallo *et al.,* 2011; Hanahan and Weinberg, 2011). Cancer cells survive and sustain themselves by continuous production of tumour blood vessels resulting in an accelerated metastasis through a process called "angiogenic switching" (Burri *et al*., 2004; Hanahan and Weinberg, 2000; Stegmann, 1998).

1.4.1.6 Genome instability

Tumour cells generally have a chromosomal deformity in their genome which increases as a tumour metastasises, and the disease develops. The microenvironment of the cancer cell is very important in tumour progression. Cancer cells cultivate a mechanism to escape controlled homeostatic pathways which is an integral part present in normal cells (Hanahan and Weinberg, 2011).

1.4.1.7 Tissue invasion and metastasis

Malignant tumours are very active cells. They left their site of origin to invade surrounding tissues and organs (metastasis) in the body. The process of invasion and metastasis is a very complex process. Tumour cells have to undergo multistep processes to invade their surrounding tissues. They achieve this by up-regulating mutated inactive E-cadherin and catenin gene responsible for the cell to cell adhesion (Hanahan and Weinberg, 2000; Hanahan and Weinberg 2011).

1.4.2 Cancer diagnosis and therapy

Cancer treatment depends on the diagnosis and stage of the disease. Cancer can be treated in various ways such as chemotherapy, surgery, radiation therapy, targeted therapy and hormonal therapy (Schaefer and Dieter, 2016). Most often than not, the choice of treatment depends on the stage of a tumour, the site or location of a tumour and the overall health status of the patient. Total elimination of cancer cells without causing damage to the surrounding organ or tissue in the system is often the main aim of cancer treatment. Removal of cancer tumours by surgery is effective if the cancer is detected early and the entire tissue removed before metastasis (National Cancer Institute, 2017); often, this is impossible. Examples of surgical removal are mastectomy and prostatectomy. More so, the use of drugs to cure cancer is known as chemotherapy. These drugs are cytotoxic anticancer drugs works by affecting the DNA of the rapidly dividing cells, but they can be non-specific. Thus they destroy some normal cells in the body. Chemotherapy drugs are used by combining two or more drugs.

Radiation therapy is a form of treatment that involves the use of x-ray to eradicate cancer cells or reduce the size of a tumour by destroying their genetic materials. During this treatment, some healthy cells are sometimes affected by the radiation, but they tend to recover with time. An approach in cancer treatment where the immune system is made to fight against a tumour is known as *immunotherapy* and remains a cancer treatment alternative. Moreso, some cancer cells that use hormones in the body to grow can be prevented from spreading and increasing by blocking or removing those hormones. Some breast and prostate cancers are treated through this process known as hormonal therapy. The change occurring in tumour microenvironments such as overexpression of proteins within a tumour are the target in targeted therapy. Monoclonal antibodies are used in targeted therapy, whereby an antibody binds to the surface of proteins found in a cancer cell, and this mechanism can then be employed as a form of therapy. Targeted therapy also involves the

use of peptides to bind cell surface receptors in the extracellular matrix of the tumour proteins leading to enhanced forms of targeted therapy (Hede and Huilgo, 2006). In recent times, nanoparticles have been used as they increase tumour specificity during treatment

1.5 Chlorotoxin (CTX): origin and biochemical components

Chlorotoxin (CTX) was first isolated as a bioactive peptide or neurotoxin obtained from the venom of scorpion of the family *Leiurus quinquestriatus* (El-Ghlban *et al.*, 2014; Sentissi and Jacoby, 2015; Wang *et al.,* 2014; Zhang *et al.,* 2014). CTX has a primary sequence made up of 36 amino acids, making it a 4 kDa peptide, maintained by four disulphide bonds, which stabilise the structure coordinating the eight cysteine residues present in the protein (Dardevet *et al.,* 2015). It was initially considered a ligand that blocks chloride channels in glioma cell migration, but that function was subsequently ascribed to CTX-mediated inhibition of MMP-2. Chlorotoxin binds mainly to tumour cells especially glioma cells and is also taken up by multiplying human vascular endothelial cells (El-Ghlban *et al.*, 2014; Zhang *et al.*, 2014). Aside from its compact structure, CTX has some unique characteristics that make it able to bind and diffuse through a tumour to be able to shrink tumour cells. (Mamelak and Jacoby, 2007; Veiseh *et al.*, 2007).

CTX as a venom causes paralysis in small insects with no toxic effect on vertebrates or any undesirable physiological significance (Dardevet *et al.,* 2015). Studies have also shown that CTX conjugates have been used to detect tumours and locate tumour microenvironments, e.g. in cutaneous cell carcinoma and breast cancer (Sentissi *et al.*, 2015; Zhang *et al.,* 2014). Recently, *in vitro* and *in vivo* tumour-targeting ability of CTX when conjugated with fluorescently-labelled Cy5.5 dye, nanoparticles and polymers have been documented (El-Ghlban *et al.,* 2014; Kittle *et al.,* 2014; Sun *et al.,* 2015; Veiseh *et al.,* 2007). Structurally, CTX is made up of an alpha-helix linked by three disulphide bridges to a small three-stranded antiparallel beta-sheet and fourth disulphide bridge linked with N-terminal cysteine to the rest

of the molecule (see figure 1.8) (Stroud *et al.*, 2011). The cysteine pattern in CTX is of the type C1–C4, C2–C6, C3–C7 and C5–C8 and its three small antiparallel β-sheets arranged against an α-helix (Dardevet *et al*., 2015).

Figure 1.8: An Amino acid sequence of CTX.
(Taken from Dardevet *et al.*, 2015)

This primary sequence shows eight cysteine residues and the four-disulphide bridge in orange colour.

1.5.1 Mode of action of CTX in tumour cells

Ion channels are essential in cell volume regulation because cells move when ions and water flow. They are also crucial for cell migration because they regulate the intracellular Ca^{2+} concentration (Schwab *et al.*, 2007). Movement or invasion of tumour cells is influenced by the activity of a Cl^- channel that is activated by cell swelling. Inhibition of these channels, possibly by ClC_3, slows down migration and invasion of tumour cells (Schwab *et al.*, 2007). Chlorotoxin was found to block chloride channel of tumour cells especially glioma cells and cancer of the brain in a dose-dependent concentration and preferentially at the positive potentials in an irreversible manner (Dalton *et al.*, 2003) hence, the name chloride-channel toxin (Lewis and Garcia, 2003) and it is an up-regulated membrane protein seen in diverse types of cancers. CTX binds to a specific Ca^{2+} activated chloride channels (Dalton *et al*., 2003) and other tumours hence; it may be a potential tool in anti-cancer treatment (Lewis and Garcia, 2003).

Stoud and co-workers (2011) proposed that the binding of chlorotoxin to cell surface receptors lead to internalisation of the entire lipid raft-anchored complex enclosing MMP-2, MT1-MMP, TIMP-2 chloride channels and other proteins expressed in tumour cells, thereby eliminating the working chloride ion channel. MMP-2 was also shown as the significant CTX receptor on the surface of glioma cells in an experiment whereby a recombinant His-CTX was used to identify and isolate the proteinase (Deshane *et al*., 2003). Furthermore, Deshane and colleagues (2003) showed chlorotoxin have dual effects MMP-2 activity; hindering enzyme activity and reducing cell surface expression of the enzyme in glioma and tumour tissues that expresses MMP-2, making CTX a specific MMP-2 inhibitor. The interaction between CTX and MMP-2 gives it the ability to stop the invasion of glioma cells (Deshane *et al*., 2003).

1.5.2 MMP-2 and chlorotoxin interaction as a diagnostic tool

The MMP2-CTX interaction was initially carried out in glioma cells using a synthetic CTX TM601. In this study, annexin A_2 was identified as the molecular target of CTX because it binds to the glioma cells *in-vitro*, thereby inhibiting their migration (Kesaran *et al.,* 2010). After that, Veiseh and colleagues (2007) also explored the CTX-MMP-2 interaction in diagnostics, where they developed a tumour paint. The tumour paint Cy5.5-CTX was used to a labelled tumour using a dye enabling surgeons to image cancer cells when carrying out surgery. Mamelak and colleague developed Iodine-131-TM-601(131I-TM-601) in 2006 for the treatment of glioma in about 18 adults, and the results showed that it was well tolerated. Jacoby and colleagues (2010) used TM601; a chemically synthesised CTX for tumour targeting. The peptide was used in the study for the angiogenic study, and it was found to bind multiplying vascular endothelial cells, reduced human umbilical vein endothelial cells (HUVEC) invasion and reduced MMP-2 level secretion. The expression of MMP-2 makes CTX a viable tool for bio-imaging and diagnostics, and this can be applied in both cancer

cells and any disease where MMP-2 expresses. Nanoparticles can be conjugated to CTX and used for diagnostics, gene and drug delivery purposes (Lee *et al.,* 2010; Veiseh *et al.,* 2011)

1.6 Gum Arabic

Gum Arabic (GA) is a leguminous tree plant that is well adapted to Sudan and sub-Saharan Africa agro-ecology (Fig1.8). About 300 species of this family exist, prominent among which is *A. senegal* used in the production of quality Gum Arabic *(*Mokwunye and Aghughu, 2010). In Nigeria and Sudan, *A. senegal* is quite abundant, while in Kenya and Senegal *A. karensis* exists. South Africa and Zimbabwe have abundant *A. rostrata* while *A. leirhochis* found in other African countries (Aghughu and Ojiekpon, 1996; Wickenss, 1995). Morphologically, GA is a dried exudate obtained from the stems and branches of *A. senegal* or *Acacia seyal* when the plant is injured, or when the injury is planned and controlled (Mokwunye and Aghughu, 2010). The injury on the plant when planned and controlled is known as tapping (Mokwunye and Aghughu, 2010).

GA is a pale white to orange-brown solid that breaks with a smooth fracture Fig (1.9). Good quality gum grades exist as spheroidal tears of varying sizes with a matt outward texture. In powdered form, the pieces are paler and have a glassy appearance. GA from *A. seyal* is more brittle than the hard tears obtained from *A. senegal*. It is also obtainable in large scale in the form of white to yellowish-white flakes, granules, powder, kibbled or spray-dried and agglomerated (soluble form) (Al Assaf *et al*., 2005). Structurally, GA is a complex polysaccharide made up of highly branched molecules which on hydrolysis yield neutral (galactose, arabinose, and rhamnose) and acidic monosaccharides (glucuronic acid), low and high molecular weight protein fractions, with some calcium, magnesium and potassium salts (Ali *et al.*, 2009; Cornelsen *et al.,* 2015; Grein *et al.*, 2013; Tischer *et al* ., 2002; Williams

and Phillips, 2000).

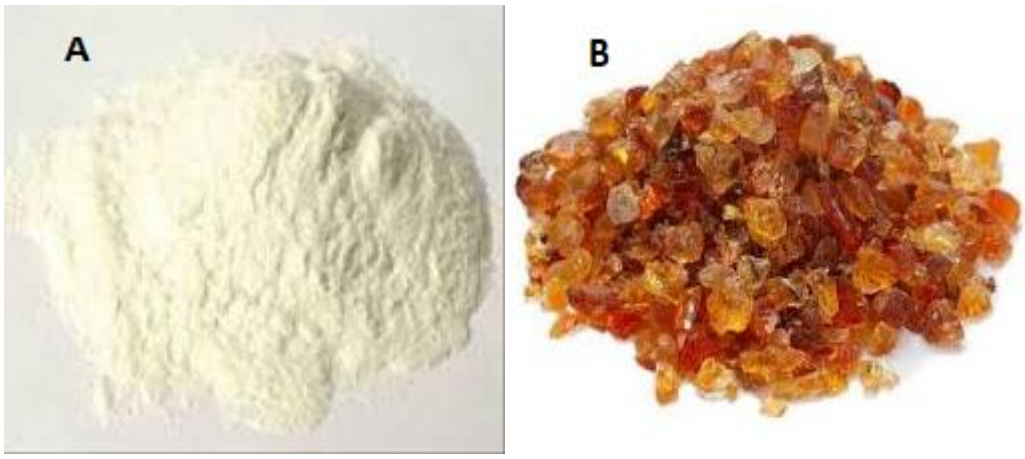

Figure 1.9: (A) Purified powder of Gum Arabic (B) Raw Gum Arabic freshly harvested from the tree.
Modified from Azzaoui et al., 2015

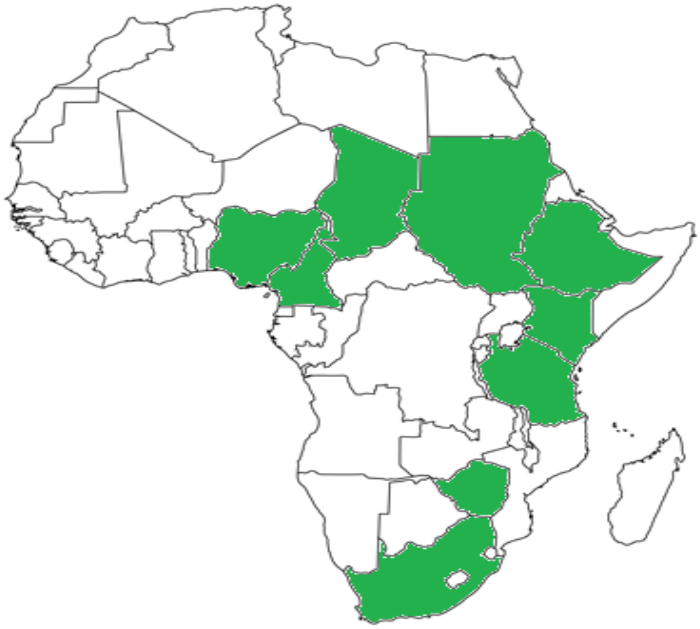

Figure 1.10: Map of Africa showing the significant Gum Arabic producing countries.
The green coloured areas on the map are the main Gum Arabic producing countries in Africa.

Apart from the ecological function which include; nourishing the soil by fixing nitrogen, and restoring fertility, giving shelter and shade to farmers and animals, wind erosion control, the

woods used as fuel (Eisa *et al*., 2008; Wekesa *et al.,* 2010; Koli *et al.,* 2013), GA performs, it is the economic live wire of some African countries such as Sudan and lately Chad. Africa supplies over 98 % of the world gum Arabic requirements with Sudan being the largest producer (Yasseen *et al*., 2014). The chemical content of GA is slightly controlled by its origin, climate, harvest season, tree age and processing methods (Al Assaf *et al.* 2005; Hassan *et al.,* 2005). It is very soluble in water and has unique features which include a high degree of branching, high protein and uronic acids content. GA is a compound with both hydrophilic and hydrophobic properties, with the functional properties, are strictly related to the structural make-up; this defines its solubility, viscosity, the degree of interaction with water and oil in an emulsion and its microencapsulation ability (Montenegro *et al.*, 2012).

1.6.1 Chemical Composition of GA

Gum Arabic (GA) is a polymer consisting of arabinogalactan-protein (AGP) complex and minor glycoprotein fractions (Dror *et al.*, 2006; Rao *et al*., 2010; Renard *et al*., 2006). This complex consists of 88% carbohydrates with D-galactose and L-arabinose as its main components with a little fraction of glucuronic acid (Montenegro *et al.,* 2012; Sanchez *et al.*, 2018) and the minor glycoprotein fractions which are about 10% and it has the highest protein fraction in GA.

1.6.2 Uses of Gum Arabic

Due to its unique characteristic, GA is made use of in the textile, ceramic, lithographic, pharmaceutical and food industries (Al-Assaf *et al.,* 2006; Montenegro *et al.*, 2012, Sanchez *et al.*, 2017). In the food industries, it is used to delay sugar crystallisation during baking and in the enhancement of wheat and rye flour. GA is similarly used in the production of chocolates and chewing gum, it acts as a stabiliser in the production of dairy products such as ice cream, as an emulsifier in beverage production, as well as a clarifying agent during winemaking (Sanchez *et al.*, 2017; Verbeken *et al.*, 2003). GA is also used as

microencapsulation (microencapsulation is the use of a substance to prevent loss and undesirable changes), to prevent food oxidation in food because of the unpredictability of food flown in the presence of oxygen, light and water (Kaushik and Roos, 2007; Sheu and Rosenberg, 1995). Microencapsulation is very vital in food and flavouring industries enhancing the biochemical stability of food flavourings (Yoshii *et al.*, 2001). These functions, are closely linked to the biological characteristics of GA such as solubility in water, active surface properties, and low viscosity in solutions when the concentration of the solids are very high (Barbosa *et al.*, 2005; Kenyon, 1995; Ortiz *et al.*, 2010).

In the pharmaceutical industries, it is used as a carrier in the drug preparations because due to its safety (Montenegro *et al.*, 2012). It has antioxidant properties (Ali *et al.*, 2009; Hinson *et al.*, 2004; Trommer and Neubert, 2005), functions in the breakdown of lipids (Tiss *et al.*, 2001), showing pronounced effects in the treatments of some degenerative diseases (multiple sclerosis, dementia), kidney failure (Ali *et al.*, 2009; Matsumoto *et al.*, 2006), cardiovascular disease (Glover *et al.*, 2009) and gastrointestinal disease (Rehman *et al.*, 2003). The sap of GA is known to be very rich in dietary fibre, hence can be used as a laxative to improve the digestive system. It is commonly used in the treatment of stomach and intestinal problems, sore throats, bleeding and the common cold. Furthermore, GA has been shown to inhibit the growth activity of some bacteria that cause tooth decay such as *Prophyromonas gingivalis* and *Prevotella intermedia* (Clark *et al.*, 1993). Which implies that GA can stop the formation of dental caries and can act as a possible preventive agent in their formation due to the high content of Ca^{2+}, Mg^{2+} and K^{+} found in this polysaccharide (Onishi *et al.*, 2008). Above all, GA contains enzymes like oxidase, peroxidases and pectinases which have been shown to exhibit antimicrobial activities (Montenegro *et al.*, 2012). Antimicrobial studies have shown that hydrophilic compounds like polyphenols, polysaccharides and tannins were found to be present in the methanol extracts of *A. catechu* and *A. nilotica*, showing maximum

antimicrobial activities. Similarly, hexane extract of the bark of *A. Senegal* showed antimicrobial activity against *S. aureus* and the fungus *C. albicans*, while the methanol extract exhibited antimicrobial activity against *E. coli, B. cereus*, *C. albicans* and *A. niger* (Montenegro *et al.*, 2012; Saini *et al.*, 2008). Antimicrobial activity of GA was assessed against food spoilage bacteria such as *Bacillus subtilis, Micrococcus luteus* and *P. aeruginosa* with results indicating a protective effect on *P. aeruginosa* but no effect on *Bacillus subtilis and Micrococcus luteus* though they reduced the growth of these bacteria (Ferreira *et al*., 2004).

1.6.3 Gum Arabic as a Nanovector

Acacia senegal gum is a natural polymer, non- toxic and an environmentally safe polymer with carboxylate and amine functional groups (Fig 1.10) (Banerjee and Chen, 2007). The challenges facing cancer chemotherapeutics like poor physicochemical properties of drugs, low tumour specificity, insufficient tumour cell internalization, various side effects of cancer drugs and low survival rate have led to the development of drug-delivery particles (Zhu *et al*., 2013), which may involve the use of proteins, peptides or chemical to detect, prevent metastasis or treat cancers (Dardevet *et al.*, 2011). Drug carriage systems are continually being improved to enhance pharmacological uses of dispensed drugs concerning therapeutics (Allen and Cullis, 2004). The benefit of nanostructured materials in biomedicine has been gaining world-wide interest, particularly in their use in selective delivery of drugs or molecules to target tissues and organs, bio-sensing and bio-imaging, optical spectroscopy including surface-enhanced Raman scattering (SERS) (Mochochoko *et al*., 2013).

Nanoparticles can enter tiny capillaries and pass through biological membranes (Ferreira *et al.*, 2015). These Nano-constructs must be large enough to consist of all the requirements for the evasion of body defences and still maintain its small size not to create undesired

obstructions to the smallest blood vessels in the body (Ferrari, 2005). A good nanovector system has the following unique features: ability to detect target cells and tissues, ability to reach disease site where target cells and tissue are located and ability of the drug to deliver multiple therapeutic agents because most cancer drugs involve the use of more than one drug due to the nature of cancer cells (Ferrari, 2005). Previously, lipid-based nanovectors like liposomes were widely used for their biological properties which include biocompatibility, biodegradability and isolation of drugs from the immediate environment. However, these nanovectors had many limitations like excessive long half life of the liposomes, wrong delivery of drugs to undesired cells and tissues. Recently, these undesirable effects have brought about the use of plant sources for nanoparticle synthesis a process called biogenic synthesis, which includes the use of whole plants, plant tissues, fruits and plant extracts (Mittal *et al.,* 2013). While considering the synthesis of plant nanoparticles, its biocompatibility is an essential parameter for biomedical applications. Synthesising biocompatible plant nanoparticles from non-toxic, cost-effective and effortlessly accessible materials with these qualities will be of significant advantage.

Various studies have shown the successful production of nanoparticles from plant sources (Ahmmad *et al.*,2013; Awwad *et al.,* 2013; Chanda *et al.*, 2010; Mochochoko *et al.,* 2013; Ortega-Arroyo *et al.*, 2013; Singh *et al.,* 2010). Hence, solubility, high binding affinity, easy functionality, good permeability, controlled pharmacokinetics and ability to protect and preserve the drug are qualities to be considered.

The use of gum Arabic is of significant advantage in nanoparticle synthesis than materials from synthetic sources (Sharma *et al.*, 2014). Collection and arrangement of specific materials exhibiting these novel characteristics can bring about cheap nanoparticle production

with useful biomedical properties. GA possess unique physicochemical qualities for it to be used in nanoparticles synthesis; these are as follows:

GA has high amino acid content, which makes it very soluble in water. It has been shown that the presence of amino acids with the peptide bond in a nanovector makes it very soluble in water (Dieckman *et al.*, 2003). GA has a high molecular weight (figure 1.11). Nanovector with high molecular weights gives good suspendability, i.e. steric stabilisation is increased by the full surface area covered by the drug that is incorporated into this vector. This characteristic protects the drug from deactivation during handling and long-term storage (Klummp *et al.*, 2006; Mayer and Mark, 1998).

More so, Chanda and colleagues (2010) in their studies showed that GA could be used in nanoparticles synthesis. Gold functionalized GA nanoparticles (radioactive GA_{198}) dispensed in Severe Combined Immune deficiency (SCID) mice bearing human prostate tumour xenografts was shown after a few weeks to have 80% reduction in tumour size and a minimal leakage of radioactive materials in the surrounding organs, and high tolerance of the nanoparticles in the blood of the treated mice. Furthermore, this study showed the GA-synthesized gold nanoparticle-delivered the drug to target tumour cells *in-vivo* with no toxicity and with high therapeutic efficiency. Kattumuri and co-workers (2007) in an *in-vivo* and *in-vitro* study used GA-functionalized and gold nanoparticles to target three different markers. These markers are known to be highly expressed in cancer cells: matrix metalloproteinases (MMPs), epidermal growth factors receptors (EGFR) and oncoproteins found in human papillomavirus (HPV). They concluded that the specifically targeted tumour cells showed a drastic reduction and complete eradication in some others. Also their results showed that intravenous administration was uniform in the organs of the animals used in the experiment (Kattumuri *et al*., 2007).

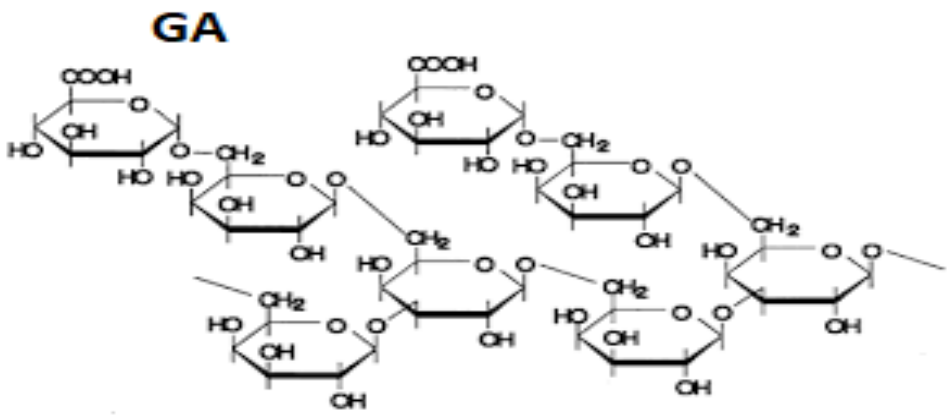

Figure 1.11: Structure of Gum Arabic.
(Modified from the book and paper group, Volume 10, American Institute for Conservation. Accessed December 2018. https://cool.conservation us.org/coolaic/sg/bpg/annual/v10/bp10-02.html

1.7 Nanotechnology

Nanotechnology in the last decade has been considered as one of the most vital developments in the field of science and technology (Banerjee and Chen, 2007). It is an interdisciplinary technology with high potentials for healthcare usage, with the field encouraging knowledge from another field of sciences such as chemistry, biology, engineering, physics and medicine. (Zhang *et al.,* 2004). These central materials in this field are nanoparticles, which are particles between 10-100nm in size with distinct properties like such as unique small sizes, morphology and distribution (Veerasamy *et al.*, 2011; Banerjee and Chen, 2007; Zargar *et al*., 2011). These particles also possess properties enhancing their applicability such as optical and magnetic properties, high surface-area-to-volume and electrical properties, among others (Gleiter, 2000).

1.7.1 Application of Nanotechnology

Current development in nanotechnology has established that nanoparticles have gained remarkable potential as drug carriers making them gain a wide range of biomedical applications, hence through bio-conjugation, nanoparticles are to be able to deliver a better

health care system and more effective diagnostic therapy (Agasti *et al.*, 2010). For examples, nanoparticles synthesised from plants can employed in the identification of proteins and nucleic acids expressed in disease conditions at early stages. More so, through nanotechnology, the major drawback in drug applications and early detection of diseases such as reduced toxicity, drug dosage, increase solubility, targeting ability and better drug specificity have been achieved. Nanotechnology has also brought about the development of fluorescent materials for molecular research (Bhatia, 2016).

1.7.2 Types of Nanoparticles

Nanoparticles can be broadly grouped into, one-dimensional nanoparticle, which includes biological sensors, optical devices and chemical sensors; while 2D nanoparticles include carbon nanotubes and three-dimensional nanoparticles; which are made up of dendrimers, quantum dots and others (Bhatia, 2016; Hett, 2004). Nanoparticles can also be classified based on their characteristics and functions.

1.8 Quantum Dots (QDs)

Quantum dots (QDs) are semiconductor nanocrystals of about two to10 nm in size made up of an inner metal core and a shell (Nguyen *et al.*, 2013; Bruchez *et al*., 1998). These molecules have quantum effects associated with the size of the QDs, i.e. smaller size particles have shorter wavelengths, while larger particles have larger wavelengths (Alivisatos *et al.*, 2005 and Kawasaki *et al.*, 2005). QDs are synthesised from group II-IV and III-V elements in the periodic table (Chan *et al*., 2002) and are mainly explored for their fluorescent properties over other organic materials for diagnostic and clinical uses (Hezinger *et al*., 2008; Jaiswal and Simon, 2004; Rodriguez-Fragoso *et al*., 2014).

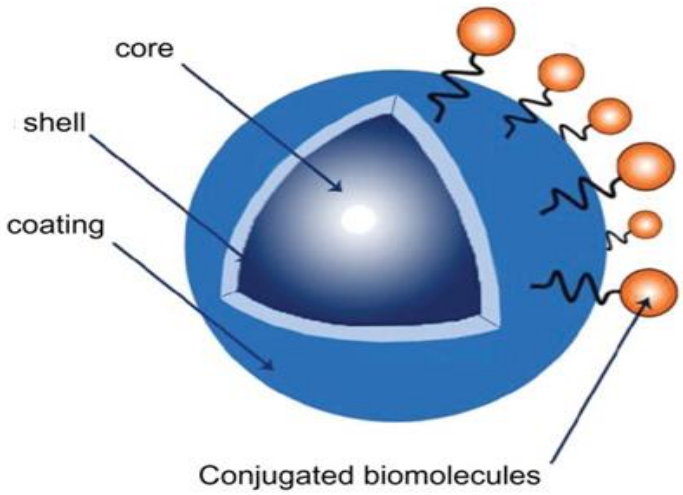

Figure 1.12: Structure of Quantum dots.
(Modified from Madani *et al.*, 2013).

1.8.1 Characteristics of Quantum Dots

Structurally, QDs comprise of a metalloid core and a 'cap/shell' that protects the core, which is mainly made of metal complexes such as semiconductors, noble metals and magnetic transition metals (Kim *et al*., 2010). QDs have a wide range of optical properties when compared to other organic fluorophores. They are about 10- 20 times brighter than other organic dyes (Gao *et al.,* 2005), have very broad excitation spectra with a distinct narrow peak giving them a brighter emission property and a higher signal to noise ratio, thereby reducing autofluorescence (the difference between emission and absorption peaks) (Fu *et al.*, 2012). QDs are very stable because of their composition preventing photobleaching in the process, (Alivisatos *et al.*, 2005; Chan *et al.,* 2002) and this stability grants their usefulness for the thick specimen is *in vivo* imaging and background-free imaging (Shin *et al.,* 2006). QDs have unique multi-coloured properties hence they can be unique when used as a probe to track the different number of targets *in-vivo* at the same time (Gao *et al.,* 2005; Chan *et al.*, 2002)

1.8.2 Uses of Quantum Dots

QDs can be manipulated for use in biological fluids or aqueous environment, by altering the chemical nature of their surfaces to affect solubility and by addition of specific chemical functionalities such as coating or capping to make them more water-soluble and to bio-functionalized them with biomolecules for targeting., polymeric coatings such as PEG has been used. Gum Arabic glycoprotein polymer can also be used (Hezinger *et al.*, 2008). More so, QDs can be targeted to specific biomolecules for promising applications in cellular labelling, deep-tissue imaging, assay labelling and as efficient fluorescence resonance energy transfer donors (Bottrill and Green, 2011; Medintz *et al.*, 2005) Fig1.13. More so, QDs are most times not affected by photo-bleaching, thus making long-term labelling and monitoring of live cells more practicable (Lovric *et al*., 2005). A summary of the uses of QDs is shown in Fig 1.13.

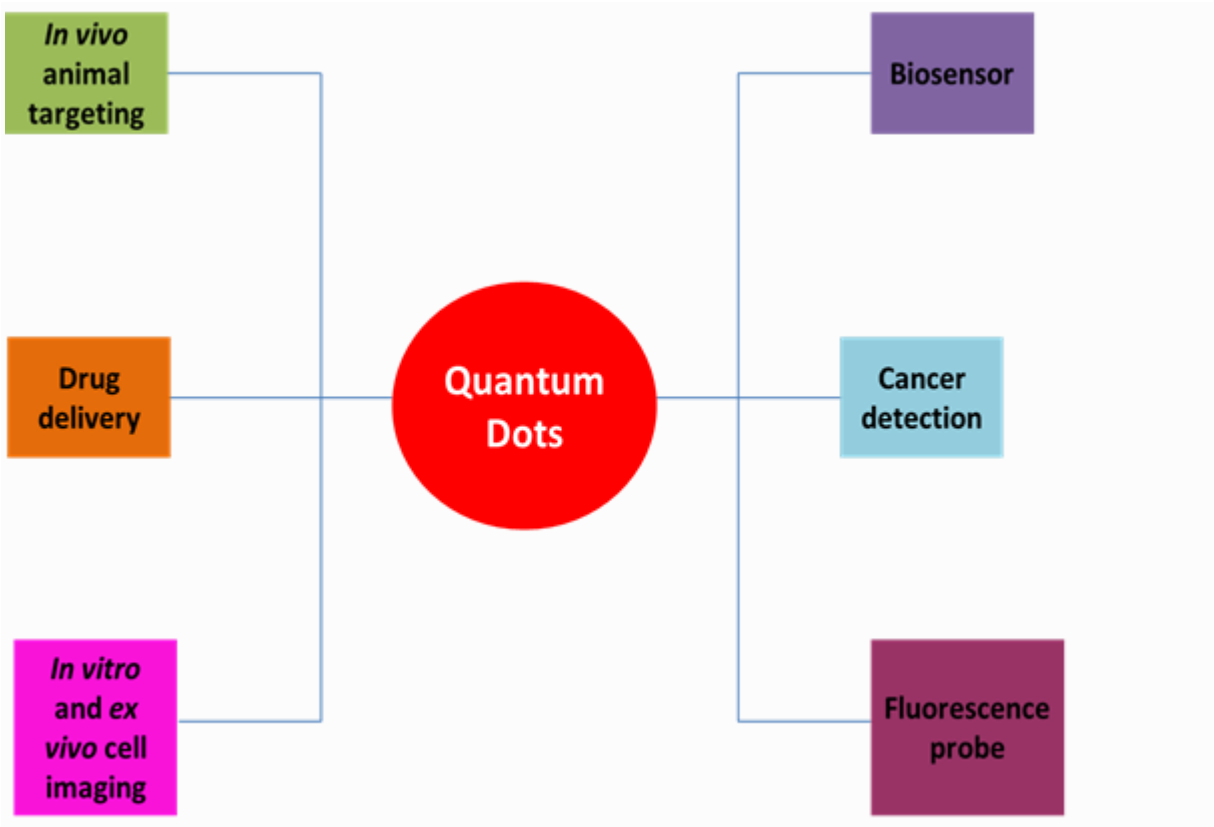

Figure 1.13: Diagram showing the different uses of quantum dots.

The various biomedical application of quantum dots in biotechnology field; they are used for delivery of drugs to many, early detection of cancer for bioimaging *in vivo* and *in vitro* as probe and biosensor.

1.8.3 Cadmium Telluride (CdTe) QDs

Amongst the different types of QDs, Cadmium Telluride (CdTe) QDs have found extensive use in biomedical and industrial purpose (Bao *et al.,* 2010). CdTe quantum dots are known to serve as a unique probe in bio-imaging of living cells because of their distinctive photoluminescence characteristics when excited, their photostability, well-regulated and narrow emission, as well as high quantum yield (Bao *et al*., 2010; Ma *et al.,* 2006; Nguyen *et al*., 2013). The method of synthesising and capping agent (CdTe) is fundamental as it determines its application in biological processes.

1.9 Cancer-specific peptide a promising agent for cancer diagnosis and therapeutics.

Evidence abounds on the usefulness of peptides as agents for cancer therapeutics and diagnosis (Reubi 2003; Xiao *et al*., 2015). These molecules comprise of amino acids connected with peptide bonds with sizes between 2-50 amino acids (Reubi 2003; Xiao *et al*., 2015). There are over 60 peptidic drugs currently on the market globally, and some of them are used directly for cancer therapeutic presently (Thayer, 2011) (Fig1.14). Peptides can exist both in the natural or synthesised form (Reubi, 2003; Iikuni *et al.*, 2009). In the past, monoclonal antibodies (mAbs) were used as targeting agents in cancer treatment, but studies have shown that peptides possess more advantages when compared to mAbs (Shadidi and Sioud, 2003). Some peptide have been discovered in the past few years for specific cancer cells as shown the Table 1.1 below

1.9.1 Peptide for Cancer diagnosis and Therapeutic

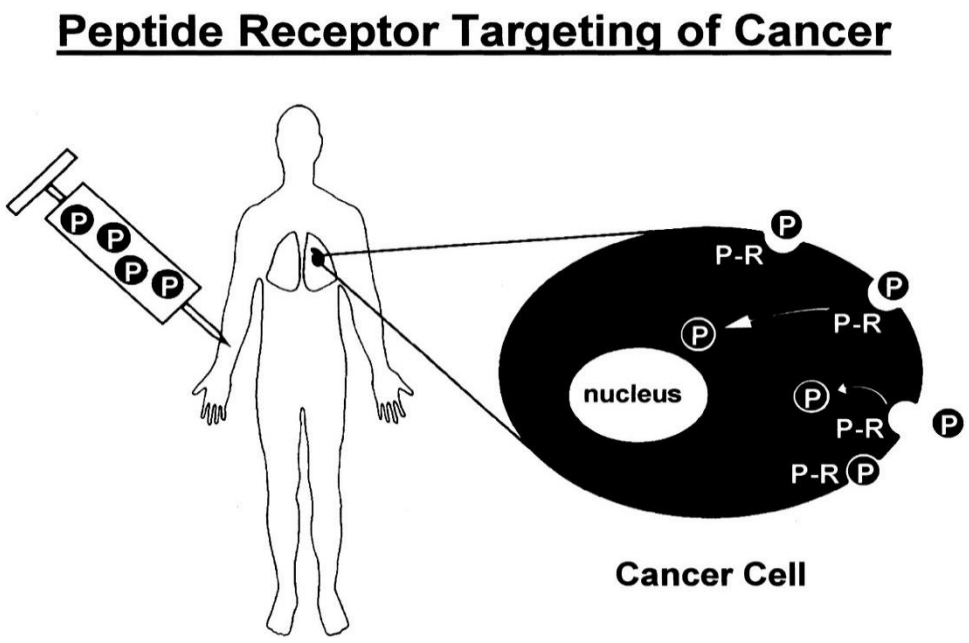

Figure 1.14: Principle of peptide receptor targeting of cancer.
(Taken and adopted from Reubi *et al.*, 2003).

Here, a tumour is expressing the peptide receptor, the peptide with conjugate nanomaterial then bind to it and internalise with the receptor into the cell. Whole body scan will detect the accumulation in a tumour, where it can be easily detected.

Table 1.1: Peptide applied in cancer diagnosis

Cancer	Peptide	Year	Author
Breast cancer	HER-2	2014	Boku *et al.*
	MUC1	2011	Zanetti *et al.*
Colorectal cancer	HNP1-3	2006	Albrethsen *et al.*
	CPAA-783-EPPT1	2012	Bloch *et al.*
	Serum C-peptide	2014	Comstock *et al.*
Gastric cancer	LGR5	2013	Zheng *et al.*
	PGI/II, CA242	2014	Lu *et al*
Pancreatic cancer	uMMP-2 and uTIMP-1	2014	Roy *et al.*
	MIC-1/GDF15	2014	Wang *et al.*
	RGS6	2014	Jiang *et al.*
Prostate cancer	EN2	2013	McGrath *et al.*
	UCP2	2013	Li *et al.*
Lung cancer	Linear peptide antigen derived from ANXA1	2014	Wang *et al.*
	HCBP-1	2014	Wang *et al*
	C-peptide in serum	2014	Zhang *et al.*

1.9 Cytotoxicity of QDs

Any cancer treatment efficacy is measured directly by its ability to decrease or totally eliminate tumour cells with little or no effect on the healthy cells (Byrne *et al*., 2008) and also

considering the unique fluorescent properties of QDs; a flow cytometer will be used *invitro* for cytotoxicity assay.

1.10 Flow Cytometry

The use of flow cytometry technology in biomedical research has increased in the past few years (Ibrahim and Engh, 2007). The technology measures the distinct characteristics of particles or cells in a fluid. The cells or particles are first labelled with fluorescent materials and then made passed through a beam of light in a single file (Brown and Wittwer, 2000; Edward *et al.,* 2004). The use of this instrument has increased notably in cancer research for cell sorting and diagnostics due to it's user-friendly and small sample size. Flow cytometry is a fast and convenient method of diagnosis because it is both a qualitative as well as a quantitative technique in biomedical research and it is also used clinical haematology.

1.11 Problem Statement

Cancer as a disease remains a global phenomenon affecting the population of all socio-economic groups, developing and developed countries. Prompt and accurate diagnosis is imperative for the proper management of the disease. The challenge is to identify specific molecules that can bind tumour cells for the early detection of the disease. Given this, scientists have resulted in the use of targeted therapy via the use of nanoparticles such as QDs conjugated peptide system, for bio-imaging for early detection of diseases. Hence, in this research studies, this has necessitated the need to synthesise and capped non-toxic QDs, bio-conjugate the QDs using nanobiotechnology with a peptide (CTX) for early detection of disease and therapeutics. CTX is a protein gotten from the venom of scorpion has emerged one of the promising targeting agents because it can bind specifically to MMP-2 protein expressed in a tumour cell, for the bio-imaging for early detection of cancer cells. Thus; it increases the chances of survival of cancer patients and serves as a point-of-care diagnostics for cancer treatment; as early diagnosis is the primary key to surviving the disease.

1.12 Aim and Objective of the Study

The primary aim of this study is to synthesise, cadmium telluride quantum dots using Gum Arabic polymer and bio-conjugate the QDs with chlorotoxin peptide for cancer bioimaging purpose.

The Research objectives include;

1. To synthesise of water-soluble cadmium telluride quantum dots (CdTe) capped with Gum Arabic polymer, biophysically characterise these Quantum Dots using various techniques and determine their stability in different Media.
2. To determine the toxicity of these Quantum Dots using WST-1 cell viability studies and using a flow cytometer assay to determine quantum dots uptake of cells.
3. To determine cell binding studies using different forms chlorotoxin protein ;
    i. Different chlorotoxin peptide labelled with FITC N and C-terminal
    ii. Protein expression (His-CTX-Gst), purification and sequencing CTX
    iii. Blocking studies using purified CTX and FITC labelled the peptide
    iv. Immunocytochemistry studies of Protein.
    v. Bio-conjugation and uptake Studies of QDs and CTX protein.

1.13 References

Agasti S.S., Rana S., Park M., Kim C.K., You C. and Rotello V.M. (2010). Nanoparticles for detection and diagnosis. *Advanced Drug Delivery Reviews* **62**(3): 316–328.

Aghughu O. and Ojiekpon I.F. Status of gum Arabic production in Nigeria. A paper presented at an international seminar/conference on the export, marketing and quality control of gum Arabic, Lagos, Nigeria, 27 – 29 November, 1996.

Ahmmad, B., Leonard, K., Islam, M. S., Kurawaki, J., Muruganandham, M., Ohkubo, T and Kuroda Y. (2013). Green synthesis of mesoporous hematite (α-Fe 2 O 3) nanoparticles and their photocatalytic activity. *Advanced Powder Technology* **24**(1), 160-167.

Al-Assaf S., Phillips G.O. and Williams P.A. (2005). Studies on acacia exudate gums. Part I: the molecular weight of Acacia senegal gum exudate. *Food Hydrocolloids* **19**(4): 647–660.

Alberts B., Johnson A., Lewis J., Raff M., Roberts K and Walter P. (2002). Extracellular control of cell division, cell growth, and apoptosis.

Albrethsen J., Moller C.H., Olsen J., Raskov H. and Gammeltoft S. (2006). Human neutrophil peptides 1, 2 and 3 are biochemical markers for metastatic colorectal cancer. *European Journal of Cancer* **42**(17): 3057-3064.

Ali B.H. (2004). Does gum Arabic have an antioxidant action in rat kidney? *Renal Failure* **26**(1): 1-3.

Ali B.H., Ziada A. and Blunden G. (2009). Biological effects of gum arabic: a review of some Recent Research. *Food and Chemical Toxicology* **47**(1): 1–8.

Allen T.M. and Cullis P.R. (2004). Drug delivery systems: entering the mainstream. *Science* **303**: 1818–1822.

Alivisatos A. P., Gu W. and Larabell C. (2005). Quantum dots as cellular probes. *Annual Review of Biomedical Engineering* **7:** 55-76.

Amălinei C., Căruntu I. D. and Bălan, R. A. (2007). Biology of metalloproteinase. *Romanian Journal of Morphology and Embryology* **48**(4): 323-334.

Anand P., Kunnumakara A. B., Sundaram C., Harikumar K. B., Tharakan S. T., Lai O. S., and Aggarwal B. B. (2008). Cancer is a preventable disease that requires major lifestyle changes. *Pharmaceutical Research* **25**(9): 2097-2116.

Arvizo R., Bhattacharya R. and Mukherjee P. (2010). Gold nanoparticles: opportunities and challenges in nanomedicine. *Expert Opinion on Drug Delivery* **7**(6): 753-763.

Arzamasov A.A., Vassilevski A.A. and Grishin E.V. (2014). Chlorotoxin and related peptides: Short insect toxins from scorpion venom. *Russian Journal of Bioorganic Chemistry* **40**(4): 359–369.

Awwad A. M., Salem N. M. and Abdeen A. O. (2013). Green synthesis of silver nanoparticles using carob leaf extract and its antibacterial activity. *International Journal of Industrial Chemistry* **4**(1): 29

Azzaoui K., Hammouti B., Lamhamdi A., Mejdoubi E. and Berrabah M. (2015). The Gum Arabic in the southern region of Morocco. *Moroccan Journal of Chemistry* ***3***(1): 3-1.

Banerjee S. S. and Chen D. H. (2007). Fast removal of copper ions by gum Arabic modified magnetic nano-adsorbent. *Journal of Hazardous Materials* **147**(3): 792-799.

Bao H., Hao N., Yang Y. and Zhao D. (2010). Biosynthesis of biocompatible cadmium telluride quantum dots using yeast cells. *Nano Research*. **3**(7): 481-489.

Barbosa M.I., Borsarelli C.D. and Mercadante A.Z. (2005). Light Stability of Spray-Dried Bixin Encapsulated with Different Edible Polysaccharide Preparations. *Food Research International* **38**(8-9): 989–994.

Bhandari G. P., Angdembe M. R., Dhimal M., Neupane S. and Bhusal C. (2014). State of non-communicable diseases in Nepal. *BMC Public Health* **14**(1): 23.

Bhatia S. (2016). Nanoparticles Types, Classification, Characterization, Fabrication Methods and Drug Delivery Applications. In *Natural Polymer Drug Delivery Systems* **2**:33-93.

Björklund M. and Koivunen E. (2005). Gelatinase-mediated migration and invasion of cancer cells. *Biochimica et Biophysica Acta (BBA)-Reviews on Cancer* **1755**(1): 37-69.

Blagosklonny M.V (2003). Cell immortality and hallmarks of cancer. *Cell Cycle* **2**(4): 295-298.

Bloch M., Kam Y., Yavin E., Moradov D., Nissan A., Ariel I. and Rubinstein A. (2012). The relative roles of charge and a recognition peptide in luminal targeting of colorectal cancer by fluorescent polyacrylamide. *European Journal of Pharmaceutical Sciences* **47**(5): 904-913.

Bonnans C., Chou J. and Werb Z. (2014). Remodelling the extracellular matrix in development and disease. *Nature Reviews Molecular Cell Biology* **15**(12): 786–801.

Bottrill M., and Green M. (2011). Some aspects of quantum dot toxicity. *Chemical Communications* **47**(25): 7039-7050.

Boku N. (2014). HER2-positive gastric cancer. *Gastric Cancer* **17**(1): 1-12.

Brown M. and Wittwer C. (2000). Flow cytometry: principles and clinical applications in haematology. *Clinical Chemistry* **46**(8): 1221-1229.

Brinckerhoff C. E. and Matrisian L. M. (2002). Matrix Metalloproteinase: a tail of a frog that became a prince. *Nature Reviews Molecular Cell Biology* **3**(3): 207-214.

Bruchez M., Moronne M., Gin P., Weiss S. and Alivisatos A. P. (1998). Semiconductor nanocrystals as fluorescent biological labels. *Science* **281**(5385): 2013-2016.

Byrne J. D., Betancourt T. and Brannon-Peppas L. (2008). Active targeting schemes for nanoparticle systems in cancer therapeutics. *Advanced drug delivery reviews* **60**(15):1615-1626.

Burri P.H., Hlushchuk R. and Djonov V. (2004). Intussusceptive angiogenesis: its emergence, its characteristics, and its significance. *Developmental Dynamics* **231**(3): 474-488.

Cancer Reasearch, U K (2014). *Worldwide Cancer*. http://www.cancerresearchuk.org/health-professional/cancer-statistics/worldwide-cancer/incidence (Accessed 2 May, 2016).

Cancer Association of South Africa and the NCR report, 2011, CANSA (https://www.cansa.org.za/south-african-cancer-statistics)(Accessed January, 2018)

Cattell M.A., Anderson J.C. and Hasleton P. S. (1996). Age-related changes in amounts and concentrations of collagen and elastin in normotensive human thoracic aorta. *Clinica Chimica. Acta* **245**(1): 73–84.

Cavallo F., De Giovanni C., Nanni P., Forni G. and Lollini P.L. (2011). The immune hallmarks of cancer. *Cancer Immunology, Immunotherapy* **60**(3): 319-326.

Chan W.C., Maxwell D.J., Gao X., Bailey R.E., Han M. and Nie S. (2002). Luminescent quantum dots for multiplexed biological detection and imaging. *Current Opinion in Biotechnology* **13**(1): 40-46.

Chanda N., Kan P., Watkinson L.D., Shukla R., Zambre A., Carmack T.L., Engelbrecht H., Lever J.R., Katti K., Fent G.M. and Casteel S.W., (2010). Radioactive gold

nanoparticles in cancer therapy: therapeutic efficacy studies of GA-198AuNP Nanoconstruct in prostate tumour–bearing mice. *Nanomedicine: Nanotechnology, Biology and Medicine* **6**(2): 201-209.

Chaudhary A.K., Singh M., Bharti A.C., Asotra K., Sundaram S. and Mehrotra R. (2010). Genetic polymorphisms of matrix metalloproteinases and their inhibitors in potentially malignant and malignant lesions of the head and neck. *Journal of biomedical science* **17**(1):10.

Cheresh D. A. and Stupack D. G. (2008). Regulation of angiogenesis: apoptotic cues from the ECM. *Oncogene*, **27**(48): 6285.

Chong K.P. (2004). Nanoscience and engineering in mechanics and materials. *Journal of Physics and Chemistry of Solids* **65**(8): 1501-1506

Clark D.T., Gazi M.I., Cox S.W., Eley B.M. and Tinsley G.F. (1993). The effects of Acacia arabica gum on the in vitro growth and protease activities of periodontopathic bacteria. *Journal of Clinical Periodontology* **20**(4): 238–43.

Colotta F., Allavena P., Sica A., Garlanda C. and Mantovani A. (2009). Cancer-related inflammation, the seventh hallmark of cancer: links to genetic instability. *Carcinogenesis* **30**(7): 1073–1081.

Cooper G.M. (2000). Development and causes of cancer. In *The Cell: A Molecular Approach. 2nd edition. Sunderland (MA):* Sinauer Associates, Sunderland(MA*).*

Cooper G.M. and Hausman R.E. (2000). Chapter 9: Protein Sorting and Transport, in the Cell: A Molecular Approach, Cooper, G.M., Editor. 2000, Sinauer Associates: Sunderland, USA

Comstock S.S., Xu D., Hortos K., Kovan B., McCaskey S., Pathak D. R. and Fenton J. I. (2014). Association of insulin-related serum factors with colorectal polyp number and type in adult males. *Cancer Epidemiology and Prevention Biomarkers* **23**(9):1843-1851.

Cornelsen P., Quintanilha R.C., Vidotti M., Gorin P.A.J., Simas-Tosin F.F. and Riegel-Vidotti I. C. (2015). Native and structurally modified gum arabic: exploring the effect of the gum´s microstructure in obtaining electroactive nanoparticles. *Artigo Submetido* 119: 35–43

Coussens L.M., Fingleton B. and Matrisian L.M. (2002). Matrix metalloproteinase inhibitors and cancer-trials and tribulations. *Science* **295**(5564): 2387-2392.

Cox T.R. and Erler J.T. (2011). Remodelling and homeostasis of the extracellular matrix: implications for fibrotic diseases and cancer. *Disease Models and Mechanisms* **4**(2): 165–178.

Dalton S., Gerzanich V., Chen M., Dong Y., Shuba Y. and Simard J.M. (2003). Chlorotoxin-sensitive Ca^{2+} activated Cl^{-} channel in type R2 reactive astrocytes from adult rat brain. *Glia* **42**(3): 325–339.

Daniel M.C. and Astruc D. (2004). Gold nanoparticles: assembly, supramolecular chemistry, quantum-size-related properties, and applications toward biology, catalysis, and nanotechnology. *Chemical Reviews* **104**(1): 293-346.

Dardevet L., Rani D., Aziz T.A.E., Bazin I., Sabatier J.M., Fadl M., Brambilla E. and De Waard M., (2015). Chlorotoxin: a helpful natural scorpion peptide to diagnose glioma and fight tumour invasion. *Toxins* **7**(4):1079-1101.

Deshane J., Garner C.C. and Sontheimer H. (2003). Chlorotoxin inhibits glioma cell invasion via matrix metalloproteinase-2. *Journal of Biological Chemistry* **278***(6)*: 4135–4144.

Devy L. and Dransfield D.T. (2011). New strategies for the next generation of matrix-metalloproteinase inhibitors: selectively targeting membrane-anchored MMPs with therapeutic antibodies. *Biochemistry Research International* 2011.

DeVita V.T. and Chu E. (2008). A history of cancer chemotherapy. *Cancer Research* **68**(21): 8643-8653.

Dhanaraj V., Williams M.G., Ye Q.Z., Molina F., Johnson L.L., Ortwine D.F. and Blundell, T.L. (1999). X-ray structure of gelatinase a catalytic domain complexed with a hydroxamate inhibitor. *Croatica Chemica Acta* **72**(2-3): 575–591.

Dror Y., Cohen Y. and Yerushalmi-Rozen R. (2006). Structure of gum arabic in aqueous solution. *Journal of Polymer Science Part B: Polymer Physics* **44**(22): 3265–3271.

Dubey M., Bhadauria S. and Kushwah B.S. (2009). Green Synthesis of Nanosilver Particles from Extract of Eucalyptus Hybrida (SAFEDA) Leaf. *Digest Journal of Nanomaterials and Biostructures* **4**(3): 537–543.

Edwards B.S., Oprea T., Prossnitz E. R. and Sklar L. A. (2004). Flow cytometry for high-throughput, high-content screening. *Current Opinion in Chemical Biology* **8**(4): 392-398.

Egeblad M. and Werb Z. (2002). New functions for the matrix metalloproteinases in cancer progression. *Nature Reviews Cancer* **2**(3): 161–174.

El-Ghlban S., Kasai T., Shigehiro T., Yin H.X., Sekhar S., Ida M. and Seno M. (2014). Chlorotoxin-Fc fusion inhibits release of MMP-2 from pancreatic cancer cells. *BioMed Research International* **2014**: 1–10.

Eisa M. A., Roth M., and Sama G. (2008). *Acacia senegal* (Gum Arabic tree): Present role and need for future conservation/Sudan. In *Deutscher Tropentag*. 1-5

Elmore S. (2007). Apoptosis: a review of programmed cell death. *Toxicologic Pathology* **35**(4): 495-516.

Erogbogbo F., Yong K.T., Roy I., Hu R., Law W.C., Zhao W., Ding H., Wu F., Kumar R., Swihart M.T. and Prasad P.N. (2010). In vivo targeted cancer imaging, sentinel lymph node mapping and multi-channel imaging with biocompatible silicon nanocrystals. *American Chemistry Society nanoletters*, **5**(1):413-423.

Esteves A.C.C. and Trindade T. (2002). Synthetic studies on II/VI semiconductor quantum dots. *Current Opinion in Solid State and Materials Science* **6**(4): 347-353.

Ferlay J., Soerjomataram I., Dikshit R., Eser S., Mathers C., Rebelo M., Parkin D.M., Forman D. and Bray F. (2015). Cancer incidence and mortality worldwide: Sources, methods and major patterns in GLOBOCAN 2012. *International Journal of Cancer* **136**(5): E359–E386

Ferreira I.C.F.R., Calhelha R.C., Estevinho L.M. and Queiroz M.J.R.P. (2004). Screening of antimicrobial activity of diarylamines in the 2,3,5-trimethylbenzo[b]thiophene series: a structure-activity evaluation study. *Bioorganic and Medicinal Chemistry Letters* **14**(23): 5831-5833.

Ferreira T.H., Rocca A., Marino A., Mattoli V., de Sousa E.M.B. and Ciofani G. (2015). Evaluation of the effects of boron nitride nanotubes functionalized with gum arabic on the differentiation of rat mesenchymal stem cells. *Royal Society of Chemistry Advance* **5**(56): 45431–45438.

Folgueras A.R., Pendás A.M., Sánchez L.M. and López-Otín C. (2004). Matrix metalloproteinases in cancer: From new functions to improved inhibition. *International Journal of Developmental Biology* **48**(5-6): 411–424.

Forouzanfar M.H., Afshin A., Alexander L.T., Anderson H.R., Bhutta Z.A., Biryukov S., Brauer M., Burnett R., Cercy K., Charlson F.J. and Cohen A.J. (2016). Global, regional, and national comparative risk assessment of 79 behavioural, environmental and occupational, and metabolic risks or clusters of risks, 1990–2015: a systematic analysis for the Global Burden of Disease Study 2015. *The Lancet* **388**(10053):1659-1724.

Frantz C., Stewart K.M., Weaver V.M., Frantz C., Stewart K.M. and Weaver V.M. (2010). The extracellular matrix at a glance. *Journal of Cell Biology* **123**:4195–4200.

Ferrari M. (2005). Nanovector therapeutics. *Current Opinion in Chemical Biology* **9**(4): 343–346.

Fu Y., An N., Li K., Zheng Y. and Liang A. (2012).Chlorotoxin-conjugated Nanoparticles as potential glioma-targeted drugs. *Journal of Neuro-Oncology* **107**(3): 457–62.

Gaddala B. and Nataru, S. (2015). Synthesis, characterisation and evaluation of silver nanoparticles through leaves of Abrus precatorius L.: an important medicinal plant. *Applied Nanoscience* **5**(1): 99-104.

Gao Y., Xie J., Chen H., Gu S., Zhao R., Shao J. and Jia L. (2014). Nanotechnology-based intelligent drug design for cancer metastasis treatment. *Biotechnology Advances* **32**(4): 761-777.

Ghafoor A, Jemal A, Ward E, Coskkinides V, Smith R.T.M. (2003). Trends in breast cancer by race and ethnicity. *CA: A Cancer Journal for Clinicians* **53**: 342–355.

Gialeli C., Theocharis A. D. and Karamanos N. K. (2011). Roles of matrix metalloproteinase in cancer progression and their pharmacological targeting. *FEBS Journal*. **278**(1):16-27.

Gleiter H. (2000). Nanostructured materials: basic concepts and microstructure. *Acta materialia* **48**(1): 1-29.

Greenberg, RA (2005). Telomeres, crisis and cancer. *Current Molecular Medicine*. **5** (2): 213–218.

Grein A., da Silva B.C., Wendel C.F.T., Ischer C.A., Sierakowski M.R., Moura A.B.D. and Riegel-Vidotti I.C. (2013). Structural characterisation and emulsifying properties of polysaccharides of Acacia mearnsii de Wild gum. *Carbohydrate Polymers* **92**(1): 312–320.

GLOBOCAN/World Health Organization (2012) Cancer facts sheets.

Glover D.A., Ushida K., Phillips A.O. and Riley S. G (2009). Acacia(sen) SUPERGUM^{TM} (Gum arabic): An evaluation of potential health benefits in human subjects. *Food Hydrocolloids* **23**(8): 2410–2415.

Gong Y., Chippada-Venkata U. D. and O, W. K. (2014). Roles of matrix metalloproteinases and their natural inhibitors in prostate cancer progression. *Cancers* ***6***(3): 1298-1327.

Hanahan D. and Weinberg R.A. (2000). The Hallmarks of Cancer Review University of California at San Francisco. *Cell* **100**: 57–70.

Hanahan D. and Weinberg R.A. (2011). Hallmarks of cancer: the next generation. *Cell* **144**(5): 646–674.

Hassan A.N, Awad S, and Muthukumarappan K. (2005). Effects of exopolysaccharide-producing cultures on the viscoelastic properties of reduced-fat Cheddar cheese. *Journal of dairy science* **88**(12): 4221-4227.

Hahn W.C., Dunn I.F., Kim S.Y., Schinzel A.C., Firestein R., Guney I. and Boehm J.S., (2009). Integrative genomic approaches to understanding cancer. *Biochimica et Biophysica Acta (BBA)-General Subjects* **1790**(6): 478-484.

Hashizume K. (2007). Analysis of uteroplacental-specific molecules and their functions during implantation and placentation in the bovine. *Molecular Reproduction and Development* **53**(1):1–11.

Hezinger A.F.E., Teßmar, J. and Göpferich A. (2008). Polymer coating of quantum dots–a powerful tool toward diagnostics and sensorics. *European Journal of Pharmaceutics and Biopharmaceutics* **68**(1): 138-152.

Hede S. and Huilgol N. (2006). "Nano" The new nemesis of cancer. *Journal of Cancer Research and Therapeutics* **2**(4): 186.

Heneghan C., Blacklock C., Perera R., Davis R., Banerjee A., Gill P. and Ward, A. (2013). Evidence for non-communicable diseases : analysis of Cochrane reviews and randomised trials by World Bank classification. *British Medical Journa*l **3**(7): 003298.

Heeneman S., Cleutjens, J.P., Faber B.C., Creemers E.E., van Suylen R.J., Lutgens E. and Daemen M.J. (2003). The dynamic extracellular matrix: Intervention strategies during heart failure and atherosclerosis. *Journal of Pathology* **200**(4): 516–525.

Hojilla C.V., Wood G.A. and Khokha R. (2008). Inflammation and breast cancer: metalloproteinases as common effectors of inflammation and extracellular matrix breakdown in breast cancer. *Breast Cancer Research* **10**(2): 205.

Hinson J.A., Reid A.B., McCullough S.S. and James L.P. (2004). Acetaminophen-induced hepatotoxicity: role of metabolic activation, reactive oxygen/nitrogen species, and mitochondrial permeability transition. *Drug Metabolic Review* **36**(3-4): 805–822.

Hua H., Li M., Luo T., Yin Y. and Jiang Y. (2011). Matrix metalloproteinases in tumorigenesis: an evolving paradigm. *Cellular and Molecular Life Sciences* **68**(23): 3853–68.

Ibrahim, S. F and van den Engh, G. (2007). Flow cytometry and cell sorting. In *Cell Separation* **19**-39

Iikuni N., H Hahn B. and La Cava A. (2009). Potential for anti-DNA immunoglobulin peptide therapy in systemic lupus erythematosus. *Expert Opinion on Biological Therapy* **9**(2): 201-206.

Islam A.M., Phillips G.O., Sljivo A., Snowden M.J. and Williams P.A. (1997). A review of recent developments on the regulatory, structural and functional aspects of gum arabic. *Food Hydrocolloids* **11**(4): 493–505.

Ingber D.E. (2007). Integrins, tensegrity, and mechanotransduction. *Gravitational and Space Research* **10**(2).

Jackson B. C., Nebert D. W. and Vasiliou V. (2010). Update of human and mouse matrix metalloproteinase families. *Human genomics* **4**(3):194.

Jacoby, D.B., Dyskin, E., Yalcin, M., Kesavan, K., Dahlberg, W., Ratliff, J., Johnson, E.W. and Mousa, S.A., 2010. Potent pleiotropic anti-angiogenic effects of TM601, a synthetic chlorotoxin peptide. *Anticancer Research **30(***1): f39-46.

Jemal A., Bray F., Center M. M., Ferlay J., Ward, E. and Forman, D. (2011). Global cancer statistics. *CA: A Cancer Journal for Clinicians*. **61**(2): 69-90.

Jaiswal J.K. and Simon S.M. (2004). Potentials and pitfalls of fluorescent quantum dots for biological imaging. *Trends in Cell Biology* **14**(9): 497-504.

Jodele S., Blavier L., Yoon J.M. and DeClerck Y.A. (2006). Modifying the soil to affect the seed: Role of stromal-derived matrix metalloproteinases in cancer progression. *Cancer and Metastasis Reviews* **25**(1): 35–43

Kass L., Erler J.T., Dembo M. and Weaver V.M. (2007). Mammary epithelial cell: influence of extracellular matrix composition and organisation during development and tumorigenesis. *International Journal of Biochemistry and Cell Biology* **39**(11): 1987-1994.

Kattumuri V., Katti K., Bhaskaran S., Boote E.J., Casteel S.W., Fent G.M. and Katti K.V. (2007). Gum Arabic as a Phytochemical Construct for the Stabilization of Gold Nanoparticles: *In Vivo* Pharmacokinetics and X-ray-Contrast-Imaging Studies. *Small* **3**(2): 333-341.

Kawasaki E.S. and Player A. (2005). Nanotechnology, nanomedicine, and the development of new, effective therapies for cancer. *Nanomedicine: Nanotechnology, Biology and Medicine* **1**(2): 101-109.

Kaushik V. and Roos Y.H. (2007). Limonene encapsulation in freeze-drying of gum Arabic–sucrose–gelatin systems. LWT-*Food Science and Technology* **40**(8):1381–1391.

Kessenbrock K., Plaks V. and Werb Z. (2010). Matrix metalloproteinases: regulators of the tumour microenvironment. *Cell* **141**(1):52–67.

Kenyon M.M. (1995). Modified starch, maltodextrin, and corn syrup solids as wall materials for food encapsulation, American Chemical Society symposium series. *American Chemical Society Symposium Series* **590**: 42–50.

Kesavan K., Ratliff J., Johnson E.W., Dahlberg W., Asara J.M., Misra P., Frangioni J.V. and Jacoby D.B. (2010). Annexin A2 is a Molecular Target for TM601, a Peptide with Tumor-targeting and Anti-angiogenic Effects. *Journal of Biological Chemistry* **285**(7):4366-4374.

Kittle D.S., Mamelak M.D.A., Parrish-Novak J.E., Hansen S., Patil R., Gangalum P.R., Ljubimova J., Black K.P. and Butte P. (2014). Fluorescence-guided Tumor Visualization Using the Tumor Paint BLZ-100. *Cureus* **6**(9): 1-18.

Kim J., Park Y., Yoon T.H., Yoon C.S. and Choi K. (2010). Phototoxicity of CdSe/ZnSe quantum dots with surface coatings of 3-mercaptopropionic acid or tri-n-octylphosphine oxide/Gum Arabic in Daphnia magna under environmentally relevant UV-B light. *Aquatic Toxicology* **97**(2): 116-124.

Klumpp C., Kostarelos K., Prato M., and Bianco A.(2006). Functionalized carbon nanotubes as emerging nanovectors for the delivery of therapeutics. Biochimica et Biophysica Acta Biomembranes **1758** (3): 404-412

Koli A. O., Eltayeb A. M., Sanjak E. M. and Mohammed M. H. (2013). Socio-economic aspects of gum arabic production in Dalanj area, South Korodofan, Sudan. *Pakistan Journal of Biological Sciences* **16**(21): 1407-1410.

Lewis R. J. and Garcia M. L. (2003). Therapeutic potential of venom peptides. *Nature Reviews. Drug Discovery* **2**(10): 790–802.

Lee S., Xie J. and Chen X. (2010). Peptide-Based Probes for Targeted Molecular Imaging. *Biochemistry* **49**:1364-1376

Lovrić J., Cho S.J., Winnik F.M. and Maysinger D. (2005). Unmodified cadmium telluride quantum dots induce reactive oxygen species formation leading to multiple organelle damage and cell death. *Chemistry and biology* **12**(11): 1227-1234.

Li W., Nichols K., Nathan C.A. and Zhao Y. (2013). Mitochondrial uncoupling protein two is up-regulated in human head and neck, skin, pancreatic, and prostate tumours. *Cancer Biomarkers* **13**(5): 377-383.

Lu P., Takai K., Weaver V.M. and Werb Z. (2011). Extracellular matrix degradation and remodelling in development and disease. *Cold Spring Harbor Perspectives in Biology* **3**(12).

Ma J., Chen J.Y., Guo J., Wang C.C., Yang W. L., Xu L. and Wang P.N. (2006). Photostability of thiol-capped CdTe quantum dots in living cells: the effect of photo-oxidation. *Nanotechnology* **17**(9): 2083.

Ma X. and Yu H. (2006). Cancer issue: global burden of cancer. *The Yale journal of biology and medicine* **79**(3-4): 85.

Madani S. Y., Shabani F., Dwek M. V., and Seifalian A. M. (2013). Conjugation of quantum dots on carbon nanotubes for medical diagnosis and treatment. *International Journal of nanomedicine* 8: 941.

Manton K. G., Akushevich I. and Kravchenko J. (2008). Cancer mortality and morbidity patterns in the US population: an interdisciplinary approach. *Springer Science and Business Media.*

Marastoni S., Ligresti G., Lorenzon E., Colombatti A. and Mongiat, M. (2008). Extracellular matrix: a matter of life and death. *Connective tissue research* **49**(3-4): 203-206.

McGrath S.E., Michael A., Morgan R. and Pandha H. (2013). EN2: a novel prostate cancer biomarker. *Biomarkers in Medicine* **7**(6): 893-901.

Marchenko G., Marchenko N., Strongin A. (2003). The structure and regulation of the human and mouse matrix metalloproteinase-21 gene and protein. *Biochemical Journal* **372:** 503–515.

Meguid K. S. A., El-Wakd M. M., Kamel A. I., Adel L. and Niazi, M. (2007) Elevated Serum Laminin Level In Postmenopausal Osteoporosis; A Novel finding. *Egyptian Rheumatologist* **29**(3):1441-1154

Murphy G. and Nagase H. (2008). Progress in matrix metalloproteinase research. *Molecular Aspects of Medicine* **29**(5): 290-308.

McClatchey A. I. and Yap A. S. (2012). Contact inhibition (of proliferation) redux. *Current Opinion in Cell Biology* **24**(5): 685-694.

Mosher D.F. and Adams J.C. (2012). Adhesion-modulating/matricellular ECM protein families: A structural, functional and evolutionary appraisal. *Matrix Biology* **31**(3): 155–161.

Morgunova E., Tuuttila A., Bergmann U., Isupov M., Lindqvist Y., Scheinder G. and Tryggvason K. (1999). Structure of Human Pro-Matrix Metalloproteinase-2: Activation Mechanism Revealed. *Science* **284**:1667-1679.

Mokwunye M. and Aghughu O. (2010). Restoring Nigeria's lead in Gum Arabic Production: Prospects and Challenges. *Report and Opinion* **2**(4): 7–13.

Manicone A.M. and McGuire J.K. (2008). Matrix metalloproteinases as modulators of inflammation. *Seminars in Cell and Developmental Biology* **19**(1): 34–41.

Mamelak A.N. and Jacoby D.B. (2007). Targeted delivery of antitumoral therapy to glioma and other malignancies with synthetic chl*orotoxin (TM-601). Expert Opinion on Drug Delivery* **4**(2):175-186.

Matsumoto N., Riley S., Fraser D., Al-Assaf S., Ishimura E., Wolever T., Phillips G.O. and Phillips A.O. (2006). Butyrate modulates TGF-beta1 generation and function: potential renal benefit for Acacia (sen) SUPERGUM. *Kidney International* **69**(2): 0085–2538.

Mayer A. B. and Mark J. E. (1998). Colloidal gold nanoparticles protected by water-soluble homopolymers and random copolymers. *European Polymer Journal **34*(**1): 103-108.

Medintz I.L., Uyeda H.T., Goldman E.R. and Mattoussi H. (2005). Quantum dot bioconjugates for imaging, labelling and sensing. *Nature Materials* **4**(6): 435-446.

Mittal A.K., Chisti Y. and Banerjee U.C. (2013). Synthesis of metallic nanoparticles using plant extracts. *Biotechnology Advances* **31**(2): 346–56.

Medintz I.L., Uyeda H.T., Goldman E.R. and Mattoussi H. (2005). Quantum dot bioconjugates for imaging, labelling and sensing. *Nature Materials* **4**(6): 435-446.

Mochochoko T., Oluwafemi O.S., Jumbam D.N. and Songca S.P. (2013). Green synthesis of silver nanoparticles using cellulose extracted from an aquatic weed; water hyacinth. *Carbohydrate Polymers* **98**(1): 290–294.

Mook O. R., Frederiks W. M. and Van Noorden C. J. (2004). The role of gelatinases in colorectal cancer progression and metastasis. *Biochimica et Biophysica Acta (BBA)-Reviews on Cancer* **1705**(2): 69-89.

Montenegro M.A., Boiero M.L., Valle L. and Borsarelli C.D. (2012). Gum Arabic : More Than an Edible Emulsifier. *Products and Applications of Biopolymers*. Intech

Nahar M., Dutta T., Murugesan S., Asthana A., Mishra D., Rajkumar V., Tare M., Saraf S and Jain N.K. (2006). Functional polymeric nanoparticles: an efficient and promising tool for active delivery of bioactive. *Critical Review in Therapeutic Drug Carrier System* **23**(4):259–318.

National Cancer Institute, (2014) http://www.cancer.gov/cancertopics/cancerlibrary/what-is-cancer

National cancer institute (2017). https://www.cancer.gov/(Accessed 18 September 2017)

Noguera R., Nieto O.A., Tadeo I., Fariñas F. and Álvaro T. (2012). Extracellular matrix, biotensegrity and tumour microenvironment. An update and overview. *Histology and Histopathology* **27**(6): 693–705.

Nelson C.M. and Chen C. S. (2002). Cell-cell signalling by direct contact increases cell proliferation via a PI3K-dependent signal. *FEBS Letters* **514**(2-3): 238-242.

Oluwafemi O.S., Lucwaba Y., Gura A., Masabeya M., Ncapayi V., Olujimi O.O. and Songca S.P. (2013). A facile completely "green" size-tunable synthesis of maltose-reduced silver nanoparticles without the use of any accelerator. *Colloids and Surfaces B: Biointerfaces* **102:** 718–723.

Onishi T., Umemura S., Yanagawa M., Matsumura M., Sasaki Y., Ogasawara T. and Ooshima T. (2008). Remineralisation effects of gum arabic on caries-like enamel lesions.*Archives of Oral Biology* **53**(3): 257-260.

Ortiz-Acevedo A., Xie H., Zorbas V., Sampson W.M., Dalton A.B., Baughman R.H., Draper R.K., Musselman I.H., and Dieckmann G.R.(2005). Diameter selective solubilisation of single-walled carbon nanotubes by reversible cyclic peptides. Journal of the American Chemical Society **127**(26): 9512-9517.

Ortega-Arroyo L., Martin-Martinez E.S., Aguilar-Mendez M.A., Cruz-Orea A., Hernandez-Pérez I., and Glorieux C. (2013). Green synthesis method of silver nanoparticles using starch as capping agent applied the methodology of surface response. *Starch-Stärke* **65** (9-10): 814-821.

Paszek M.J. and Weaver V.M. (2004). The tension mounts: mechanics meets morphogenesis and malignancy. *Journal of Mammary Gland Biology and Neoplasia*. **9**(4). 325-342.

Pardee A.B., Dubrow R., Hamlin J.L. and Kletzien R.F. (1978). Animal cell cycle. *Annual Review of Biochemistry* **47**(1): 715-750.

Pereira I.T., Ramos E.A.S., Costa E.T., Camargo A.A., Manica G.C.M., Klassen L.M.B. and Klassen G. (2014). Fibronectin affects transient MMP2 gene expression through DNA demethylation changes in non-invasive breast cancer cell lines. *PloS One* **9**(9): e105806

Raveendran P., Fu J. and Wallen S.L. (2003). Completely "green" synthesis and stabilisation of metal nanoparticles. *Journal of the American Chemical Society* **125**(46): 13940–13941.

Ra H.J. and Parks W.C. (2007). Control of matrix metalloproteinase catalytic activity. *Matrix Biology* **26**(8): 587-596.

Rao Y.N., Banerjee D., Datta A., Das S.K., Guin R. and Saha A. (2010). Gamma irradiation route to synthesis of highly re-dispersible natural polymer capped silver nanoparticles. *Radiation Physics and Chemistry* **79**(12): 1240–1246.

Rehman K.U., Wingertzahn M.A., Teichberg S., Harper R.G. and Wapnir R.A. (2003). Gum arabic. (GA) Modifies paracellular water and electrolyte transport in the small intestine. *Digestive Diseases and Sciences* **48**(4): 755–760.

Reubi J.C. (2003). Peptide receptors as molecular targets for cancer diagnosis and therapy. *Endocrine Reviews* **24**(4): 389-427

Rauch U. (1997). Modelling an extracellular environment for axonal pathfinding and fasciculation in the central nervous system. *Cell and Tissue Research* **290**(2): 349–356.

Raffetto J.D. and Khalil R.A. (2008). Matrix metalloproteinases and their inhibitors in vascular remodelling and vascular disease. *Biochemical Pharmacology* **75**(2): 346–359.

Renard D., Lavenant-Gourgeon L., Ralet M.C. and Sanchez C. (2006). Acacia senegal Gum: Continuum of Molecular Species Differing by Their Protein to Sugar Ratio, Molecular Weight, and Charges. *Biomacromolecules* **7**(9): 2637–2649.

Rodriguez-Fragoso L., Gutiérrez-Sancha I., Rodríguez-Fragoso P., Rodríguez-López A. and Reyes-Esparza J. (2014). Pharmacokinetic Properties and Safety of Cadmium-Containing Quantum Dots as Drug Delivery Systems. In *Application of Nanotechnology in Drug Delivery*. InTech.

Roy R., Zurakowski D., Wischhusen J., Frauenhoffer C., Hooshmand S., Kulke M. and Moses M. A. (2014). Urinary TIMP-1 and MMP-2 levels detect the presence of pancreatic malignancies. *British Journal of Cancer* **111**(9): 1772-1779.

Rizvi S. B., Ghaderi S., Keshtgar M. and Seifalian, A. M. (2010). Semiconductor quantum dots as fluorescent probes for in vitro and in vivo bio-molecular and cellular imaging. *Nano reviews* **1**(1): 5161.

Sanchez C., Nigen M., Tamayo V.M., Doco T., Williams P., Amine C. and Renard D. (2018). Acacia gum: History of the future. *Food Hydrocolloids* **78**:140-160.

Said A.H., Raufman J. P. and Xie G. (2014). The role of matrix metalloproteinase in colorectal cancer. *Cancers* **6**(1): 366-375.

Sariahmetoglu M., Crawford B.D., Leon H., Sawicka J., Li L. and Ballermann B.J. and Regulation R. (2007). Regulation of matrix metalloproteinase-2 (MMP-2) activity by phosphorylation. *FASEB Journal* **21:** 2486–2495.

Saini M., Saini R., Roy S. and Kumar A. (2008). Comparative pharmacognostical and antimicrobial studies of Acacia species (Mimosaceae). *Journal of Medicinal Plants Research* **2**(12): 378-386.

Sheu T.Y. and Rosenberg M. (1995). Microencapsulation by spray drying ethyl caprylate in whey protein and carbohydrate wall systems. *Journal of Food Science* **60**(1): 98–103

Schaefer L and Dieter P. R (2016). "Special issue: extracellular matrix: therapeutic tools and targets in cancer treatment. *Advanced in drug Delivery Reviews* **97**: 1-3.

Schwab A., Nechyporuk-Zloy V., Fabian A. and Stock C. (2007). Cells move when ions and water flow. *Pflügers Archiv : European Journal of Physiology* **453**(4): 421–32.

Shadidi M. and Sioud M. (2003). Selective targeting of cancer cells using synthetic peptides'. *Drug Resistance Updates* **6**(2003): 363 – 371.

Sentissi A. and Jacoby D.B. (2015). "Chlorotoxin polypeptides and conjugates and uses thereof. *U.S. Patent No. 9,018,347*. Washington, DC: U.S. Patent and Trademark Office.

Stegmann T.J. (1998). FGF-1: a human growth factor in the induction of neoangiogenesis. *Expert Opinion on Investigational Drugs* **7**(12): 2011-2015.

Sharma G., Kodali V., Gaffrey M., Wang W., Minard K. R., Karin N. J. and Thrall, B. D. (2014). Iron oxide nanoparticle agglomeration influences dose rates and modulates oxidative stress-mediated dose-response profiles in vitro. *Nanotoxicology* ***8***(6): 663-675.

Siegel R., Naishadham D. and Jemal A. (2013). Cancer statistics, 2013. *CA: a cancer journal for clinicians* **63**(1): 11-30.

Spitz W.U., Asphyxia. *W.U., Spitz; D.J., Spitz R.C.* Spitz and Fisher's Medicolegal Investigation of Death–Guidelines for the Application of Pathology to Crime Investigation. 4ª ed. Spr*ingfield:* Editora Charles C Thomas, United States of America, 833-841.

Stroud M.R., Hansen S.J. and Olson J.M. (2011). In vivo bio-imaging using chlorotoxin-based conjugates. *Current Pharmaceutical Design* **17**(38): 4362.

Singh, A., Jain, D., Upadhyay, M. K., Khandelwal, N and Verma, H. N. (2010). Green synthesis of silver nanoparticles using *Argemone mexicana* leaf extract and evaluation of their antimicrobial activities. *Digest Journal of Nanomaterials and Biostructure* **5**(2), 483-489.

Siegel R., Ma J., Zou Z. and Jemal A. (2014). Cancer statistics, 2014. *CA: A Cancer Journal for Clinicians* **64**(9): 9–29.

Smith A. M., Duan H., Mohs, A. M. and Nie S. (2008). Bioconjugated quantum dots for in vivo molecular and cellular imaging. *Advanced drug delivery reviews* **60**(11):1226-1240.

South African Medical research cancer Report, 8th April 2014. http://www.mrc.ac.za. (Accessed Dec, 2017).

Strongin A.Y. (2006). Mislocalization and unconventional functions of cellular MMPs in cancer. *Cancer Metastasis Reviews* **25**: 87–98.

Sun Z., Zhang W., Zhang P., Gao D., Gong P., Yu X.-F and Cai L. (2015). Neurotoxin-directed synthesis and in vitro evaluation of Au nanoclusters. *Royal Society of Chemistry Advance* **5**(38): 29647–29652.

Tang Z., Kotov N. A. and Giersig M. (2002). Spontaneous organization of single CdTe nanoparticles into luminescent nanowires. *Science* **297**(5579): 237-240

Thayer A.M. (2011). Improving peptides. *Chemical & Engineering News* **89**(22): 13.

Theocharis A.D., Skandalis S.S., Gialeli C., Karamanos N.K. (2016). Extracellular matrix structure. *Advance Drug Delivery Reviews* **97**: 4–27.

Tentes I., Asimakopoulos B., Mourvati E., Diedrich K., Al-Hasani S. and Nikolettos N. (2007). Matrix metalloproteinase (MMP)-2 and MMP-9 in seminal plasma. *Journal of Assisted Reproduction and Genetics* **24**(7): 278-281.

Trexler M., Briknarová K., Gehrmann M., Llinás M. and Patthy L. (2003). Peptide ligands for the fibronectin type II modules of matrix metalloproteinase 2 (MMP-2). *Journal of Biological Chemistry* **278**(14): 12241–6.

Tischer C. A., Gorin P.A.J., and Iacomini M. (2002). The free reducing oligosaccharides of gum arabic: aids for structural assignments in the polysaccharide. *Carbohydrate Polymers* **47**(2):151-158.

Tiss A., Carrière F. and Verger R. (2001). Effects of gum arabic on lipase interfacial binding and activity. *Analytical Biochemistry* **294**: 36–43.

Torre L. A., Bray F., Siegel R. L., Ferlay J., Lortet-Tieulent J. and Jemal A. (2015). Global cancer statistics, 2012. *CA: A Cancer Journal for Clinicians*. **65**(2): 87-108.

Trommer H. and Neubert R.H. (2005). The examination of polysaccharides as potential antioxidative compounds for topical administration using a lipid model system. *International Journal of Pharmaceutics* **298:** 153–163.

Tutt A. and Ashworth A. (2002). The relationship between the roles of BRCA genes in DNA repair and cancer predisposition. *Trends in Molecular Medicine.* **8**(12): 571-576.

Uria, J. A. and Werb, Z. (1998). Matrix metalloproteinases and their expression in mammary gland. *Cell research* **8**(3): 187.

Van der Worp H.B., Howells D.W., Sena E.S., Porritt M.J., Rewell S., O'Collins V. and Macleod M. R. (2010). Can animal models of disease reliably inform human studies? *PLoS Medicine* **7**(3).

Vandooren J., Van den Steen P.E. and Opdenakker G. (2013). Biochemistry and molecular biology of gelatinase B or matrix metalloproteinase-9 (MMP-9): the next decade. *Critical Reviews in Biochemistry and Molecular Biology* **48**(3): 222–72.

Veiseh M., Gabikian P., Bahrami S.B., Veiseh O., Zhang M., Hackman R.C. and Olson J.M. (2007). Tumour paint: A chlorotoxin: Cy5.5 bioconjugate for intraoperative visualisation of cancer foci. *Cancer Research* **67**(14): 6882–6888.

Verbeken D., Dierckx S. and Dewettinck K. (2003). Exudate gums: occurrence, production, and applications. *Applied Microbiology and Biotechnology* **63**(1): 10–21.

Veerasamy R., Xin T. Z., Gunasagaran S., Xiang T. F. W., Yang E. F. C., Jeyakumar N. and Dhanaraj S. A. (2011). Biosynthesis of silver nanoparticles using mangosteen leaf extract and evaluation of their antimicrobial activities. *Journal of Saudi Chemical Society* **15**(2): 113-120

Venkitaraman A. R. (2002). Cancer susceptibility and the functions of BRCA1 and BRCA2. *Cell* **108**(2): 171-182.

Visse R. and Nagase H. (2003). Matrix metalloproteinases and tissue inhibitors of metalloproteinases: Structure, function, and biochemistry. *Circulation Research* **92**(8): 827–839.

Wang X., Bo J., Bridges T., Dugan K.D., Pan T.C., Chodosh L.A., and Montell D.J. (2006). Analysis of cell migration using whole-genome expression profiling of migratory cells in the Drosophila ovary. *Developmental cell* **10**(4): 483-495.

Wang H., Gu W., Xiao N., Ye L. and Xu Q. (2014). Chlorotoxin-conjugated graphene oxide for targeted delivery of an anticancer drug. I*nternational Journal of Nanomedicine* **2014**(9): 1433–1442.

Wang X., Li Y., Tian H., Qi J., Li M., Fu C. and Zhang C. (2014). Macrophage inhibitory cytokine 1 (MIC-1/GDF15) as a novel diagnostic serum biomarker in pancreatic ductal adenocarcinoma. *BMC Cancer* **14**(1): 578.

Wekesa, C., Makenzi P., Chikamai B., Luvanda A. and Muga M. (2010). Traditional ecological knowledge associated with Acacia *senegal* (Gum Arabic tree) management and Gum Arabic production in northern Kenya. *The International Forestry Review* **12**(3): 240-246.

Werb Z. (1997). ECM and cell surface proteolysis: regulating cellular ecology. *Cell* **91**(4): 439–442.

Wickens G.E., El Din A.S., Sita G. and Nahal I. (1995). Role of Acacia species in the rural economy of dry Africa and the Near East. *Food and Agriculture Organisation*. 27

Williams P.A. and Phillips G.O. (2000). Gum arabic. In G. O. Phillips, and P. A. Williams (Eds.), *Handbook of Food Hydrocolloids. England: CRC Press (Ch 9)*.

World Health Organization Report, 2014. http://www.who.int/gho/publications /world health statistics/2014/en (Accessed November 1st, 2017).

World Health Organisation Report, 2015. http://www.who.int/gho/publications/ world_health statistics/2015/en/(Accessed November 20, 2016).

Wu X.S., Jian X.C., Yin B. and He Z.J. (2010). Development of the research on the application of chlorotoxin in imaging diagnostics and targeted therapies for tumours. *Chinese Journal of Cancer* **29**(6): 626–630.

Xue M. and Jackson C.J. (2008). Autocrine actions of matrix metalloproteinase (MMP)-2 counter the effects of MMP-9 to promote survival and prevent terminal differentiation of cultured human keratinocytes. *Journal of Investigative Dermatology* **128** (11): 2676–85.

Xiao Y. F., Jie M.M., Li B.S., Hu C.J., Xie R., Tang B. and Yang S. M. (2015). Peptide-based treatment: a promising cancer therapy. *Journal of Immunology Research*. ***2015***.

Yasseen G. A., Salih A. A. and Ahmed M. E. (2014). Competitiveness and profitability of Gum Arabic in North Kordofan state, Sudan. *Procedia-Social and Behavioural Sciences* **120:** 704-710.

Yoshii H., Soottitantawat A., Liu X.D., Atarashi T., Furuta T., Aishima S., S., Ohgawara and Linko, P. (2001). Flavour release from spray-dried maltodextrin/gum arabic or soy matrices as a function of storage relative humidity. *Innovative Food Science and Emerging Technologies* **2**(1):55–61.

Yun Lu., Bin Z., Guangqi G., Ding L., Xingdang L. and Biao H. (2014). Clinical significance in combined detection of serum pepsinogen I, pepsinogen II and carbohydrate antigen 242 in gastric cancer. *Hepato-Gastroenterology* **61**(129): 255-258

Zhang M., Ellenbogen R.G., Sze R.W., Veiseh O., Olson J.M., Veiseh M. and Bahrami S. B. (2014). Fluorescent chlorotoxin conjugate and method for intra-operative visualisation of cancer. *U.S. Patent No. 8,778,310*. Washington, DC: U.S. Patent and Trademark Office. *Molecular Pharmaceutics*.

Zhang T., Hu Y., Tang M., Kong L., Ying J., Wu T., Xue Y. and Pu Y. (2015). Liver toxicity of cadmium telluride quantum dots (CdTe QDs) due to oxidative stress in vitro and in vivo. *International Journal of Molecular Sciences* **16**(10): 23279-23299.

Zanetti J. S., Soave D. F., Oliveira-Costa J. P., Da Silveira G. G., Ramalho L. N. Z., Garcia S. B. and Ribeiro-Silva A. (2011). The role of tumour hypoxia in MUC1-positive breast carcinomas. *Virchows Archive* **459**(4): 367.

Zargar M., Hamid A. A., Bakar F. A., Shamsudin M. N., Shameli K., Jahanshiri F. and Farahani F. (2011). Green synthesis and antibacterial effect of silver nanoparticles using *Vitex negundo L. Molecules* **16** (8): 6667-6676.

Zheng Z. X., Sun Y., Bu Z.D., Zhang L.H., Li Z.Y., Wu, A.W. and Du H. (2013). Intestinal stem cell marker LGR5 expression during gastric carcinogenesis. *World Journal of Gastroenterology* **19**(46): 8714.

Zhu L., Wang T., Perche F., Taigind A. and Torchilin V. P. (2013). Enhanced anticancer activity of nano preparation containing an MMP2-sensitive PEG-drug conjugate and cell-penetrating moiety. *Proceedings of the National Academy of Sciences of the United States of America* **110**(42): 17047–52.

CHAPTER TWO

Synthesis and cytotoxic evaluation of Gum Arabic surface modified cadmium telluride quantum dots

Edwina .O. Uzunuigbe [a,d], Ayabei Kiplagat [b,c], Nicole R. S. Sibuyi [c], Mervin Meyer [c], Abidemi Paul Kappo [a] and Martin O. Onani*[b,c]

Corresponding Author *; monani@uwc.ac.za

[a]*Department of Biochemistry and Microbiology, University of Zululand, KwaDlangezwa 3886, South Africa.*

[b] *Department of Chemistry, University of the Western Cape, Private BagX17, Bellville, 7535, South Africa*

[c]*DST/Mintek Nanotechnology Innovation Centre Department of Biotechnology, University of the Western Cape, Private BagX17, Bellville, 7535, South Africa.*

[d]*Rubber Research Institute of Nigeria, Iyanomo, PMB 1049, Benin City, Edo State, Nigeria*

Abstract

In this experiment water-soluble cadmium telluride (CdTe) quantum dots (QDs), capped with Gum Arabic (GA, were characterised using Ultraviolet-visible (UV-vis) spectroscopy, photoluminescence (PL) spectroscopy, X-ray diffraction (XRD), high-resolution transmission electron microscopy, particle size distributions and zeta potential were evaluated. Cytotoxicity of these QDs-MPA and QDs-GA were examined with using four different human cell lines; HeLa, MCF-7, PC-3 and U87 cells line. The QDs-MPA capped with 3-mercaptopropionic acid, QDs-GA2 was stabilized and capped with GA at 60°C for 2hours, and QDs-GA12 was stabilized and capped with GA for 12hours at room temperature (25°C) with continuous stirring; These QDs-MPA, QDs-GA2 and QDs-GA12 were found to be highly luminescent with PL values of 675nm, 678nm and 677nm

respectively. The average polydispersity index (PDI) were 0.36±0.02, 0.27±0.02, 0.35±0.01 for QDs-MPA, QDs-GA2 and QDs-GA12 respectively. The average particles size from HRTEM, XRD and hydrodynamic size showed that the QDs-GA have bigger particle sizes of 56.12 nm ±1.14, 68.69 nm ±2.08 and 77.85 nm ±1.69 for QDs-MPA, QD-GA2 and QD-GA12. Cytotoxicity studies of these QDs were carried out using WST-1 cell proliferation assay on four different tumour cell line. The results showed that these cells were over 50 per cent viable and the QDs-GA capped had higher cell percentage viability.

Keywords: Gum Arabic (GA), Quantum Dots (QD), Cadmium Telluride (CdTe), Cancer cells, Cytotoxicity.

2.1 Introduction

Semiconductor nanoparticles have been widely explored based on novelties, their unique properties.[1,2,3,] and their synthesis has also improved in recent years. This may be attributed to the development in the instrumentation and the broad application of QDs in different fields.[4-7] In the midst of the numerous forms of QDs, cadmium telluride (CdTe) QDs have found full application for industrial and biomedical applications.[8] These CdTe QDs show exceptional promise for imaging of cells because of their unique characteristics, including; small size range of 1-10 nm,[3,5,9] photoluminescence, narrow emission, which is size dependent, photo-stability and relatively high quantum yield.[2,8-11] They are also unique in the sense that they can be excited by a single wavelength and emit different wavelength with different spectra this is determined by the size of the QDs [2,9,11,12] The method used to synthesise CdTe as well as the capping agent for CdTe is very important as this determines its application what application it can be used for. QDs are made up of the inner core and a shell which help to increase their optical property and stability,[2] making them an outstanding choice as fluorescent probes in biological applications, cellular bio-imaging and diagnosis, especially in cancer research.[3,9] Gum Arabic (GA) is an edible glycoprotein polymer from acacia plants

that is non-toxic and odourless. It is a heterogeneous polymer of the arabinogalactan type made up of carboxyl and amine groups and mainly used in the food and pharmaceutical industries as an emulsifier and a stabiliser.[13,14] In the synthesis of nanoparticles GA can provide functional groups which may act as a reducing agent and give colloidal stability to the nanoparticles.[8,15,16] Most recently, the biological research focal point is shifting to the use of natural materials for synthesising nanoparticles, which are characteristically non-toxic to the metabolic system.[17] The use of GA for surface modification is termed green surface modification considering the numerous advantages including economic, safe and produces less waste with minimal risk.[18-20] The use of Gum Arabic in nanoparticles synthesis can serve as a capping, stabilising agent and a source of carboxyl group for the attachment of molecules in nanoparticles synthesis.

In this research, we are reporting for the first time the use of Gum Arabic polymer to cap and stabilise CdTe quantum dots using two different routes; at 25ºC for 12hours and 60ºC for 2 hours with continuous stirring respectively. The GA maintains the integrity of the quantum dots and enhances its applicability.

2.2 Experiment

Chemicals:

The reagents were used as purchased from the manufacturers without any additional purification. Cadmium chloride ($CdCl_2$), 3-mercaptopropionic acid (MPA, 99%), sodium borohydride ($NaBH_4$), tellurium (99.8%), zinc acetate (99.9%), thiourea (99%), ethanol (99%) and acetone were purchased from Sigma–Aldrich, and were used without further purification. WST-1 Cell Proliferation Reagent 4-[3-(4-iodophenyl)-2-(4-nitrophenyl)-2H-5-tetrazolio]-1,3-

benzene disulfonate (Roche Diagnostics, Mannheim, Germany), RPMI1640, Penicillin and Streptomycin, Sterile phosphate buffer, Trypsin, Dulbecco's modified Eagle's medium

(DMEM) was from gotten from Lonza, FBS (Fetal bovine serum) was obtained from Gibco Life technologies and 96-well Flat bottom clear microplate (Greiner) and the Gum Arabic (GA) was obtained from the Rubber Research Institute of Nigeria (RRIN).

The optical characterisation and photoluminescence (PL) of CdTe-QDs was carried out using Polar Star Omega Spectrophotometer (BMG Lab tech) and Nano log HORIBA FL3-22-TRIAX, respectively. X-Ray diffraction (XRD) crystalline phase analysis of the dried sample QDs was ascertained using an AXS D8 diffractometer (Bruker) with nickel-filtered Co Ka radiation (k = 1.5418 A °) CuKα¼1.5418Åat 40 kV at a scanning rate of 0.01 per min in a range of 2 theta = 15 to 70^{o}.

High-Resolution Transmission Electron Microscope (model TECNAIF3OST-TEM) was used to determine the morphology and the elemental distribution of the QDs. The sample was prepared by putting a drop of the QDs solution on a nickel grid and allowing to dry it before analysis. Fourier transform infrared (FTIR) analysis was carried out on a PerkinElmer spectrum100 series s instrument using potassium bromide (KBr) pellets, this was done with the dry sample of the QDs. The hydrodynamic size distribution and the zeta potential of the QDs were measured using a Malvern Zeta sizer Nano-ZS (Malvern, Worcestershire, UK).

2.3 Synthesis and Characterization of CdTe-QDs

The synthesis of the CdTe was carried out using methods described previously [12,28] but with some slight modifications [21-23]. All reactions were carried out under an inert atmosphere using nitrogen gas. All the flasks were washed, rinsed with acetone and dried in the oven before synthesis. Sodium hydrogen Telluride complex (NaHTe) made by dissolving 1mmol sodium borohydride ($NaBH_{4)}$ and 0.04 mmol tellurium powder (Te) in deionised water. The solution was heated at 80^{o}C for 30 minutes with continuous stirring, which resulted in a colour change from black to the purple colour solution of NaHTe. The Cd/MPA precursor was prepared by mixing 0.4 mmol

$CdCl_2$ and 0.6 mmol MPA in deionised water, which raised the initial pH of 2.48 to pH 11.7. The solution was heated to 80ºC under inert atmospheric conditions in a three-neck flask, and the NaHTe solution was injected. The reaction was maintained at 100ºC for 2 hours allowing the growth of CdTe nanocrystals. Afterwards, the solution was rapidly cooled down on the ice, and two mL 0.1M zinc acetate and 0.1 M thiourea in deionised water was added to the CdTe solution and which raise the pH to 11.5. The solution was degassed and subsequently heated to 90ºC for 1 hour in a three-neck flask which allowed the growth of MPA-capped CdTe QDs. The solution ultimately changed colour from purple to greenish yellowish. The solution was aliquot in 2mL Eppendorf tubes and centrifuged for 3minutes at a speed of 13000 rpm using Eppendorf mini spin plus microcentrifuge to remove impurities and unreacted materials. The supernatant was collected in sterile 15ml tubes, and the pellets were discarded.

2.4 Preparation of QDs-GA Using Gum Arabic Polymer

The QDs-GA preparation experiment was carried out according to the method as previously by. [24] The Gum Arabic (GA) capped CdTe QDs was prepared by adding 1mL of (5%) GA solution to 5mL of MPA-capped CdTe QDs and stirred for 12-15 hours at room temperature 25ºC to form QDs-GA12. Stirring of QDs-GA2 was done for 2hours at 60ºC after addition of 1mL 5% GA solution was added to 5 mL of QD solution. The samples recovery was by addition of absolute ethanol in a 15mL tube, the resulting solution then centrifuged at 14000 rpm for five mins, then discarded the supernatant, and the pellet was resuspended in distilled water for further characterisation.

2.5 Investigation of the effect of CdTe QDs in cancer cells

The cytotoxicity of CdTe QDs on selected cancer cell lines was assessed using 4-[3-(4-iodophenyl)-2-(4-nitrophenyl)-2H-5-tetrazolio]-1, 3-benzene disulfonate (WST-1) *in vitro* assay. The four cell lines: HeLa (cervical cancer), MCF-7 (breast cancer), PC-3 (prostate cancer) and U-87 (brain cancer). MCF-7 (from ATCC), HeLa and U-87 cells were cultured in

Dulbecco's modified Eagle's medium (DMEM) (incomplete) and PC-3 cells in on RPMI1640(incomplete) (BioWhattaker, Lonza) that was supplemented with 10% FBS (Fetal bovine serum) (Gibco life technologies) and Pen-strep (BioWhattaker, Lonza) to make it a complete media. The cells were grown in about 6mL of complete media in T75 tissue culture flask for about 2 to 3 days for all the cell lines except U87 cells that took upto 4 to 5 days at 37°C in a humidified atmosphere with 5% CO_2 in a Shel Lab incubator until ~70% confluency reached. When cells reach the desired confluence, trypsinisation was done; briefly, cell media in the T75 culture flask was decanted, cells were washed with sterile 1XPBS and media decanted. The cells were trypsinised using 1X trypsin and centrifuged at 3000xg for 3minutes 15ml Eppendorf tubes. The supernatant was removed, and media was added to tubes. Cells were counted using an automated cell counter, and the cells were seeded (100 µL per well) at a density of 1 x 10^5 cells per mL in a 96 well plate and cultured for 24 hours at 37 °C. After 24 hours of incubation, the media was removed, and cells washed with 1XPBS. After that, the cells were treated for another 24 hours with different concentrations of QDs-MPA, QD-GA2 and QD-GA12. The positive control cells were treated with 6% DMSO. After treatment, the spent media was replaced with 100µL fresh media. WST-1 reagent 10µL then added to each well, and the plate was incubated for 4 hours at 37 °C. Absorbance measured at 440 nm and 630 nm, using BMG Labtech Polar Star Omega microplate reader and the experiment was carried in triplicate of experiments. The percentage cell viability calculated as the percentage mean absorbance ratio of treated cells against percentage means absorbance ratio of untreated cells multiplied by 100 as shown in the formula below:

$$\text{Percentage (\%) Cell viability} = \frac{\text{treated cells}}{\text{untreated cells}} \text{ X } 100$$

2.6 Results and discussion

2.6.1 Optical characterisation

The QDs solutions were centrifuged immediately after synthesis to remove impurities and unreacted materials. The UV-vis and PL were used to monitor and confirm the formation of the CdTe QDs, and GA capped nanoparticles respectively. The UV-vis absorption spectra of the QDs-MPA was about 466 nm while for QD-GA2, and QD-GA12 was 453 nm and 455nm respectively as seen Fig2.1

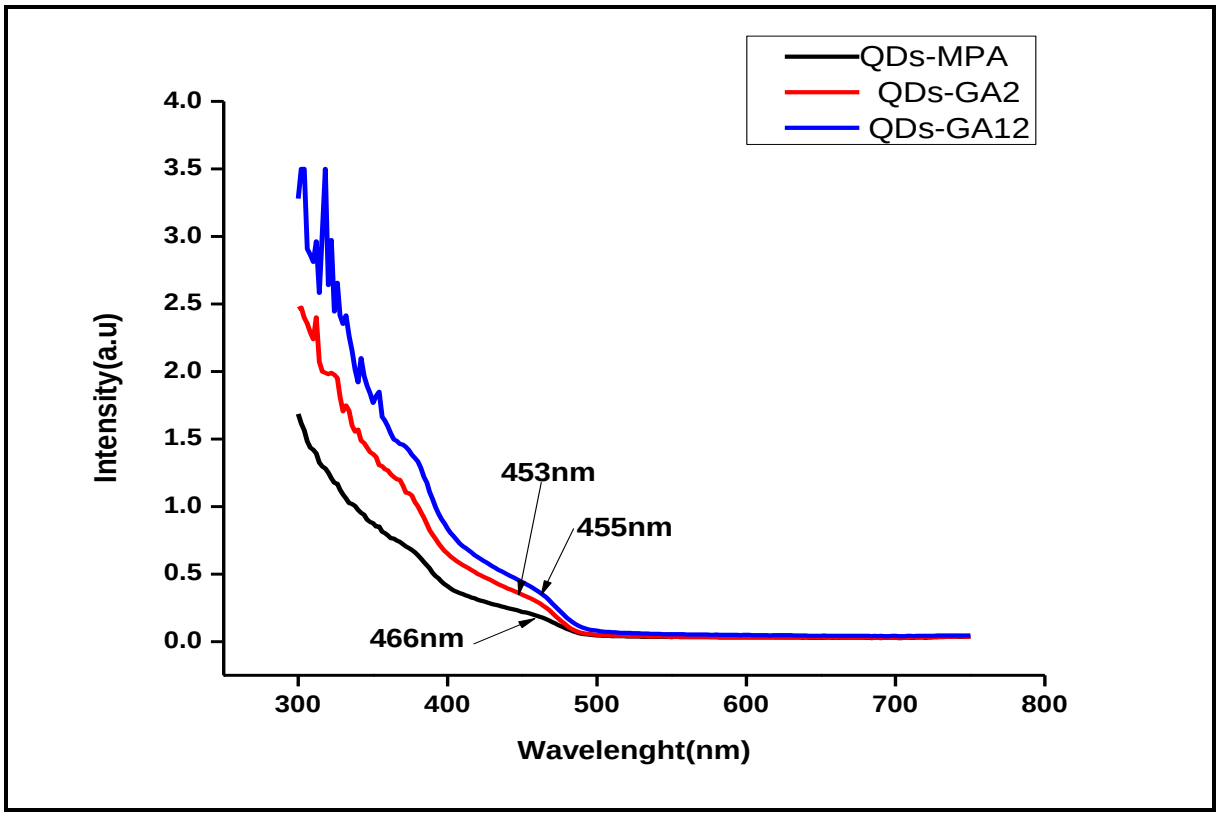

Figure2.1: UV–vis spectra of the QDs-MPA, QDs-GA2 and QDs-GA12

The PL wavelengths and peaks are in agreement with other studies.[8,11] Photoluminescence peak showed a red shift in emission spectra. PL spectra of the QDs-MPA and the GA-capped QDs was in the same range of 676 to 678nm. PL peaks were overlaid, the QDs-GA12 had the highest intensity peak as shown in Figure 2.2. This is probably due to the bigger particle size of QDs-GA12 from TEM analysis (3.9 nm) and hydrodynamic size (77.85 nm).

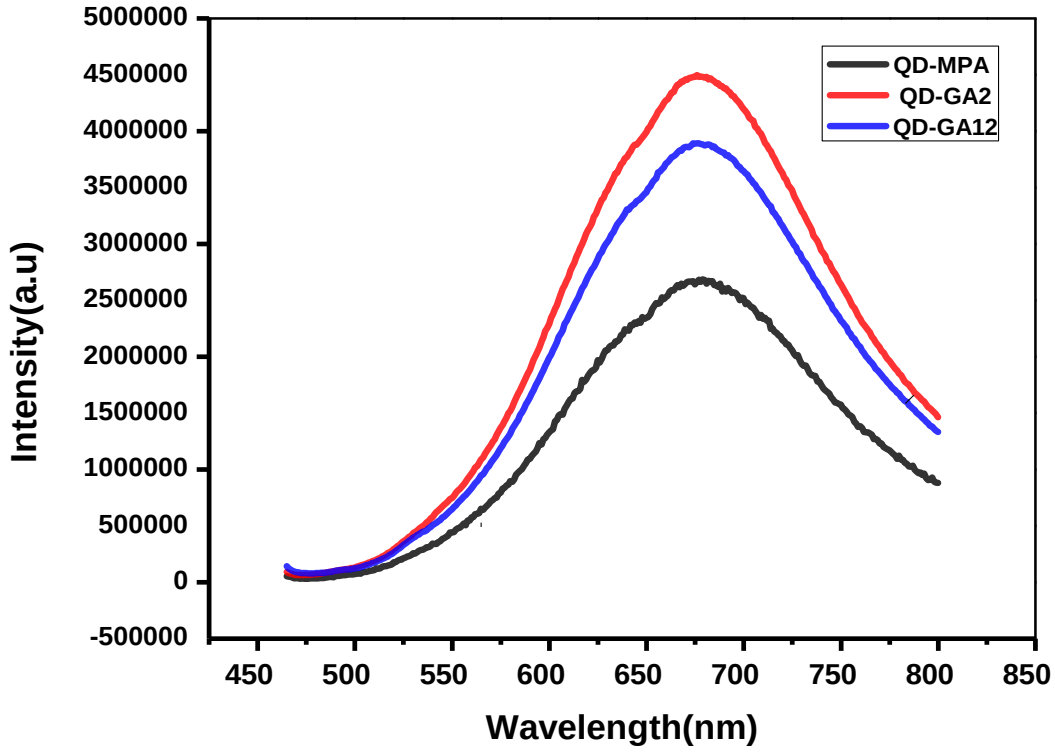

Figure 2.2: The photoluminescence spectrum of the QDs-MPA, QDs-GA2 and QDs-GA12

The full width at half maxima (FWHM) of particles increases with incubation time, and this also depends on the increase in the size of particles.[8] Hence was observed that in the quantum dots synthesized and capped for 12 hours (QD-GA12) at room temperature showed bigger particle sizes and the largest FWHM values for PL spectra, this was followed by the QDs-GA2 and QDs-MPA which were 103.5nm, 93.5nm and 70nm respectively; this is consistent with the increase in size of QDs-GA12 having the most significant particle size**.**

2.6.2 X-Ray Diffraction (XRD) Powder Analysis

This XRD was used to ascertain the crystal nature of the QDs. XRD powder analysis pattern of QDs-MPA, QDs-GA2 and QDs-GA12 are shown in figure2.3 below.

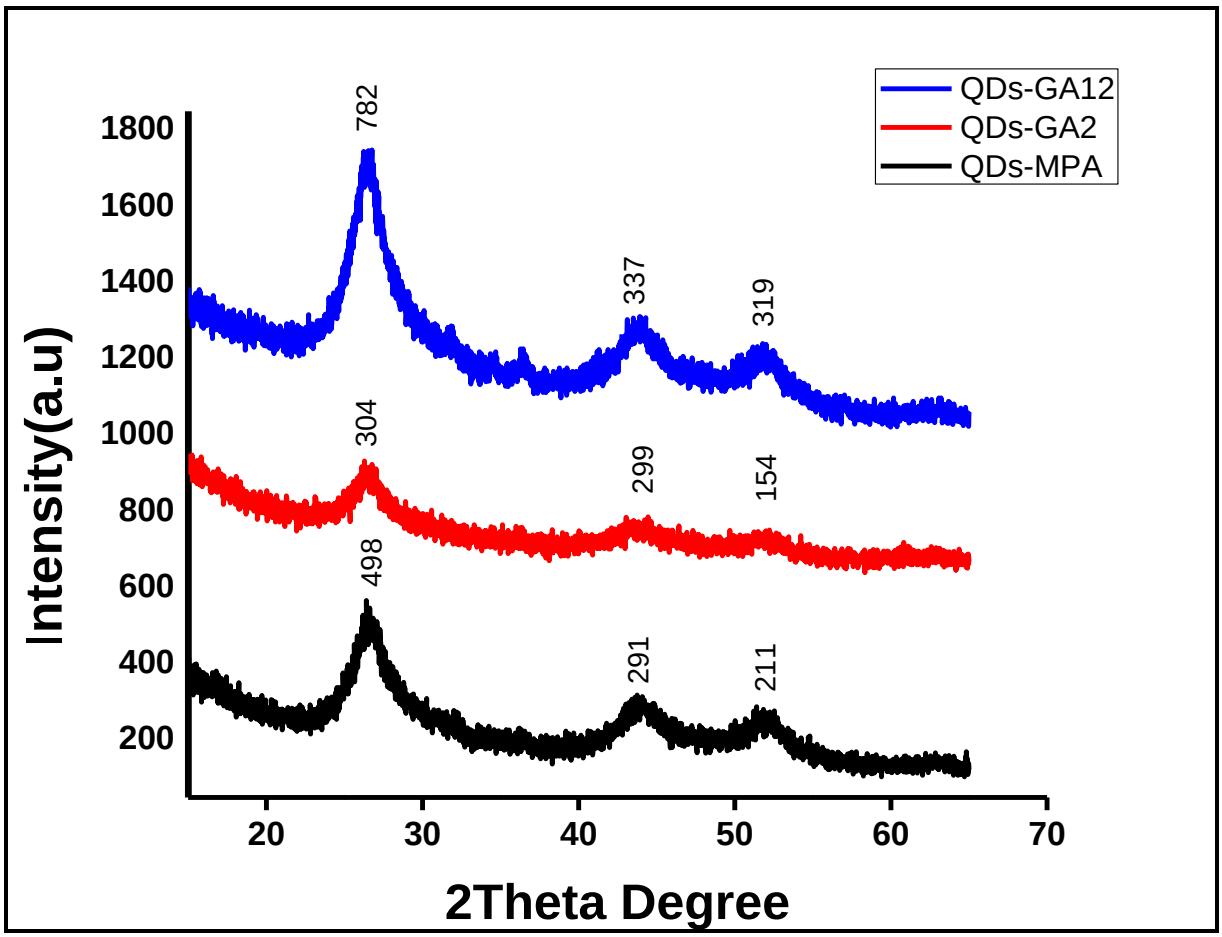

Figure2.3: XRD pattern of the QDs-MPA, QDs-GA2 and QDs-GA12

The figure shows a major distinctive broad peak at 2θ of 26.7, 26.5and 26.52 corresponding to the indices (498), (304) and (782) respectively. The two minor small peaks correspond to 2θdegree; 43.88, 52.02 for QDs-MPA; 43.67, 52.03 for QDs-GA2 and 43.98, 51.91 for QDs-GA12 as shown in (Fig 3). The crystalline cubic phase of the QDs was established, and this corresponds to the cubic CdTe standard pattern (JCPDS card no: 065-1047), similar to the work of.[25] Broad distinctive peaks imply the presence of small-sized nanoparticles.[8,6]

The Derby Scherer equation was also used to calculate the particle size of the quantum dots from the XRD graph

Particle Size (S) = $\frac{k\lambda}{\beta \cos\theta}$

Where S is the size of particles (nm), λ=1.5406Åis a constant which is the wavelength of the X-ray radiation, B = 0.91, β is full width at half maximum (FWHM) of the XRD pattern, θ is the Bragg's angle in degree. The average sizes of the different quantum dots using XRD peaks were; 3.78, 3.97 and 4.2nm for QDs-MPA, QDs-GA2, and QDs-GA12 respectively, these values measure up with the previous data obtained for particle sizes using image J. This observation was then confirmed with HRTEM and particle size analysis.

2.6.3 High-Resolution Transmission Electron Microscope

The CdTe QDs were characterised using HRTEM to determine shape, size and structure. The HRTEM results are shown in fig 2.4c, 2.5c and 2.6c.

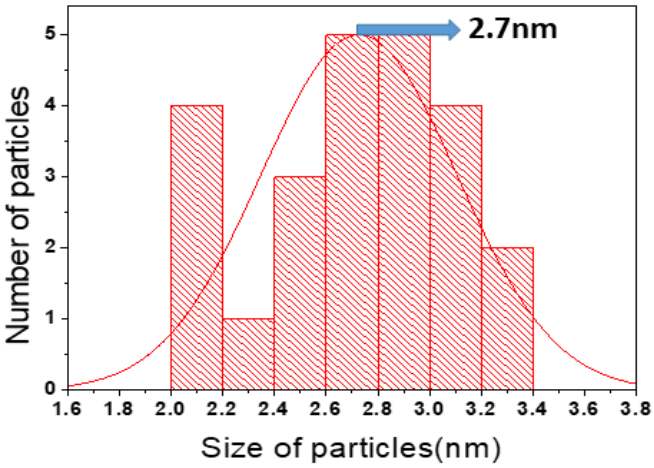

Figure2.4a: Particle size distribution of QDs-MPA

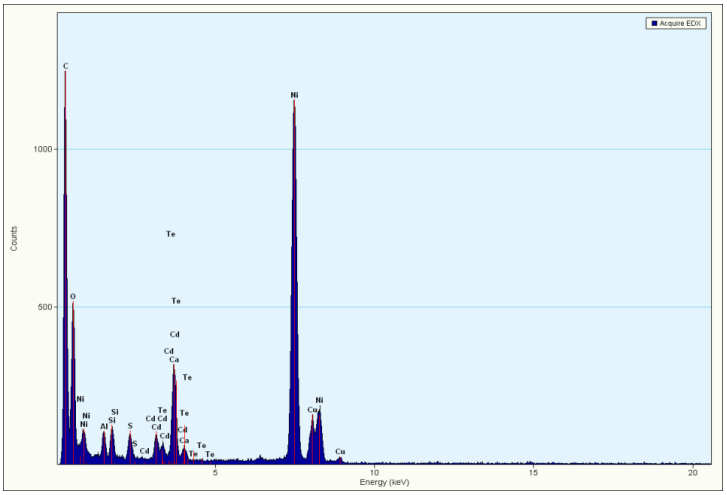

Figure2.4b: EDX Spectra of QDs-MPA

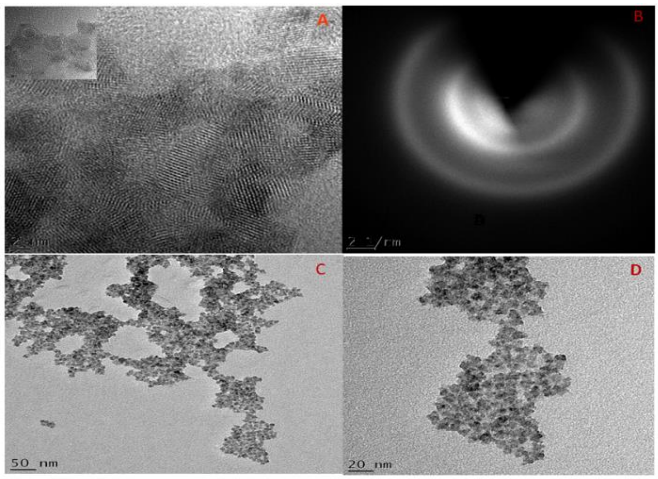

Figure2.4c: HRTEM and SAED images of QDs-MPA

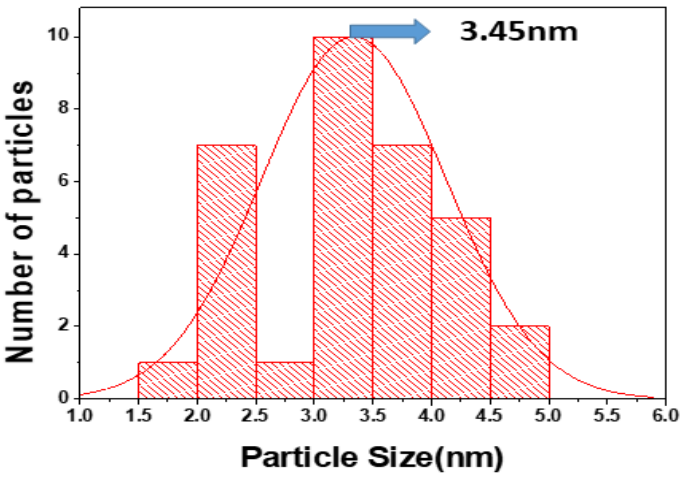

Figure2.5a: Particle size distribution of QDs-GA2

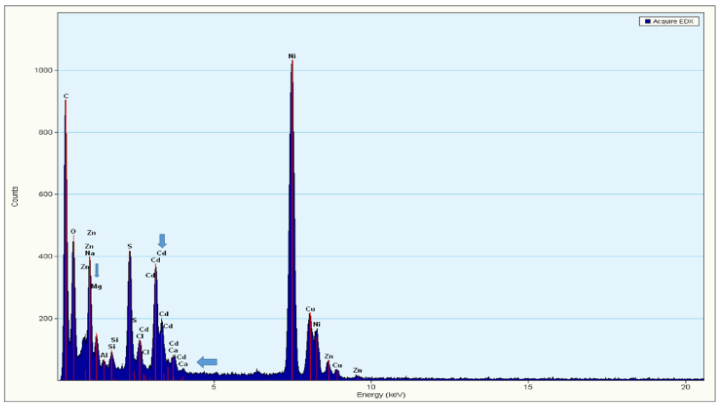

Figure 2.5b: EDS spectra of QDs-GA2

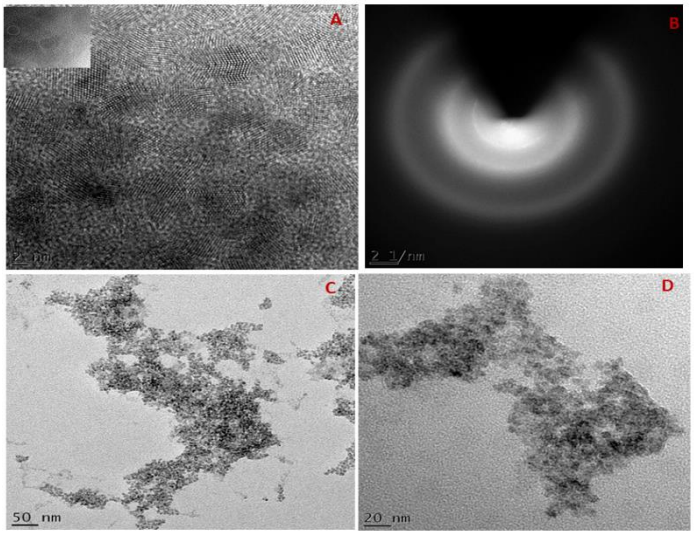

Figure 2.5c: HRTEM and SAED images of QDs-GA2

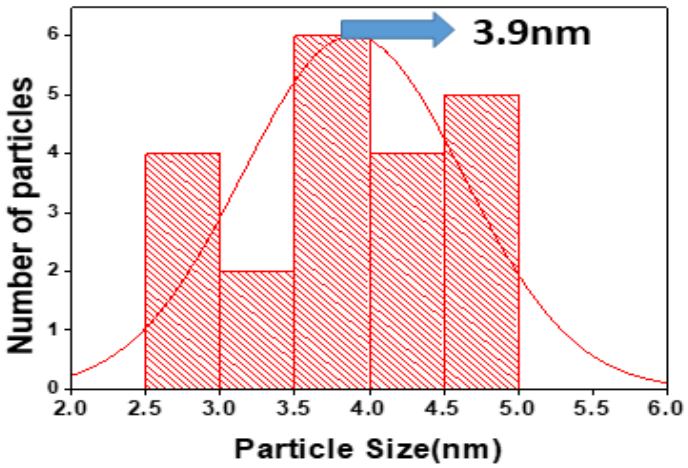

Figure 2.6a: Particle size distribution of QDs-GA12

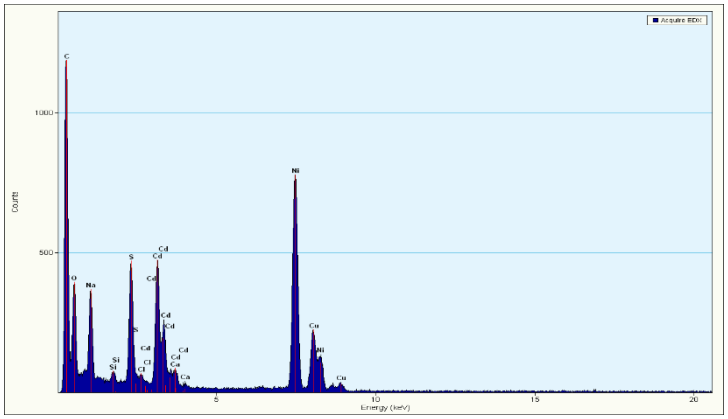

Figure2.6b: EDS spectra QDs-GA12

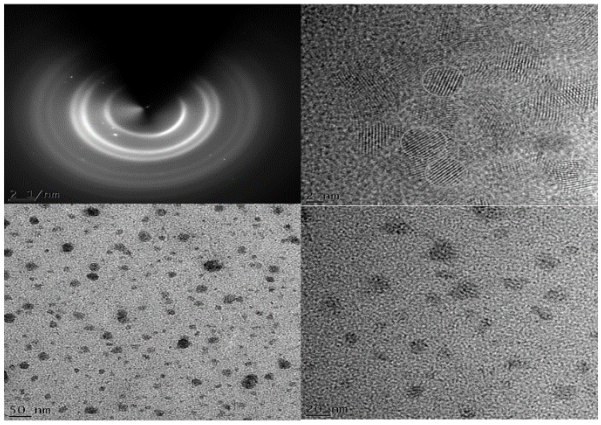

Figure 2.6c: HRTEM and SAED images of QDs-GA12

Image J software was used on the HRTEM images to determine the diameter of the QDs; The average particle size was 2.7nm,3.45nm and 3.9nm for QDs-MPA, QDs-GA2 nad QDs-GA12 respectively. The particle size distribution from image J was presented in fig2.4a, 2.5a and 2.6a for each of the QDs. The QDs were dispersed adequately from HRTEM images. The EDS was used for elemental analysis of the individual elements present in sections of the sample; The spectra show traces of cadmium, tellurium, carbon, oxygen, zinc, sodium and chlorine in the spectra, Fig2.4b, 2.5b and 2.6b for the different QDs respectively. Research has shown that particles capped with polymer tend to have bigger sizes compared to MPA capped particles. This result is consistent with the literature. Also, the difference in the size of the 2hour QDs-GA and QDs-GA12 may probably be due to the effect of temperature on the participles. Fig2.4c, 2.5c and 2.6c showed the HRTEM and SAED images for QDs-MPA, QDs-GA2 nad QDs-GA12 respectively.

2.6.4 Fourier Transform Infrared Spectroscopy (FT-IR)

FTIR analysis shows the functional groups that are present in the compound. The spectroscopy was measured from range of 4000 to 350cm^{-1} range and was used to confirm the capping of QDs with GA polymer, as shown in Fig2.7.

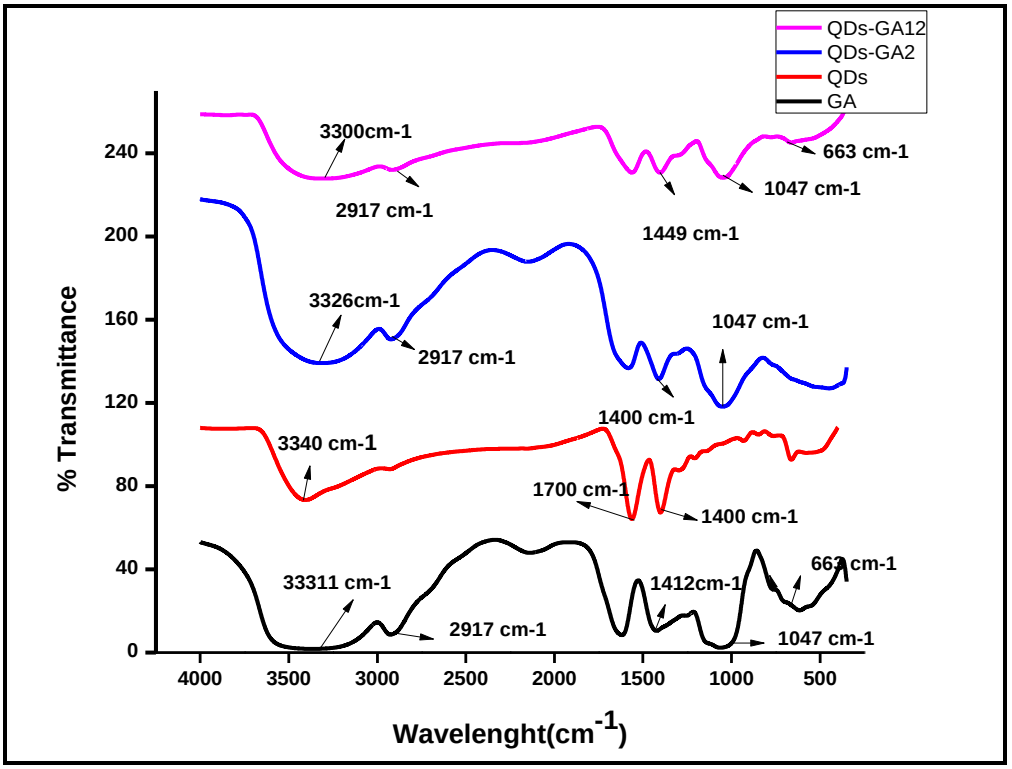

Figure2.7: The FT-IR plot of all three; QDs-MPA, QDs-GA2 and QDs-GA12

The FTIR spectra of the GA powder, QDs and QDs-GA were analysed overlaid and compared. FTIR spectra of GA powder and QDs-GA2 and QDs-GA12 showed similar peaks confirming the capping of the CdTe QDs, the characteristic stretch at 3300 cm^{-1} to 3328cm^{-1} for –OH stretching is attributed to the monosaccharide which makes up the GA polymer possessing some free-OH, [26,27] the band at 2917cm^{-1} stretching is R-CH_2-R found in the GA capped QDs and GA powder. The stretch between 995 cm^{-1} and 1047 $cm^{-1}$are commonly referred to as GA "fingerprint" and represents the C=O and C-N frequencies stretching. There was also aliphatic amine stretching vibration of the arabinogalactan chains of GA [27] at 1290 cm^{-1}which a is a particular band of aliphatic amine. The broad QDs stretch between 3340 cm^{-1} to 3200$cm^{-1}$is O-H associated with acid in the sharp peak at 1700cm^{-1} is assigned to carboxylic acid (R-COOH) associated with the capping mercaptopropionic acid (MPA).[28] Surface chemistry of nanoparticles has some crucial impact on their application biologically.

2.6.5 Zeta Potential, Hyrodynaymic Sizes and Polydispersity Index

The zeta potential of nanoparticles is a vital marker for predicting the long-term stability of nanoparticles in solution and also to determine the surface charge and a high zeta potential values of about ±25 mV to ±60 mV which indicates that the particle is stable.[29] the hydrodynamic particle size and Polydispersity index (PDI) of the QDs was also measured. In each case, measurements were done in triplicate at room temperature at 25^0C, and the average value was obtained. The bar chat distribution of the Zeta potential, PDI and hydrodynamic sizes of the quantum dots are shown in Fig: 2.8 with the bars having different alphabet indicating that they are significantly different from each other.

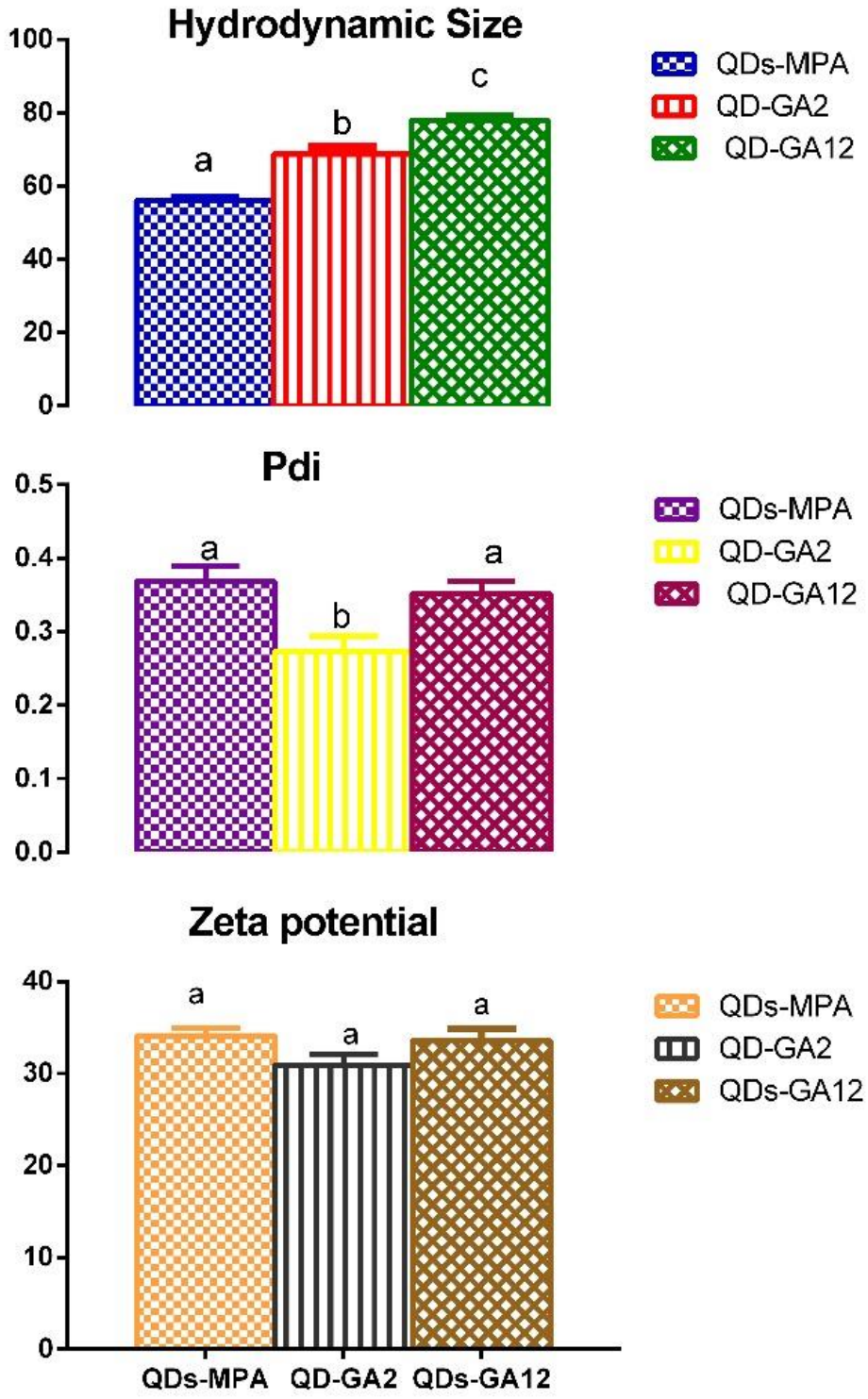

Figure 2.8: Histogram showing the Zeta potential, Polydispersity index (PDI) and hydrodynamic distribution of the different quantum dots.

Zeta potential is an important parameter used to ascertain long-term stability and investigative assessment of the nanoparticles.[30] Zeta potential of the quantum dots was not significantly different from each other and with a mean value of (34.12±0.8), (30.87±1.18) and (33.56±1.3) for QDs-MPA, QDs-GA2 and QDs-GA12 respectively. Particles with zeta potential value of above ±30 are said to be very stable according to literature.[31] The zeta potential of the QDs was above ±30 with QD-GA12 having the highest zeta value and QDs-GA2 having the lowest zeta potential. The number of particle ratio to total number particles present in a solution is termed polydispersity index. The colloid solution with low PDI values of less than one for the particles is said to be monodispersed.[32] The mean PDI values of QDs were (0.37±0.02), (0.27±0.02) and (0.35±0.01) for QDs-MPA, QDs-GA2 and QDs-GA12 respectively. The PDI values of QDs-MPA and QDs-GA12 were not significantly different from each other but differed over p values ($P<0.05$). The hydrodynamic size of the three quantum dots showed significant differences in their sizes with p values of ($P>0.0001$) with a mean value of (56.12 nm ±1.14), (68.69 nm ±2.08) and (77.85 nm ±1.69) for QDs-MPA, QDs-GA2 and QDs-GA12 respectively.

QDs capped with GA polymer had a larger hydrodynamic size which was probably due to the effect of the capping agent. Zeta potential is an essential parameter for ascertaining the long and short-term stability of a material. This substance with high zeta potential values are said to be highly stable and low values tends to coagulate or agglomerate making them unstable. The zeta potential of the QDs were (34.12±0.8), (30.87±1.18) and (33.56±1.3) for QDs-MPA, QDs-GA2 and QDs-GA12 respectively. QDs-MPA and QDs-GA12 had higher zeta potential value when compared to QDs-GA12 which implies these particles are more very stable.

2.7 Cytotoxicity Studies of the Bare and GA capped Quantum Dots

Nanoparticles capped with polymers are presumed to be less toxic compared to those capped with synthetic materials because of the displayed stabilities. Research has shown that water-soluble quantum dots have a low level of toxicity. Fig: 2.9, 2.10, 2.11 and 2.12 showed the cytotoxicity of the MPA and GA capped QDs on selected cancer cell lines after 24-hour exposure.

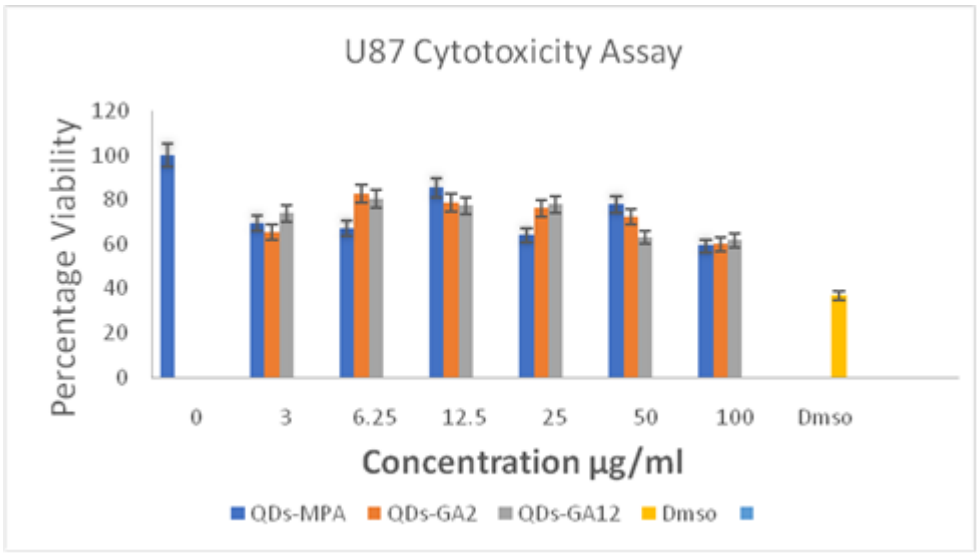

Figure 2.9: Bar chart showing U87 Cytotoxicity assay using QDs-MPA and QDs-GA

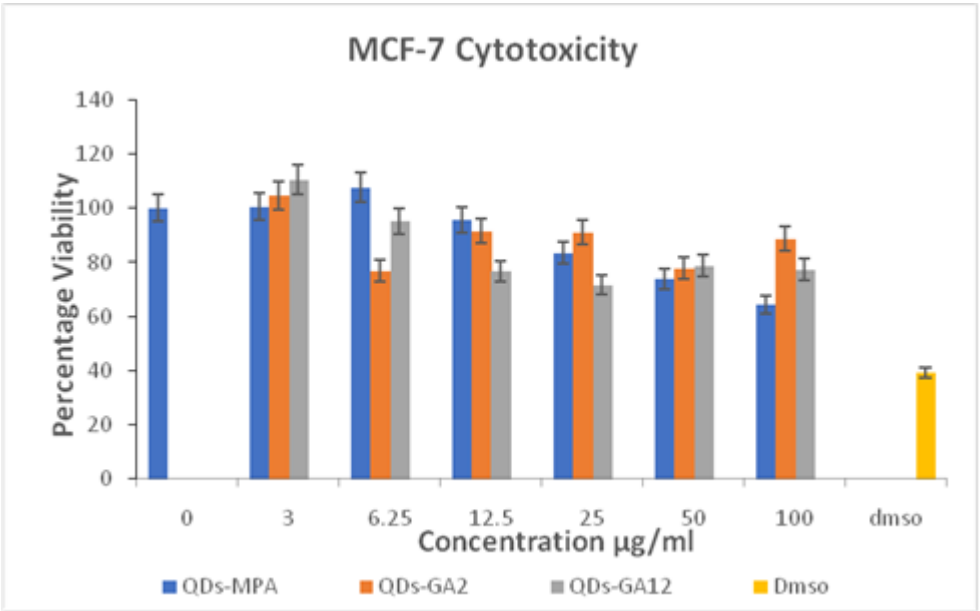

Figure 2.10: Bar chart showing MCF-7 cytotoxicity assay using QDs-MPA and QDs-GA

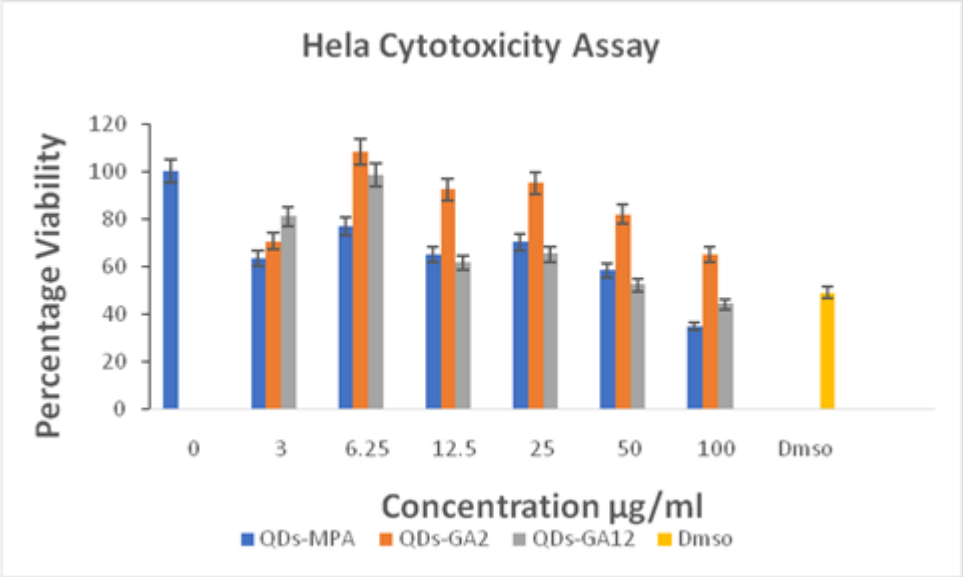

Figure 2.11: Bar chart showing HeLa cytotoxicity assay using QDs-MPA and QDs-GA

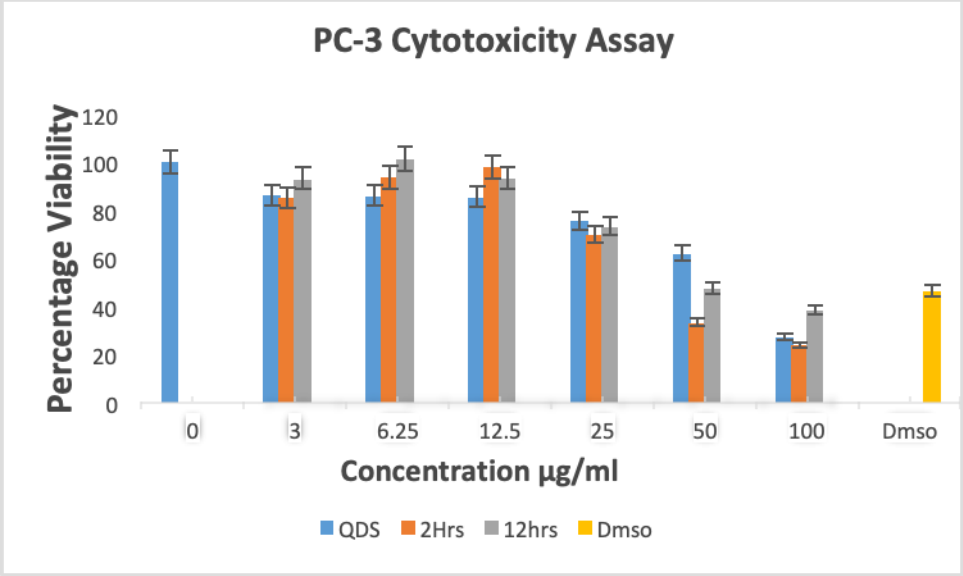

Figure 2.12: Bar chart showing PC-3 cytotoxicity assay using QDs-MPA and QDs-GA

In this study, the viability of QDs was carried out in triplicate, and the average is taken. QDs capped with GA and uncapped were over 50% for all cell lines.

Published literature has shown that quantum dots coated with polymer shows excellent colloidal stability in solution [33-35].

PC-3 cells were very viable for all the concentrations except at 100µg/ml for MPA capped QDs and QDs-GA2 our results were in concordance with other published work [36] in literature. Surface coating plays a vital role in the cytotoxicity of quantum dots. [37,38]

All other cell lines were over 50% viable when compared with control 6% DMSO used in the experiment as control treatment and the toxicity is dose-dependent. For all cell lines especially HeLa and MCF-7, we observed an increase in cell viability at 6.25µg/ml comparable to the untreated cell (0 concentration) probably due to an increase in cell proliferation.

2.8 Conclusion

In this experiment Luminescent CdTe QDs capped with GA was synthesised and capped at two different temperatures (60 degrees for 2 hours and at room temperature for 12hours with continuous stirring).

Capping of nanoparticles with other materials can help to stabilise the particle and provide functional groups. QDs that were capped with GA for 12hours were found to be very stable and monodispersed. Cytotoxicity analyses show the cells were over 50% viable. GA capped QDs were found to be less toxic in a concentration-dependent manner.

We conclude that QDs synthesised from our studies can be potentially serve bio imaging purposes due to their low toxicity and significantly higher cell viability.

2.9 References

1. H. Zhang, Z. Zhou, B. Yang, and Gao, M, *J. Phys. Chem*., B 2003, **107,** 8-13
2. K.C. Nguyen, G.W.William, and F. T. Azam, *Toxicol*, 2013, **306,** 114-123.
3. X. Wu, H. Liu, J. Liu, K.N Haley, J.A.Treadway, J.P. Larson, N.Ge, F. Peale, and M.P. Bruchez, 2003, *Nat. Biotechnol*., ***21,*** 452.
4. T. Jamieson, R. Bakhshi, D. Petrova, R. Pocock, M. Imani, and A.M. Seifalian, 2007, *Biomaterials*, **28**, 4717-4732.
5. A. M Smith, H. Duan, A.M. Mohs, and S. Nie, 2008, *Adv. Drug Deliv. Rev*. ***60***, 1226-1240
6. J. W. Kyobe, E. B. Mubofu, Y.M. Makame, S. Mlowe, and N. Revaprasadu, 2016, Physica E Low Dimens Syst Nanostruct **76**, 95-102..
7. H. Y Ramirez, J. Flórez, and A.S.Camacho, Á. S. 2015, *Phys. Chem. Chem. Phys*, ***17*** 23938-23946.
8. H. Bao, N. Hao, Y. Yang, and D. Zhao, 2010, *Nano. Research*, ***3***, 481-489.
9. J. Weng, X. Song, L. Li, H. Qian, K. Chen, X. Xu, and J. Ren 2006, *Talanta*, ***70***, 397-402.
10. M.A. Walling, J.A. Novak, and J.R. Shepard, 2009, *Int. J. Mol. Sci.* **10,** 441-491
11. L. Li., H. Qian, N. Fang, and J Ren, 2006, *Journal of Luminescence*, **116**, 59-66.
12. P. Mushonga, M.O. Onani, A.M. Madiehe, and M. Meyer, 2013, *Mater. Lett*, **95**, 37-39.
13. V. Kattumuri, K. Katti, S Bhaskaran, E.J. Boote, S.W Casteel, G.M. Fent, D.J. Robertson, M. Chandrasekhar, R. Kannan, and K.V. Katti, 2007, *Small*, ***3,*** 333-341.

14. M. A. Montenegro, M. L. Boiero, L. Valle, and C. D. Borsarelli, 2012, In *Products and applications of biopolymers*. InTech.
15. L. Zhang, F. Yu, A.J Cole, B. Chertok, A.E David, J. Wang, and V.C.Yang, 2009, *The AAPS Journal*, **11**, 693-699.
16. J.S. Djajadisastra, P. Purnamasari and A. Pujiyanto, 2014, *Int. J Pharm. Pharm. Sc*, **6,** 462-465.
17. B. Kang, T. Opatz, K. Landfester, and F. R. Wurm, 2015, *Chem. Soc. Rev*. **44**, 8301-8325
18. R. R. Bhosale, A. S., Kulkarni, S. S Gilda, N. H. Aloorkar, R. A Osmani, and B. R Harkare, 2014, *Int J Pharm. Sci. Nanotech*, **7**, 2328-2337.
19. P. Rauwel, S. Küünal, S. Ferdov, and E. Rauwel, 2015, *Adv. Mater. Sci. Eng*, ***2015*.**
20. S. M. Yakout and A. A. Mostafa, 2015, *Int J Clin Exp Med*, **8**, 3538.
21. J. Chomoucka, J. Drbohlavova, P. Majzlikova, J. Prasek, J. Pekarek, R. Hrdy, and J. Hubalek, 2013, In *Conference proceedings 5th international conference Nanocon*, **1** 566-571.
22. Z.J. Li, X.B. Li., J. J. Wang, S. Yu, C. B. Li, C.H. Tung, and L. Z. Wu, 2013, *Energy Environ. Sci*, **6**, 465-469.
23. P. Yang, A. Zhang, H. Sun, F. Liu, Q. Jiang, X. Cheng, 2010, J. Colloid Interface Sci, **345**, 222-227
24. J. Kim, Y. Park, T.H. Yoon, C.S. Yoon, and k. Choi, 2010, *Aquatic Toxicology*, **97**, *Aquat. Toxicol.* 116-124
25. A. Arivarasan, G. Sasikala, and R. Jayavel, 2014, *Mater Sci Semicond Process*, **25**, 238-243.

26. F. E. Vasile, M. J. Martinez, V. M. P. Ruiz-Henestrosa, M. A., Judis, and M. F Mazzobre, 2016, *Food Hydrocoll*, ***56,*** 245-253.

27. R. C. Quintanilha, E. S. Orth, A. Grein-Iankovski, I.C. Riegel-Vidotti, and M Vidotti, 2014, *J. Colloid Interface Sci*. ***434***, 18-27.

28. Z. Paulsen, M.O. Onani, G.R. Allard, A. Kiplagat, J.O. Okil, F.B Dejene, and G.M. Mahanga, G. M. 2016, *Physica B Condens Matter*, ***480,*** 156-162.

29. M. J. Haider, and M. S. Mehdi, 2014 IJSER, **5**, 381-385.

30. R. Tantra, P. Schulze, and P. Quincey, 2010, *Particuology*, ***8***, 279-285.

31. S. Sharma, P. Shukla, A. Misra, and P.R Mishra, 2014, In *Colloid and Interface Science in Pharmaceutical Research and Development*, 149-172.

32. A.M. Elbagory, C.N. Cupido, M. Meyer, and A. A. Hussein, 2016, *Molecules*, **21**, 1498.

33. M. T. Fernández-Argüelles, A. Yakovlev, R. A. Sperling, C. Luccardini, S. Gaillard, M. Sanz and W.J. Parak, 2007, *Nano Letters*, **7**, 2613-2617.

34. N. Tomczak, R., Liu, and J.G. Vancso, 2013, *Nanoscale*, **5,** 12018-12032.

35. H. M. Xiong, 2010, *J. Mater. Chem*, ***20***, 4251-4262.

36. S. J. Soenen, J. Demeester, S.C De Smedt, and K. Braeckmans, 2012, *Biomaterials*, **33**, 4882-4888.

37. R. Dhar, S. Singh, and A. Kumar, 2015, *Bull. Mater. Sci*, **38**, 1247-1252.

38. H. R. Rajabi, and M. Farsi, 2016, *Mater. Sci. Semicond. Process*, **48**, 14-22

CHAPTER THREE

Stability of QD-MPA and QD-GA CdTe Quantum dots in some biological media

3.1 Introduction

In recent times, there has been an increase in the use of core-shelled nanoparticles like quantum dots because of their applications.

Studying the responses of the interaction of nano-materials with other biological materials can reveal valuable information of their therapeutic applications (Iijima and Kamiya 2009; Hwang *et al.*, 2008; Kumar *et al.*, 2014; Tso *et al*., 2010; Zhang *et al*., 2009). Biologically, stable quantum dots are expected to have a minimum shift in their UV-Vis spectra in buffer or media. The stability of nanoparticles in biological media is an essential property because it is crucial to their application in *invitro* and *invivo* studies (De Barros *et al*., 2016; Elbagory *et al*., 2016; Lazzari *et al*., 2012). Nanoparticles have the propensity to aggregate in biological media, thereby bringing about changes in their physicochemical properties (De Barros *et al*., 2016; Khademi-Azandehi *et al*., 2015; Yu *et al.*, 2017; Hwang *et al*., 2007). Understanding the changes that could occur when these particles are used at different conditions, concentrations and time is essential in determining their applications and possibly their level of toxicity. The stability test is a routine biophysical experiment used to determine the colloidal constancy of nanoparticles (Tejamaya *et al.*, 2012).

This study evaluated the stability of QDs-MPA and QDs-GA quantum dots incubated in three different tissue culture media: Complete Roswell Park Memorial Institute Medium (RMPI 1640) media, Complete Dulbecco's Modified Eagle's medium (DMEM) media and 10 % Fetal Bovine Serum (FBS) and two commonly used buffers in cell biology: 0.5 % Bovine Serum Albumin (BSA) and Phosphate buffer saline (PBS). More so, these experiments were

evaluated at different time points, and UV-Vis spectra were used to monitor their stability over time.

3.2 Experimental design

3.2.1 Materials used

Dulbecco's modified Eagle's medium (DMEM) (BioWhattaker, Lonza), Complete RPMI-1640 (BioWhattaker, Lonza), 10 % Fetal bovine serum (Gibco Life Technologies), Phosphate Buffer (BioWhattaker, Lonza), Bovine Serum Albumin (Roche Diagnostics, Germany), 96-well plates and sterile glass tubes.

3.2.2 Method

The synthesised QDs-MPA, QDs-GA2 and QDs-GA12 were centrifuged for 2 minutes at 4500 rpm using a microcentrifuge to remove impurity and unreacted materials. The quantum dots were after that recovered with ethanol by centrifugation at 4300 rpm for 10 minutes to obtain nanoparticle pellets, after which, they were dried and re-suspended in a distilled water. The QDs *invitro* stability was carried out according to the method of Elbagory *et al.* (2016), with minor modifications. Briefly, an equal volume of QDs solution (100 µL) was incubated with 100µL of either buffer or media in a 96 well plate to make a total volume of 200 µL and set up in triplicates at the same time. After that, the stability of the QDs determined by measuring the changes in the UV-Vis spectra of the nanoparticle solutions at time intervals of 0, 1, 6, 12, 24, and 48 and 360 hours in 10% FBS, complete DMEM, complete RPMI, 0.5 % BSA and PBS buffers.

3.3 Results and Discussion

Studies have shown that nanoparticles capped with polymers are sterically stable (Pavlin and Bregar, 2012; Tejamaya *et al*., 2012). In this study, the effect of four media (Complete DMEM, 0.5% BSA, 10% FBS and complete RPMI) and PBS buffer composition, time and

concentration on the stability of quantum dots capped with MPA (QDs-MPA) and Gum Arabic powder (QDs-GA) was investigated. Ordinarily, nanoparticles that can be applied biologically should show slight or no aggregation in biological media and buffer, hence the need for these biological materials to be stable (Iijima and Kamiya, 2009; Zhang *et al*., 2009). Added to this, several studies in literature alluded to the fact that capping confers stability on nanoparticles, particularly with polymers (Kvitek *et al.,* 2008; Pavlin and Bregar, 2012; Rao and Kulkarni, 2002).

3.4 Stability of QDs-MPA and QDs-GA in 0.5% BSA

In this study, the stability of QD-MPA and QDs-GAs was monitored using UV-Vis spectra over time. Figures 3.1, 3.2 and 3.3 showed the UV spectra of the stability studies of QDs-MPA, QDs-GA2 and QDs-GA12 in 0.5% BSA from 0-360 hours.

As shown in Figure 3.1, there was no shift in the absorbance spectra of QDs-MPA from 0-48 hours, which implies that the nanoparticles were very stable in this medium within this time range. However, there was a notable shift in the spectra of this nanoparticle at 360 hours; which may be indicative of an increase in particle size and agglomeration of the nanoparticles leading to the formation of supramolecular structures (Hrubý *et al.,* 2016; Ling *et al.,* 2009).. Figure 3.2 depicts the stability of QDs-GA2 in 0.5% BSA in which these nanoparticles were displayed to be very stable from 0-48 hours with a slight change at 360 hours, potentially due to an increase in nanoparticle size.

The QDs-GA12 stability in 0.5% BSA was shown as displayed in the spectra of Figure 3.3. It was observed that the nanoparticles followed the same pattern as earlier depicted for QDs-MPA and QDs-GA2 from 0-360 hours, but at 48 hours there was a slight increase in the absorbance spectra upward indicative of an increase in the size of the nanoparticles. It is still not clear why there is a shift in the spectra at 48 hours and not at 360 hours.

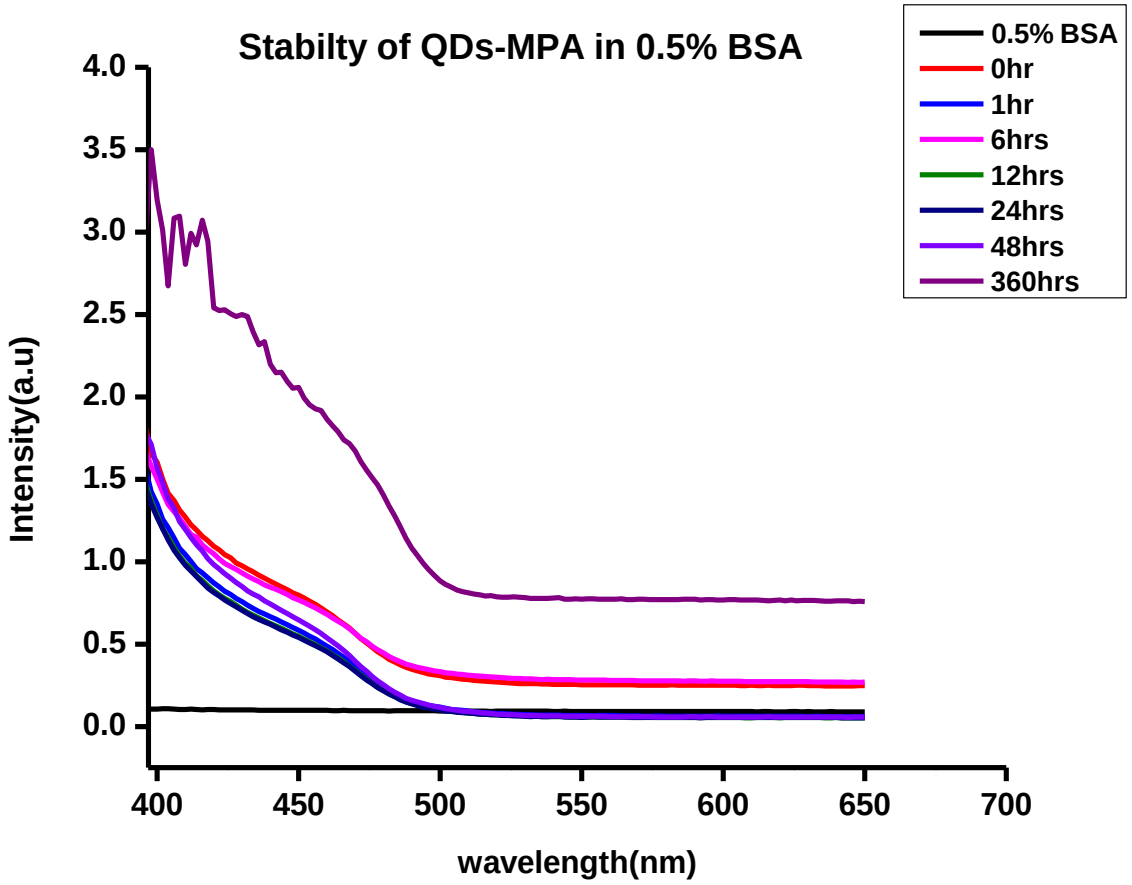

Figure 3.1: Stability of QDs-MPA in 0.5% BSA

U-Vis spectra showing the stability of QDs-MPA at time intervals 0, 1, 6, 12, 24, 48 and 360 hours. The black spectra represent the 0.5% BSA only (control). The spectra showed that the particles were stable from 0-48 hours, but a shift was observed at 360 hours which is indicative of instability probably due to an increase in particle size.

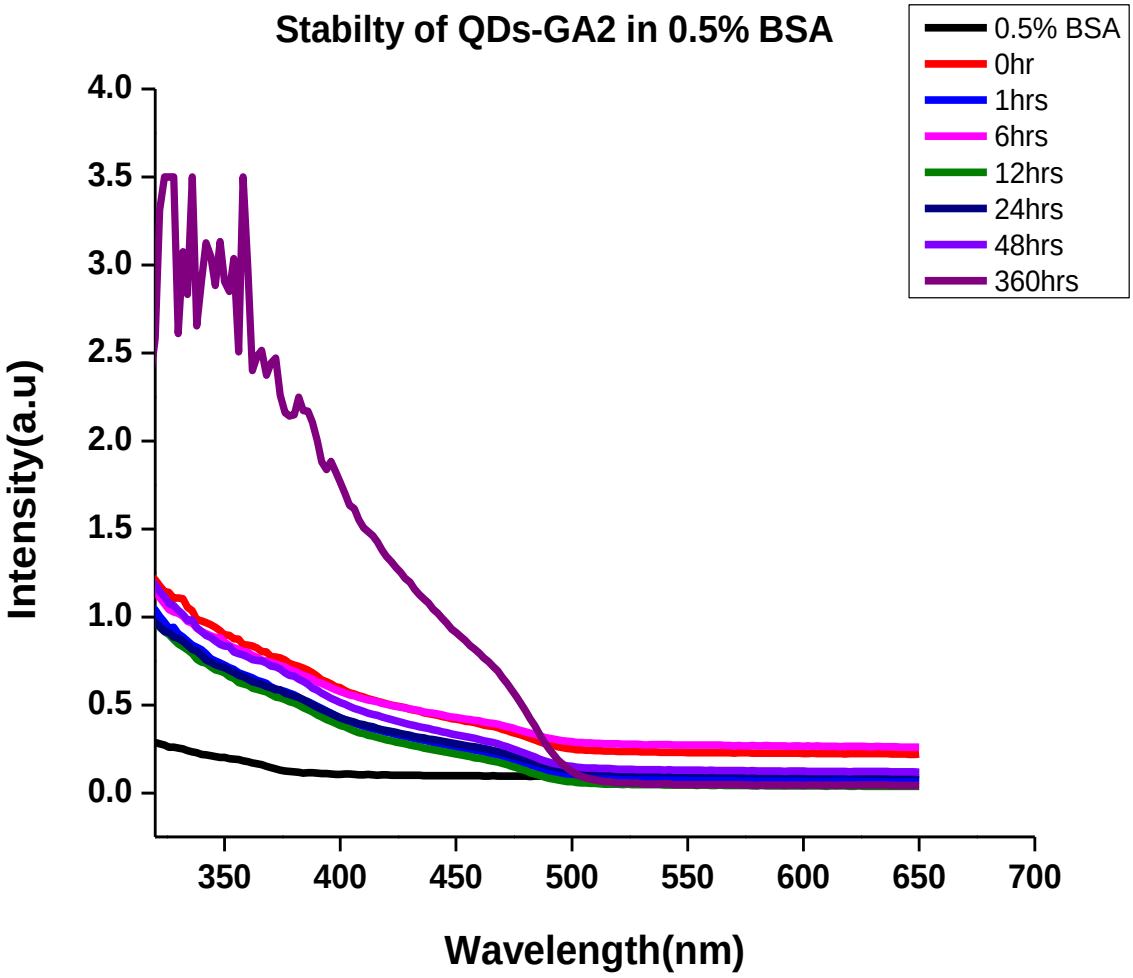

Figure 3.2: Stability of QDs-GA2 in 0.5% BSA:
U-Vis spectra showing the stability of QDs-GA2 at time intervals 0, 1, 6, 12, 24, 48 and 360 hours. The black spectra represent the 0.5% BSA only (control). The spectra of the QDs from 0-48 hours showed the stability of the QDs was not compromised until at 360 hours when there was a slight shift.

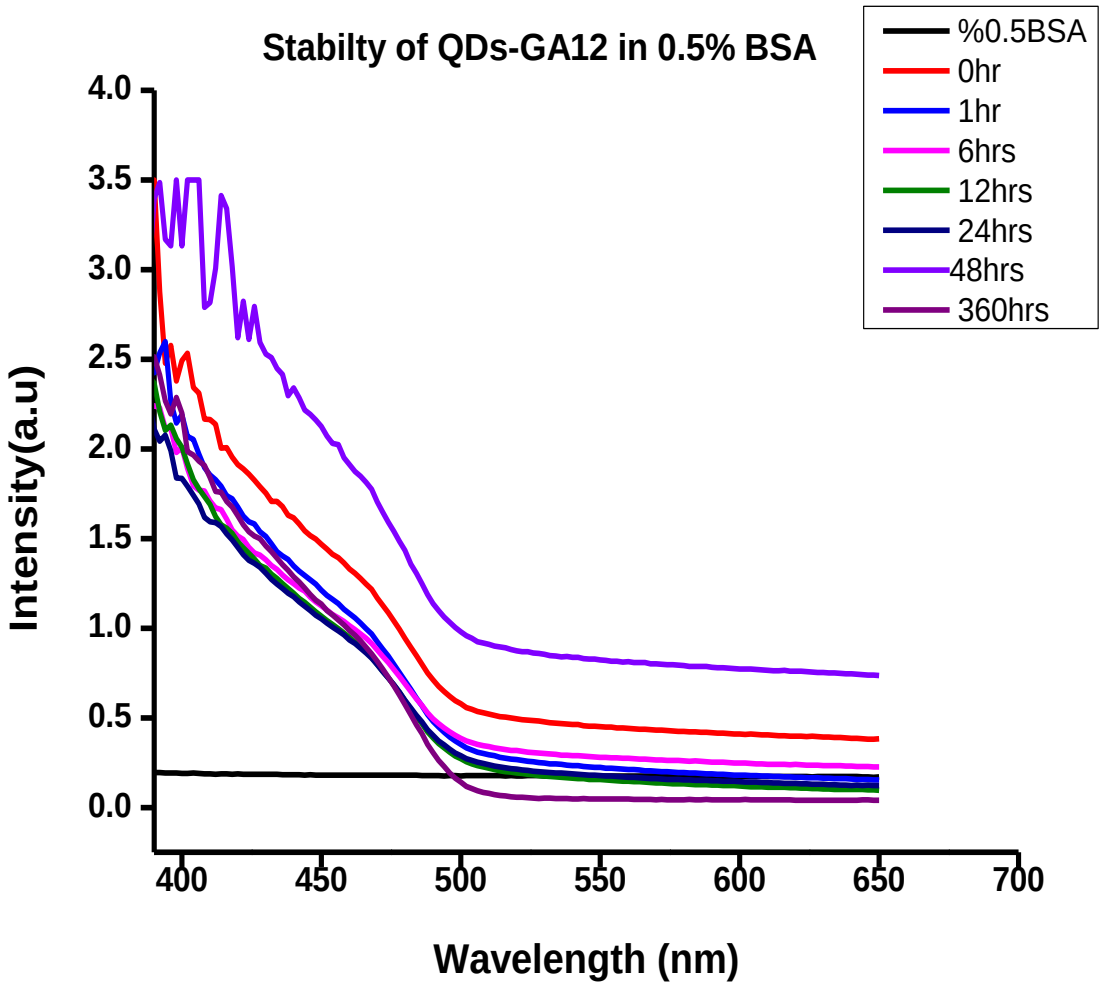

Figure 3.3: Stability of QDs-GA12 in 0.5% BSA:
U-Vis spectra showing the stability of QDs-GA12 at time intervals 0, 1, 6, 12, 24, 48 and 360 hours. The black spectra represent the 0.5% BSA only (control). QDs spectra from 0-24 hours showed that there was no shift signifying that these particles are stable, but there was a slight shift upward at 48 hours. A downward spectra shift at 360 hours was observed and could be indicative of gradual recovery of the QDs at this time interval.

3.5 Stability of QDs-MPA and QDs-GA in DMEM

In Figures 3.4, 3.5 and 3.6, results obtained showed the stability of QDs-MPA, QDs-GA2 and QDs-GA12 quantum dots in DMEM. The spectra in Figure 3.4 revealed that there is a gradual shift in spectra with time between 0-360 hours, confirming a time-dependent increase in the size of quantum dots. It is possible that the spectral absorbance from DMEM interferes with that of the nanoparticles. The absorbance of the nanoparticles shown in Figures 3.5 (QDs-GA2) and 3.6 (QD-GA12) when dissolved in DMEM also shows there is a gradual shift in spectra to the right with an increase in time, suggesting an increase in nanoparticle sizes. Additionally, both quantum dots showed a very noticeable broad shift at 360 hours, which may be due to aggregation as the QDs grow in size.

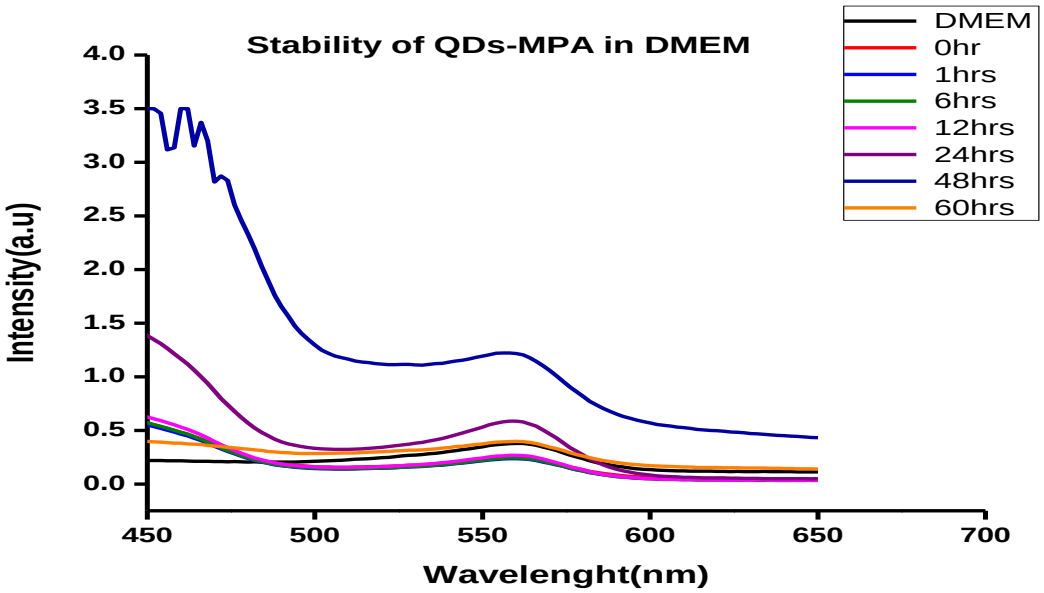

Figure 3.4: Stability of QDs-MPA in DMEM:
U-Vis spectra showing the stability of QDs-MPA at time intervals 0, 1, 6, 12, 24, 48 and 360 hours. The black spectra represent the DMEM buffer only (control). The spectra showed that there is a gradual shift in spectra with time, which may be due to the DMEM absorbance interfering with the absorbance of the nanoparticles from 0-360 hours but a notable shift was observed at 48hour.

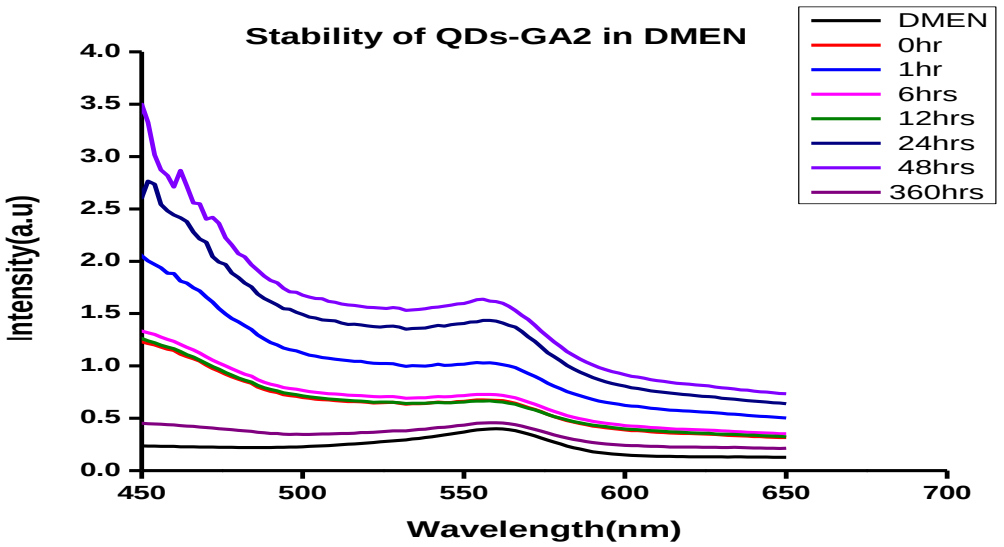

Figure 3.5: Stability of QDs-GA2 in DMEM:
U-Vis spectra are showing the stability of QDs-GA2 at various time intervals 0, 1, 6, 12, 24, 48 and 360 hours. The black spectra represent the DMEM media only (control). The spectra showed that there is a gradual shift in spectra with time it can vary due in DMEM absorbance interfering with the absorbance of the nanoparticles from 0-360 hours.

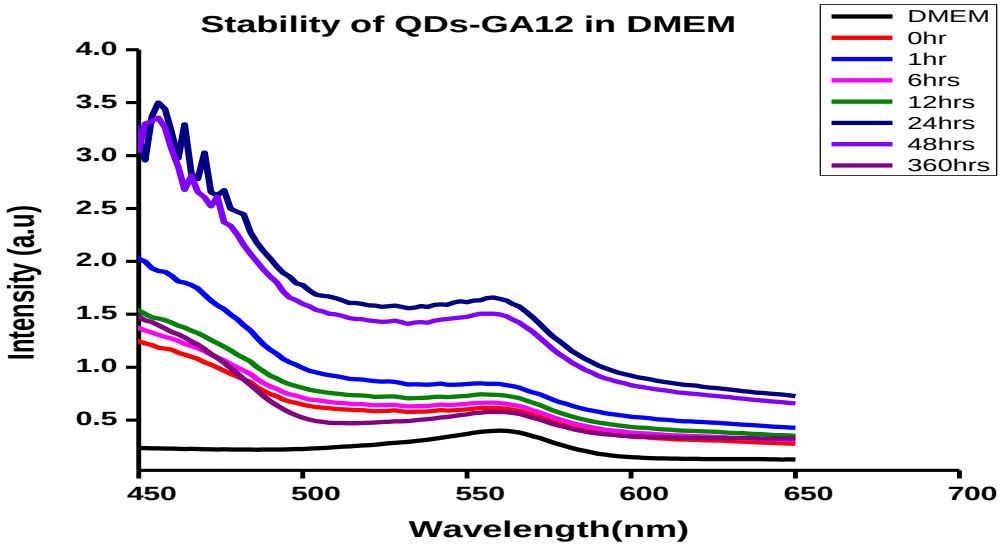

Figure 3.6: Stability of QDs-GA12 in DMEM:
U-Vis spectra are showing the stability of QDs-GA12 at various time intervals 0, 1, 6, 12, 24, 48 and 360 hours. The black spectra represent the DMEM media only (control). There is a gradual shift in the absorbance of the spectra of the QDs with time, which may be due to the absorbance of the DMEM interfering with the absorbance of the nanoparticles from 0-360 hours.

3.6 Stability of QDs-MPA and GA-QDs in 10% FBS

The stability of QDs-MPA, QDs-GA2 and QDs-GA12 in 10 % FBS were depicted in Figures 3.7, 3.8 and 3.9 respectively. Figure 3.7 showed very uniform QDs spectra which reflect the stability of the QDs between 0-48 hours with a slight shift at 360 hours. Conversely, the absorbance spectra of the QDs-GA2 shown in figure 3.8 revealed there was no shift in the QDs absorbance spectra from the beginning of the stability experiment at 0 hours through to 360 hours. More so, the same pattern of spectral absorbance is depicted in Figure 3.9, whereby the QDs-GA12 showed uniform absorbance spectra at all the time intervals revealing the uniform stability of the QDs from 0-360 hours.

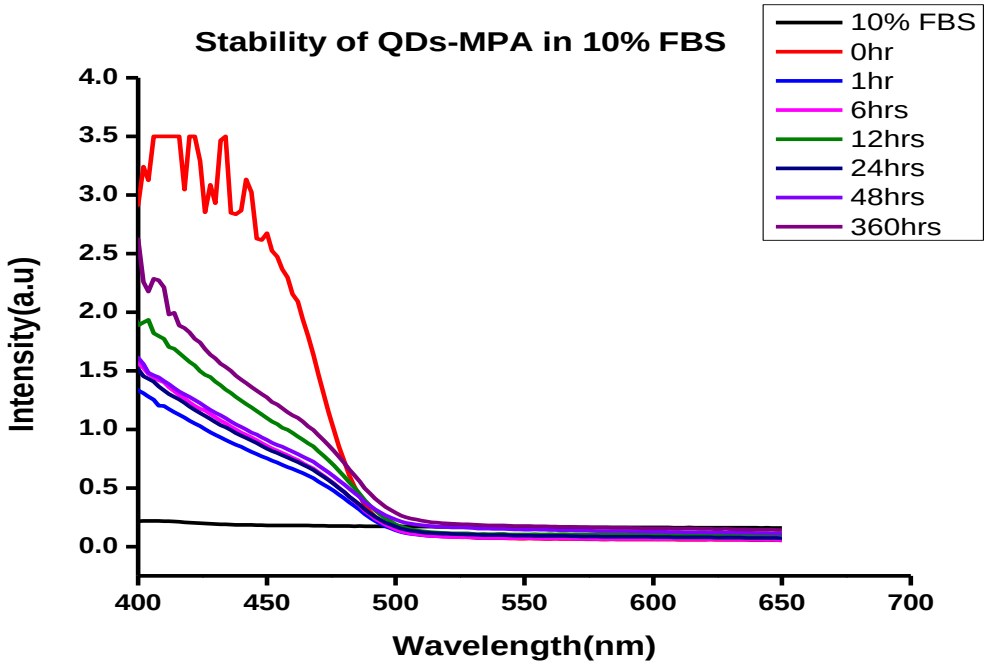

Figure 3.7: Stability of QDs-MPA in 10% FBS:
U-Vis spectra showing the stability of QDs-MPA at time intervals 0, 1, 6, 12, 24, 48 and 360 hours. The flat black spectra represent the 10% FBS only (control). The figure showed that the QDs spectra were very uniform indicative of the stability of the QDs at 0 – 48 hours with a slight shift noticeable at 360 hours.

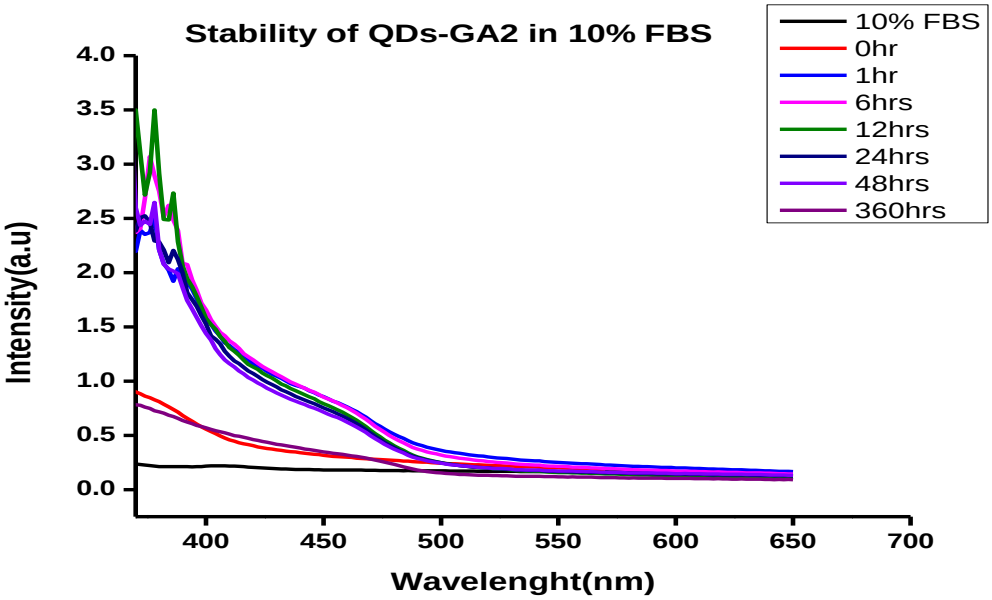

Figure 3.8: Stability of QDs-GA2 in 10% FBS:
U-Vis spectra showing the stability of QDs-GA2 at time intervals 0, 1, 6, 12, 24, 48 and 360 hours. The flat black spectra represent the 10% FBS only (control). The figure showed that the QDs spectra were very uniform revealing the stability of the QDs at 0-360 hours.

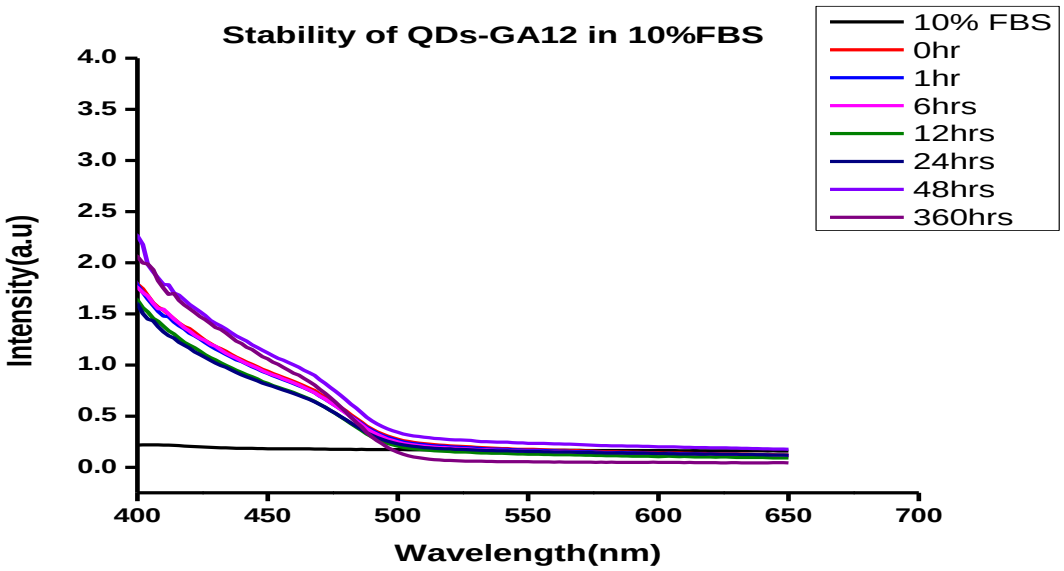

Figure 3.9: Stability of QDs-GA12 in 10% FBS:
U-Vis spectra showing the stability of QDs-GA12 at time intervals 0, 1, 6, 12, 24, 48 and 360 hours. The flat black spectra represent the 10% FBS only (control). The figure showed that the QDs spectra were very uniform revealing the stability of the QDs at 0-360 hours.

3.7 Stability of QDs-MPA and QDs-GA in PBS

Furthermore, Figure 3.10 depicts the absorbance spectra of QD-MPA in PBS showing the QDs spectra were very uniformly stable between 0-12 hours, a noticeable slight shift between 24-48 hours indicative of a gradual increase in particles size, but with a noticeable shift at 360 hours. Conversely, the QDs-GA2 in PBS absorbance spectra reflect in figure 3.11 wherein the QDs spectra absorbance were at the same wavelength showing that the QDs from 0-360 hours were very uniformly stable and that the particle sizes remain the same. The QD-GA12 dissolved in PBS (shown in Figure 3.12) displayed QDs spectra absorbance at the same wavelength between 0-48 hours showing the very uniform stability of the QDs within the periods, but a very noticeable shift at 360 hours reflecting aggregation due to increase in particle size(Elbagory *et al.*, 2016; Krutyakov *et al.,* 2008; Khademi-Azandehi *et al.,* 2015).

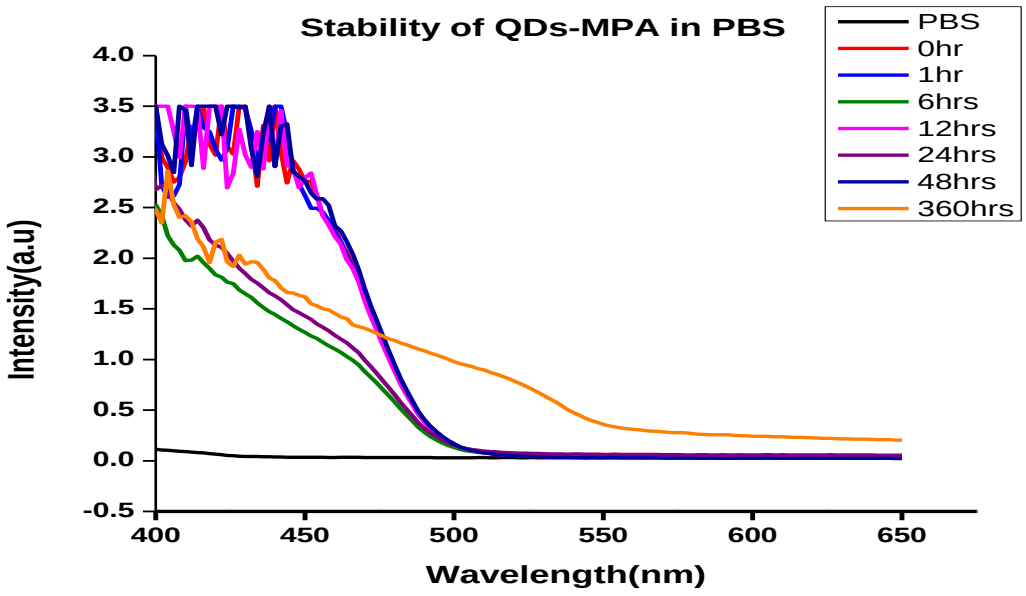

Figure 3.10: Stability of QDs-MPA in PBS:
U-Vis spectra are showing the stability of QDs-MPA at time intervals of 0, 1, 6, 12, 24, 48 and 360 hours. The flat black spectra represent the PBS buffer only (control). The figure showed that the QDs spectra were very uniform revealing the stability of the QDs at 0-48 hours, but a noticeable shift is seen at 360 hours.

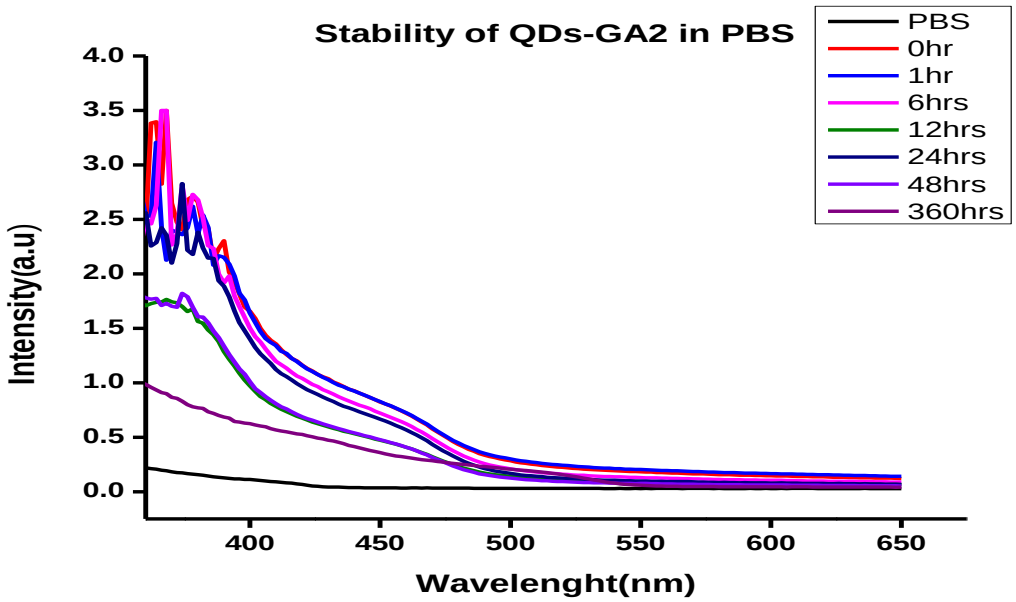

Figure 3.11: Stability of QDs-GA2 in PBS:
U-Vis spectra showing the stability of QDs-GA2 at a time interval of 0, 1, 6, 12, 24, 48 and 360 hours. The flat black spectra represent the PBS buffer only (control). The figure showed the QDs spectra were very uniform showing the stability of the QDs at 0-360 hours.

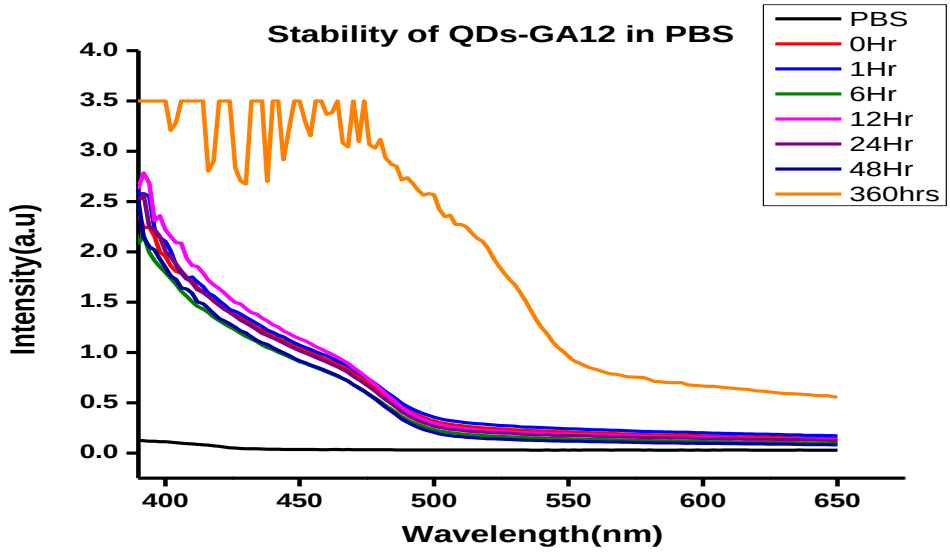

Figure 3.12: Stability of QDs-GA12 in PBS:
U-vis spectra are showing the stability of QDs-GA12 at time intervals of 0, 1, 6, 12, 24, 48 and 360 hours. The flat black spectra represent the PBS buffer only (control). The figure showed that the QDs spectra were very uniform revealing the stability of the QDs between 0 – 48 hours, but with a very bulging shift at 360 hours which may be due to time-dependent particle size aggregation.

3.8 Stability of QDs-MPA and QDs-GA in RPMI

In Figure 3.13, the QDs-MPA particle spectra showed absorbance at the same wavelength from 0-48 hours, which implies the particles were very stable. However, at 360 hours, the presence of a very prominent spectra shift suggestive of aggregation or an increase in particle size can be observed. Additionally, the QDs-GA2 spectra shown in Figure 3.14 presents uniform QDs spectra between 0-48 hours suggesting these particles are stable in this media, but a flattened spectrum at 360 hours as seen in the control spectra could be an indication of loss quantum dots. Figure 3.15 showed that the QDs spectra were very stable with the same absorbance at 0-48 hours but shifted at 360 hours probably due to particle size increase (Elbagory *et al*., 2016).

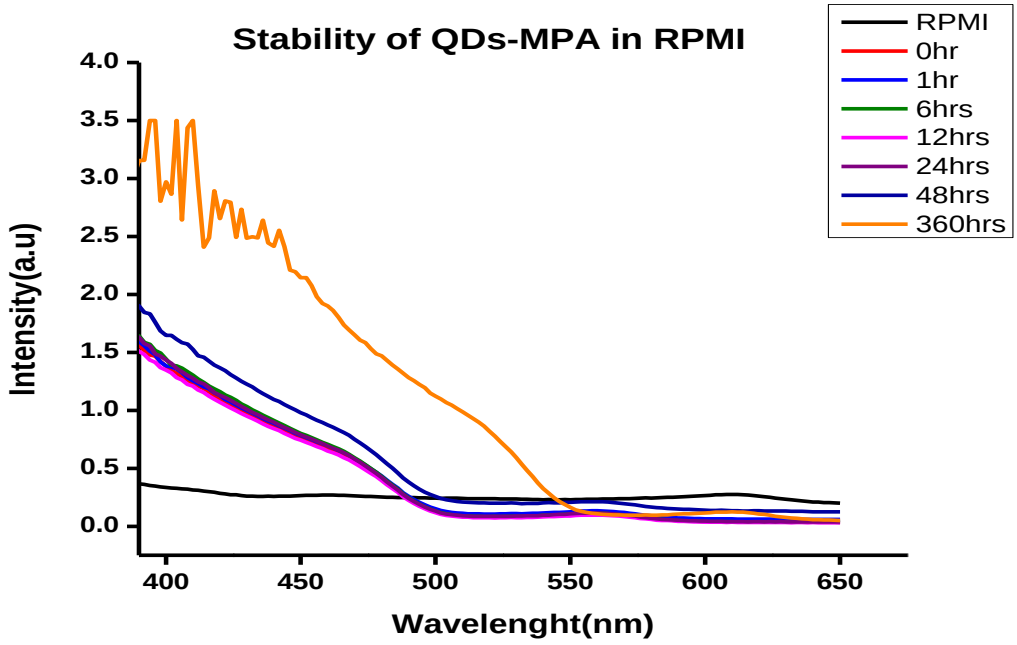

Figure 3.13: Stability of QDs-MPA in RPMI:
U-Vis spectra are showing the stability of QDs-MPA at time intervals of 0, 1, 6, 12, 24, 48 and 360 hours. The flat black spectra represent RPMI only (control). These nanoparticle spectra showed they were very stable from 0-48 hours, but at 360 hours, a noticeable spectra shift which may be due to aggregation or an increase in particle size is observed.

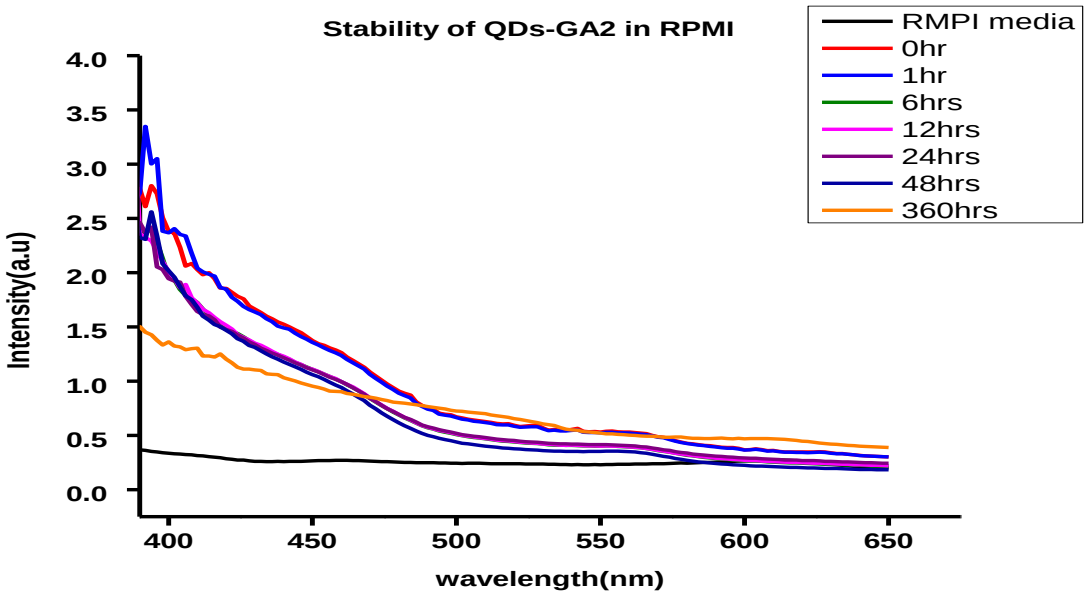

Figure 3.14: Stability of QDs-GA2 in RPMI:
U-Vis spectra are showing the stability of QDs-GA2 at various time intervals of 0, 1, 6, 12, 24, 48 and 360 hours. The flat black spectra represent RPMI only (control). The figure showed that the QDs spectra were very uniform and stable even at 360 hours as against the control spectrum.

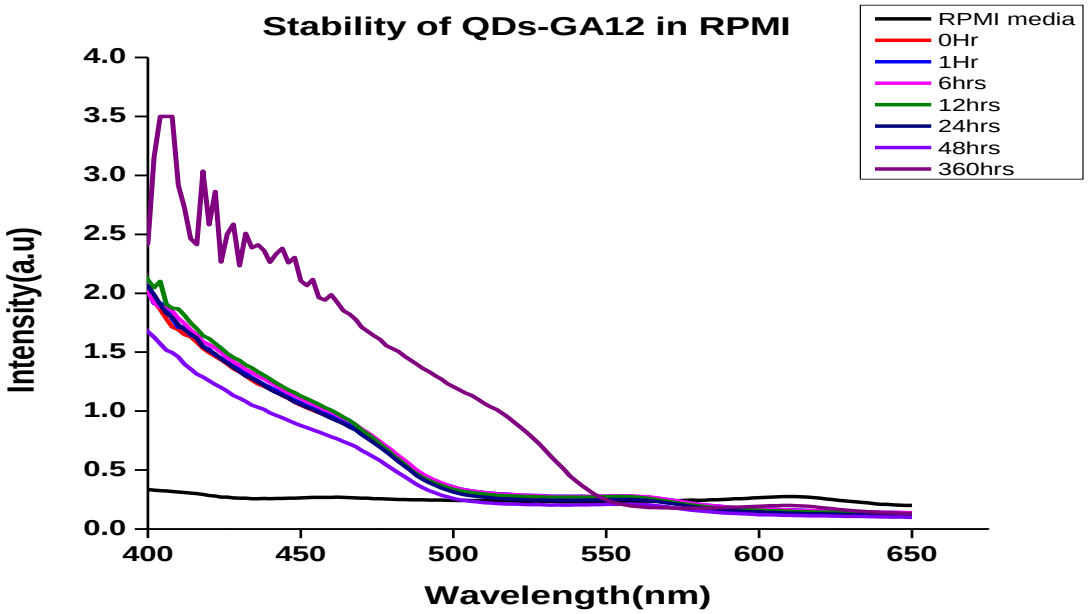

Figure 3.15: Stability of QDs-GA12 in RPMI:
U-Vis spectra are showing the stability of QDs-GA12 at various time intervals of 0, 1, 6, 12, 24, 48 and 360 hours. The flat black spectra represent RPMI only (control). The figure showed the QDs spectra were very stable with the same absorbance between 0-48 hours but with a significant shift at 360 hours.

3.9 Conclusion

In conclusion, this experiment investigated the stability of CdTe quantum dots capped with MPA and GA in a buffer and four different media. We observed that most of the quantum dots were very stable for 48 hours except in figure 3.3 and figure 3.10 that showed a shift in absorbance spectra at this period. Moreover, most of the QDs showed spectra shift at 360 hours indicating an increase in particles size due to particle aggregation (Elbagory *et al*., 2016). Interestingly, Figure 3.14 at 360 hours showed a flat spectrum as seen in the control; this could be indicating a loss in quantum dots particles (Elbagory *et al*., 2016; DeBarros *et* al., 2016). On the whole, the results of this stability study showed that the GA polymer-capped particles are very stable and this is in agreement with literature as seen in other similar studies (Tejamaya *et al*., 2012; Pavlin *et al*., 2012) that nanoparticles capped with polymers exhibit uniform steric stability.

3.10 References

De Barros H.R., Cardoso M.B., de Oliveira C.C., Franco C.R..C, de Lima Belan D., Vidotti M., Riegel-Vidotti I.C. (2016). Stability of Gum Arabic-gold nanoparticles in physiological simulated pHs and their selective effect on cell lines. *Royal Society Chemistry Advance.* **6**(12): 9411-9420.

Elbagory A. M., Cupido C. N., Meyer M. and Hussein A. A. (2016). Large-scale screening of Southern African plant extracts for the green synthesis of gold nanoparticles using microtitre-plate method. *Molecules* **21**(11): 1498.

Hwang Y., Lee J. K., Lee J. K., Jeong Y. M., Cheong S. I., Ahn Y. C. and Kim, S. H. (2008). Production and dispersion stability of nanoparticles in nanofluids. *Powder Technology* **186**(2):145-153.

Iijima M. and Kamiya H. (2009). Surface modification for improving the stability of nanoparticles in liquid media. *KONA Powder and Particle Journal* **27:**119-129.

Labille J and Brant J. (2010). Stability of nanoparticles in water. *Nanomedicine.* **5**(6)985-998.

Lazzari S., Moscatelli, D., Codari F., Salmona M., Morbidelli M. and Diomede L. (2012). Colloidal stability of polymeric nanoparticles in biological fluids. *Journal of Nanoparticle Research* **14**(6): 920.

Shankar S., Rai A., Ahmad A., Sastry M. (2004). Rapid synthesis of Au, Ag, and bimetallic Au core-Ag shell nanoparticles using Neem (Azadirachta indica) leaf broth. *Journal of Colloid Interface Science*. **275**:496-502.

Tso C.P., Zhung C.M., Shih Y.H., Tseng Y.M., Wu S.C. and Doong, R.A., 2010. Stability of metal oxide nanoparticles in aqueous solutions. *Water science and technology* **61**(1): 127-133.

Kumar A., Das S., Munusamy P., Self W., Baer D. R., Sayle D. C. and Seal S. (2014). Behaviour of nanoceria in biologically relevant environments. *Environmental Science: Nano* **1**(6): 516-532.

Khademi-Azandehi P and Moghaddam J. (2015). Green synthesis, characterisation and physiological stability of gold nanoparticles from Stachys lavandulifolia Vahl extract. *Particuology*. **19**:22-6.

Kvitek L., Panáček A., Soukupova J., Kolář M., Večeřová R., Prucek R., Holecova M. and Zbořil R. (2008). Effect of surfactants and polymers on stability and antibacterial activity of silver nanoparticles (NPs). *Journal of Physical Chemistry* **115**(1): 5825–5834.

Krutyakov Y.A., Kudrinskiy A.A., Olenin A.Y., Lisichkin G.V. (2008). Synthesis and properties of silver nanoparticles: advances and prospects. *Russian Chemical Review*. **77** (3):233-57.

Ling XY, Reinhoudt DN, Huskens J. (2009) From supramolecular chemistry to nanotechnology: assembly of 3D nanostructures. *Pure and Applied Chemistry*. **81**(12):2225-33.

Pavlin, M. and Bregar, V. B. (2012). Stability of nanoparticle suspensions in different biologically relevant media. *Digest Journal of Nanomaterials and Biostructures* **7**(4).

Tejamaya M, Romer I, Merrifield RC, Lead JR. Stability of citrate, PVP, and PEG-coated silver nanoparticles in ecotoxicology media. Environ Sci. tech 2012; 46(13): 7011-7017. doi.10.1021/es2038596

Rao A. V. and Kulkarni, M. M. (2002). Hydrophobic properties of TMOS/TMES-based silica aerogels. *Materials Research Bulletin* **37**(9): 1667-1677.

Sharma V.K., Siskova K.M., Zboril R., Gardea-Torresdey J.L.(2004). Organic-coated silver nanoparticles in biological and environmental conditions; fate, stability and toxicity. Advances in Colloid and Interface Science. 204:15-34.

Shankar S., Rai A., Ahmad A. and Sastry M. (2004). Rapid synthesis of Au, Ag, and bimetallic Au core-Ag shell nanoparticles using Neem (Azadirachta indica) leaf broth. Journal of *Colloid and Interface Science*. **275**:496-502.

Yu F., Chen Y., Liang X., Xu J., Lee C., Liang Q., Tao P., Deng T. (2017). Dispersion stability of thermal nanofluids. *Journal of Progress in Natural Science*. **27**(5):531-42.

Zhang Y., Chen Y., Westerhoff P. and Crittenden J. (2009). Impact of natural organic matter and divalent cations on the stability of aqueous nanoparticles. *Water Research **43***(17): 4249-4257.

CHAPTER FOUR

Cell Binding Studies and Immunocytochemistry Assay

4.1 Introduction

Globally, cancer remains one of the leading public health problems (Siegel *et al.*, 2017), it causes over 9 million deaths yearly, and about 10 million new cases (WHO Report, 2015). When the disease is discovered early and treated, it increases the rate of survival. Presently, chemotherapy, surgery and radiation are the primary treatment option for cancer (Arvizo *et al*., 2010). However, they are associated with some side effects. It is therefore imperative that modern technologies for treatment and early diagnosis emerge (Arvizo *et al*., 2010). Several disciplines like chemistry, material science and clinical studies are now involved in the fight against cancer, especially in the area of diagnosis and imaging which is key to the survival of the disease. Many cancer cell lines are used for various analysis invitro, and changes in their physiology and morphology can provide information on the effect of the substances they are exposed to for example, nanoparticles and this can provide information on the toxicity level of these nano-materials (Buzea *et al*., 2007; Shin et al., 2015).

Understanding the safety and toxicity of these nanoparticles is very important in their overall application (Holsapple *et al.,* 2005). This provides information on the biological interaction between nanoparticles and biological environment of interest for the future therapeutic application (Oberdörster, 2010; Wittmaack, 2007).

4.2 Types of cancer cell lines

There are numerous types of cancer cells. A tumour that is formed determines by the type of cell or tissue in the body that was originally altered. HeLa cells are human cervical cancer cell lines associated with human papillomavirus infections. There are different strains of the virus (Crosby *et al.,* 2013). PC-3 are prostate cancer cell lines used in cancer research. Prostate cancer is the second most common type of cancer in men (Krumwiede and Krumwiede, 2012), most diagnosed (about 95.5%) and second leading cause of death (CDC report, 2017; Siege *et al.*, 2012; Tai *et al.*, 2011). The prostate is a small gland found under the bladder in males and forms part of the reproductive system, producing seminal fluid that is important for semen production. MCF-7 is from breast adenocarcinoma (Liyanage *et al.*, 2002), also, an epithelial cancer cell line with physical characteristics of differentiated mammary epithelium (Polyak and Kalluri, 2010). MCF-7 cells are helpful for *invitro* studies because they retain several essential features of the mammary epithelium (Holliday and Speirs, 2011; Neve *et al*., 2006). Generally, breast cancer is the most common cancer in females, accounting for most cancer mortality in women (Ferlay, 2012; IARC, 2014). U87 cells are glioblastoma cell lines found in the human brain; they are the most common type of brain tumour developing from glial cells (NCI, 2017).

4.3 Immunocytochemistry

Immunocytochemistry is a very dynamic technique in cancer research to detect proteins, peptides and some macromolecules in tissues and cells cultures (Burry, 2011). This method has been employed in the discovery of many types of cancer. The use of antibodies has been found to be an essential tool that indicates the presence of subcellular location and presence of an antigen. In immunocytochemistry, cell samples are collected and fixed appropriately to ensure that their cell morphology is maintained, and the antigenicity of the targeted protein or peptide is not compromised. Flow cytometry, is an established platform used for evaluating

multi-parameter measurement of cell fluorescence from a single cell particle (Edwards *et al*., 2004). The flow cytometer can be sensitive to the minimal concentration of fluorescent molecules. Hence, it can detect several molecules. In this study (binding study), it was used to determine the binding of the N-terminal, and C-terminal FITC labelled chlorotoxin peptide 1 and peptide 2 respectively.

4.4 Materials and Method

4.4.1 Materials

WST-1 Cell Proliferation Reagent 4-[3-(4-iodophenyl)-2-(4-nitrophenyl)-2H-5-tetrazolio]-1, 3-benzene disulfonate (Roche), RPMI-1640 (Lonza), Dulbecco's modified Eagle's medium (DMEM), FBS (Fetal bovine serum) (Gibco life technologies), Penicillin and Streptomyc -in (Lonza), Sterile phosphate buffer (Lonza), Trypsin (Lonza), Peptide 1 (FITC attached to the N-terminal of chlorotoxin peptide, CTX-FITC) and Peptide 2 (FITC attached to the C-terminal, CTX-FITC) (GL Biochem), 6-well culture plates (Greiner), 12 well culture plates, 96-well Flat bottom clear microplate (Greiner), coverslips 22 x 22 mm (Lasec), slides (Lasec), FluoroShield with DAPI (Sigma), Paraformaldehyde (Sigma), Triton X-100 (Fluka), the four cell lines: HeLa, MCF-7, PC-3 and U-87 (ATCC), MMP-2 antibody (ThermoFischer), Leica bond autostainer.

4.4.2 Cell Culture

The cytotoxicity of CdTe QDs synthesised from the previous chapter was used on selected cancer cell lines, and cell viability was assessed *in vitro* using 4-[3-(4-iodophenyl)-2-(4 nitrophenyls)-2H-5-tetrazolio]-1, 3-benzene disulfonate (WST-1) assay. MCF-7, HeLa and U-87 cells were cultured in Dulbecco's Modified Eagle Medium (DMEM), PC-3 on RPMI-1640 with L- glutamine which was supplemented with 10 % FBS (Fetal bovine serum) and 1% Penicillin and 50 mg/mL of Streptomycin. The cells were grown at 37°C in a

humidified atmosphere with 5% CO_2 in an SL (Shel Lab) incubator for about 2 to 3days until ~70 % confluence. After that, the cells were washed gently with 1×PBS, trypsinised and the density determined using Invitrogen Countess Automat ed Cell Counter. The cells were seeded at a density of 1 x 10^5 cells per mL in a 96 well plate, 100 µL of the cells were plated in each well and cultured for 24 hours at 37 °C. After 24 hours of incubation, the cells were treated for another 24 hours with different concentrations of the QDs capped with MPA and GA (100µg/mL, 50µg/mL, 25µg/mL, 12.5µg/mL, 6.25µg/mL and 3.125µg/mL) and the positive control cells were treated with 6% DMSO. The media was replaced with fresh media containing 10µL WST-1 per 100 µL media and incubated for 4 hours at 37°C, and the absorbance was measured at 440 nm and 630 nm using BMG Labtech polar star omega microplate reader. All media were equilibrated at 37 ºC using a water bath and all the experiments were carried out in sterile laminar flow (Labotec bio-flow). The viabilities of the cells were expressed as the percentage ratio of mean absorbance of the treated cells against the mean absorbance of untreated cells using the formula below;

Percentage (%) Cell viability = $\frac{\text{treated cells}}{\text{untreated cells}}$ X 100

4.5 Cell binding study of FITC labelled Chlorotoxin peptide 1 and 2

Cell binding study was carried out using chlorotoxin labelled with FITC on the N-terminal (peptide 1) and C-terminal (peptide 2). The cells were grown to 70 % confluence in a flask, washed gently with PBS and trypsinised gently without scraping cells. Subsequently, the cells were counted using automated cell counter (Invitrogen) and seeded in a 6-well plate at a cell density of 3 × 10^5 per mL. The cells were allowed to grow for 24 hours in a six-well plate at 37°C in a humidified atmosphere with 5% CO_2 in an SL (Shel Lab) incubator. The cells were washed with 1xPBS and treated with different concentration of FITC-

peptide 1 and 2 (0.05 mM, 0.0125 mM, 0.006 mM and 0.001mM). After an hour, the plate was removed from the incubator and washed again with 1× PBS. A 300 µL of trypsin was added to each well to trypsinise the cells and was collected in a 15 mL tube. Approximately, 3mL of 1×PBS was added to the cells in the tube and centrifuged for 3 minutes using Beckman Coulter X12 centrifuge. The supernatant was discarded, and about 300µL of the complete media was added to the pellet which was mixed gently and incubated on ice. Cells binding analysis was carried out using BD Accuri C6 flow cytometer.

4.6 Seeding of cells in culture plate cells

MCF-7, HeLa, PC-3 and U-87 cells were cultured in a T75 flask and allowed to grow to about 70% confluence, the cells were washed with 1×PBS, and four mL of 2×trypsin was added to each flask to trypsinise the cells. The cells were counted using countess automated cell counter. Sterilised coverslips were placed in a 6-well cell culture plate with a tweezer, and the cells seeded onto coverslips at a cell density of $3x10^5$ cells/mL. Also, the cells were allowed to grow for 24 hours in six-well plates at 37 °C in a humidified atmosphere with 5% CO_2 in an SL (Shel Lab) incubator. When the cells have grown up to about 60% confluence, they were treated with 20 µL/mL of quantum dot solution for about 12 hours in order for the cells to take up the QDs and the FITC labelled peptide one was used for treating the cells for an hour with a concentration of 0.0125mM.

4.7 Fixing and permeabilisation of cells on slides

After 12 hours of treatment, the cells treated with quantum dots were removed from the incubator. Subsequently, the media was removed from the culture plates and cells were washed twice with 1x PBS. 4% formaldehyde solution was added to each well to cover the cover-slip in the well; to fix the cells on the coverslips for 20 minutes at room temperature. After that, the cells were washed with 1×PBS twice, PBS removed and 0.1% Triton X-100 was added to each well and left for 5 minutes for permeabilisation of the cell membrane to

take place, afterwards, the cells were washed twice again with 1×PBS. This process was also carried out using FITC-peptide 1.

4.8 Staining of fixed cells

FluoroShield DAPI mounting media (Sigma-Aldrich) then dropped on well-labelled microscope slides, and a tweezer was used to pick the cover-slips containing the cells. These cells were washed two times with 1× PBS and drained properly. After that, the cover-slips containing the cells were placed on the mounting media and mounted on the microscope slide. This was wrapped with foil paper and allowed to dry in 4ºC before images were captured using Zeiss Axiovert 200M fluorescence microscope at 10X magnification, and a mercury arc lamp (HBO100) was used to illuminate the slides.

4.9 Immunocytochemistry Assay

HeLa, PC-3, MCF-7 and U87 cell lines were cultured and trypsinised as described in section 4.6. The microscope slides were placed in a sterile 150 mm × 15 mm petri dish, and the cells were seeded on the slides and gently placed in an SL (Shel Lab) incubator to allow the cells to grow on the slides at 37°C in a humidified atmosphere with 5% CO_2. When cells have grown to confluence, they were washed three times with 1XPBS for 5 minutes, and 4% formaldehyde was added to the petri dish to cover the slides in the dish, this was done to fix the cells on the slides for 20 minutes. Afterwards, the slides were washed three times with 1XPBS and were allowed to dry at 4°C, and viewed under the microscope to confirm if the cells were properly fixed. A Leica bond autostainer was used to stain the slide. MMP-2 antibody from Thermo Fischer was used as the primary antibody; then images were taken using Zeiss primo vert light microscope.

4.10 Results and Discussion

4.10.1 WST-1 viability assay images of cells treated with different QDs concentrations

The cytotoxicity of QDs-MPA, QDs-GA2 and QD-GA12 were evaluated using four cancer cell lines; HeLa, PC-3, MCF-7 and U87 and images of the cells then taken when treated with QDs after 24hours cells were viewed using a microscope. Although changes were observed in the morphology of the cells, viability assay revealed that the cells were still over 70% viability. This may imply that the QDs were not toxic to cells although it changed the morphology of the cell, but it did not kill the cells. Figure 4.1 showed images of HeLa cells treated with different concentration of QDs-GA, QDs-GA2, and QDs-GA12 respectively, in a 96 well plate, with a 6% DMSO was used as positive control. The images revealed that the HeLa cell morphology did not change at low concentrations (<50µg/mL) of the QDs but slight changes in the morphology of the cells were observed at 50µg/mL and 100µg/mL.

4.10.2 WST-1 cell viability of HeLa cells treated with different QDs concentrations

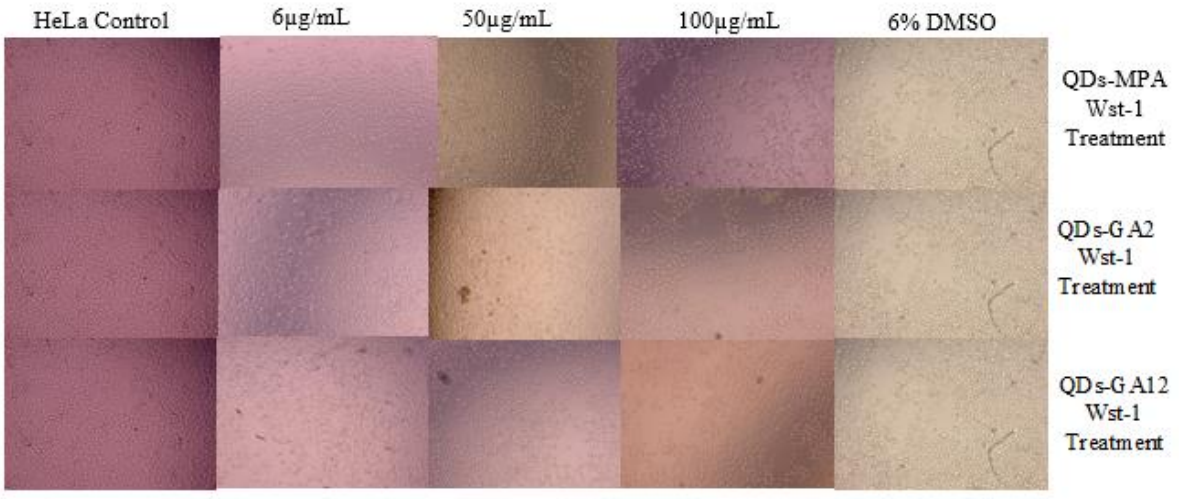

Figure 4.1: Images of HeLa cells treated with different concentration of QDs-MPA, QDs-GA2, and QDs-GA12 respectively, in 96 well plates.
At 50µg/mL, changes were observed in the morphology of the cells.

4.10.3 WST-1 cell viability of PC-3 cells treated with different QDs concentrations

PC-3 cells treated with different concentration of QDs images are shown in Figure 4.2 revealing changes in cell morphology with an increase in the concentration of QDs.

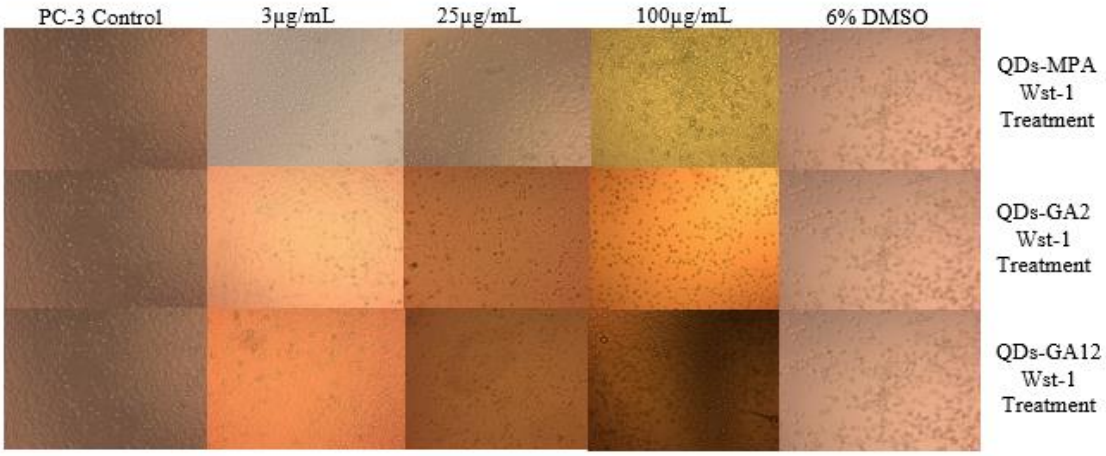

Figure 4.2: Images of PC-3 cells treated with different concentration of QDs-MPA, QDs-GA2 and QDs-GA12 respectively.
The changes in morphology of the cells were observed with the increase in the concentration of QDs.

4.10.4 WST-1 cell viability of MCF-7 cells treated with different QDs concentrations

Figure 4.3 are images of QDs-MPA, QDs-GA2, and QDs-GA12 treated MCF-7 cells with various concentrations of QDs-MPA, QDs-GA2 and QDs-GA12. Morphologically changes in the cells were observed with an increase in the concentration of the QDs treatment.

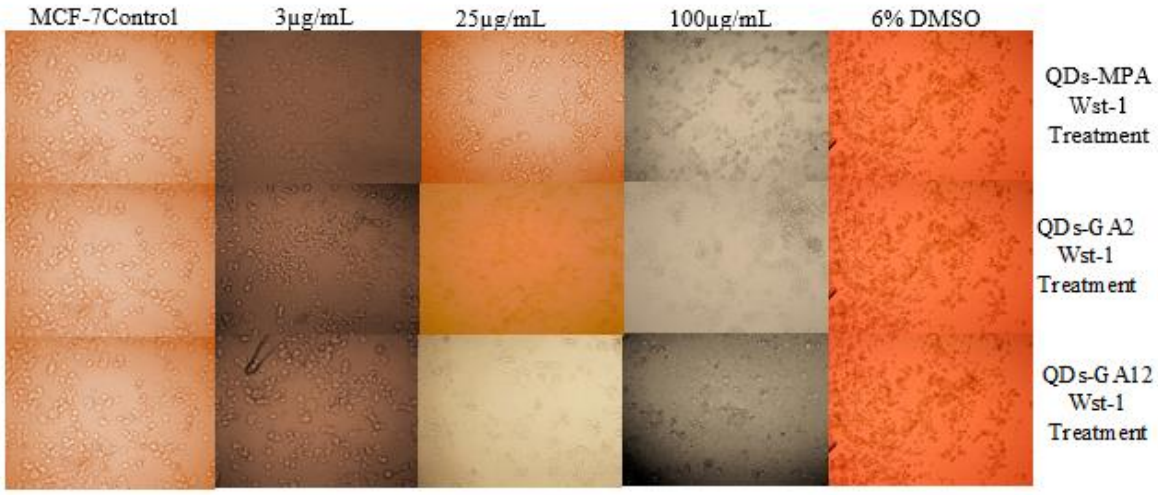

Figure 4.3: Images of MCF-7 cells treated at a different concentration of QDs-MPA, QDs-GA2, and QDs-GA12 respectively.
Morphological changes in cells were observed with the increase in the concentration of quantum dots.

4.10.5 WST-1 cell viability of U87 cells treated with different QDs concentrations

Figure 4.4 showed images of U-87 cells treated at a different concentration of QDs-GA, QDs-GA2, and QDs-GA12. Morphological changes were observed with increase in the concentration of QDs treatment and 6% DMSO was used as positive control.

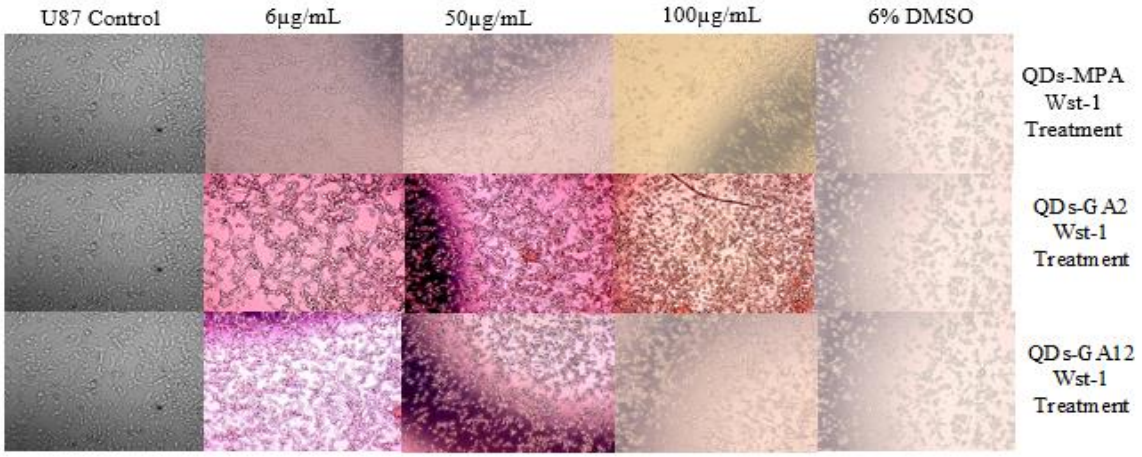

Figure 4.4: Images of U-87 cells treated at a different concentration of QDs-GA, QDs-GA2, and QDs-GA12 respectively.
The changes in morphology of the cells were observed with the increase in the concentration of QDs

4.11 Cell binding studies using CTX-FITC (Peptide-1) and CTX-FITC (Peptide-2)

Several studies have shown the binding of CTX to MMP-2 protein (Dardevet et al., 2015; Deshane et al., 2003; Othman et al., 2017; El-Ghlban et al., 2014). MMP-2 is a metalloproteinase whose activity is increased in tumour formation (Ali et al., 2016; El-Ghlban et al., 2014). However, chlorotoxin, venom from a scorpion is known to inhibit MMP-2 activity by binding to the proteinases (Fu et al., 2012; Huang et al., 2011; Ojeda et al., 2016; El-Ghlban et al., 2 014). In this study, FITC was attached to the N-terminal and C-terminal of chlorotoxin, and these were labelled as peptide-1 and peptide-2 respectively. Various concentration of these peptides (CTX-FITC-1 and CTX-FITC-2) were used to treat the cell lines known to express MMP-2 for one hour (HeLa, MCF-7, PC-3, U87 and CHO cell lines) (Hagemann et al., 2012; Nuttall et al., 2003). The degree of binding was evaluated by measuring fluorescence intensity in percentage. This experiment was carried out in triplicate, and the average percentage binding was taken for each plot.

Figures 4.5a to 4.11 shows CTX-FITC peptide 1 and 2 binding studies with different cell lines. The cell binding studies using CTX-FITC-1 and 2 for HeLa cells is shown in Figure 4.5a and 4.5b using the following concentrations, the black (untreated cell), pink (0.001mM), green (0.006mM), red (0.0125mM) and blue (0.05mM). Histogram plot of HeLa cells treated with CTX-FITC-1 at various concentrations showed cells spectra movement shift to the right (+CTX-FITC) this is an indication of cells that bind to CTX-FITC-1 and this shift increases with concentration while moving to the left shows no binding (-CTX-FITC) as seen in the control cells (black colour in the plot).

4.11.1 Binding studies for HeLa cells using CTX-FITC (Peptide-1) and CTX-FITC (Peptide-2)

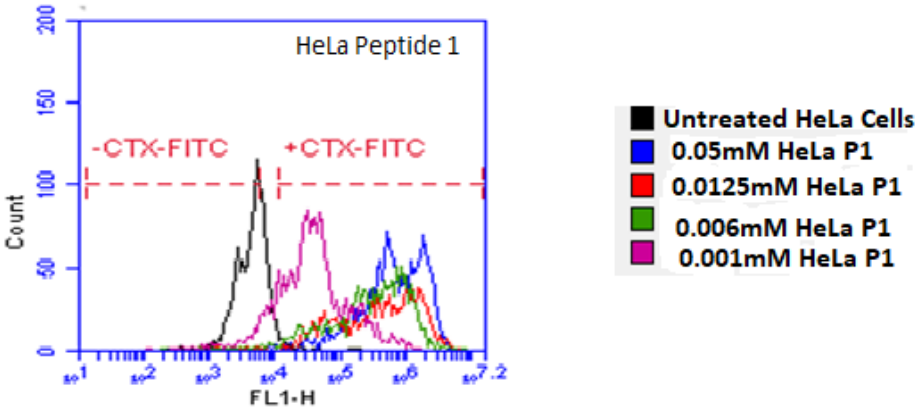

Figure 4.5a: Histogram of HeLa cells treated with FITC peptide1 at various concentrati ons.

The black, pink, green, red and blue colour represent; untreated cell, 0.001mM, 0.006mM, 0. 0125mM, and 0.05mM of Peptide1 concentration used for HeLa cells respectively. The shift of the cells to the right (+CTX-FITC) is an indication that cells bind to CTX-FITC peptide 1, and the shift increases with increase in concentration. The movement to the left shows no binding (-CTX-FITC) as seen in the untreated cells (black colour).

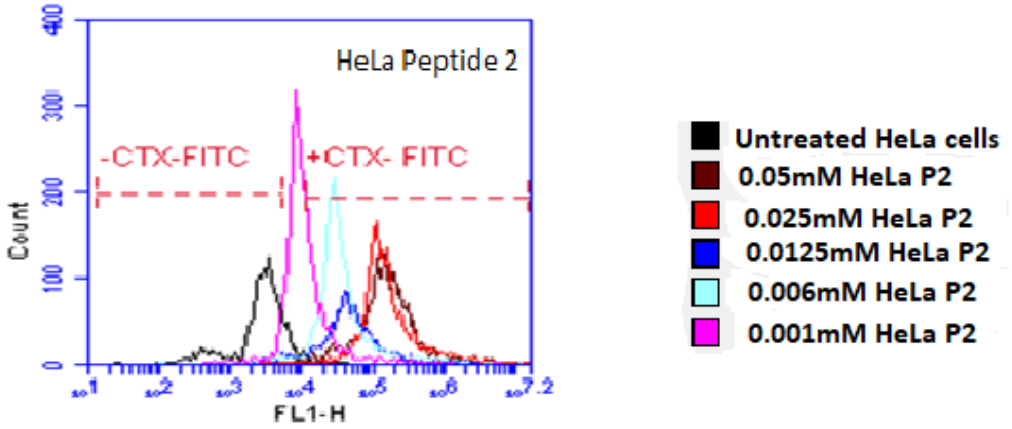

Figure 4.5b: Histogram of HeLa cells treated with various concentrations of FITC peptide-2.

Black, pink, green, blue, red and brown colour spectra represent; untreated HeLa cells, 0.001mM, 0.006mM, 0.0125mM, 0.025mM and 0.05mM of peptide 2 concentrations respectively. Cells fluorescence movement to the right (+CTX-FITC) is an indication that the cells bind to CTX-FITC Peptide 2 and this shift increases with concentration while a movement to the left shows no binding (-CTX-FITC) as seen in the control (black colour).

4.11.2 Binding studies for PC-3 cells using CTX-FITC (Peptide-1) and CTX-FITC (Peptide-2).

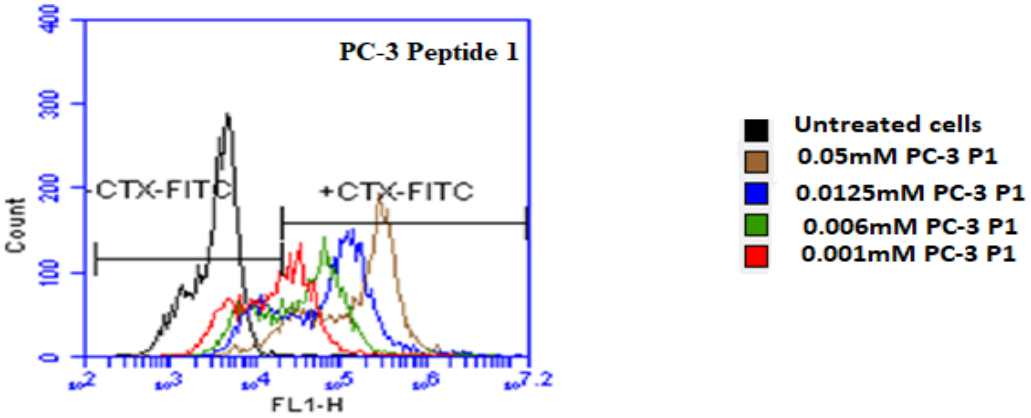

Figure 4.6a: Histogram of PC-3 cells treated with FITC peptide1 at different concentrat ions.

The black, red, green, blue and brown colour represent; untreated cell PC-3, 0.001mM, 0.006mM, 0.0125mM, and 0.05mM concentrations of Peptide 1 used for PC-3 treatment respectively. Cells movement to the right (+CTX-FITC) is an indication of cells that bind to CTX-FITC Peptide1 and this shift increases with concentration while a movement to the left shows no binding (-CTX-FITC) as seen in the untreated cell (black colour).

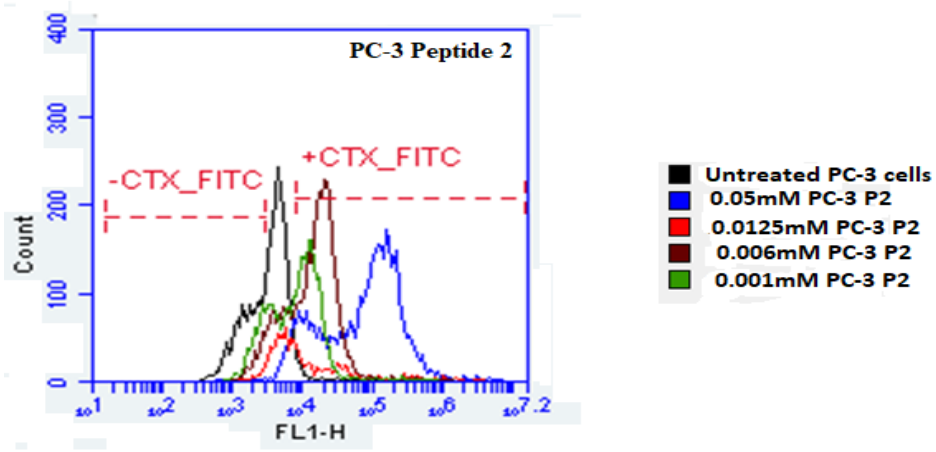

Figure 4.6b: Histogram of PC-3 cells treated with FITC peptide-2 at varying concentrations.

The black, red, green, blue and brown represent; untreated cell PC-3, 0.001mM, 0.006mM, 0.0125mM, and 0.05mM concentrations of Peptide 2 used for PC-3 treatment respectively. Cells fluorescence movement to the right (+CTX-FITC) is an indication that the cells bind to CTX-FITC Peptide 2 and this shift increases with concentration while a movement to the left showed no binding (-CTX-FITC) as observed in untreated cells (black colour)

4.11.3 Binding studies for MCF-7 cells using CTX-FITC (Peptide-1) and CTX-FITC (Peptide-2).

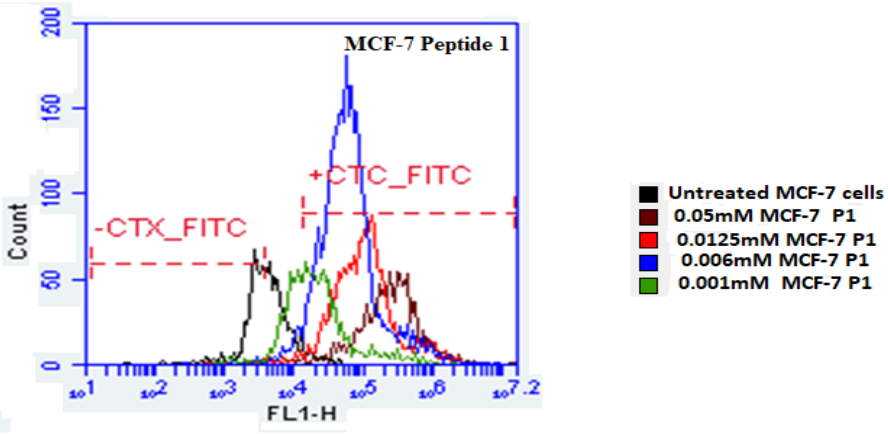

Figure 4.7a: Histogram of MCF-7 cells treated with FITC peptide-1 at various concentrations.

The black, green, blue, red and brown represent; untreated cell MCF-7, 0.001mM, and 0.006, 0.0125mM and 0.05mM concentrations of Peptide 1 used for MCF-7 treatment respectively. Cells movement to the right (+CTX-FITC) is an indication that the cells bind to CTX-FITC Peptide 1 and this shift increases with concentration while a movement to the left showed no binding (-CTX-FITC) observed in untreated cells (black colour spectra).

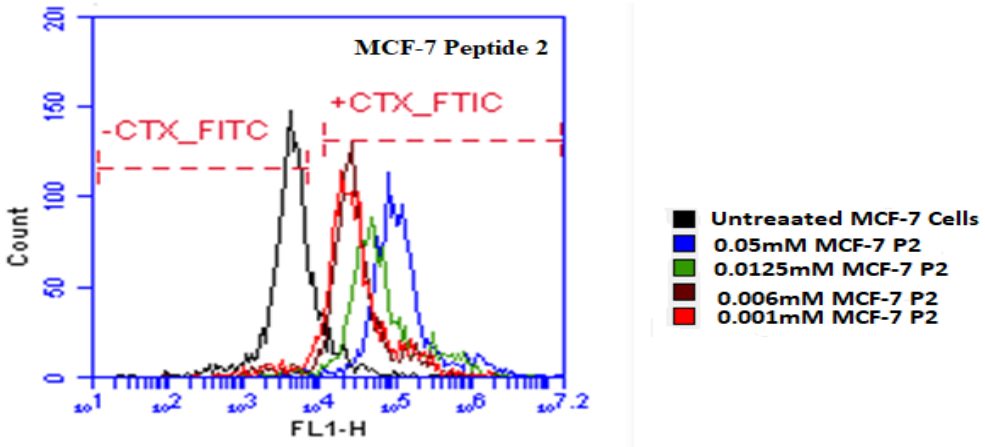

Figure 4.7b: Histogram of MCF-7 cells treated with FITC peptide-2 at varying concentrations.

The black, red, brown, green and blue represent; untreated cell MCF-7, 0.001mM, 0.006mM, 0.0125mM and 0.05mM concentrations of Peptide 2 used for MCF-7 treatment respectively. Cells fluorescence movement to the right (+CTX-FITC)is an indication that the cells bind to CTX-FITC Peptide 2 and this shift increases with concentration while a movement to the left shows no binding (-CTX-FITC) as in the untreated cells (black colour).

4.11.4 Binding studies for U87 cells using CTX-FITC (Peptide-1) and CTX-FITC (Peptide-2).

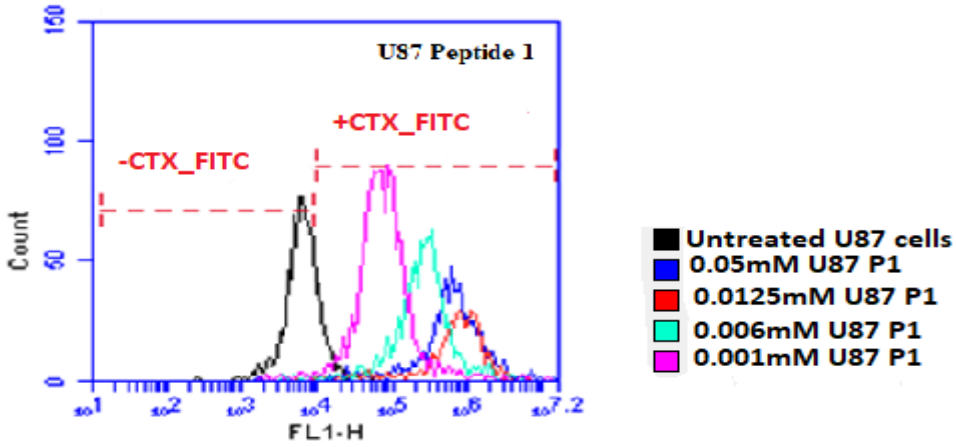

Figure 4.8a: Histogram of U87 cells treated with FITC peptide-1 at various concentrations.

The black, pink, green, red and blue represent; untreated cell U87, 0.001mM, 0.006mM, 0.0125mM and 0.05mM concentrations of Peptide 1 used for U87 treatment respectively. Cells movement to the right (+CTX-FITC) is an indication that the cells bind to CTX-FITC Peptide 1 and this shift increases as concentration increases while a movement to the left indicates no binding (-CTX-FITC) as seen in untreated black colour spectra.

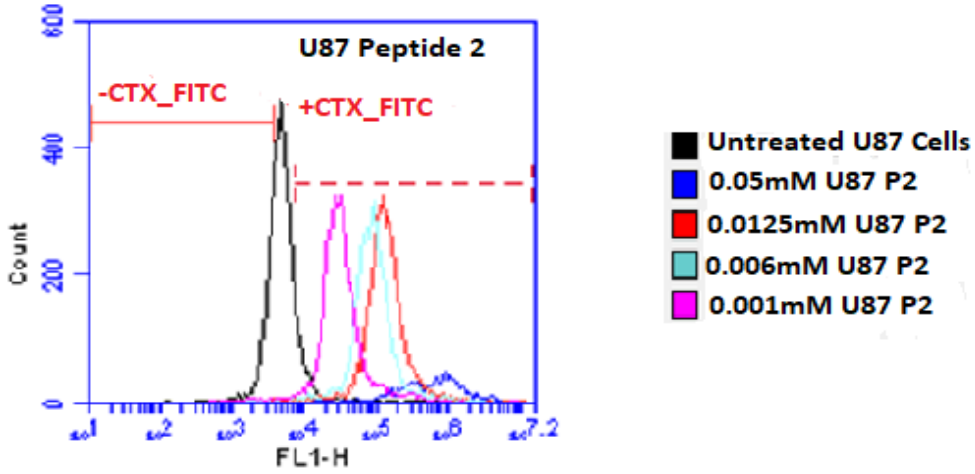

Figure 4.8b: Histogram of U87 cells treated with FITC peptide-2 at varying concentrations.

The black, pink, green, red and blue represent; untreated cell U87, 0.001mM, 0.006mM, 0.01 25Mm and 0.05Mm concentrations of Peptide 2 used for U87 treatment respectively. Cells fluorescence movement to the right (+CTX-FITC) is an indication that the cells bind to CTX-FITC Peptide 2 and this shift increases with concentration while a movement to the left shows no binding (-CTX-FITC) as seen in the untreated cells (black colour).

4.11.5 Binding studies for CHO cells using CTX-FITC (Peptide-1) and CTX-FITC (Peptide-2).

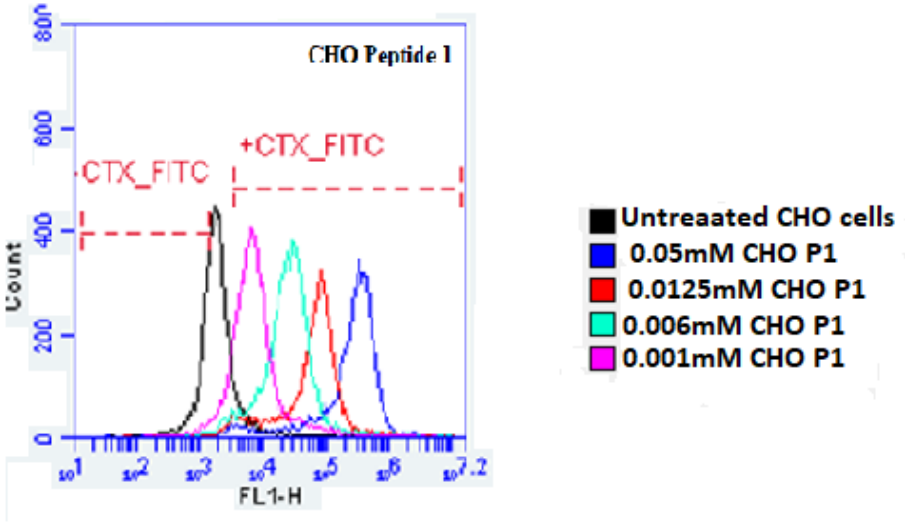

Figure 4.9a: Histogram of CHO cells treated with FITC Peptide-1 at various concentrations.

The black, pink, green, red and blue represent; untreated cell CHO, 0.001m M, 0.006mM, 0.0125mM and 0.05mM concentrations of Peptide 1 used for CHO treatment respectively Cells movement to the right (+CTX-FITC) is an indication that the cells bind to CTX-FITC Peptide 1 and this shift increases with concentration while a movement to the left shows no binding (-CTX-FITC) as seen in untreated cells (black colour)

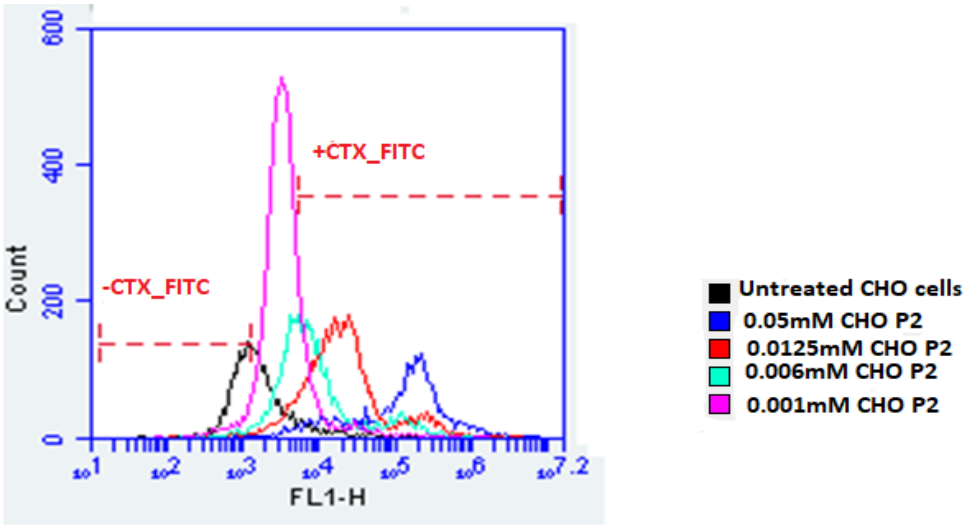

Figure 4.9b: Histogram of cells treated with FITC peptide-2 at varying concentrations.

The black, pink, green, red and blue represent; untreated cell CHO, 0.001mM, 0.006mM, 0.0125mM and 0.05mM concentrations of Peptide 2 used for CHO treatment respectively. fluorescence movement to the right (+CTX-FITC) is an indication that the cells bind to CTX-FITC Peptide 2 and this shift increases with concentration while a movement to the left shows no binding (-CTX-FITC) as seen in the control(untreated cells) cells (black colour)

4.12 Percentage of cells binding of CTX-FITC Peptide 1 for all cell line

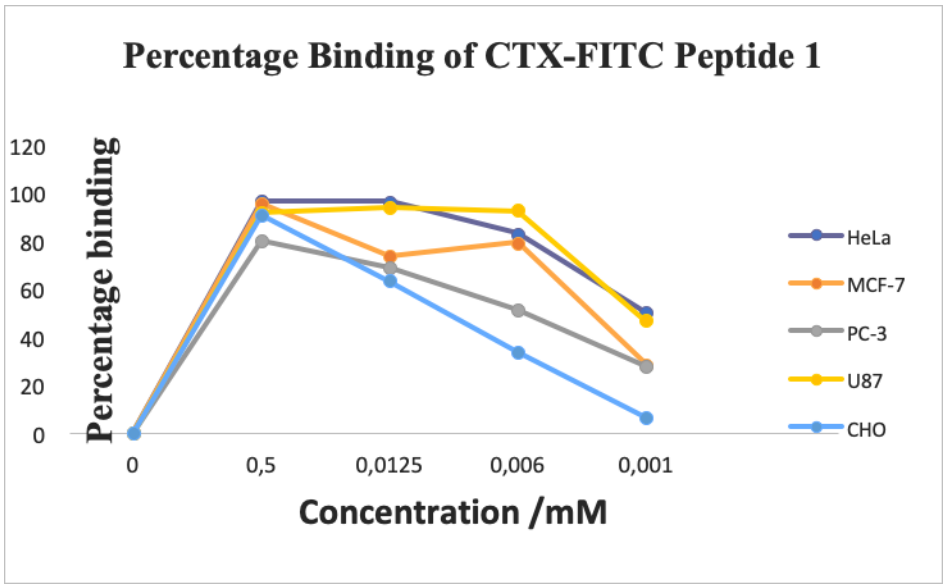

Figure 4.10: Plot of percentage binding of peptide 1 to cell lines (HeLa, PC-3, MCF-7, U87 and CHO cells).

Plots showed the binding of cells to CTX-FITC peptide 1 is concentration dependent. HeLa and U87 cells had the highest binding percentage.

4.12.1 Percentage of cells binding of CTX-FITC Peptide 2 for all cell line

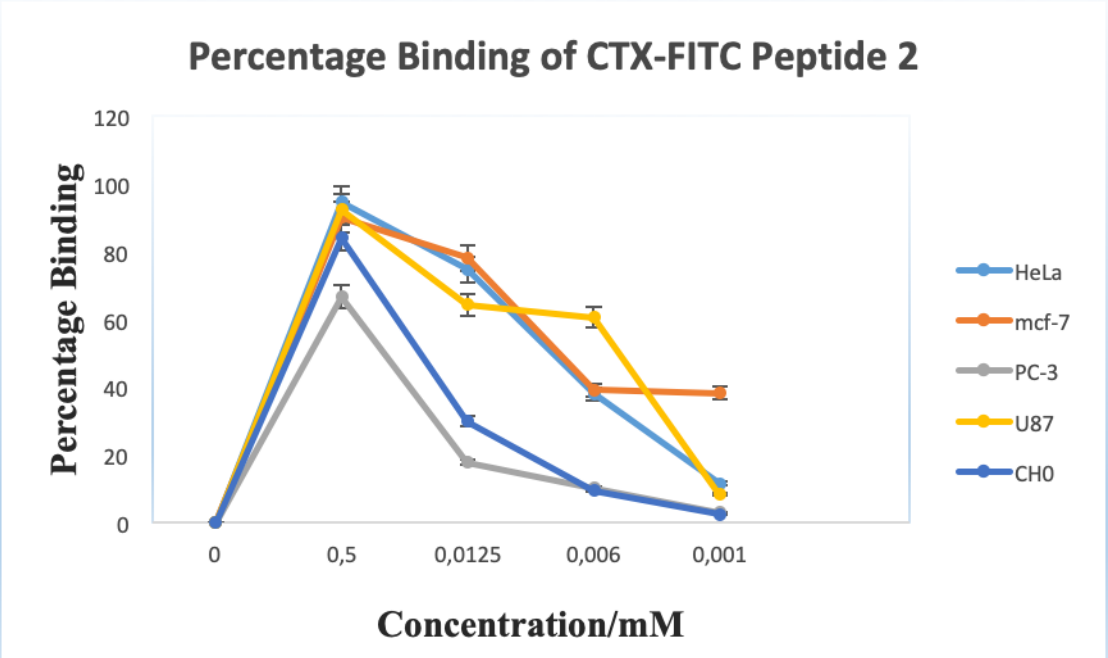

Figure 4.11: Plot of percentage binding of peptide 2 to cell line (HeLa, PC-3, MCF-7, U87 and CHO cells). (HeLa, PC-3, MCF-7, U87 and CHO cells).
Plots showed the binding of cells to this CTX-FITC peptide 2 is concentration dependent. HeLa and U87 cells had the highest binding percentage.

The cell binding studies using CTX-FITC-1 and 2 for HeLa cells is shown in Figure 4.5a and 4.5b respectively using concentrations (0.001mM, 0.006mM, 0.0125Mm and 0.05mM). Histogram fluorescence intensity plots of HeLa cells treated with CTX-FITC showed that cells spectra movement to the right (+CTX-FITC) this is an indication that HeLa cells bind to CTX-FITC-1 and this shift in spectra increases with concentration while moving to the left shows no binding (-CTX-FITC) as seen in the control cells (black colour spectra in both plots). It was also observed that HeLa binds more to CTX-FITC-1 (Figure 4.5a) than CTX-FITC-2 (Figure 4.5b), this corresponds to the percentage binding plots for peptide 1(Figure 4.10) where HeLa cells have the highest percentage binding.

Figure 4.6a and Figure 4.6b are histogram spectra plots for PC-3 cell binding studies using CTX-FITC-1 and 2 respectively with 0.01mM, 0.006mM, 0.0125mM and 0.05mM

concentrations. Cells fluorescence spectra movement to the right (+CTX-FITC) is an indication that the cells bind to the peptides with an increase in concentration. PC-3 has the lowest binding percentage for both peptide 1 and 2 (Figure 4.10 and Figure 4.11), but the binding percentage is higher peptide 1 (CTX-FITC-1).

Figure 4.7a and Figure 4.7b are histogram fluorescence binding spectra plots for MCF-7 cell binding studies using CTX-FITC-1 and 2 corresponding to 0.01mM, 0.006mM, 0.0125mM and 0.05mM concentrations. MCF-7 binds more with peptide 1 (CTX-FITC-1) than CTX-FITC-2 as seen Fig 4.7a and Fig 4.7b respectively.

Figure 4.8a, 4.8b, 4.9a, and 4.9b represents histogram fluorescence binding spectra plots for U87 cells peptide 1 (CTX-FITC-1), (CTX-FITC-2), and CHO cells (CTX-FITC-1), CTX-FITC-2 respectively. For both peptides binding is concentration dependents as seen in the cells fluorescence plot movement to the right which signifies that these cells bind to the peptide. Percentage binding is higher in peptide 1 for U87 and CHO cells respectively. U87 cells bind more to (CTX-FITC-1) as seen in the movement of the spectra to the right (Fig 4.8a) when compared to peptide 2 (CTX-FITC-2) (Fig 4.8b). This is in agreement with (Fig 4.11) the percentage binding of all five cell lines to peptide 1 that showed that percentage binding is higher in peptide 1.

Figure 4.10 and 4.11 showed the percentage binding of the five cell lines (HeLa, PC-3, MCF-7, U87 and CHO) to peptide 1 and 2 respectively. Plots suggest that cells bind more to peptide 1 (CTX-FITC-1) than peptide 2 (CTX-FITC-2). The plot (Fig 4.10) revealed that the binding of cells to chlorotoxin-FITC peptide 1(CTX-FITC-1) is also concentration dependent. HeLa and U87 cells had the highest binding percentage at 0.05mM. Thus, this could suggest that these cells have high receptors for FITC peptide 1 (Thovhogi *et al.,* 2015) as a result of the presence of MMP-2 protein in the cells.

Plots (Fig 4.11) showed that the binding of cells to this CTX-FITC-2 is concentration dependent. It is observed that U87 and HeLa cells have the highest percentage binding and high fluorescence for peptide 2 (Fig 4.11). This implies that they have high receptors for the peptide, this may be due to high expression of MMP-2 by these cells (Abe *et al*., 1994; Hagemann *et al*., 2012; Nuttall *et al*., 2003; VanMeter *et al.*, 2001; Yamamoto *et al.*, 1996) and hence high receptor available for binding. MCF-7 and by PC-3 binds discreetly (Nuttall *et a*l., 2003) and these cells moderately express this MMP-2 hence the available receptor binding are also moderately available. Percentage binding of peptide1 and peptide 2 when compared showed that cell binds more to peptide1 than peptide 2 and this could be as a result that suggests that MMP-2 expressed in the cancerous cells probably binds to the N-terminal of chlorotoxin peptide because the N-terminal of chlorotoxin peptide 1 is free and available for binding. Cells without peptide were used as a control, and their spectra showed movement to the left. This is an indication of lack of peptide treatments hence no fluorescence. Hence, results obtained from this study correlates with that of Ali and co-workers 2016, where they documented that chlorotoxin conjugates can be developed for targeting and imaging.

4.13 Cell Microscopy Studies

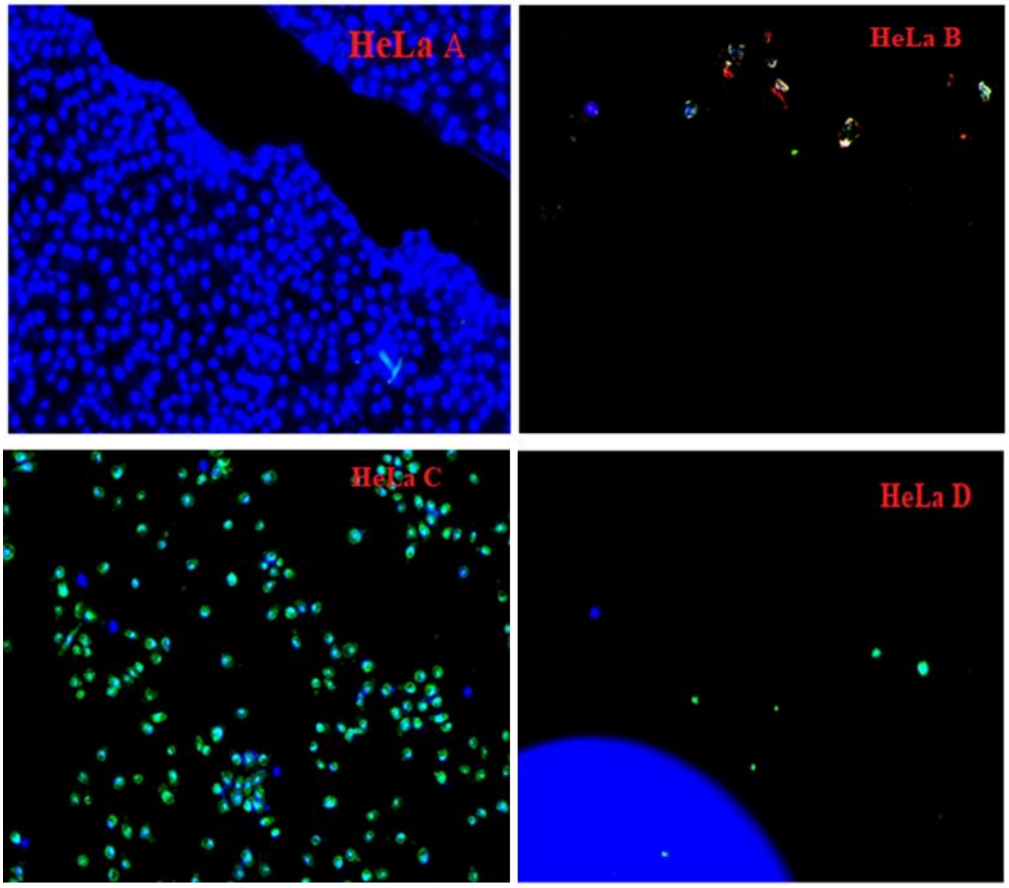

Figure 4.12: Microscopy study of the binding of the QDs to HeLa cells.
(A) HeLa cell and DAPI, (B) HeLa cells with DAPI and quantum dots, (C) HeLa, DAPI, peptide and quantum dots, (D) Hela cells and quantum dots only. This result indicates that DAPI is taken up by the nucleus (blue colour), QDs and peptide (green) and Quantum dots only is green and red fluorescence emission.

.

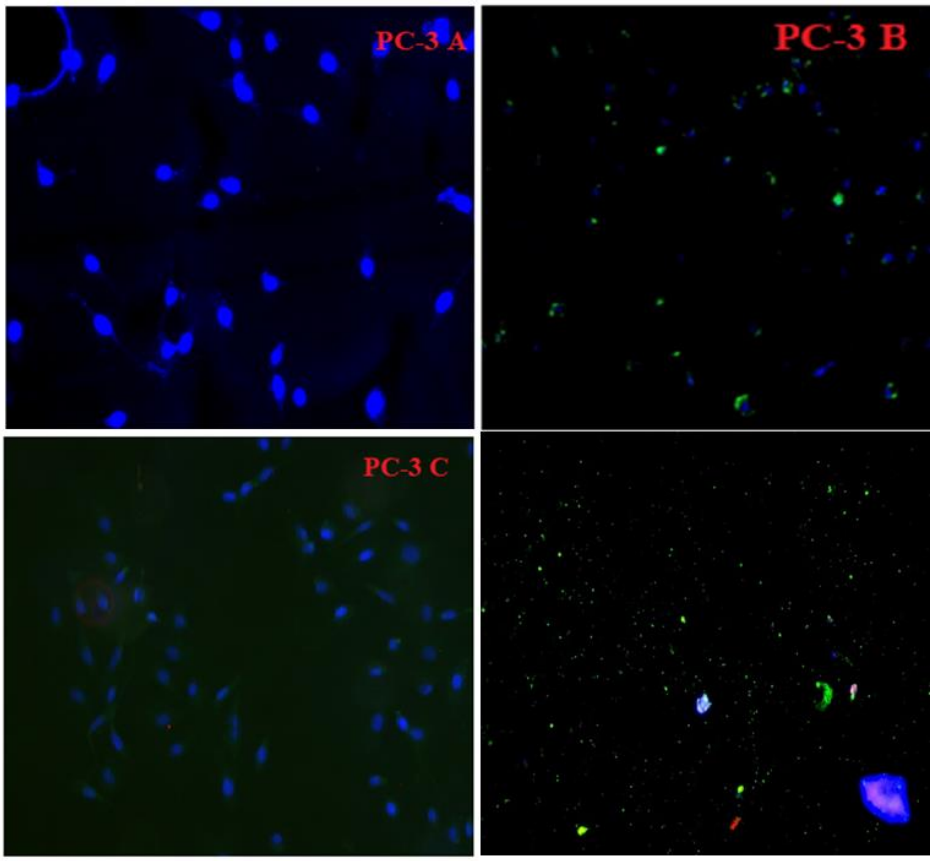

Figure 4.13: Microscopy study of the binding of the QDs to PC-3 cells.
(A) PC-3 cell and DAPI, (B) PC-3cells with DAPI and quantum dots (C) PC-3, DAPI, and peptide. This results showed DAPI is taken up by nucleus (blue colour), QDs and peptide (green) and Quantum dots only is green fluorescence emission.

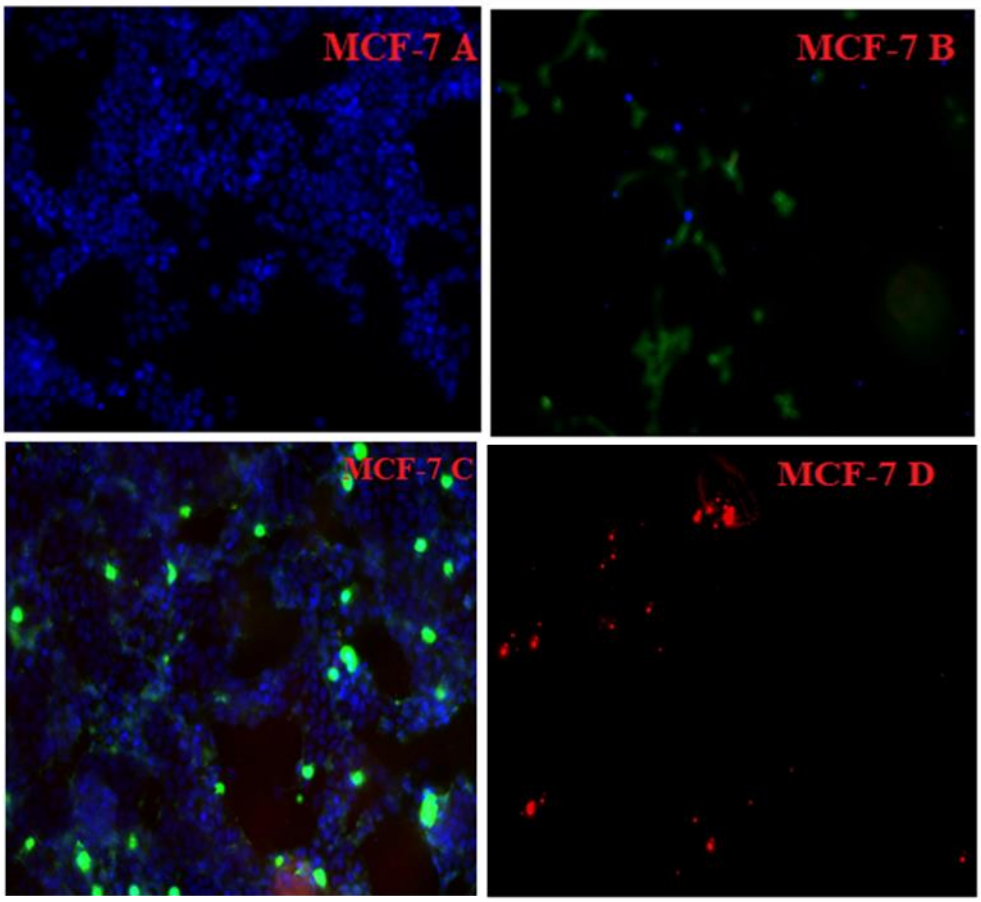

Figure 4.14: Microscopy study of the binding of the QDs to MCF-7 cells.
(A) MCF-7 cell and DAPI, (B) MCF-7 cells, DAPI and quantum dots (C) MCF-7, DAPI, and peptide. (D) Quantum Dots only. This results showed DAPI is taken up by nucleus (blue colour), QDs and peptide (green) and Quantum dots only is green fluorescence emission.

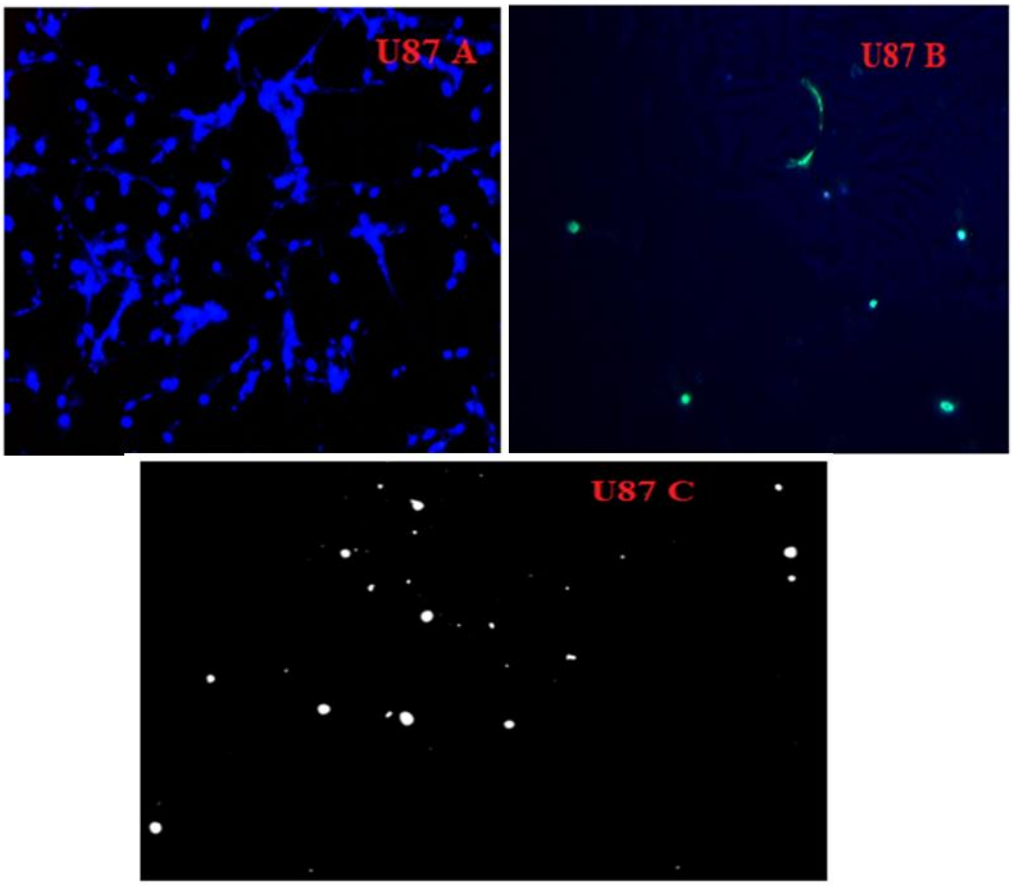

Figure 4.15: Microscopy study of the binding of the QDs to U8-7 cells.
(A) U87 cell and DAPI, (B) U87 cells, DAPI and quantum dots (C) U87, DAPI, and peptide. This results showed DAPI is taken up by nucleus (blue colour), QDs and peptide (green) and Quantum dots only is green fluorescence emission.

Microscopy study of the binding of the QDs to HeLa cells is seen in Figure 4.12. Cells were incubated with QDs and peptide, followed by counterstaining with DAPI and were examined under the microscope at 40× magnification. Cells were fixed and treated with peptide and quantum dots to ascertain if peptide and quantum were taken and internalise in the nucleus of the cells. HeLa (A) images showed cells treated with DAPI (4', 6-diamidino-2-phenylindole) only with a characteristic blue colour that shows nuclei localisation; this implies that they bind to the DNA to emit blue colour. Hence, it was observed that DAPI was internalised in the cell's nucleus while HeLa B is images of cells treated with quantum dots only showing red and green emission fluorescence of the QDs. Cells with peptide, DAPI and QDs are

shown in HeLa C images. The micrographs revealed cellular uptake of the QD (red and green), peptide (green) and localisation of the nucleus (blue) in both cell lines.

Figures 4.13 and 4.14 shows microscopy study of the binding of the QDs to PC-3 and MCF-7 cells. These cells were incubated with QDs and peptide and counterstained with DAPI. Image (A) for both cell lines showed the nuclei localisation (blue) in the two cell lines. QDs and peptide (green), DAPI (blue) and Quantum dots only. This image shows efficient cell uptake of peptide and QDs.

Microscopic study of the binding of the QDs to U8-7 cells is shown in Figure 4.15. Cells were incubated with QDs and peptide and counterstained with DAPI as aforementioned; (A) U87 cell and DAPI, (B) U87 cells, DAPI and quantum dots (C) U87, DAPI, and peptide. These results showed that DAPI is taken up by the nucleus (blue colour), QDs and peptide (green) and Quantum dots only displays green fluorescence emission. Hela cells micrograph showed the highest cell uptake of QDs, peptide and nuclei localisation.

4.14 Immunocytochemistry Assay

Immunocytochemistry is an assay used to visualise the localisation of a protein in the cells using a specific type of antibody that can bind the protein of interest. It shows if a protein is expressed in the cells but revealed in the intracellular location (Hesam, 2012).

The immunocytochemistry assay was used as described by Hesam (2012) to visualise the localisation of the protein (MMP-2) in the cells using a specific antibody that can bind the protein of interest (MMP-2 primary antibody) as seen in Figures 4.16 to 4.19. The MMP-2 antibody was used for the analysis to ascertain if these cells express MMP-2 proteins. The presence of bluish-brown stain observed using the light microscope is indicative that the cells

were positive to MMP -2 proteins when stained with the antibody. However, this technique has some limitation especially when visualise using fluorescence microscope because some molecules fluorescence by themselves and can bind specifically to other molecules present in the cells. Hence this technique is a preliminary method to detect the presence of these proteinases; other more specific technique can be employed (Hesam, 2012).

Figure 4.16 represents immunocytochemistry images of HeLa Cells. Immunocytochemistry assay images using MMP-2 primary antibodies for HeLa cells at X40 and X100 magnifications, the bluish-brown colour is an indication of the presence of MMP-2 protein. The intensity of the brownish stain seen in the cell images varies, and it was observed HeLa cells had high intensity; this agrees with the work of Nutall *et al*., 2003 which demonstrated that HeLa cells are very high in MMP-2 protein.

Immunocytochemistry images of PC-3, MCf-7 and U87 cells is shown in Figure 4.17, Figure 4.18 and Figure 4.19 respectively. These assays were carried out using MMP-2 primary antibodies for these cells. The blue-brown colouration is a positive test for the presence of MMP-2 protein. From the images, the intensity of the stain is high in U87 cells probably because of the presence of high concentration of MMP-2 which is by the literature (Nutall *et al*., 2003, Hagemann *et al*., 2010). MMP-2 is highly expressed in U87 (glioma) cells and moderately expressed in PC-3 and MCF-7 as shown in Figure 4.17 and 4.18.

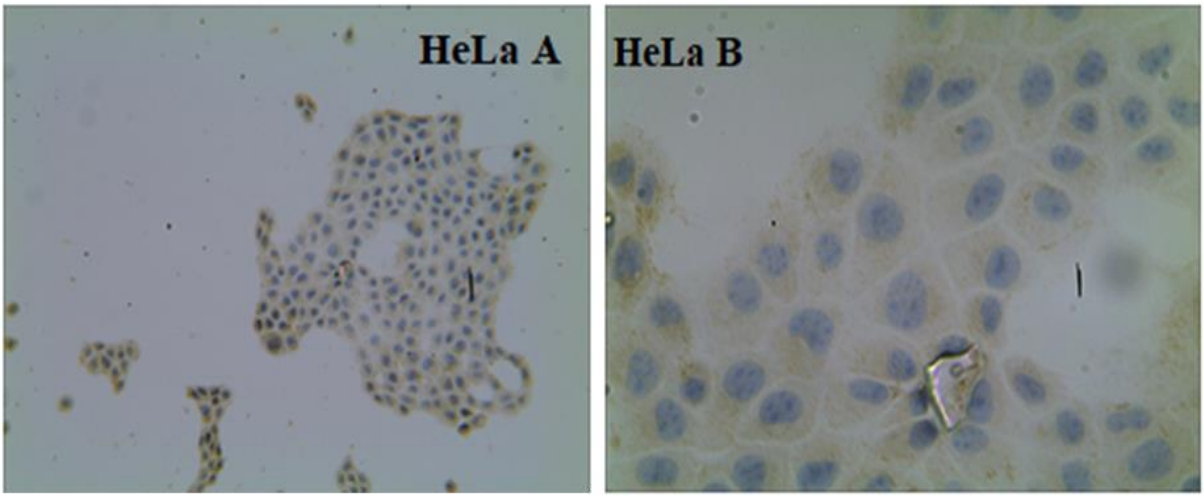

Figure 4.16: Immunocytochemistry images of HeLa Cells.
HeLa cells are showing the presence of MMP-2 using a primary antibody **(A)** at x40 magnification **(B)** at x100 magnifications. The presence of bluish-brown colour is an indication of the presence of MMP-2 protein.

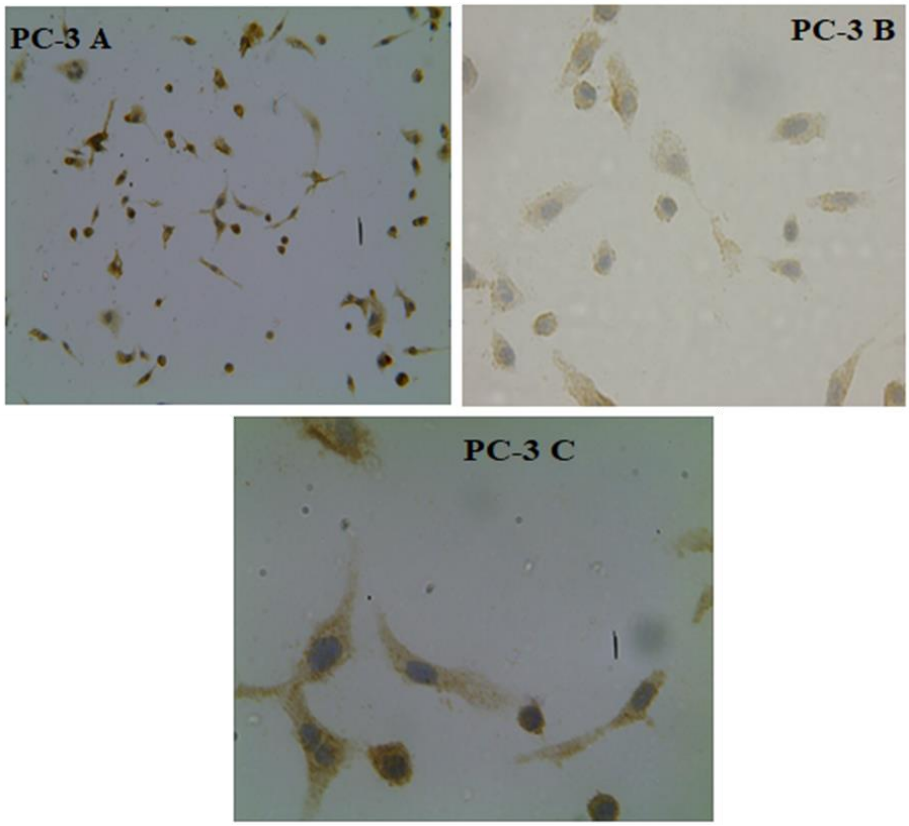

Figure 4.17: Immunocytochemistry images of PC-3 Cells.
Immunocytochemistry assay images using MMP-2 primary antibodies for PC-3 cells at x40 and x100 magnifications. The presence of bluish-brown colour is an indication of the presence of MMP-2 protein.

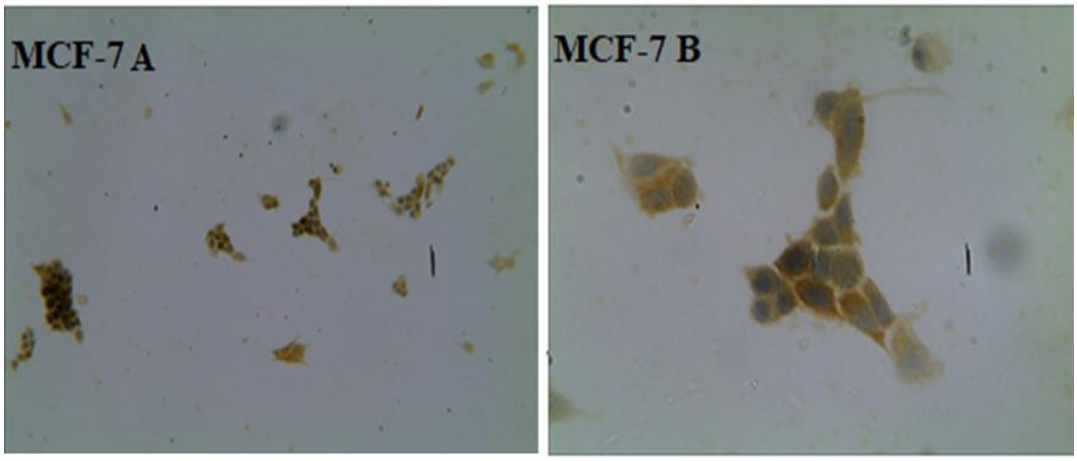

Figure 4.18: Immunocytochemistry images of MCF-7 Cells.
Immunocytochemistry assay images using MMP-2 primary antibodies for MCF-7 cells **(A)** at x40 **(B)** at x100 magnifications. The presence of bluish-brown colour is an indication of the presence of MMP-2 protein.

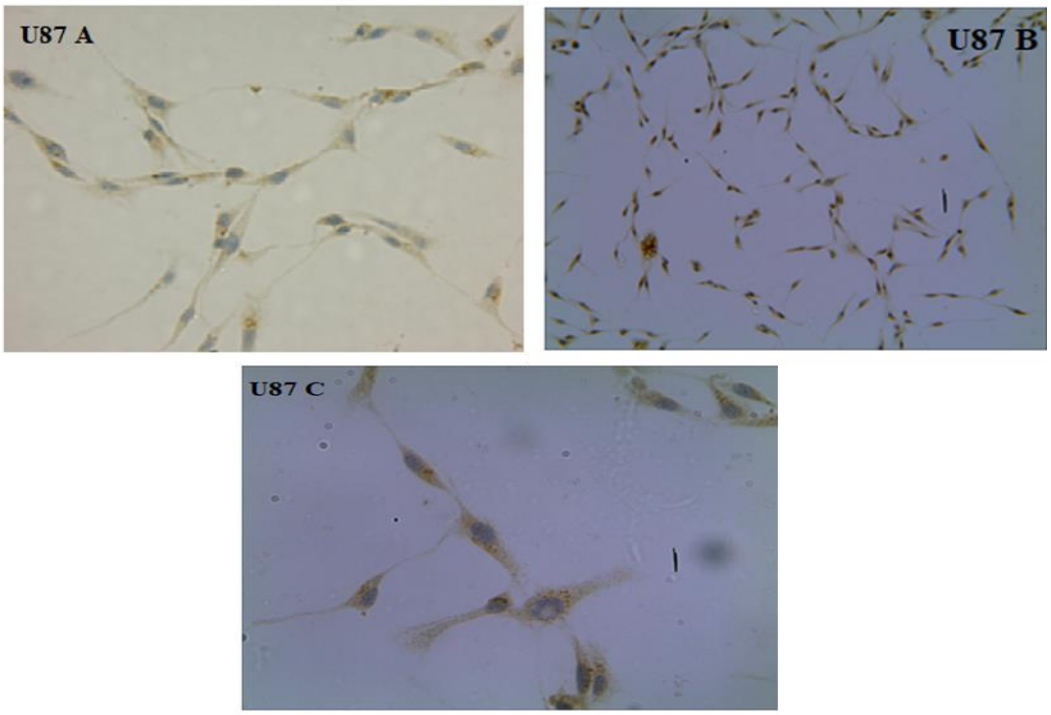

Figure 4.19: Immunocytochemistry images of U87 Cell.
Immunocytochemistry assay images using MMP-2 primary antibodies for U87 cells at x40 and x100 magnifications. The presence of bluish-brown colour is an indication of the presence of MMP-2 protein.

In conclusion, the QDs synthesised in this study can be applicable for biological purposes because they have low cytotoxicity and high fluorescence intensity. Also, it was established that the cancer cell lines could bind chlorotoxin from the binding studies, in a concentration depended manner and these cells have receptors for CTX protein.

4.15 References

Abe T., Mori T., Kohno K., Sciki M., Hayakawa T., Welgus H.G., Hori S. and Kuwano, M. (1994). Expression of 72 kDa type IV collagenase and invasion activity of human glioma cells. *Clinical and experimental metastasis* **12**(4): 296-304.

Aguilar Z.P. (2013). Quantum Dots for Bio imaging. **3**:41-70.

Ali S.A., Alam M., Abbasi A., Undheim E.A., Fry B.G., Kalbacher H. and Voelter W. (2016). Structure-activity relationship of chlorotoxin-like peptides. *Toxins* **8**(2):36.

Arvizo R., Bhattacharya R. and Mukherjee P. (2010). Gold nanoparticles: opportunities and challenges in nanomedicine. *Expert Opinion on Drug Delivery* **7**(6):753-763.

Burry R. W. (2011). Controls for immunocytochemistry: an update. *Journal of Histochemistry and Cytochemistry* **59**(1): 6-12.

Breast cancer statistics. https://www.cdc.gov/cancer/breast/statistics/index.htm (Accessed October 09 2017)

Buzea C., Pacheco I.I. and Robbie K. (2007). Nanomaterials and nanoparticles: Sources and toxicity. *Biointerphases* **2**(4): 17-71.

Centres for disease control and Prevention (CDC), 2017 report. https://www.cdc.gov/ (Accessed November 2017)

Crosby T., Hurt C.N., Falk S., Gollins S., Mukherjee S., Staffurth J., Ray R., Bashir N., Bridgewater J.A., Geh J.I. and Cunningham D. (2013). Chemoradiotherapy with or without cetuximab in patients with oesophageal cancer (SCOPE1): a multicentre, phase 2/3 randomised trial. *The Lancet Oncology* **14**(7): 627-637.

Dardevet L., Rani D., Aziz T.A.E., Bazin I., Sabatier J.M., Fadl M., Brambil E. and De Waard M. (2015). Chlorotoxin: a helpful natural scorpion peptide to diagnose glioma a nd fight tumour invasion. *Toxins* **7**(4):1079-1101.

Deshane J., Garner C.C. and Sontheimer H. (2003). Chlorotoxin inhibits glioma cell invasion via matrix metalloproteinase-2. *Journal of biological chemistry* **278**(6): 4135-4144.

Othman H., Wieninger S.A., ElAyeb M., Nilges M. and Srairi-Abi N. (2017). In Silico Prediction of the molecular basis of ClTx and AaCTx interaction with matrix metalloproteinase-2 (MMP-2) to inhibit glioma cell invasion. *Journal of Biomolecular Structure and Dynamics* **35**(13): 2815-2829.

Huang R., Han L., Li J., Liu S., Shao K., Kuang Y., Hu X., Wang X., Lei H. and Jiang C.(2011). Chlorotoxin-modified macromolecular contrast agent for MRI tumour diagnosis. *Biomaterials* **32**(22): 5177-5186.

Ojeda P.G., Wang C.K. and Craik, D.J. (2016). Chlorotoxin: structure, activity, and potential uses in cancer therapy. *Peptide Science **106*(**1): 25-36.

Fu Y., An N., Li K., Zheng Y. and Liang A. (2012). Chlorotoxin-conjugated nanoparticles as potential glioma-targeted drugs. *Journal of Neuro-oncology* **107**(3): 457-462.

Edwards B.S., Oprea T., Prossnitz E.R. and Sklar L.A. (2004). Flow cytometry for high-throughput, high-content screening. *Current Opinion in Chemical Biology* **8**(4): 392-398

El-Ghlban S., Kasai T., Shigehiro T., Yin H. X., Sekhar S., Ida M. and Seno M. (2014). Chlorotoxin-Fc fusion inhibits release of MMP-2 from pancreatic cancer cells. *BioMed Research International* 2014.

Ferlay J., Soerjomataram I., Dikshit R., Eser S., Mathers C., Rebelo M., Parkin D.M., Forman D. and Bray F. (2015). Cancer incidence and mortality worldwide: sources, methods and major patterns in GLOBOCAN 2012. *International journal of cancer* **136**(5).

Hagemann C., Anacker J., Ernestus R. I. and Vince G. H. (2012). A complete compilation of matrix metalloproteinase expression in human malignant gliomas. *World journal of clinical oncology* **3**(5): 67.

Hesam Dehghani (2012). Applications of Immunocytochemistry Croatia. Intech open science/open.www.intechopen.com. **1**:3

Holsapple M.P., Farland W.H., Landry T.D., Monteiro-Riviere N.A., Carter J.M., Walker N.J. and Thomas K.V. (2005). Research strategies for safety evaluation of nanomaterials, part II: toxicological and safety evaluation of nanomaterials, current challenges and data needs. *Toxicological Sciences* **88**(1): 12-17.

Holliday D.L. and Speirs V. (2011). Choosing the right cell line for breast cancer research. *Breast Cancer Research* **13**(4): 215.

IARC Cancer Base No.11 [Internet]. Lyon, France: International Agency for Research on Cancer; 2014. Available from: http://globocan.iarc.fr, (Accessed November 16 2017).

Krumwiede K. A., and Krumwiede N. (2012). The lived experience of men diagnosed with prostate cancer. In *Oncology Nursing Forum* **39**(5).

Liyanage U. K., Moore T. T., Joo H. G., Tanaka Y., Herrmann V., Doherty G. and Linehan D. C. (2002). Prevalence of regulatory T cells is increased in peripheral blood and tumour microenvironment of patients with pancreas or breast adenocarcinoma. *The Journal of Immunology* **169** (5): 2756-2761.

Neve R.M., Chin K., Fridlyand J., Yeh J., Baehner F.L., Fevr T. and Speed T. (2006). A collection of breast cancer cell lines for the study of functionally distinct cancer subtypes. *Cancer Cell* **10** (6): 515-527.

National Cancer Institute (NC1), 2017. https://www.cancer.gov/ (Accessed 18 September 2017)

International Agency for Research on Cancer; 2014.(IARC). http://globocan.iarc.fr/Pages /factsheets_cancer.aspx. (Accessed 17 December 2017)

Nguyen K. C., Seligy V. L. and Tayabali A. F. (2013). Cadmium telluride quantum dot nanoparticle cytotoxicity and effects on model immune responses to Pseudomonas aeruginosa. *Nanotoxicology*. **7**(2): 202-211

Nuttall R.K., Pennington C.J., Taplin, J., Wheal A., Yong V.W., Forsyth P.A. and Edwards D.R. (2003). Elevated Membrane-Type Matrix Metalloproteinases in Gliomas Revealed by Profiling Proteases and Inhibitors in Human Cancer Cells1 1 Norfolk and Norwich Big C Appeal; *Molecular Cancer Research* **1**(5):333-345.

Oberdoerster et al. and Stoeger et al. *Environmental Health Perspectives.* **115**(6): A291.

Oberdörster G. (2010). Safety assessment for nanotechnology and nanomedicine: concepts of nanotoxicology. *Journal of Internal Medicine.* **267**(1): 89-105.

Pai V.B. and Nahata M.C. (2000). Cardiotoxicity of chemotherapeutic agents. *Drug Safety.* **22**(4): 263-302.

Polyak K. and Kalluri R. (2010). The role of the microenvironment in mammary gland development and cancer. *Cold Spring Harbor Perspectives in Biology*. **2**(11): a003244.

Shin S.W., Song I.H. and Um S.H. (2015). Role of physicochemical properties in nanoparticle toxicity. *Nanomaterials* **5**(3): 1351-1365.

Siegel R., DeSantis C., Virgo K., Stein K., Mariotto A., Smith T. and Lin C. (2012). Cancer treatment and survivorship statistics, 2012. *CA: A Cancer Journal for Clinicians*. **62**(4): 220-241.

Siegel R.L., Miller K.D. and Jemal A. (2017). Cancer statistics, 2017. CA: *A Cancer Journal for Clinicians* **67**: 7–30.

Tai S., Sun Y., Squires J. M., Zhang H., Oh W. K., Liang C.-Z. and Huang J. (2011). PC3 Is a Cell Line Characteristic of Prostatic Small Cell Carcinoma. *The Prostate* **71**(15): 1668–1679.

Thovhogi N., Sibuyi N., Meyer M., Onani M and Madiehe A. (2015). Targeted delivery using peptide-functionalised gold nanoparticles to white adipose tissues of obese rats. *Journal of Nanoparticle Resea*rch **17**(2): 112.

VanMeter T. E., Rooprai H. K., Kibble M. M., Fillmore H. L., Broaddus W. C., and Pilkington, G. J. (2001). The role of matrix metalloproteinase genes in glioma invasion: co-dependent and interactive proteolysis. *Journal of neuro-oncology* **53**(2): 213-235.

WHO Report, 2015. http://www.who.int/mediacentre/factsheets/fs297/en/Accessed on November, 2017.12.21

Xu S., Li D. and Wu P. (2015). One-pot, facile, and versatile synthesis of monolayer MoS2/WS2 quantum dots as bioimaging probes and efficient electrocatalysts for hydrogen evolution reaction. *Advanced Functional Materials.* **25**(7): 1127-1136.

Yamamoto M., Mohanam S., Sawaya R., Fuller GN., Seiki M., Sato H., Gokaslan ZL., Liotta LA., Nicolson GL., and Rao J.S.(1996). Differential expression of membrane-type matrix metalloproteinase and its correlation with gelatinase A activation in human malignant brain tumours in vivo and in vitro. *Cancer Research* **56**(2): 384-392

Zhang L., Xing Y., He N., Zhang Y., Lu Z., Zhang J. and Zhang Z. (2012). Preparation of graphene quantum dots for bioimaging application. *Journal of Nanoscience and Nanotechnology* **12**(3): 2924-2

CHAPTER FIVE

Recombinant Expression and Purification of Chlorotoxin (CTX)

5.1 Introduction

Protein expression can be defined as the synthesis, modification and regulation of protein in living organisms using a cellular system (Meagher *et al.,* 1977). Current developments in genomics and proteomics have simplified the use of recombinant DNA technology to assess most protein of concern, without previous knowledge of the protein's location or function in the cells (Young *et al.,* 2012; Koehn and Hunt, 2009). In the past few years some technologies have been established for the manufacture of recombinant proteins for therapeutic studies. These include the use of rapid cloning systems, miniaturization of cell growth conditions, and a variety of innovative automation systems for expression and purification of recombinant protein. Recombinant expression of proteins can easily be achieved through the use of a strong promoter system and there several of them available they include; T7, lambda Pl, and araB. Perhaps the most popular is the T7-based pET expression plasmids (Makrides, 1996; Hannig and Makrides, 1998)

The method of recombinant protein expression involves transfecting cells with DNA and culturing them to generate the desired protein. There are different microorganisms used for the producing recombinant protein, the most common being *Escherichia coli*. (*E. coli*); due to its low cost, easily scalable, short turnaround time, it is highly expressed and production of hetergenous protein (Rosano and Ceccarelli, 2014; Koehn and Hunt, 2009; Hannig, and Makrides, 1998; Baneyx, 2009; Hunt 2005)

Recombinant expression facilitate the production of proteins in large quantities for the biochemical and industrial application (Rosano and Ceccarelli, 2014; Kigawa and Yokoyama, 2002).

Here, Recombinantly expressed and purify CTX was to be used to probe its interaction between the commercial form of the peptide using simple experiment like blocking study and cell migration assay.

5.2 Materials and Method

5.2.1 Materials

Ammonium persulphate, Bacteriological agar (Merck), Tryptone (Merck), NaCl (Merck), Tryptone powder (Merck), Yeast (Merck), EDTA, Coomassie® Brilliant Blue, Ampicillin (Sigma), Tris-Cl (Merck), lysozyme (Sigma), Complete ^{TM}, EDTA-free protease inhibitor cocktail tablet (Roche), TEMED, acrylamide–Bis ready to use solution 40 % (Promega).

5.2.3 Transformation and Expression screening of Chlorotoxin (CTX)

Transformation reaction of Chlorotoxin was carried out using competent *E. coli* BL21 cells. Firstly, the cells were thawed on ice, then 100 µL of the competent BL21 cells were placed in a tube with 2µL of the vector plasmid DNA. This was gently mixed by tapping, the tube and incubated on ice for 30 minutes, transformation mixture was heat shocked at 42°C for one minute and incubated immediately on the ice again for 5 minutes. Heat shocked transformatio n mix was added to 900µL pre-warmed Luria Broth (LB) in a sterile tube with no antibiotics added. The mixture was incubated at 37 °C for one and a half hours in a shaker. LB Agar plate with ampicillin (Amp positive) and some without ampicillin (Amp negative) was prepared to evaluate if the transformation has taken place. Four plates were labelled as follows: One LB agar plate only (Amp^-) and three LB agar + Ampicillin with 100 µg/mL concentration of ampicillin (Amp+). 50µL of the transformation mixture was plated onto the

LB agar plate (Amp^-) and LB + Ampicillin (Amp+) plates respectively. Also, the rest of the transformation mixture was centrifuged for about three minutes and centrifuged at about 14500. 50 µL of the pellet was also plated on an LB agar Amp+ plate, and finally, 50 µL of the BL21 competent cells were plated on LB agar Amp+ plate, serve as a control, to confirm that the BL21 competent cells did not have plasmid DNA before the transformation reaction was carried out. These plates were wrapped in foil paper and incubated overnight at 37 °C using a 211DS Shaking Incubator (Labnet).

After overnight incubation, a single colony was picked from the LB + Ampicillin plates and was inoculated into 10mL pre-warmed LB containing 100 µg/mL Ampicillin. The tube was incubated overnight at 37 °C shaking incubator and glycerol stocks of the colony were prepared from the overnight culture and were stored at -80 °C. From the overnight culture, 1mL was taken and was added to 9mL LB containing Ampicillin of 100µg/mL concentration and the culture mixture was further incubated for an additional 1 hour 30 minutes at 37 °C, in a shaker. After the incubation, 2mL was taken from the cell culture solution mixture, and this was labelled un-induced sample. The un-induced culture was centrifuged at 14500 RPM for 5 minutes using a 5417R Benchtop Microcentrifuge from Eppendorf. The pellets were subsequently stored at -80 °C for Sodium dodecyl sulphate polyacrylamide gel, electrophoresis (SDS-PAGE) analysis.

5.2.4 Large Scale Expression of Chlorotoxin

A 1mL of glycerol stock of the sample culture was added into 100 mL LB supplemented with 100 µg/mL ampicillin, and the mixture was incubated overnight at 37 °C with shaking. The overnight culture was added to 900 mL LB with 100 µg/mL ampicillin concentration in a 2 Litre Erlenmeyer flask to ensure adequate aeration. The sample was incubated at 37 °C until an optical density (OD) of 0.8 to 1.0 was attained. As soon as this OD range was reached,

10mL of the sample was removed which represented the un-induced sample, spilt into 2mL Eppendorf tubes and centrifuged at 14500 rpm for 5 minutes with a bench centrifuge 5417R Benchtop Microcentrifuge from Eppendorf and pellets were stored at -80 °C for SDS-PAGE. The 990 mL of the remaining cell culture was induced with 1mM IPTG for induction of protein expression and was incubated for three hours at 37 °C with shaking. The induced culture was then centrifuged in 50 mL tubes using a Heraeus Megafuge 1.0R centrifuge at 4300xg RCF for 20 minutes. Two 50 mL tubes of the pellet was re-suspended in 10 mL Sodium Chloride-Tris-EDTA (STE)/lysozyme (lysis buffer), 5mM of imidazole was added to the pellet, and the sample mixtures were put together in a one 50 mL tube, one tablet of 1X Complete^{TM}, EDTA-free protease inhibitor cocktail tablet (Roche) was added, appropriately mixed with vortex and this was incubated on ice for 30 minutes. The culture sample was sonicated on ice for three cycles (one-minute sonication and two minutes rest on ice). This procedure then repeated until the lysate was clear and it was centrifuged at 4300xg RCF for 20 minutes at 4 °C, the pellet and supernatant (this was labelled total lysate) was stored at -80 °C for protein purification.

5.3 Purification of Recombinant HIS-CTX-GST Protein

5.3.1 Preparation of Column

This was carried out following the manufacturer's instructions to effectively isolate the protein. Briefly, a column of a 4mL slurry of Nickel-NTA agarose gel (about 2mL bed volume) was taken and pipetted into 15mL tubes and centrifuged briefly for 5 minutes at 4000xg, and the supernatant was discarded. Then about 8mL of lysis buffer was then added in a ratio 2:1 (Ni-NTA-Lysis buffer) this was repeated twice, and the supernatant discarded each time.

5.3.2 Purification of HIS-CTX-GST Protein

Subsequently following the preparation of the column, the protein lysate (12 mL) was added to the equilibrated beads in the column (4 mL) and mixed on the Tube roller (Stuart SRT9dD) at 4 °C for 60 minutes. The mixture was allowed to settle in the tube the sample was collected as flow through 1. This step was repeated twice and labelled flows through 2 and flow through 3 for SDS-PAGE analysis. The HIS-CTX-GST protein was eluted by adding 3mL of elution buffer. The elution buffer and HIS-CTX-GST suspension were mixed at 4 °C for 10 minutes on the Tube roller (Stuart SRT9dD) to detach the HIS-CTX-GST protein from the beads, and this was collected as Elution 1. This step was repeated twice to generate Elution 2 and Elution 3, and the solutions were also collected and stored on ice for SDS page analysis. The beads were then washed with MES buffers to remove any excess protein within the column, then with distilled water and finally with 20 % ethanol using X10 column volume and finally, stored in 20 % ethanol at 4 °C.

5.3.3 Analysis of Extracted HIS-CTX-GST Protein

The protein samples collected during purification were analysed by a 12 % SDS-PAGE. SDS-PAGE solutions were prepared and cast using a Mini-PROTEAN Tetra Cell, TEMED was added right before the gel was cast as shown in the table below. For the expression screening samples, ten µL of protein sample was mixed with 10mL of 2X SDS sample buffer, and heated at 95 °C for 5 minutes and vortexed for 2 minutes. They were centrifuged to sediment the debris, and 10µL of the sample then loaded on the SDS-PAGE gel. The purified samples were loaded as follows; 10µLof the unstained protein, marker was loaded first, followed by 10µL of the sample and 10 µL of 2X SDS sample buffer mixed with 10µL of the sample also loaded onto the gel. The gel was run for 70 minutes at 150 Volts. Moreover, then stained with Coomassie Brilliant Blue R-250 stain for 15 minutes and destained overnight, it

was put on a Stovall Belly dancer shaker, and Canon Cano Scan LiDE 120 electronic scanner was used to scan the gels.

Table 4.1: The preparation of 12 % SDS-PAGE.

Reagents	12 % separation buffer	5 % stacking buffer
dH_2O	4.3 mL	3.65 Ml
1.5 M Tris-Cl pH 8.8	2.5 mL	-
0.5 M Tris-Cl pH 6.8	-	630.0 Ml
10 % SDS	100.0 µL	50.0 Ml
Acry/Bis (30 %)	3.0 mL	400.0 Ml
10 % APS	200.0 µL	50.0 Ml
TEMED	20.0 µL	20.0 Ml

5.3.4 The Cleavage of HIS-GST-CTX with 3C Protease.

All the elution collected were put together, and a 5mL aliquot taken, and 500 µL of HRV 3C protease was added, this was allowed to cleave overnight at 4^{o}C on a Tube roller. The following morning, the protein solution was passed over the Ni-NTA beads to remove the tag which binds to the beads, and the pure proteins were collected in the flow through and freeze-dried overnight at -51 ^{o}C to concentrate the peptide and after that it was dialysed at 4 ^{o}C overnight with continuous stirring with 0.5X PBS. The sample was poured out of the dialysis tubing into a 15 mL tube and analysed with SDS-PAGE.

5.3.5 Quantification of Chlorotoxin Protein

The Qubit Fluorometer was used to quantify the protein, and Nanodrop 2000 (Thermo scientific) spectrophotometer was also used. Briefly, three standard qubits working solution was prepared in a ratio of 1:200 in a Qubit™ protein with a qubit reagent in qubit buffer in small tubes wrapped with foil because the reaction is sensitive to light.

Standard 1: 10 µL of standard sample 1 and 190 µL of working solution

Standard 2: 10 µL of standard sample 2 and 190 µL of working solution

Standard 3: 10 µL of standard sample 3 and 190 µL of working solution

Protein sample: 10 µL of protein and 190 µL of working solution

It was vortexed for about 2-3 seconds and incubated in the dark for 15 minutes before reading. Standard assay samples were read first before protein samples were read. The protein solution then kept for further use.

5.4 Analysis of Sequences

Glycerol stocks previously prepared from overnight cultures were taken out from -80 ^{o}C freezer with the use of a sterile loop it was streaked onto Nutrient agar plates in a sterile hood and left to grow overnight at 37 °C. Parafilm was used to seal the plates, and it was sent to Inqaba Biotechnologies for sequencing. Primary sequencing method was used. The sequencing was done using two colonies picked from two different plates with specific primers in both forward and reverse directions. All sequences were run on the ABI 3500XL Genetic Analyzer, POP7™ (ThermoScientific). Bio Edit© Sequence Alignment editor was used to do multiple sequence alignments as well as generate a consensus sequence. The GenBlast (Genbank) algorithm was used to align the sequence with the oligonucleotide sequences.

5.5 Results

5.5.1 SDS GEL of CTX Expression Screening

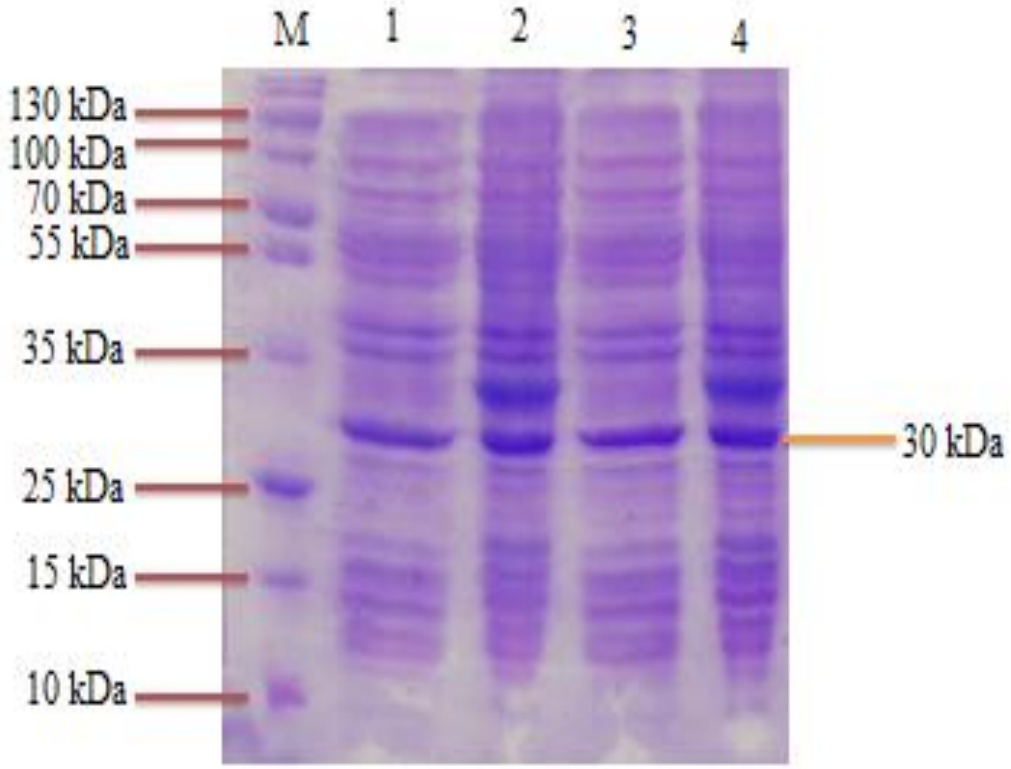

Figure 5.1a: Expression screening results of Chlorotoxin (CTX).
From the SDS-PAGE gel; Lane M is a molecular weight for protein marker in kDa, Lanes 1and 3 is the un-induced bacterial culture without 1mM IPTG while lanes 2 and 4, is the total bacterial cell culture overnight with added 1mM of IPTG.

5.5.2 SDS GEL of CTX Purification

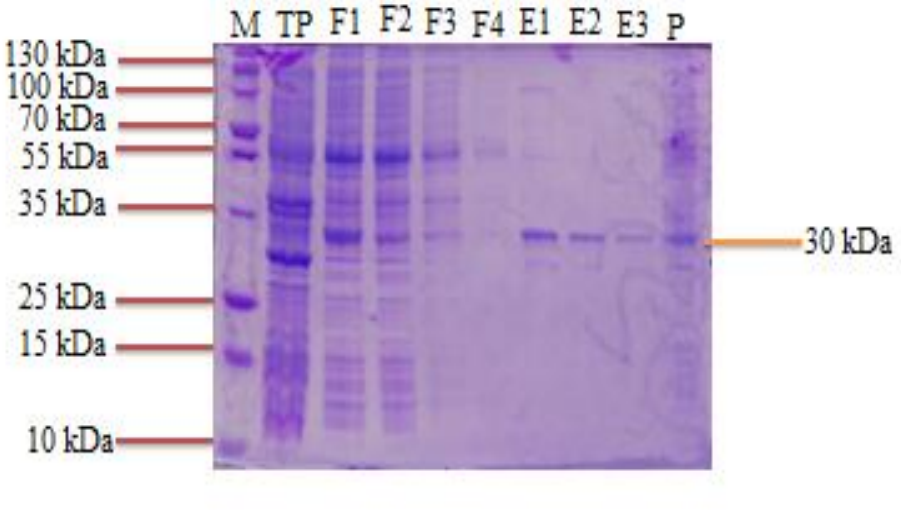

Figure 5.1b: SDS-PAGE analysis of Purification of Chlorotoxin protein.
M is protein molecular weight marker in kDa. TP is total protein lysate before purification, F1 to F4 flows through from nickel beads affinity column, E1, E2, E3: are the elution 1, elution 2, and elution 3 and P is the pellet. The protein band at 30 kDa on the SDS gel correlates with the expected size of CTX protein.

5.5.3 SDS Gel is showing the CTX Digestion.

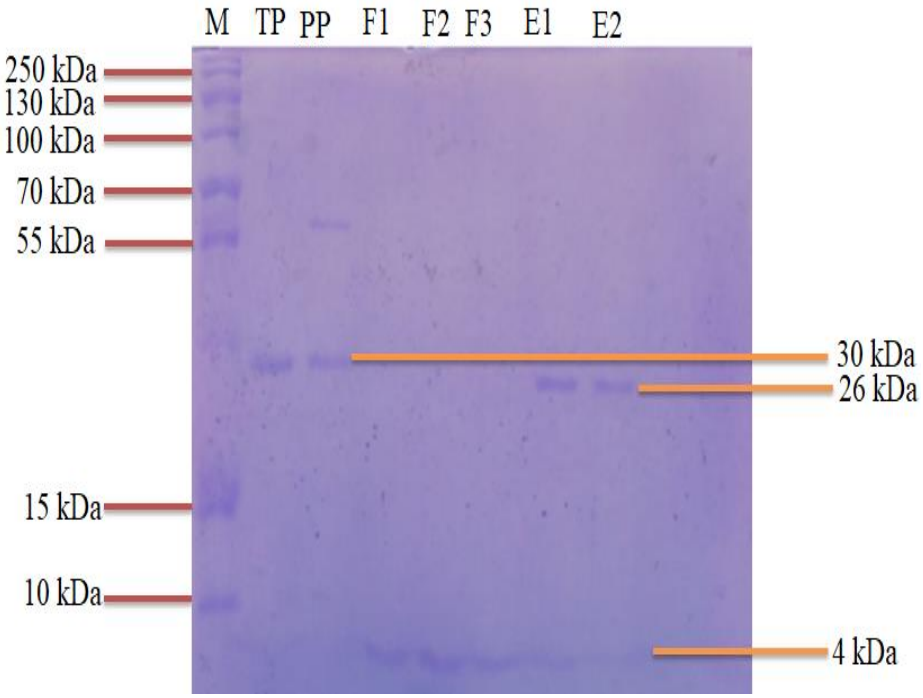

Figure 5.1c: SDS Gel showing the Digestion of CTX.
M is protein molecular weight marker in kDa. TP is total protein lysate before purification; PP is Protein with 3C Protease after the overnight cleavage, F1 to F3 is flow through from nickel beads affinity column, E1, E2 are the elutions. The protein band on the SDS gel correlates with the size of the CTX protein expected after the cleavage which is 4kDa.

5.6 Sequence of Chlorotoxin

AGTCAGAGGTTTTCACCGTCATCACCGAAACGCGCGAGGCARATCGTCAGTCAG

TCACGATGCGGCCGCTCGAGTCAATGATGATGATGATGACGACACAGGCAC

TGCGGGCCATAACATTTACCGCGGCCTTTACCGCCACAGCAATCATCGCATTTAC

GCGCCATCTGATGATCCGTGGTAAAACACGGCATGCACATGGATCCCAGGGGCC

CCTGGAACAGAACTTCCAGATCCGATTTTGGAGGATGGTCGCCACCACCAAACG

TGGCTTGCCA

Figure 5.2a: Amino acid sequence of Chlorotoxin

agtcagaggttttcaccgtcatcaccgaaacgcgcgaggcaratcgtcagtcagtcacga

S Q R F S P S S P K R A R X I V S Q S R

tgcggccgctcgagtcaatgatgatgatgatgatgacgacacaggcactgcgggccataa

C G R S S Q - - - - - - R H R H C G P -

catttaccgcggcctttaccgccacagcaatcatcgcatttacgcgccatctgatgatcc

H L P R P L P P Q Q S S H L R A I - - S

gtggtaaaacacggcatgcacatggatcccaggggcccctggaacagaacttccagatcc

V V K H G M H M D P R G P W N R T S R S

gattttggaggatggtcgccaccaccaaacgtggcttgcca

D F G G W S P P P N V A C

Figure 5.2b: Nucleotide sequence of CTX protein retrieved from ExPASy translate tool.

5.7 Discussion on the purification and recombinant expression of chlorotoxin

Chlorotoxin peptide used in this study is approximately a 4kDa peptide, tagged with GST of molecular weight 26 kDa. Expression screening and purification showed that the protein (HIS-CTX-GST) was expressed at the right molecular weight (30kDa) as represented in (Fig 5.1a and 5.1b respectively), Qubit Fluorometer showed that the concentration of the protein was 2.75mM. Subsequently, the protein was cleaved with 3C protease, however, after several attempts of using lower concentrations of protease, the concentration of the 3C protease was increased to ratio 1:10 (500 µL was added to 5 mL). After that, the 3C protease and protein were mixed overnight in a roller mixer and was eventually cleaved. The right size of the CTX protein (4 kDa) was obtained as shown in Figure 5.1c. Two bands showing the HIS-GST tag and CTX protein were seen on the SDS-PAGE when the overnight cleaved protein was analysed before purification. Furthermore, glycerol stock of the starter culture was streaked on agar plates with ampicillin and allowed to grow overnight in an incubator at 37^{o}C. These plates were used for sequencing using universal primers, The sequence results were analysed using Bio Edit, and the amino acid and nucleotide sequences were then determined using

ExPASy blast form (https://web.expasy.org/translate/). The result gave a 100% similarity for an amino acid sequence of chlorotoxin (Figure 5.2a and figure 5.2b)

5.8 Blocking Studies

Blocking studies were carried out using FITC-CTX labelled peptide 1 and purified CTX peptide, to determine FITC-CTX binding was specific and competitive.

5.8.1 Material and Method

Six-well culture plate, purified CTX, FITC peptide, 1X PBS, Trypsin, complete DMEM media, complete RPMI media, and tips (yellow tips and blue tips).

5.8.2 Method

A modification of Thovhogi *et al.,* 2015 protocol was used for this experiment. Briefly, cells were seeded in a 6well plate for 24hrs at a cell density of 3×10^5. They have grown for about 2 to 4 days depending on each cells line and about 60-70% confluence, they were washed with 1X PBS. Different concentration of purified peptide (0.125 mM and 0.5 mM) was used as the blocking peptide, and FITC-CTX (0.0125 Mm) was prepared. They were added at the same time to each well in 6 well tissue culture plate and incubated for one hour at 37 ºC. After incubation, cells first washed with 1X PBS, trypsinised and centrifuged at 3000 rpm for 3 minutes, and the pellets were suspended in 300 µL media in the tube and placed on ice, and the cells were analysed using (BD accuri) flow cytometer. A minimum of 10^3 cells was analysed and this done for all four cells lines. The experiment was carried out in triplicates, and the average of the experiments was taken.

5.9 Results

5.9.1 Histogram of cell blocking studies using labelled chlorotoxin and purified chlorotoxin

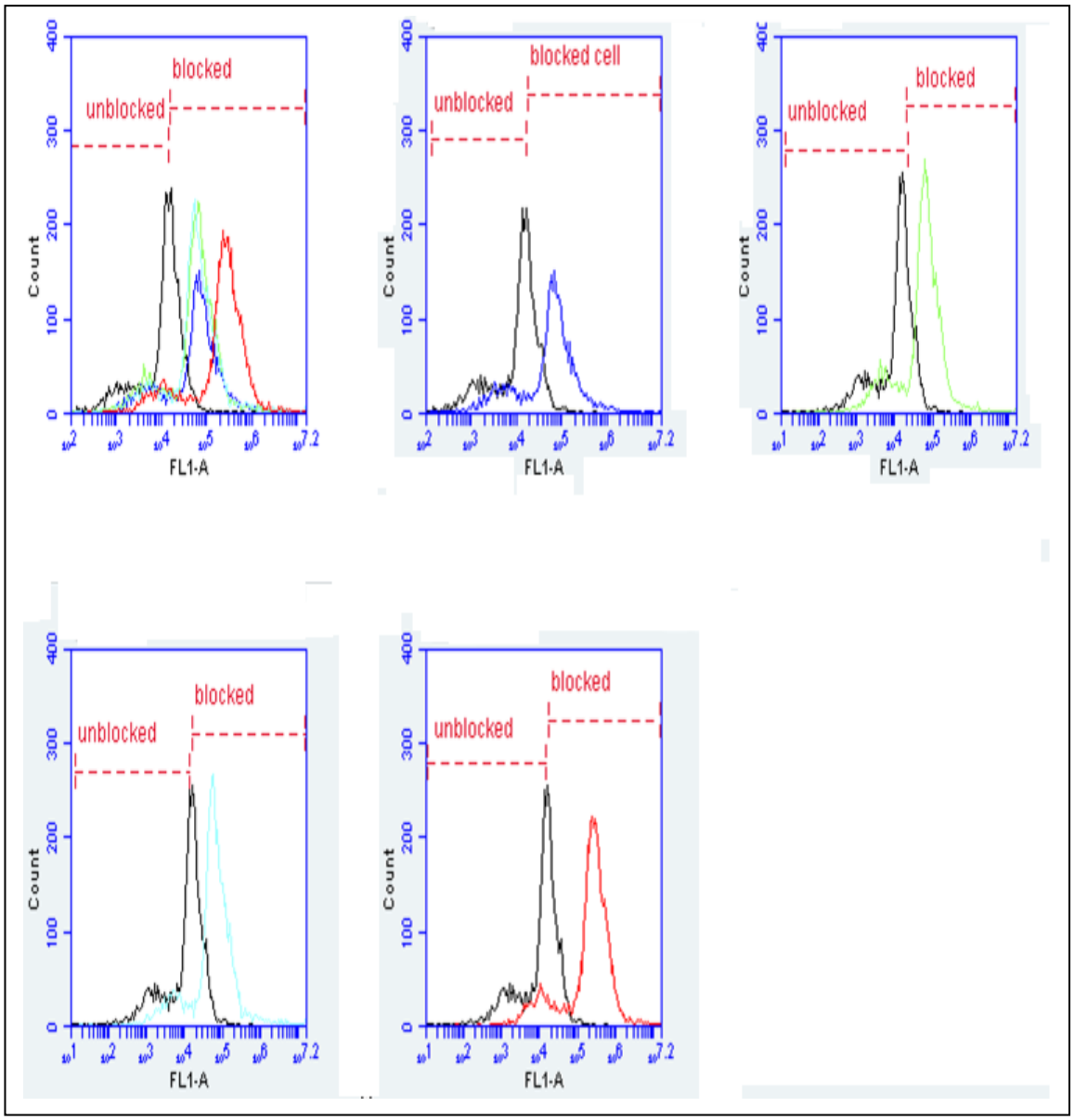

Figure 5.3: Histogram of cell blocking studies.
Here we use FL1-A filter of the flow cytometer showing the blocked, and unblocked cells spectra using FITC labelled chlorotoxin and unlabelled CTX.

5.9.2 HeLa Cells Block Study Analysis using CTX Peptides 1

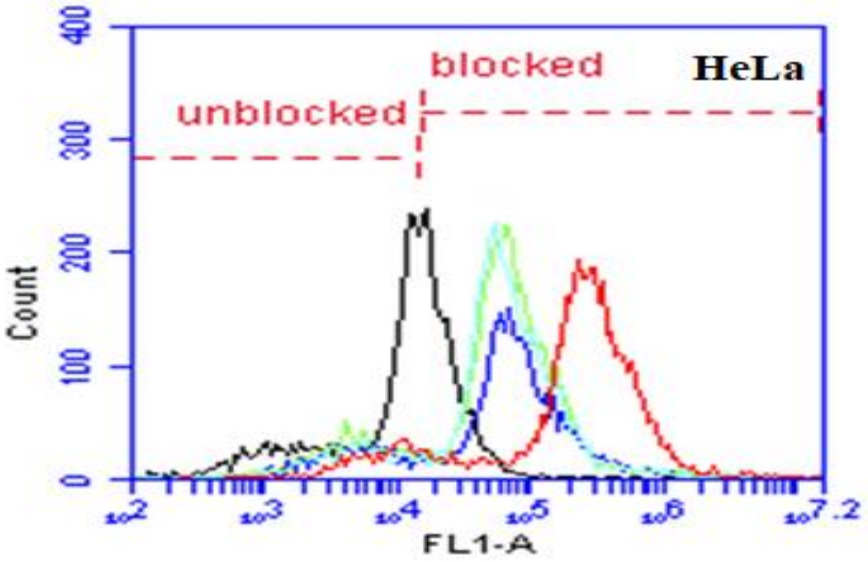

Figure 5.4: Histogram showing is blocking experiment of HeLa cells using Chlorotoxin peptide.

Black, green, aqua, blue, and red colour represent untreated cells, 0.0125mM, 0.125mM, 0.5mM of blocking peptide (unlabelled CTX) and 0.0125mM labelled peptide1(FITC-CTX) respectively. The spectra showed blocking of receptors at high concentration of unlabelled peptide with gradual movement to the left.

5.9.3 PC-3 Cells Block Study Analysis using CTX Peptides 1

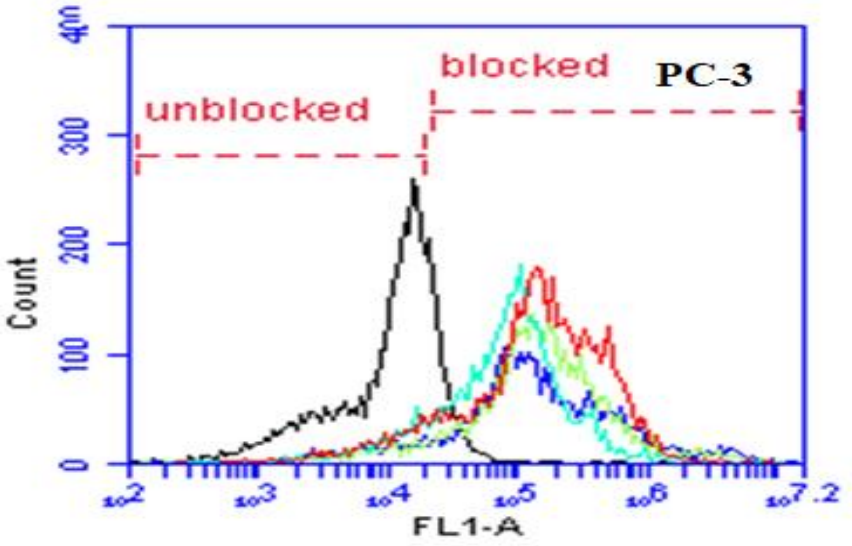

Figure 5.5: Histogram showing is blocking experiment of PC-3 cells using chlorotoxin peptide.

Black, green, aqua, blue, and red colour represent untreated cells, 0.0125mM, 0.125mM, 0.5mM of blocking Peptide (unlabelled CTX) and 0.0125mM Labelled Peptide1(FITC-CTX).

The spectra showed that the spectra were all at the same point hence cells were not blocked, but the binding of the peptide to cells was competitive.

5.9.4 U87 Cells Block Study Analysis using CTX Peptides 1

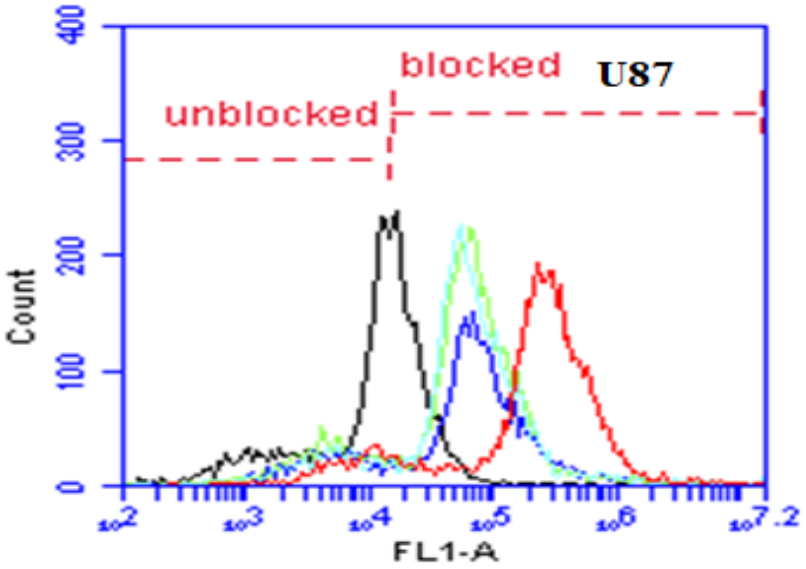

Figure 5.6: Histogram showing is blocking experiment of U87 cells using chlorotoxin peptide.
Black, green, aqua, blue, and red colour represent untreated cells, 0.0125mM, 0.125mM, 0.5Mm of blocking Peptide (unlabelled CTX) and 0.0125mM labelled peptide1(FITC-CTX). The spectra showed blocking of cells receptors as the concentration of unlabelled peptide increases with gradual movement to the left

5.9.5 MCF - 7 Cells Block Study Analysis using CTX Peptides 1

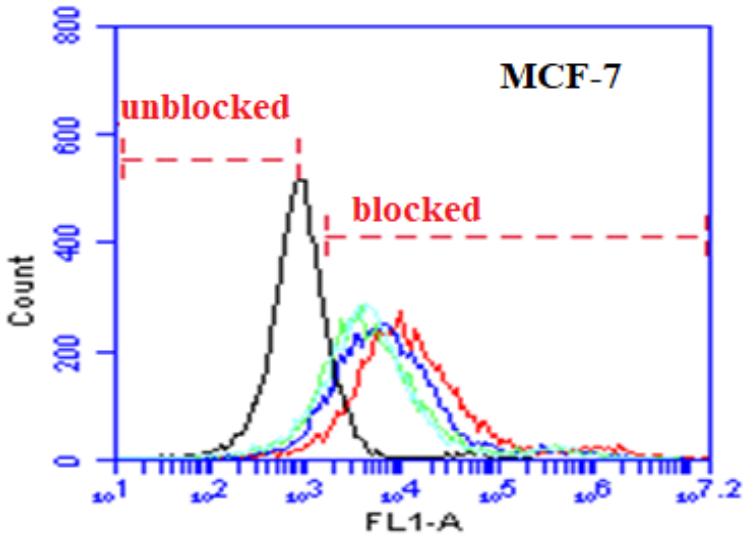

Figure 5.7: Histogram showing is blocking experiment of MCF-7 cells using chlorotoxin peptide.

Black, green, aqua, blue, and red colour represent untreated cells, 0.0125mM, 0.125mM, 0.5Mm of blocking Peptide (unlabelled CTX) and 0.0125mM labelled peptide1(FITC-CTX). The spectra showed a slight spectra movement to the left, but the binding of the peptide to cells was competitive with small as concentration increases.

5.9.6 HeLa, PC-3, U87 and MCF-7 Blocked Cells Percentages

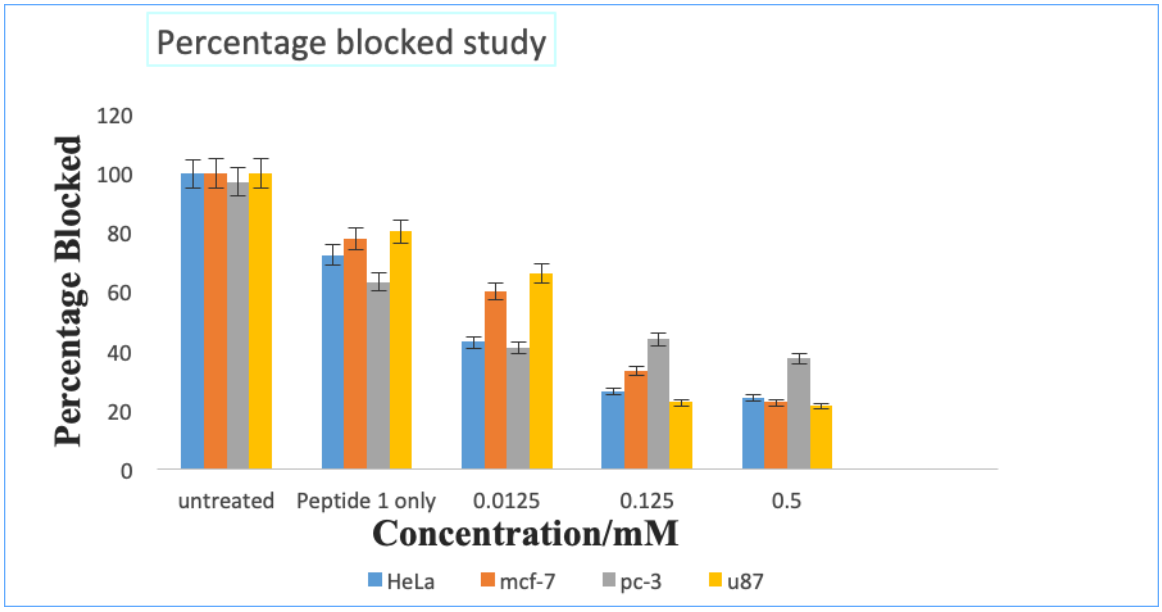

Figure 5.8: Chart showing percentage blocked cells of HeLa, PC-3, U87 and MCF-7. This shows that the blocking of cells is dependent on receptors available for binding and concentration.

5.10 Discussion on Blocking Studies

Chlorotoxin CTX is a promising tumour ligand for *in-vivo* and *in-vitro* fluorescence imaging study (Kittle et al., 2014). Hence, in this work, blocking studies were carried out to determine if the binding of the peptide to protein receptors in the cell lines were specific or concentration dependent. Cells were incubated with different concentrations of unlabeled peptide (CTX) which was used as the blocking peptide. The cells were incubated with three different concentration (0.0125mM, 0.125mM, 0.5mM) of chlorotoxin peptide purified (unlabelled CTX) with a fixed concentration of FITC-CTX labelled peptide (0.0125 mM).

Figure 5.3 represents one of the histogram plots of cell blocking studies showing all the filters in the flow cytometry. Here, we used FL1-A filter of the flow cytometer showing the blocked, and unblocked cells spectra using FITC labelled chlorotoxin and unlabelled CTX. Figure 5.4 shows the blocking studies using HeLa cells with the following concentration 0.0125mM, 0.125mM, 0.5mM of blocking peptide (unlabelled CTX) and 0.0125mM labelled Peptide1(FITC-CTX). In the study, it was observed that in the presence of purified unlabelled peptide the binding of labelled peptide FITC-CTX decreases, hence, the spectra shifted to the left and it is concentration dependent (Thovhogi *et a*l .,2015)

Blocking studies of PC-3 cells using Chlorotoxin labelled and the unlabelled peptide is shown in figure 5.5. The cell movement is seen to slightly shift to the left towards the untreated cell only (black spectra) when compared to the spectra for peptide only (red). This implies that the binding is concentration and receptor-dependent. Additionally, U87 cells blocking studies were carried out. Several concentrations [0.0125mM, 0.125mM, 0.5Mm of blocking Peptide (unlabelled CTX) and 0.0125mM labelled peptide (FITC-CTX)] were used. Results displayed in figure 5.6 showed that there was a clear shift of the spectra to the left as the concentration of the unlabelled peptide increases indicating a reduction in the receptors available for binding.

Histogram of cell blocking studies using CTX-FITC peptide on mcf-7 is shown in figure 5.7. It was observed that as purified unlabelled peptide concentration increases the binding of labelled peptide (FITC-CTX) decreases. Hence, the spectra shifted to the left when compared to the spectra that are peptide only (red).

Figure 5.8 represents the percentage of four blocked cells (HeLa, PC-3, U87 and MCF-7) and this was carried in triplicates. The chart shows the percentage of untreated cells, 0.0125mM labelled peptide (FITC-CTX) and the different concentration of the unlabelled proteins used. From the chart, it was observed that the blocking of the cell is concentration dependent, in

other words, as the concentration of the unlabelled protein increases the receptor available for binding with the labelled protein decreases.

In conclusion, this study shows that the mechanism of cell binding uptake depends on the receptors of the cells available for binding. Combined percentage chart of blocked cells for HeLa, PC-3, U87 and MCF-7 is presented in (Figure 5.8). As the concentration of the unlabelled peptide increases the receptors available for the labelled peptide (CTX-FITC) to bind decreases hence decrease in fluorescence intensity. This is in accordance with (Thovh -ogi *et al*., 2015).

5.11 Scratch Migration Assay

5.11.1 Experimental

This was carried out according to the method described by Kasai *et al.*, (2012) and Al-Asmari *et al*., (2016) with some modifications. Cells(HeLa, PC-3, MCF-7 and U87) were seeded in 24 well plates with their respective media. After 24 hours, cells were found to be about 70-80 % confluence, they were washed with PBS, and a yellow tip 200μL plastic pipette was used to make a scratch on the confluent cells creating a wound, and the wells were rinsed with media to remove cell debris. The cells were incubated with various concentration of purified CTX peptide at 0.025 Mm, 0.05 Mm and 0.1 mM prepared in cell media and a control which was not supplemented with the peptide. They were incubated at 37 ^{o}C, and picture image was taken at 0, 8hrs, 12hrs and 24hrs using Zeiss Primo vert light microscope. The area migrated was obtained from the difference in the distance between 0hour and each time measured in micrometre (µm) using Image J Software and the percentage gap closure was expressed as

$$\frac{0\,hrs}{24\,hrs}\times 100$$

5.11.2 Result and discussion of Scratch Migration Assay

5.11.2.1 HeLa cells percentage gap closure of scratch migration assay

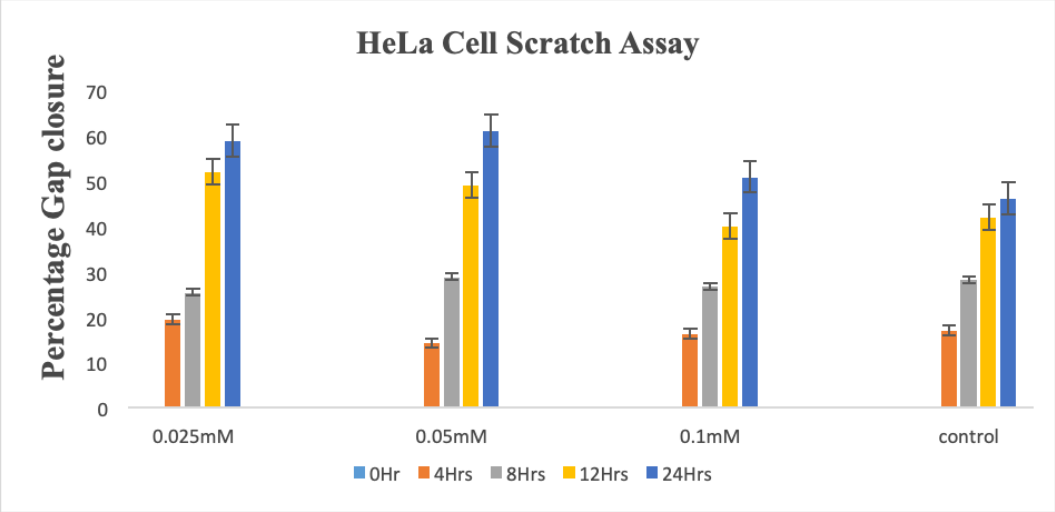

Figure 5.9: Chart showing percentage gap closure of HeLa cells
when treated with various concentrations of CTX and Gap closure was measured at a different time interval from image pictures taken at 0, 4, 8, 12, and 24hours. Percentage gap closure was high at a lower concentration of the peptide, and it increases with time.

5.11.2.2 U87 Cells Percentage Gap Closure of Scratch Migration Assay

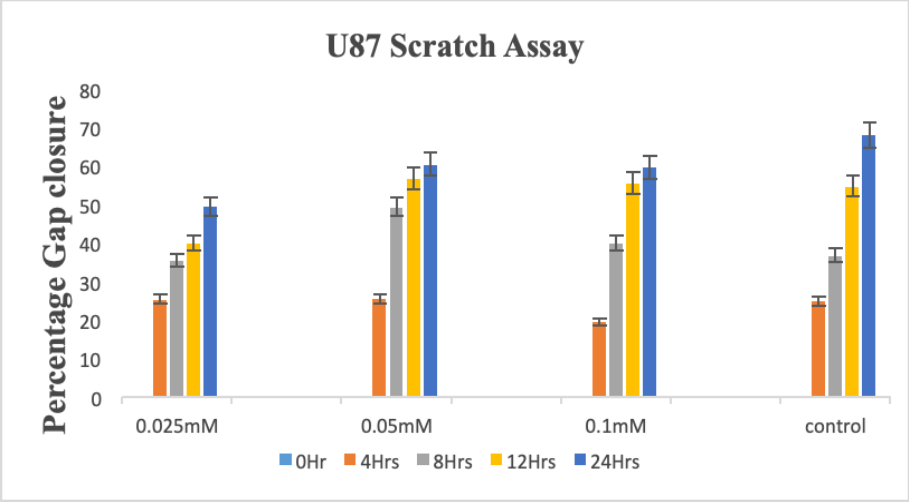

Figure 5.10: Chart showing percentage gap closure of U87 cells
when treated with various concentrations of CTX and Gap closure was measured at a different time interval from image pictures taken at 0hr, 4hrs, 8hrs, 12hrs, and 24hrs. Percentage gap closure was highest at 0.05mM concentration of the peptide at 24hours, and the gap closure was increasing with time.

5.11.2.3 MCF-7 Cells Percentage Gap Closure of Scratch Migration Assay

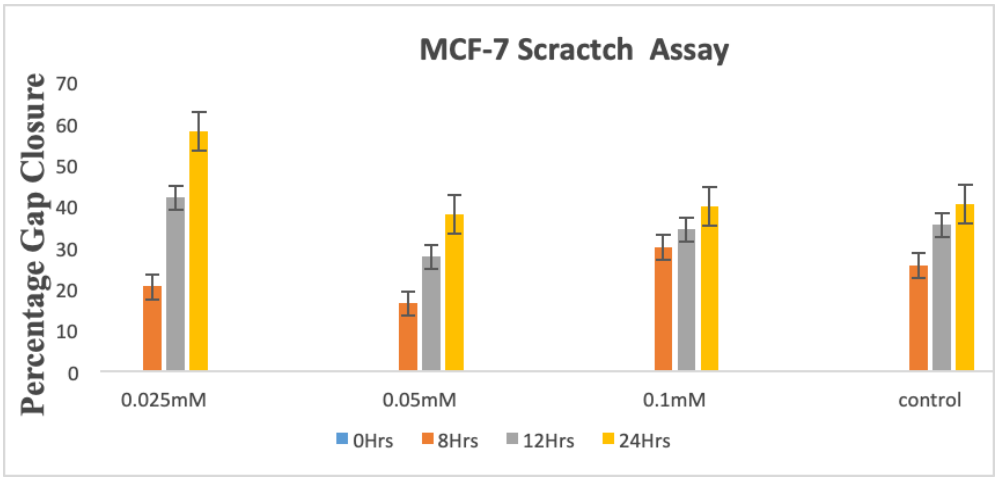

Figure 5.11: Chart showing percentage gap closure of MCF-7 cells
when treated with varying concentrations of CTX and Gap closure was measured at a different time interval from image pictures at 0hr, 8hrs, 12hrs, and 24hrs. Percentage gap closure was high at a lower concentration of the peptide and increases with time.

5.11.2.4 PC-3 Cells Percentage Gap Closure of Scratch Migration Assay

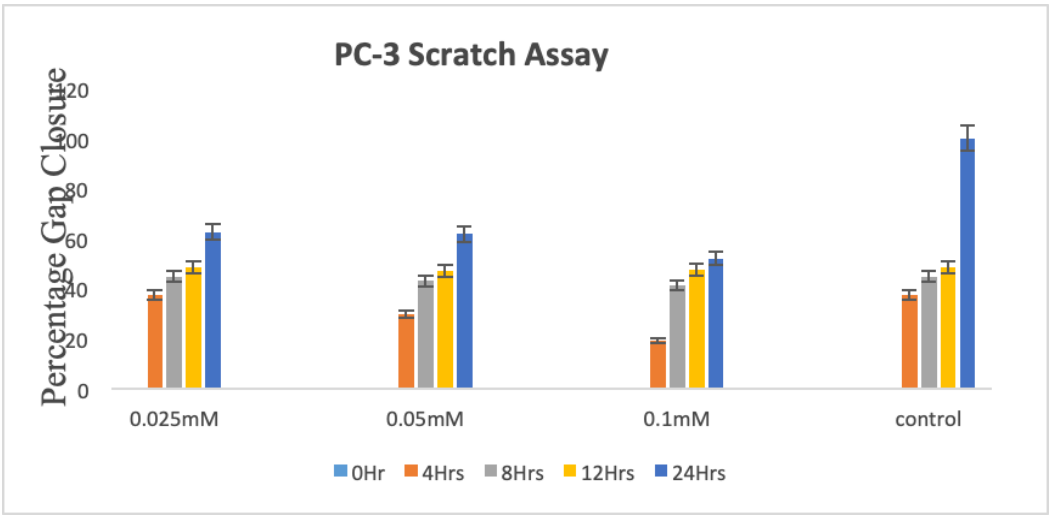

Figure 5.12: Chart showing percentage gap closure of PC-7 cells
when treated with varying concentrations of CTX and Gap closure was measured at different time intervals from image pictures taken at 0hr, 4hrs, 8hrs, 12hrs, and 24hrs. Percentage gap closure was high at a lower concentration of the peptide and increases with time.

5.12 Discussion

Cell migration and proliferation are necessary for the development of all forms of cancer (Brabletz *et al*., 2005; Coussens and Werb, 2002; Guo *et al.*, 2013; Mantovani *et al*., 2008). Chlorotoxin peptide is a 36 amino acids peptide isolated initially from scorpion *Leiurus quinquestriatus v*enom. It acts as an anticancer agent, by binding to tumour cells and less affinity for normal human cells because MMP2 is expressed in cancer cells (Arzamasov *et al*., 2014; El-Ghlban *et al*., 2014; Kittle *et al*., 2014; Stroud *et al*.,2014). The migration of cells was accessed by *in-vitro* scratch assay, and purified unlabelled CTX was used in the scratch study.

Percentage gap closure of HeLa cells, when treated with varying concentrations of unlabelled purified CTX and different time interval exposure reveal that gap closure increases with time from 0 to 24hours for HeLa cells at a lower concentration of the peptide (0.025mM and 0.05mM). Also, we observed that percentage gap closure was highest at 0.05mm concentration of the peptide at 24hours (60.3%) for U87 cells, with gap closure increasing with time. It was observed that the gap closure for the untreated cell was almost closed after 24 hours.

Figure 5.11 represents percentage gap closure of MCF-7 cells when treated with varying concentrations of CTX and Gap closure was measured at different time intervals. Percentage gap closure was high at a lower concentration of the peptide; this might probably be due to the inability of the lower concentration of the peptide to inhibit cells migration and the gap closure increases with time. Finally, Figure 5.12 displayed the percentage gap closure of PC-7 cells scratch assay when treated with varying concentrations of unlabelled CTX. Percentage gap closure was high at a lower concentration of the peptide and increases with time.

MMP-2 has been found to be expressed in several tumour cells (Deshane et *al.,* 2003; Kähäri and Saarialho-Kere, 1999) and tissue remodelling diseases (Deryugina *et al.,* 1998). Previous

studies have also shown that CTX inhibits tumour cells by binding to MMP-2 expressed in these cells.

In this studies, the percentage gap closure of cells treated with unlabelled peptide was increasing with time, and for some of the cell lines, it was concentration dependent. This implies that CTX was able to inhibit cells migration this is in agreement with previous findings (Deshane *et al*., 2003; Veiseh *et al*., 2009). This can probably be attributed to some factors; availability of receptors in the cells for the peptide to bind, mechanism of action of the CTX to inhibit these tumour cells movement (Deshane *et al*., 2003; Veiseh *et al*., 2009).

Secondly, unlabelled CTX peptide was able to inhibit cell migration slightly this was expressed as percentage closure, and the difference in percentage closure is an indication probably that the level of CTX receptors in each tumour cells is different. Also, an increase in the concentration of the peptide probably may have led to the lower percentage closure indicating a high inhibition of tumour cells.

These findings in this study will be useful in tumour cell diagnosis and therapeutic.

In conclusion, it was observed that the percentage gap closure was time-dependent that is it increased with time in some of the cells, and it also depends on concentration. Although, there was no concentration of the peptide used that inhibit the cancer cells migration between 0 and 12 hrs slight inhibitions was observed in PC-3 cells at 0.1mM. The increase in gap closure was minimal. This implies that there was slight inhibition in cell migration.

5.13 References

Al-Asmari A.K., Islam M and Al-Zahrani A.M. (2016). In vitro analysis of the anticancer properties of scorpion venom in colorectal and breast cancer cell lines. *Oncology Letters* **11**(2): 12.

Arzamasov A.A., Vassilevski A.A. and Grishin E.V. (2014). Chlorotoxin and related peptides: Short insect toxins from scorpion venom. *Russian Journal of Bioorganic Chemistry* **40**(4): 359-369.

Brabletz T., Jung A., Spaderna S., Hlubek F. and Kirchner T (2005). Migrating cancer stem cells-an integrated concept of malignant tumour progression. *Nature Reviews Cancer* **5(**9): 744.

Baneyx F. (1999). Recombinant protein expression in Escherichia coli. *Current opinion in biotechnology*. **10**(5):411-421.

Coussens L. M. and Werb Z. (2002). Inflammation and cancer. *Nature* **420**(6917): 860

Deshane J., Garner C. C. and Sontheimer H. (2003). Chlorotoxin inhibits glioma cell invasion via matrix metalloproteinase-2. *Journal of Biological Chemistry* **278**(6):4135-4144.

Deryugina E. I., Bourdon M. A., Reisfeld R. A. and Strongin A. (1998). Remodeling of collagen matrix by human tumour cells requires activation and cell surface association of matrix metalloproteinase-2. *Cancer Research* 58(16): 3743-3750.

El-Ghlban S., Kasai T., Shigehiro T., Yin H.X., Sekhar S., Ida M., Sanchez A., Mizutani A., Kudoh T., Murakami H. and Seno M. (2014). Chlorotoxin-Fc fusion inhibits release of MMP-2 from pancreatic cancer cells. *Biomedical Research International 2014*.

Hunt I. (2005). From gene to protein: a review of new and enabling technologies for multi-parallel protein expression. *Protein expression and purification*. **40**(1):1-22.

Guo P., Lan J., Ge J., Mao Q and Qiu Y. (2013). ID1 regulates U87 human cell proliferation and invasion. *Oncology Letters* **6**(4): 921-926.

Hannig G and Makrides S.C. (1998). Strategies for optimizing heterologous protein expression in Escherichia coli. *Trends in biotechnology*, **16**(2): 54-60.

Kähäri V. M. and Saarialho-Kere U. (1999). Trendsin Molecular Medicine: Matrix metalloproteinases and their inhibitors in tumour growth and invasion. *Annals of Medic ine* **31**(1): 34-45.

Kasai T., Nakamura K., Vaidyanath A., Chen L., Sekhar S., El-Ghlban S. and Seno M. (2012). Chlorotoxin fused to IgG-Fc inhibits glioblastoma cell motility via receptor-mediated endocytosis. *Journal of Drug Delivery* 2012.

Koehn J., and Hunt I., (2009). High-Throughput Protein Production (HTPP): a review of enabling technologies to expedite protein production. In *High Throughput Protein Expression and Purification* (1-18). *Humana Press*.

Kigawa T and Yokoyama S. (2002). High-throughput cell-free protein expression system for structural genomics and proteomics studies. *Tanpakushitsu kakusan koso. Protein, nucleic acid, enzyme* **47**(8): 1014

Kittle D.S., JE P.N., Hansen S., Patil R., Gangalum P.R., Ljubimova J., Black K.L. and Butte P.(2014). Fluorescence-guided tumour visualisation using the tumour paint BLZ-100. *Cureus* **6**(9).

Makrides S.C. (1996). Strategies for achieving high-level expression of genes in Escherichia coli. *Microbiological reviews*. **60**(3):512-538.

Mantovani A., Allavena P., Sica A. and Balkwill F. (2008).Cancer-related Inflammation. *Nature* **454**(7203):436.

Meagher R.B., Tait R.C., Betlach M. and Boyer H.W. (1977). Protein expression in E. coli minicells by recombinant plasmids. Cell **10**(3):521-536.

Rosano G. L and Ceccarelli E. A. (2014). Recombinant protein expression in Escherichia coli: advances and challenges. *Frontiers in Microbiology* **5**:172

Stroud R.M., Hansen J.S., and Olson J.M. (2011). In vivo bio-imaging using chlorotoxin-based conjugates. *Current pharmaceutical design* **17**(38): 4362-4371.

Thovhogi N., Sibuyi N., Meyer M., Onani M and Madiehe A. (2015). Targeted delivery using peptide-functionalised gold nanoparticles to white adipose tissues of obese rats. *Journal of Nanoparticle Resea*rch **17**(2): 112.

Veiseh O., Gunn J. W., Kievit F. M., Sun C., Fang C., Lee, J. S. and Zhang M. (2009). Inhibition of tumour-cell invasion with chlorotoxin-bound superparamagnetic nanoparticles. Small 5(2): 256-264.

Young, C. L., Britton, Z. T., & Robinson, A. S. (2012). Recombinant protein expression and purification: a comprehensive review of affinity tags and microbial applications. *Biotechnology journal* **7**(5):620-634.

CHAPTER SIX

Bio-Conjugation of Biotinylated Chlorotoxin with Quantum Dots

6.1 Introduction

Bio-conjugation is a chemical approach used to form a stable link between two molecules. The use of quantum dots for biological application in research has encountered two major challenges over the years; these are its solubility and functionalization. QDs have some unique features that make it very useful for functionalization in the biological application (*in vivo* and *invitro*) (Resch-Genger *et al.,* 2008 and Zhang *et al*., 2012). Early diagnosis and localised application of drugs are required for most cancer diseases to be treated effectively. More so, exposure of the whole body to drugs and radiation is highly discouraged, hence, there is a need for bio-conjugation towards targeted therapy (Karakoti *et al.,* 2015). In order to understand the intricacy of some diseases and the efficacy of their treatments, the biological molecules involved in the cellular processes is vital (Patra *et al*., 2007; Krakatoa *et al.*, 2015). Nanoparticles like QDs when functionalized possesses some great promises for easy, fast disease diagnosis and imaging (Asati *et al*., 2009; Ambrosi *et al*., 2010; Cui *et al*., 2011 and Karakoti *et al*., 2015). Quite a lot of studies have used CTX to a target tumour cells their binding affinity (Calderon *et al.,* 2014; Kasai *et al*., 2012; Olubiyi *et al.,* 2015; Stroud *et al.,* 2011). In recent times, CTX is conjugated to proteins and some fluorescent materials to target a tumour (Kasai *et al.,* 2012)

6.2 Materials and Method

6.2.1 Materials

Sulfo-NHS-SS-Biotin (Thermos fisher scientific), streptavidin (Sigma), Biotinylated chlorotoxin (GL Biochem), quantum dots, WST-1 Cell Proliferation Reagent 4-[3-(4-iodophenyl)-2-(4-nitrophenyl)-2H-5-tetrazolio]-1, 3-benzene disulfonate (Roche Diagnostics,

Mannheim, Germany), Dulbecco Modified Eagle Medium (DMEM) (Lonza), Phosphate buffered saline (PBS), RPMI media(Lonza), 96 well tissue culture plates.

6.2.2 Synthesis and characterisation of QDs-MPA and QDs-GA CdTe quantum dots

The QDs-MPA and QDs-GA quantum dots were synthesised and characterised using the method described previously in chapter 2.

6.2.3 Bio-conjugation of quantum dots to Biotinylated Chlorotoxin Peptide

A known mass of quantum dots was weighed and dissolved in water. 1mL of the QDs solution was mixed with 80 µL of Sulfo-NHS-SS-Biotin (6 mg/mL). This was prepared fresh every time it was used. The reaction was stirred on a stirring mantle with a stirring bar for about an hour. An equal amount of streptavidin (80 µL) of 250 µg/mL was added to the QDs-biotin solution, stirred and incubated for 6 hours at room temperature with stirring. The absorbance was measured, and the solution was centrifuged for 10 minutes to remove the unreacted compound. One (1) mg/mL of the CTX-biotin which was prepared in water was added to an equal amount of QDs-biotin-Strep, and the resulting solution was incubated at room temperature with stirring for about 6 hours. UVis was used to confirm the conjugation.

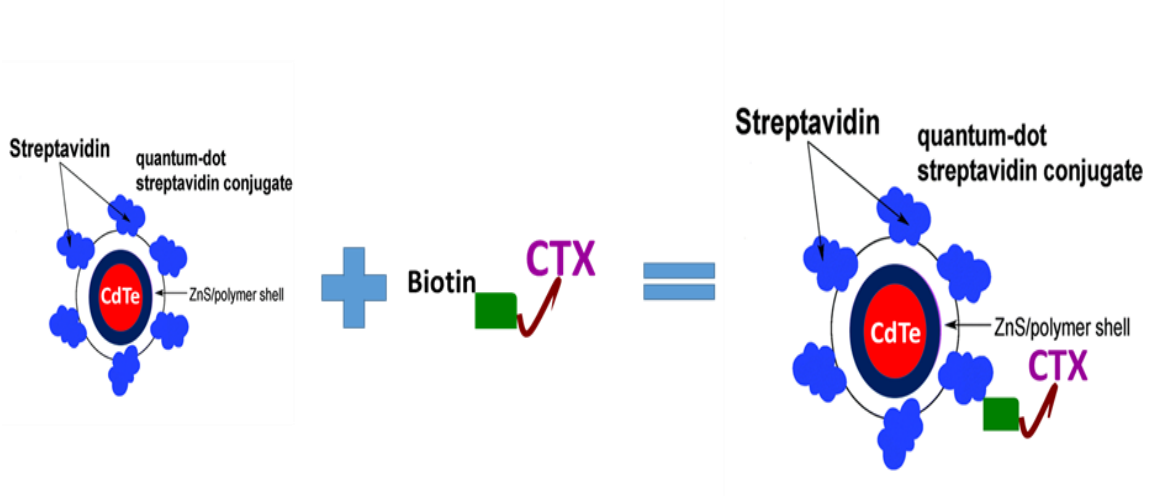

Figure 6.1: Diagram showing the mechanism of conjugation of biotinylated chlorotoxin to Quantum dots.

6.2.4 Investigation of the cell binding of QDs

The fluorescence intensity of the quantum dots and peptide were evaluated using a flow cytometer. Cells were seeded in 6 well plates with a cell density of $3X10^5$ for 24 hrs. After which cells were treated with 25 µg/mL and 50 µg/mL of QDs for 24 hours. Then cells were washed with PBS, trypsinised using 300µl of trypsin, washed with 1X PBS again and centrifuged for 3 minutes at 3000 rpm after that about 300ul of media was added to cells in tubes, and this was kept on ice. A flow cytometer was used to analyse cell binding. This method was used to investigate cell binding of studies for QDs-MPA and QDs-GA12. These were carried out in triplicate.

6.2.4 Cell culture and WST-1 cell viability

Cells were seeded in 96 well tissue culture plates at a cell density of $1\times 10^{-6,}$ and after 24 hours cell was washed with 1X PBS and treated with conjugated chlorotoxin Quantum dot peptide (QDs-Biotin-CTX) for 24 hours. The media was removed from the wells, and 100 µL of reconstituted WST-1 cell proliferation assay reagent with media was added to each well and incubated for 4 hours at 37 °C and absorbance was measured at 440 nm and 630 nm using BMG Labtech polar star omega microplate reader

6.3 Results and Discussion

UVis absorbance of QDs-MPA, QDs-Streptavidin and QDs-MPA-CTX is presented in Figure 6.2; Absorbance spectra are showing an upward shift in UV spectra when streptavidin was an attachment to the QDs and a further shift was also observed after conjugating with CTX. This is probably due to an increase in the size of QDs after conjugation. Also, Figure 6.3 showed UVis absorbance of QDs-GA, QDs-GA-Strep and QDs-GA-CTX. Absorbance spectra showed a shift in UV spectra after conjugation; which implies that conjugation was successful and an increase in the size of the QDs.

The cytotoxicity studies of QDs-GA and QDs-MPA chlorotoxin conjugate (QDs-GA-CTX) and (QDs-MPA-CTX) respectively using HeLa, MCF-7, PC-3 and U87 cell line at various concentration of 3.125µg/mL, 6.25µg/mL, 12.5µg/mL, 25µg/mL, 50µg/mL and 100µg/mL are shown in Figure 6.4 and 6.5. We observed cell viability at over 70% with viability decreasing as the concentration of the conjugate QDs increasing.

U87 cell lines had the lowest reduction in cell viability of 21%, and HeLa cells had the highest reduction in viability (47%). QDs-MPA-CTX viability studies suggested that MCF-7 and U87 displayed the lowest reduction in cell viability (4.3 % and 13 % respectively) while HeLa displayed the highest reduction in viability and it is concentration dependent. This corresponds to the work of Malvindi *et al*., 2014, where they carried out *invitro* cytotoxicity studies using InP/ZnS and CdSe/ZnS QDs to demonstrate that cytotoxicity of the QDs was concentration-dependent when cells were exposed to QDs treatment within 24 hours and 48 hours. Reduction in percentage cell viability after conjugation may probably be due to the presence of CTX because studies have shown that CTX can binds MMP-2 expressed in some tumours and reduced cell proliferation and migration. An increase in the size of the QDs after conjugation can also be attributed to the reduction in viability. From our chart, the optimum concentration for all cells line is 6.25µg/mL because at this concentration the cell lines displayed over 70% cell viability.

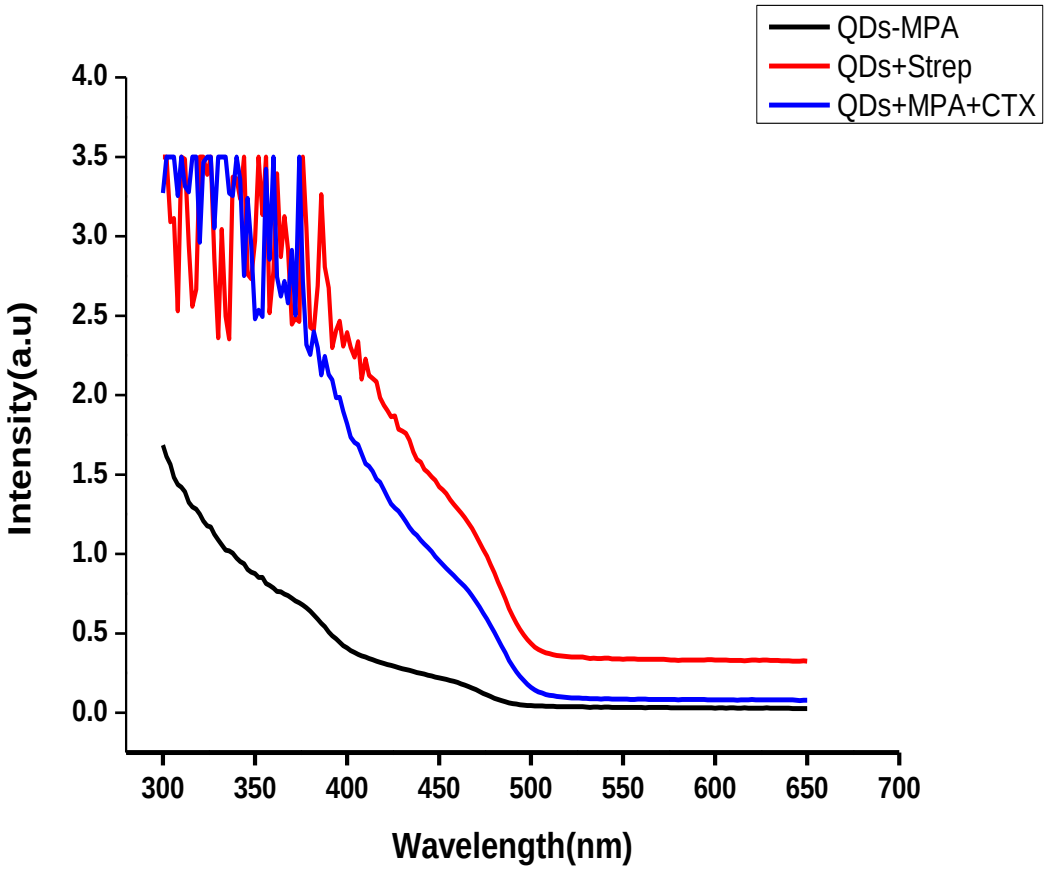

Figure 6.2: UV absorbance of QDs-MPA, QDs-Streptavidin and QDs-MPA-CTX.
Absorbance spectra showed an upward shift in UV spectra after conjugation. The black spectra indicate QDs-MPA before conjugation, the red spectra represent the addition of streptavidin, and the blue spectra represent QDs-MPA-CTX.

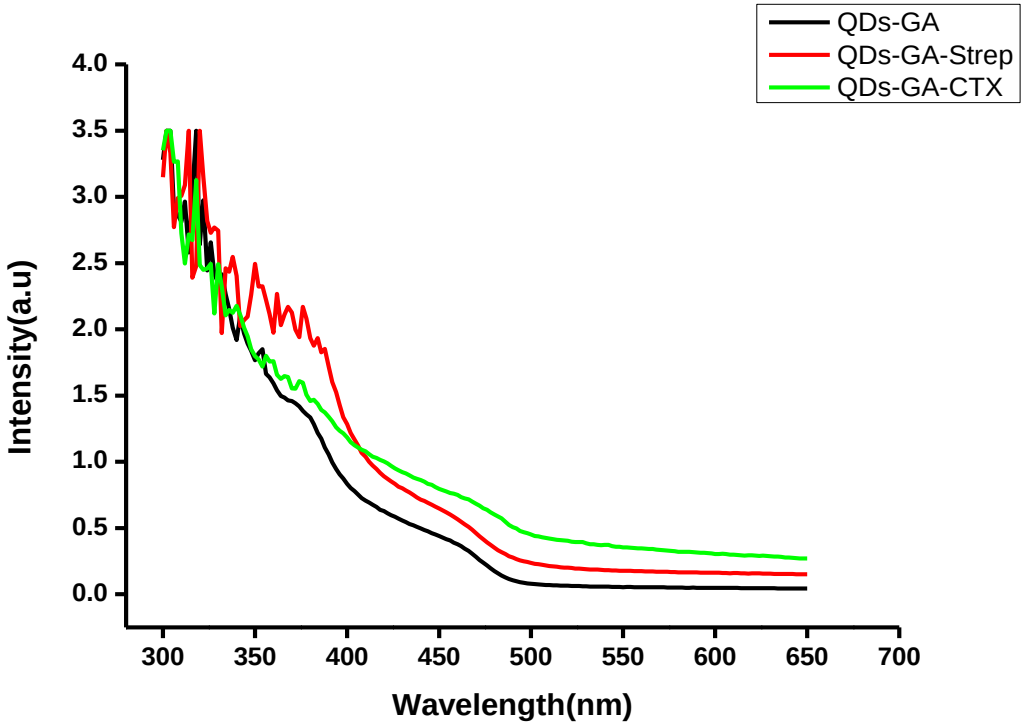

Figure 6.3 UVis absorbance of QDs-GA, QDs-GA-Strep and QDs-GA-CTX.
Absorbance spectra showed a shift in UV spectra after conjugation. The black spectra indicate QDs-GA before conjugation, the red spectra represent the addition of streptavidin, and the green spectra represent QDs-GA-CTX.

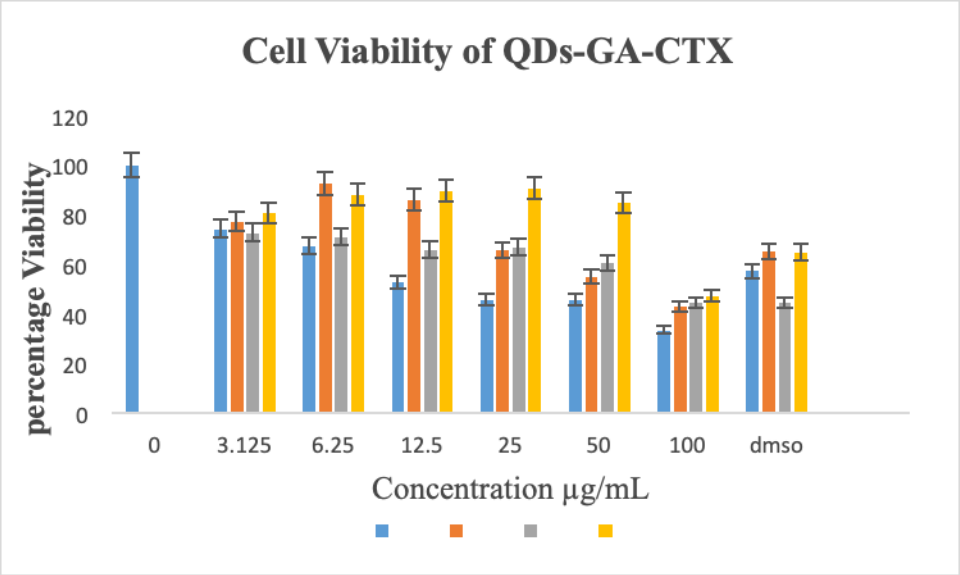

Figure 6.4: The cytotoxicity studies of QDs-GA chlorotoxin conjugate (QDs-GA-CTX) using HeLa, MCF-7, PC-3 and U87 cell line.
The chart showed over 70% cells viability with viability decreasing with increase in concentration.

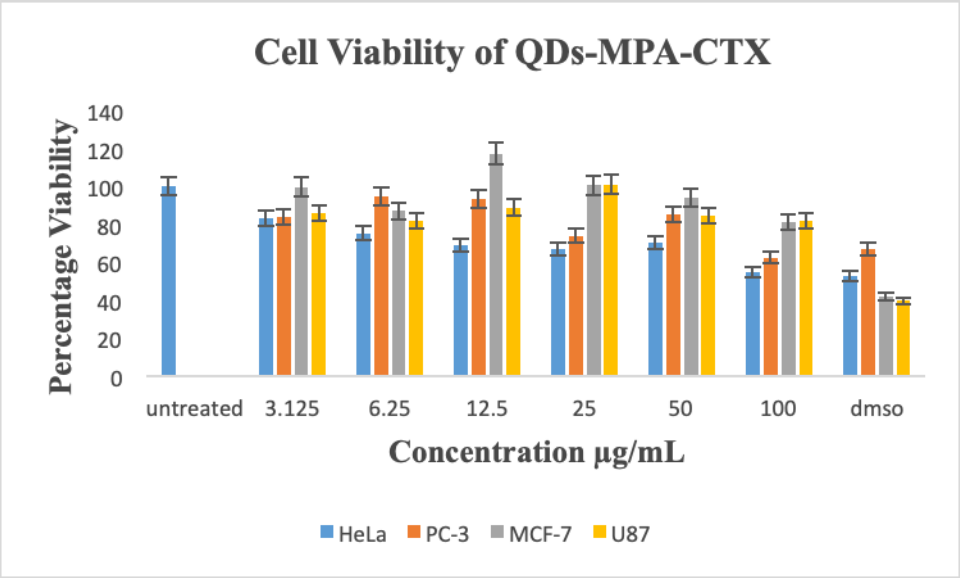

Figure 6.5: The cytotoxicity studies of QDs-MPA chlorotoxin conjugate.
The chart showed over 70% cells viability with viability decreasing with an increase in the concentration of CTX Conjugate.

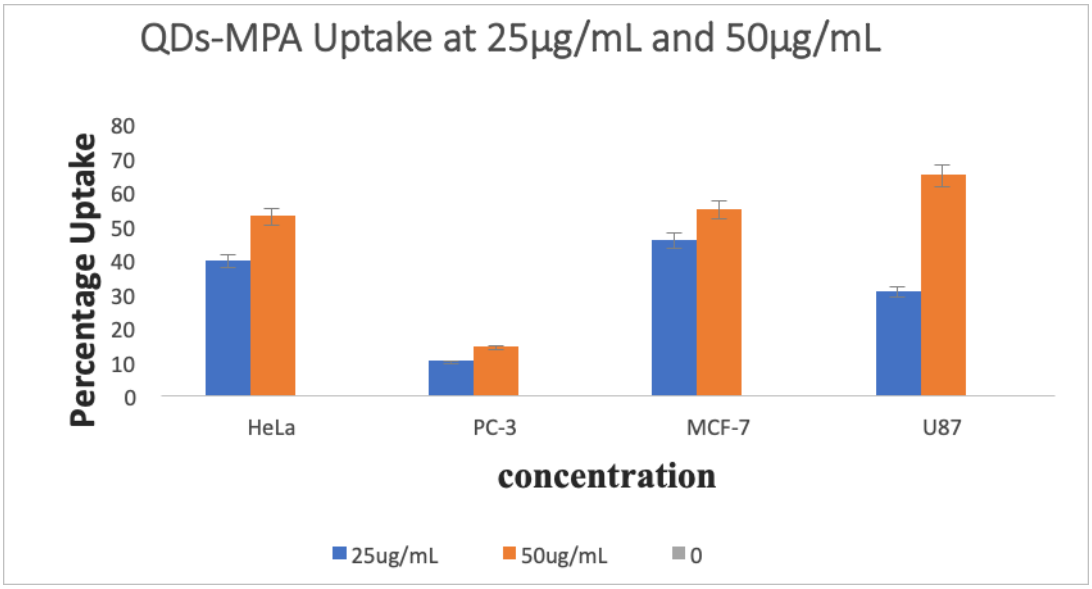

Figure 6.6: Percentage QDs-MPA uptake at 25µg/mL (blue bar) and 50µg/mL (orange bar).

The QDs-MPA uptake showed that the percentage uptake was high in HeLa and U87 cells and low uptake was observed in PC-3 cells

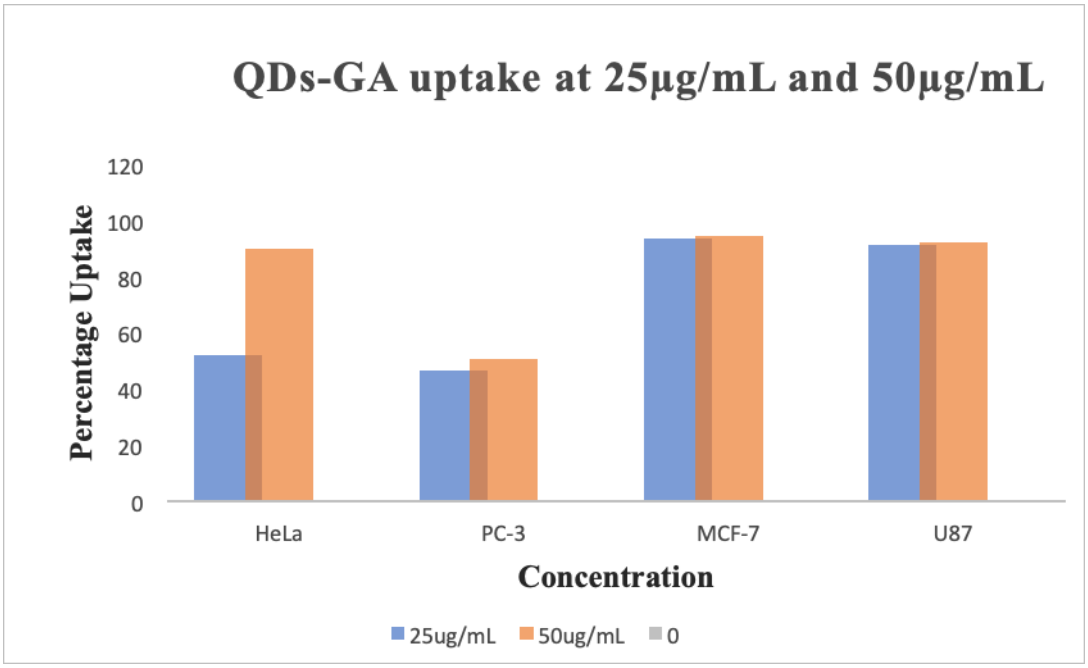

Figure 6.7: Percentage QDs-GA uptake at 25µg/mL (blue bar) and 50µg/mL (orange bar).

The QDs-GA uptake showed that the percentage uptake was high in HeLa, MCF-7 and U87 cells and low uptake was observed in PC-3 cells.

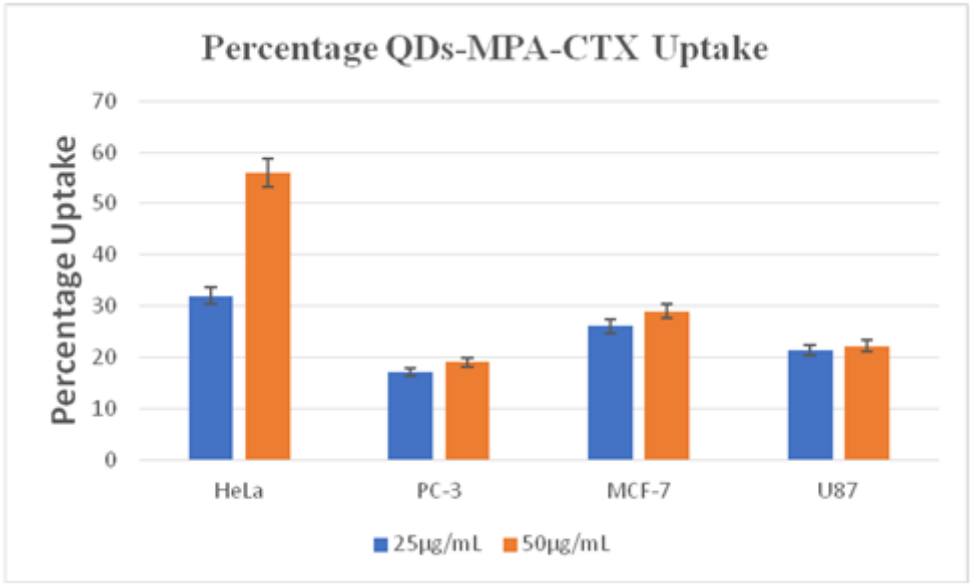

Figure 6.8: Percentage uptake of the QDs-MPA chlorotoxin conjugate in HeLa, PC-3, MCF-7 and U87 Cell lines (QDs -MPA-CTX) at 25 µg/mL and 50 µg/mL concentration. High QDs-MPA-CTX uptake was observed in HeLa cells at both concentrations when compared to MCF-7, PC-3 and U87 cell lines.

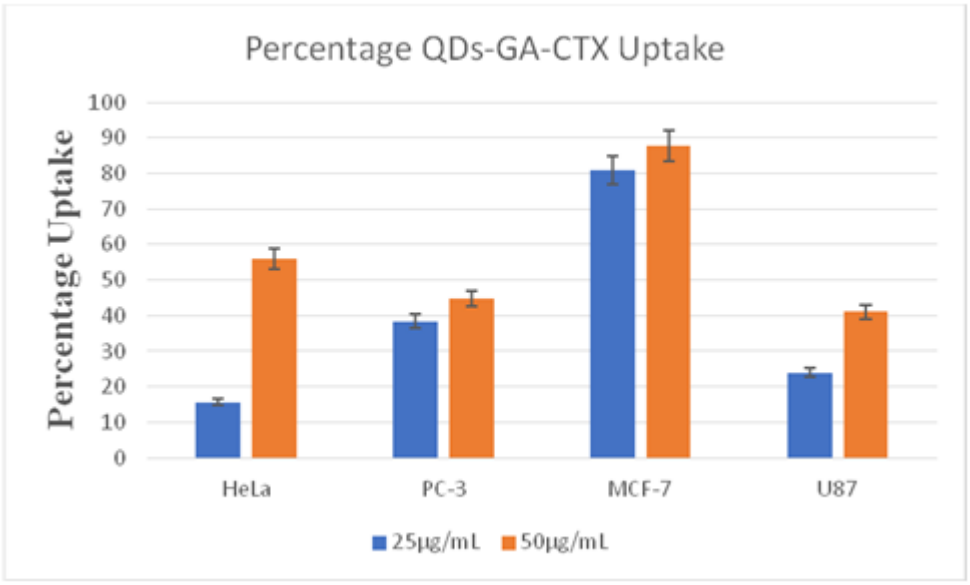

Figure 6.9: Percentage uptake of the QDs-GA chlorotoxin conjugate in HeLa, PC-3, MCF-7 and U87 Cell lines (QDs-GA-CTX) at 25 µg/mL and 50 µg/mL concentration. A very high uptake was observed in MCF-7 cells for both concentrations, HeLa cells had the next high uptake at 50µg/mL.

.

Figure 6.6 represent percentage QDs-MPA uptake using two concentrations of Quantum dots; 25µg/mL and 50µg/mL. QDs-MPA percentage uptake after 24 hours using flow cytometer to analyse cell revealed that QDs were well taken up by all four cell line but percentage uptake was highest in U87, MCF-7 and HeLa cells with percentage value of 64.8, 54.7 and 52.7% at 50µg/mL respectively and the least uptake was seen in PC-3 cells with the percentage value of 14.13%. The uptake was observed to depend on concentration, hence at 25µg/mL uptake was seen to be lower in all cell line when compared to the concentration at 50µg/mL. The P-Values were (>0.05) hence not insignificantly different for HeLa, PC-3 and MCF-7 when concentration of QDs-MPA (Figure 6.6) uptake was compared at 25 and 50µg/mL but for U87cells the P-values was less (<0.05), this implies that percentage uptake at 25 and 50µg/mL significantly different. Percentage QDs-GA uptake at 25µg/mL and 50µg/mL (Figure 6.7). QDs-GA was highly taken up by cells at 50µg/mL. This infers that percentage uptake increases with concentration. QDs-GA uptake was 91 %, 94.6 %, 89.8 % and 50 % at 50µg/mL for U87, MCF-7, HeLa and PC-3 respectively and 92.2 %, 93.6 %, 52 % and 46.5 % for U87, MCF-7, HeLa a and PC-3 respectively at 25µg/mL. Their P-values at 25 and 50µg/mL for each cell were not significant (>0.05) Figure 6.7 for all cell lines. Also, these results also suggest the QDs uptake may also be cell lines specific.

The percentage uptake of the QDs-MPA chlorotoxin conjugate (QDs-MPA-CTX) is in Figure 6.8 and Figure 6.9 respectively. The results indicate that the percentage uptake of the QDs-GA-CTX for HeLa, PC-3, MCF-7 and U87 cells at 25µg/mL and 50µg/mL was moderately increasing with concentration. HeLa and MCF-7 cells had the highest percentage uptake for both QDs conjugate, and PC-3 had the lowest. Their P-values are (>0.05) hence not significant,

6.5 References

Ambrosi A., Airo F. and Merkoci A., Enhanced gold nanoparticle-based ELISA for a breast cancer biomarker (2010). *Analytical Chemistry* **82**(3):1151–6.

Asati A., Santra S., Kaittanis C., Nath S and Perez J.M (2009). Oxidase-like activity of polymer coated cerium oxide nanoparticles. *Angewandte Chemie* **121** (13): 2344-2348

Calderon L.A., Sobrinho J.C., Zaqueo K.D., de Moura A.A., Grabner A.N., Mazzi M.V., Marcussi S., Nomizo A., Fernandes C.F., Zuliani J.P. and Carvalho B. (2014). Antitumoral activity of snake venom proteins: new trends in cancer therapy. *BioMed research international* 2014.

Cui R., Han Z., and Zhu J.J. (*2*011). Helical carbon nanotubes: intrinsic peroxidase catalytic activity and its application for biocatalysis and biosensing. *Chemistry-A European Journal* **17**(34):9377–84.

Karakoti A.S., Shukla, R., Shanker R., and Singh S., (2015). Surface functionalization of quantum dots for biological applications. *Advances Colloid and Interface Science* **215**: 28-25

Kasai T., Nakamura K., Vaidyanath A., Chen L., Sekhar S., El-Ghlban S., Okada M., Mizutani A., Kudoh T., Murakami H. and Seno M. (2012). Chlorotoxin fused to IgG-Fc inhibits glioblastoma cell motility via receptor-mediated endocytosis. *Journal of drug delivery 2012*.

Malvindi M.A., De Matteis V., Galeone A., Brunetti V., Anyfantis G.C., Athanassiou A., Cingolani R. and Pompa P.P., 2014. Toxicity assessment of silica-coated iron oxide nanoparticles and biocompatibility improvement by surface engineering. *Public Library of Science* **9**(1): e85835

Olubiyi O.I., Lu F.K., Calligaris D., Jolesz F.A. and Agar N.Y. (2015). Advances in molecular imaging for surgery. In *Image-Guided Neurosurgery* 407-439.

Patra C.R., Bhattacharya R., Patra S., Basu S., Mukherjee P., Mukhopadhyay D. and Lanthanide (2007). Phosphate nanorods as inorganic fluorescent labels in cell biology research. *Clinical Chemistry* **53**(11):2029–31.

Resch-Genger U., Grabolle M., Cavaere-Jaricot S., Nitschke R., Nann T.(2008). Quantum dots versus organic dyes as fluorescent labels. *Nature Methods* **5**(9):763–75

Sabella S., Carney R.P., Brunetti V., Malvindi M.A., Al-Juffali, N., Vecchio G., Janes, SM., Bakr O.M., Cingolani R., Stellacci F and Pompa P.P. (2014). A general mechanism for intracellular toxicity of metal-containing nanoparticles. *Nanoscale* **6**(12):7052-7061.

Stroud RM., Hansen J.S. and Olson M.J. (2011). In vivo bio-imaging using chlorotoxin-based conjugates. *Current pharmaceutical design* **17**(38): 4362-4371.

CHAPTER SEVEN

General Discussion and Conclusion

7.1 General Discussion

In this study we described, for the first time the synthesis of small, water-soluble CdTe QDs with high luminescent properties for *in-vivo* and *invitro* bio-imaging. Two different routes were used for the synthesis, and these QDs were capped and stabilised with gum Arabic polymer to reduce the toxicity. Toxicity of quantum dots has been a major concern for years, and research has shown that the use of capping agents like polymers helps to reduce toxicity. There is here the need to cap these QDs with proper capping agent in order to increase their solubility and reduce their toxicity for useful application in the bio-imaging system (Hezinger *et al*., 2008). Cancer is a progressive, complex and life-threatening disease that is a significant cause of death worldwide (Pal and Nayak, 2010). It has been reported that about 1 in 6 deaths are caused by cancer, and it is the second leading cause of death. About 8.8 million deaths were caused by cancer in 2015, and about 16 million deaths are projected to occur from cancer in 2020 (Thundimadathil, 2012). These cancer data insinuate that the present therapeutic remedies with the high death rate, seem not to be effective in the fight against this disease. This calls for a need need to devise an alternative therapeutic system to improve existing diagnostic strategies (Sumer and Gao, 2008). Another challenge is the use of chemotherapy drugs which are not non-specific in action because they can be toxic to both normal and cancer cells (Wang *et al*., 2009). Therefore, this challenge has led to the need for innovative and novel nanomaterials for targeted therapy to improve treatment and for early diagnosis. Targeted therapy is one of the most promising and developing areas in the use of nanoparticles in medical research (Thovhogi *et al*., 2015; Dykman and Khlebtsov 2011).

In this study chapter two highlights the synthesis and characterisation of CdTe Quantum Dots. CdTe QDs were synthesised capped with MPA (QDs-MPA) and GA polymer to

increase solubility and reduce toxicity. QDs were capped with GA polymers using two different routes by varying temperature; QDs were capped at 60 ºC for 2hours (QDs-GA2), and 12 hours at room temperature (QDs-GA12); The nanoparticles were then characterised using Ultraviolet-visible (UV–vis) spectroscopy which was used to confirm the formation of the QDs, Photoluminescence (PL) spectroscopy spectrum was seen to be sharp and narrow with an emission wavelength of 700 nm, 686 nm and 659 nm for QDs-MPA, QDs-GA2 and QDs-GA12 respectively. The QDs emit green and red fluorescent.

High resolution transmission electron microscopy (HRTEM) showed that particle size was be tween 2nm to 4.9nm and Fourier transform infrared spectroscopy (FTIR) confirm the biomolecules present in QDs. Also, the hydrodynamic particle size, polydispersity index (PDI) and zeta potential were also evaluated to ascertain the colloid stability of QDs. XRD was used to determine the crystalline nature of the QDs as well as calculate the particle size using Debye Scherrer equation and FWHM, and this confirms the results gotten from HRTEM that the particle size range is less than 10nm. The detailed investigations of the *in-vitro* cytotoxicity assay using the WST-1 cell proliferation assay were investigated. Proliferation assay of the QDs capped with GA and MPA were evaluated *in vitro* using four cell lines MCF-7, PC-3, HeLa and U87 cancer cell lines at different concentrations range of 100µg/mL, 50µg/mL, 25µg/mL, 12.5µg/mL, 6.5µg/mL and 3.125µg/mL. It was used to establish that GA capped QDs particles were less toxic to the cells and the toxicity increases with increase in concentration. Also for most of the cancer cells lines the quantum dots were not toxic at a concentration less than of 50µg/mL.

Stability studies of the nanoparticles in various cell culture medium and buffer were also evaluated in chapter three. The results showed that most of the QDs particles were stable for about 48 hours. The particles started growing bigger after 48hours for all the media this was

evident in the shift in spectra except for DMEN medium, whose absorbance spectra was shifting with an increase in time this corresponds with the work of Elbagory *et al.,* 2016. The increasing shift in the absorbance spectra of DMEN medium was probably due to the fact the DMEN media is coloured, and the absorbance of the medium was probably interfering with the absorbance of the QDs present in the media.

Cell microscopy studies showed that QDs were internalised in the nucleus when stained with DAPI nucleus dye (blue) and the micrographs of the all four cell line showed that HeLa cells have the highest cell uptake of QDs (green and red), peptide (green) and nuclei localisation (blue). The binding affinity study was evaluated by measuring the fluorescence intensity in percentage using a flow cytometer.

Chapter five evaluated the recombinant expression and purification of chlorotoxin peptide using SDS gel to confirm protein expression. The protein was cleaved using 3C protease and pure chlorotoxin peptide obtained was sequenced. In recent years CTX has emerged as one of the promising agents for targeting because of its ability to accurately identify a wide range of cancers, like the brain and prostate tumour cells (Kievit *et al*., 2010) and its unique size (Veiseh *et al.,* 2009). Binding experiment was done using the recombinantly expressed protein, and FITC labelled chlorotoxin. This study was carried out using some cell lines to determine the specificity of FITC-CTX binding to cell lines. It was used to evaluate specific and competitive binding of cells to FITC-CTX peptide. The extent of binding was evaluated using fluorescence flow cytometry by measuring fluorescence intensity in percentage. The histogram shift to the right indicates an increase in binding with a corresponding increase in concentration and fluorescence and it is receptor mediated. Cell migration or scratch assay was used to determine the effect of the unlabelled purified CTX peptide on the migration of cell and four cell lines were used. Cell migration and proliferation is necessary for the development of all forms of cancer (Coussens and Werb, 2002; Evan and Vousden, 2001)

In chapter six QDs was conjugated to biotinylated chlorotoxin and a shift in the UV spectra was used to confirm the attachment of streptavidin to quantum dots for both QDs-MPA and QDs-GA. The QDs-CTX conjugate was used on four cell lines to ascertain viability and cell uptake in percentage using flow cytometer.

7.2 Conclusion

The objective of this study was to synthesise quantum dots using GA polymer to cap and stabilise the QDs nanoparticle towards the development of a bio-imaging agent for diagnostic purpose thorough a conjugated peptide system. We synthesised for the first time CdTe QDs with high luminescent properties using two different methods of synthesis. They were biophysically characterised and stabilised with gum Arabic polymer to decrease the toxicity and improve the solubility of the QDs. These QDs were found to be very small in size less than 10nm from HRTEM analysis and very soluble in water these attributes makes them very suitable for biomedical purposes. This is in accordance with existing literature that QDs with the characteristic features is extensively applied as imaging agents (Chan *et al*., 1998; Chan *et al*., 2012; Mattheakis *et al*., 2004; Resch-Genger *et al*., 2008; Jamieson *et al*., 2007). Several studies have shown that nanoparticles conjugate with biomolecules are used in nanobiotechnology due to their ease of chemical synthesis, flexibility, less toxicity and biocompatibility (Fontes *et al*., 2012; McNeil, 2005). Chemotherapy drugs have been shown to be non-specific and inflict severe toxicity on patients hence, scientists in the field of molecular biology have resulted to the use of targeted therapy for easier diagnosis and treatment of a tumour. The general results from this study have been able to show the evidence that the QDs synthesised from this study is small in size, soluble, highly luminescent, with low toxicity and emit both red and green fluorescence which offer good evidence of applicability for *invivo* and *invitro* bio-imaging system.

7.3 Recommendation for Further Work

The results from this study showed that we successfully synthesised QDs that are water soluble and which have low toxicity. It will be essential to carry out a long-term study on exposure of these QDs on cells lines for any possible toxic effect *in-vitro* and other cancer cell lines. These will enable us to know if these quantum dots are toxic to other cancer cells or are cell line specific. Also, the concentration can be increased to ascertain the cause,of toxicity and the possible damage to RNA and DNA by assaying for the parameters that are responsible for these damages.

Furthermore, *in-vivo* studies using animal model QDs is also highly recommended, this will help check for the efficacy of the quantum dots especially for bio-imaging using MRI technique and a possible side effect of its accumulation in various of organ examined. Long-term stability assay is vital. Also, other types of the polymer may be used for capping the QDs. Their biophysical characterisation and toxicity evaluated, and the findings can be compared to GA capped QDs.

7.4 References

Chan W.C. and Nie S. (1998). Quantum dot Bioconjugates for ultrasensitive non-isotopic detection. *Science* 281(5385): 2016-2018.

Chan W. C., Maxwell D. J., Gao X., Bailey R. E., Han M. and Nie S. (2002). Luminescent quantum dots for multiplexed biological detection and imaging. *Current opinion in biotechnology* 13(1): 40-46.

Coussens and Werb Z. (2002). Inflammation and cancer. *Nature* **420**(6917: 860.

Dykman and Khlebtsov (2011) Gold nanoparticles in biology and medicine: recent advances and prospects. *Acta Naturae* **3**(2):34–55

Elbagory A. M., Cupido C. N., Meyer M. and Hussein A. A. (2016). Large-scale screening of Southern African plant extracts for the green synthesis of gold nanoparticles using microtitre-plate method. *Molecules,* **21**(11): 1498

Evan G.I. and Vousden K.H. 2001. Proliferation, cell cycle and apoptosis in cancer. *Nature* **411**(6835): 342.

Fontes A., de Lira R. B., Seabra M.A. B. L., da Silva T.G., de Castro Neto A.G., and Santos, B.S. (2012). Quantum dots in biomedical research. In *Biomedical Engineering-Technical Applications in Medicine*. InTech.

Hezinger A. F. E., Teßmar J. and Göpferich A. (2008). Polymer coating of quantum dots–a powerful tool toward diagnostics and sensorics. European Journal of *Pharmaceutics and Biopharmaceutics 68*(1): 138-152.

http://www.who.int/mediacentre/factsheets/fs297/en/ Accessed 1 November 2017

Jamieson T., Bakhshi R., Petrova D., Pocock R., Imani M., and Seifalian A. M. (2007). Biological applications of quantum dots. *Biomaterials* **28**(31): 4717-4732.

Mattheakis L.C., Dias J.M., Choi Y.J., Gong J., Bruchez M.P., Liu J., and Wang E. (2004). Optical coding of mammalian cells using semiconductor quantum dots. *Analytical Biochemistry* ***327***(2): 200-208.

Kievit F. M., Veiseh O., Fang C., Bhattarai N., Lee D., Ellenbogen R. G. and Zhang M. (2010). Chlorotoxin labelled magnetic nanovectors for targeted gene delivery to glioma. *ACS Nano* **4**(8): 4587-4594.

Pal D and Nayak, A.M. (2010). Nanotechnology for targeted delivery in cancer therapeutics. *International Journal of Pharmaceutical Sciences Review and Research* **1**(1): 1 – 7.

Resch-Genger U., Grabolle M., Calaviere-Jaricot S., Nitschke R and Nann T. (2008). Quantum dots versus organic dyes as fluorescent labels. *Nature Methods* **5** (9):763 – 775.

Sumer B and Gao J. (2008). Theranostic medicine for cancer. *Nanomedicine* **3** (2):137 – 140.

Thovhogi N., Sibuyi N., Meyer M., Onani M and Madiehe A. (2015). Targeted delivery using peptide-functionalised gold nanoparticles to white adipose tissues of obese rats. *Journal of Nanoparticle Resea*rch **17**(2): 112.

Thundimadathil J. (2012). Cancer treatment using peptides: Current therapies and future prospects. *Journal of Amino Acids***. 2012**: 1–13

Tomczak N., Jańczewski D., Han M. and Vancs, G. J. (2009). Designer polymer-quantum dot architectures. *Progress in Polymer Science* 34(5) 393-430.

Veiseh O., Gunn J. W., Kievit F. M., Sun C., Fang C., Lee J. S. and Zhang, M. (2009). Inhibition of tumour-cell invasion with chlorotoxin-bound superparamagnetic nanoparticles. *Small* **5**(2): 256-264.

Wang X., Wang Y., Chen Z.G and Shin D.M. (2009). Advances of cancer therapy by nanotechnology. *Cancer Research Treatment* **41**(1): 1 – 11.

APPENDIX

BUFFERS AND SOLUTIONS

2 X SDS Sample buffer:

62.5 mM Tris-HCl (pH 6.8), 2 % SDS, 25 % glycerol,

0.01 % bromophenol blue, 5 % β-mercaptoethanol.

10 X TBE

0.9 M Tris, 0.89 M boric acid,

0.032 M EDTA stored at room temperature.

10 X Tris-EDTA (TE)

10 mM Tris-HCl, 1 mM EDTA, pH 7.5

10 X Phosphate-buffered saline (PBS)

150 mM NaCl, 2.7 mM KCl,

10 mM Na_2HPO_4, 2.0 mM KH_2PO_4, pH 7.4.

Ampicillin

100 mg/ml ampicillin in distilled water; filter sterilized.

Sodium Chloride-Tris-EDTA/lysozyme (Lysis buffer)

10 mM Tris, pH 8, 150 mM NaCl, 1mM EDTA and 100 μg/ml lysozyme

Ammonium persulphate (APS)

A 10 % stock solution was prepared in deionised water.

Coomassie Brilliant Blue R-250 Staining Solution

0.25 g Coomassie Brilliant Blue R 250, 50 % ethanol and 10 % acetic acid

Destaining solution

16.5 % ethanol and 5 % acetic acid.

Dithiothreitol (DTT)

A 1 M stock solution was prepared in 0.01 M Sodium acetate, pH 5.2.

This solution was sterilized by filtration.

Ethylenediaminetetraacetic acid (EDTA)

A stock solution was prepared at a concentration of 0.5 M in deionised water, pH 8.0. 10 % Sodium dodecyl sulphate (SDS) 10 % SDS in distilled water.

Isopropyl β-D-thiogalactopyranoside (IPTG)

A 1 M stock solution was prepared in deionised water. The solution was sterilised by filtration.

Luria Agar

14 g/l Bacteriological agar, 10 g/l Tryptone, 5 g/l Yeast Extract and 5 g/l NaCl

Luria Broth

s10 g/l Bacto-tryptone, 5 g/l Bacto-Yeast Extract and 5 g/l NaCl

Lysozyme

A stock solution was prepared at a concentration of 50 mg/ml in deionised water.

PBS-T

150 mM NaCl, 2.7 mM KCl, 10 mM Na_2HPO_4, 2 mM KH_2PO_4 and 1 % Triton-X 100)

6XHis Wash Buffer (25 ml)

50 mM Phosphate Buffer pH 7.0

300 mM NaCl

1 mM Imidazole

Adjust pH to 7.0 with NaOH

6X His Elution Buffer (10 ml)

50 mM Phosphate Buffer pH 7.0

300 mM NaCl

150 mM Imidazole

Adjust pH to 7.0 with NaOH

4% formaldehyde

Paraformaldehyde powder

1X PBS solution

		Mean (mV)	Area (%)	St Dev (mV)
Zeta Potential (mV): -23.0	Peak 1:	-23.0	100.0	4.21
Zeta Deviation (mV): 3.89	Peak 2:	0.00	0.0	0.00
onductivity (mS/cm): 0.202	Peak 3:	0.00	0.0	0.00

Result quality : Good

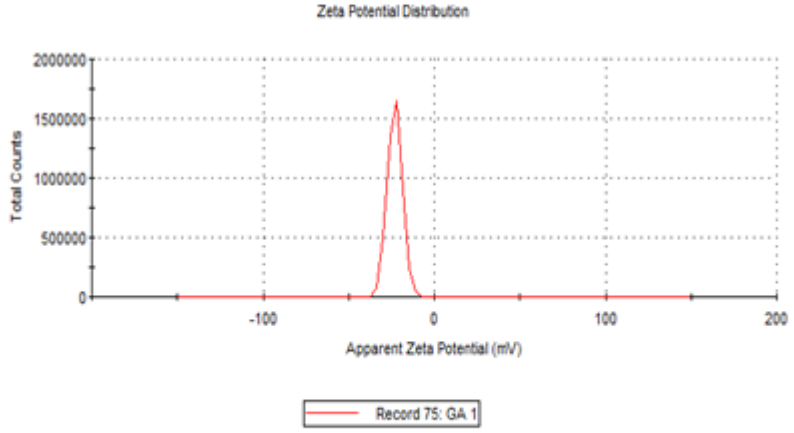

Zeta potential of GA Powder

ass Spectra of Peptide 1 and 2 from GL Biochem (Shanghai) Ltd.

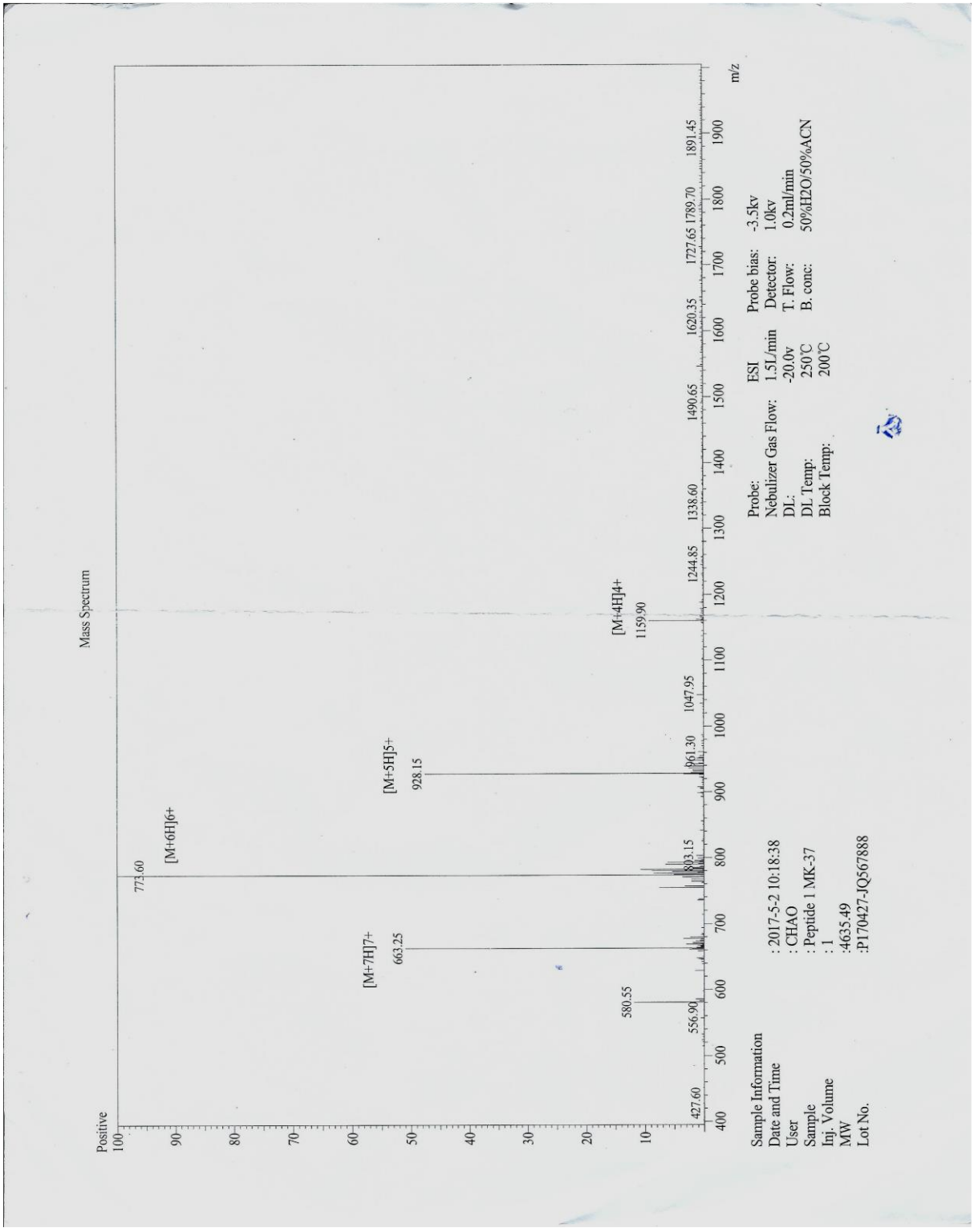

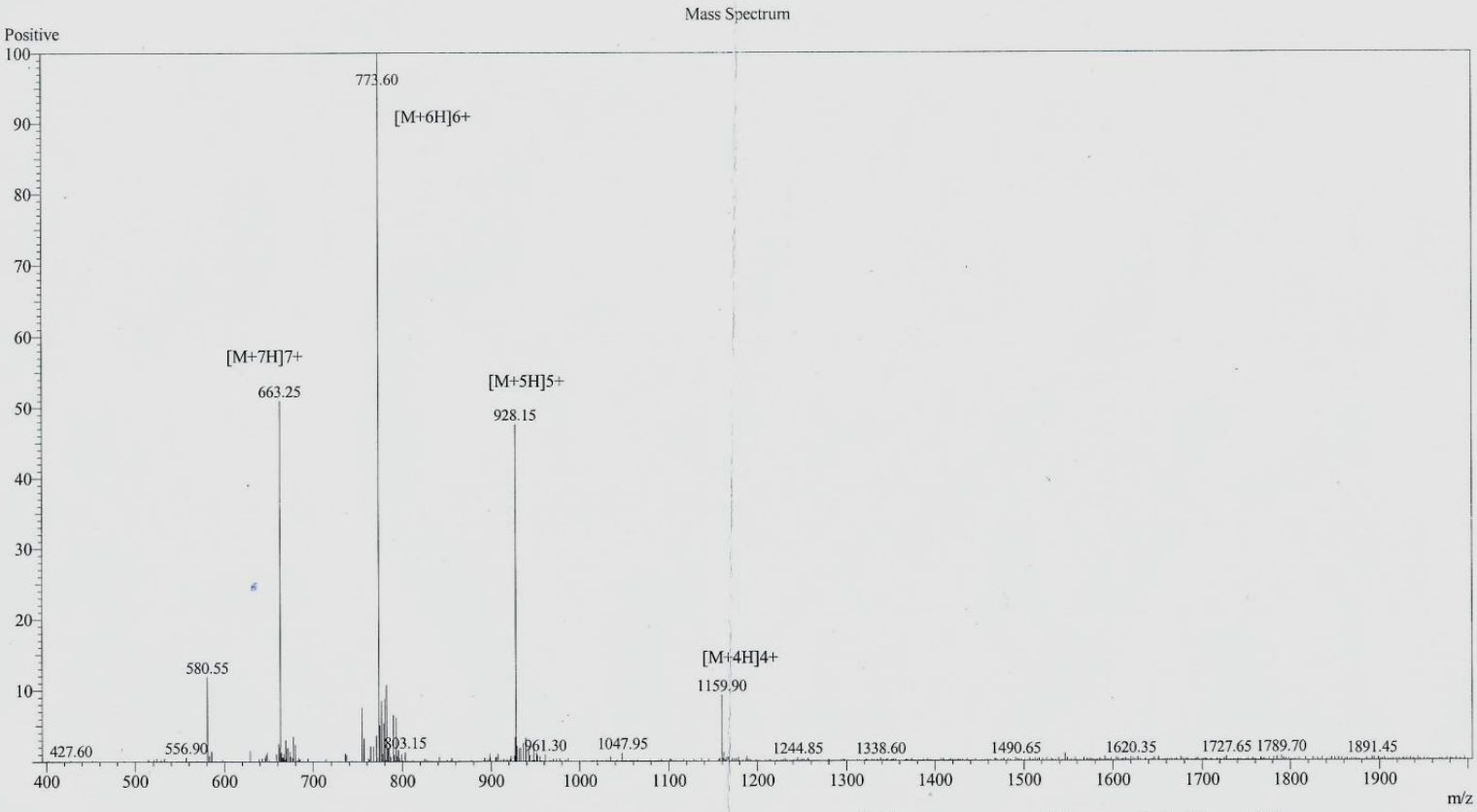

Sample Information

Date and Time	: 2017-5-2 10:18:38
User	: CHAO
Sample	: Peptide 1 MK-37
Inj. Volume	: 1
MW	:4635.49
Lot No.	:P170427-JQ567888

Probe:	ESI	Probe bias:	-3.5kv
Nebulizer Gas Flow:	1.5L/min	Detector:	1.0kv
DL:	-20.0v	T. Flow:	0.2ml/min
DL Temp:	250℃	B. conc:	50%H2O/50%ACN
Block Temp:	200℃		

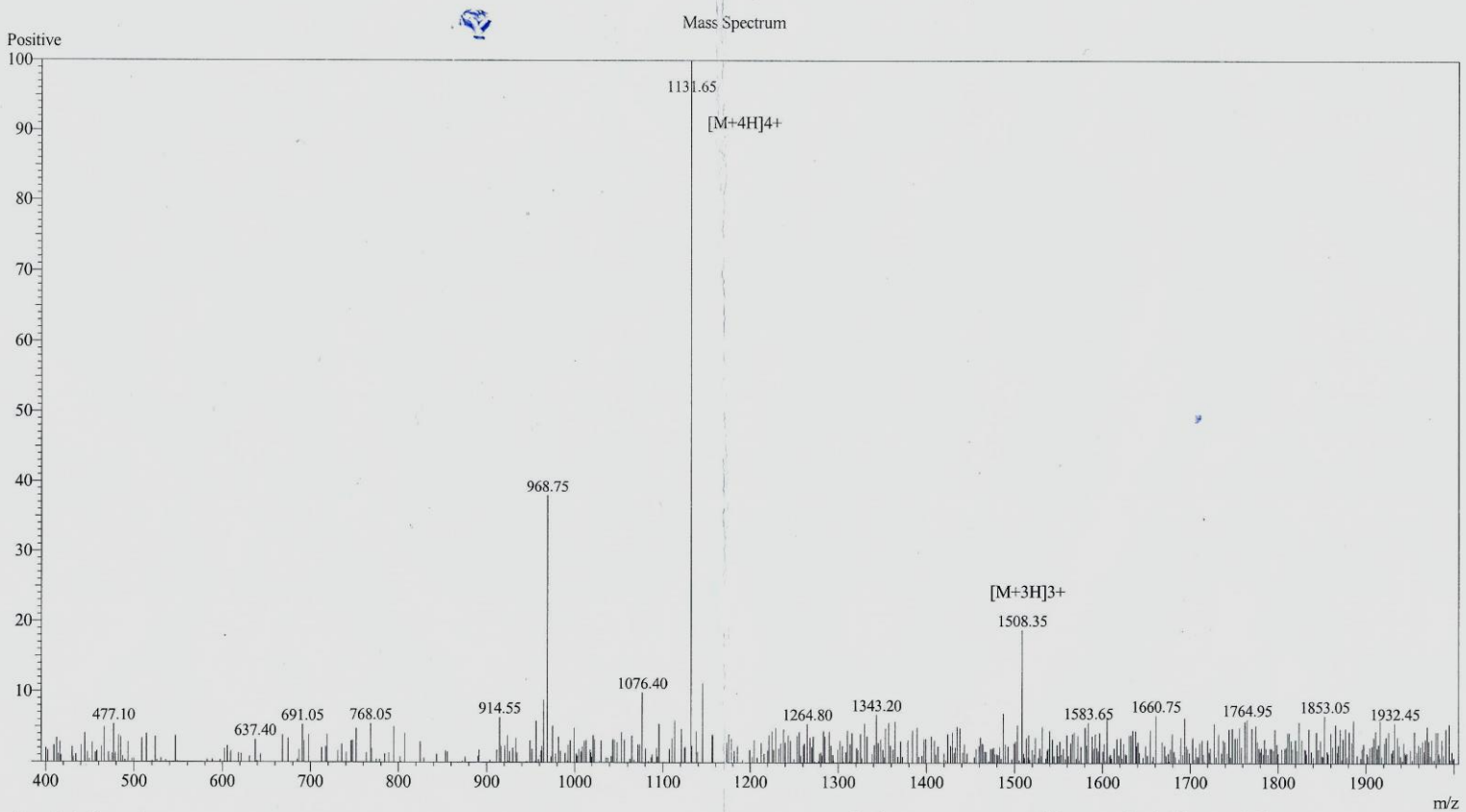

Sample Information	
Date and Time	: 2017-5-3 14:04:14
User	: CHAO
Sample	: peptide 2 MK-37
Inj. Volume	: 1
MW	:4522.33
Lot No.	:P170427-JQ567891

Probe:	ESI	Probe bias:	-3.5kv
Nebulizer Gas Flow:	1.5L/min	Detector:	1.0kv
DL:	-20.0v	T. Flow:	0.2ml/min
DL Temp:	250℃	B. conc:	50%H2O/50%ACN
Block Temp:	200℃		

Date/Time: 2017-5-3,PM 03:35:59
Data File: E:\HPLC\2017\MK-37-F 567891 170503.mdy

Analyst: HCM
Date/Time: 2017-5-3,PM 03:36:01

Sample Description:
Structure : Peptide 2 MK-37
Number : 0200046
Lot No : P170427-JQ567891
Column : 4.6mm*250mm, Kromasil 100-5 C18
Solvent A : 0.1% trifluoroacetic in 100% acetonitrile
Solvent B : 0.1% trifluoroacetic in 100% water
Gradient :

	A	B
0.01min	30%	70%
25min	55%	45%
25.1min	100%	0%
30.0min	STOP	

Flow rate : 1.0ml/min
Wavelength : 220nm
Volume : 5ul

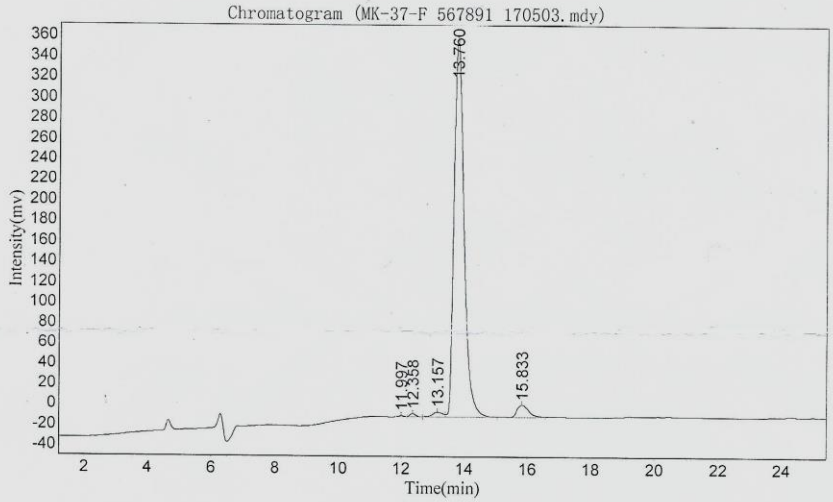

Results

Peak No.	Peak ID	Ret Time	Height	Area	Conc.
1		11.997	980.145	13019.314	0.1534
2		12.358	3172.277	40457.168	0.4765
3		13.157	4594.014	104291.828	1.2284
4		13.760	368667.313	8037651.500	94.6731
5		15.833	11594.700	294476.875	3.4686
Total			389008.448	8489896.686	100.0000

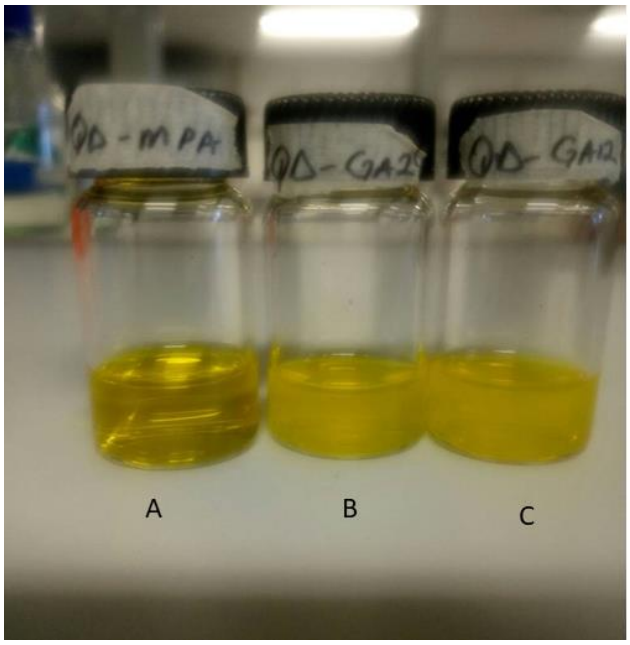

Pictures of the different quantum dots (A) quantum capped with MPA (QD-MPA) (B) Quantum Dots capped with GA powder at 60^0C for two hours (QD-GA2) (C) Quantum dots capped with GA powder at room temperature with for 12 hours.